Silver nanomaterials: synthesis and (electro/photo) catalytic applications†

Rakesh Kumar Sharma[a], **Sneha Yadav**[a], **Sriparna Dutta**[a], **Hanumant B. Kale**[b], **Indrajeet R. Warkad**[b], **Radek Zbořil**[c,d], **Rajender S. Varma**[c,e], **Manoj B. Gawande**[b]

[a]Green Chemistry Network Centre, University of Delhi, New Delhi-110007, India.

[b]Department of Industrial and Engineering Chemistry, Institute of Chemical Technology, Mumbai-Marathwada Campus, Jalna-431213, Maharashtra, India.

[c]Regional Centre of Advanced Technologies and Materials, Czech Advanced Technology and Research Institute, Palacký University, Šlechtitelů 27, 779 00 Olomouc, Czech Republic

[d]Nanotechnology Centre, CEET, VŠB-Technical University of Ostrava, 17. listopadu 2172/15, 708 00 Ostrava-Poruba, Czech Republic

[e]U. S. Environmental Protection Agency, ORD, Center for Environmental Solutions and Emergency Response Water Infrastructure Division/Chemical Methods and Treatment Branch, 26 West Martin Luther King Drive, MS 483 Cincinnati, Ohio 45268, USA.

Abstract

In view of their unique characteristics and properties, silver nanomaterials (Ag NMs) have been used not only in the field of nanomedicine but also for diverse advanced catalytic technologies. In this comprehensive review, light is shed on general synthetic approaches encompassing chemical reduction, sonochemical, microwave, and thermal treatment among the preparative methods for the syntheses of Ag-based NMs and their catalytic applications. Additionally, some of the latest innovative approaches such as continuous flow integrated with MW and other benign approaches have been emphasized that ultimately pave the way for sustainability. Moreover, the potential applications of emerging Ag NMs, including sub nanomaterials and single atoms, in the field of liquid-phase catalysis, photocatalysis, and electrocatalysis as well as a positive role of Ag NMs in catalytic reactions are meticulously summarized. The scientific interest in the synthesis and applications of Ag NMs lies in the integrated benefits of their catalytic activity, selectivity, stability, and recovery. Therefore, the rise and journey of Ag NM-based catalysts will inspire a new generation of chemists to tailor and design robust catalysts that can effectively tackle major environmental challenges and help to replace noble metals in advanced catalytic applications. This

Conflicts of interest
There are no conflicts to declare.

overview concludes by providing future perspectives on the research into Ag NMs in the arena of electrocatalysis and photocatalysis.

1. Introduction

The pioneering report on the synthesis of silver nanoparticles (Ag NPs) by M. C. Lea in 1889 sparked great interest among the research community and marked the beginning of a new era in the field of nanoscience and nanotechnology. Ag NPs are usually ranging from 1 to 100 nm in size. The unique properties of these nanometric sized Ag particles and their versatility spurred innovation in the contemporary society.[1] Silver possesses three unique attributes—ultimate electrical and thermal conductivity and excellent brilliance. Scientific enthusiasm further stems from the fact that nanosilver not only serves a wide range of applications in academia, but also brings a number of key advantages to medicine, the agricultural sector, electronics, robotics, the food industry, the textile industry, *etc.*[2–9] Therefore, significant research efforts have been invested in the design and synthesis of Ag NPs of varied size and shapes such as rods, cubes, wires, prisms, tubes, and plates.[10–25] The different shapes and sizes of Ag NPs considerably alter their chemical, optical, and electromagnetic properties.[26–28] Numerous synthetic strategies and assemblies have been developed so that Ag NPs can fit various applications.[29–37] Moreover, researchers have shifted the focus onto preparing more complex or hybrid Ag-based nanomaterials (NMs) as their tunable features enable noteworthy applications in technology-driven fields.[38–43] It is worth mentioning here that Ag NPs have led, in particular, to pragmatic advancement in catalytic processes.[44–50] The unique proliferation emerges from the fact that these nano sized particles not only have high surface area but also possess a large fraction of coordinatively unsaturated atoms (located at various steps, kinks or terraces), which, by coordinating with substrates, enhance the overall catalytic efficiency.[51–55] Ag NPs are of particular interest due to their remarkable antimicrobial and localized surface plasmon resonance properties, which endow them with unique attributes useful in areas such as broad-spectrum antimicrobials, chemical/biological sensors and biomarkers,[56] biomedicine materials,[57] surface-enhanced Raman spectroscopy (SERS),[58,59] and so on. The biological activity of Ag NPs depends on factors including shape, size distribution, surface chemistry, particle composition, particle morphology, coating/capping, particle reactivity in solution, agglomeration, dissolution rate, efficiency of ion release, and the involved cell type, the kind of reducing agents used for the synthesis of Ag NPs are a crucial factor for the determination of cytotoxicity.[60–62] These excellent features of Ag NPs have inspired the scientific community to design powerful catalysts that can act as excellent candidates for industrial processes. Also, the notable progress on Ag-based materials can be directly correlated with the steady increase in the number of publications dedicated to this area.

Nanosilver and nanosilver-based materials are now undergoing extensive research. Much of the debate is predicated on the premise that nanosilver is a versatile material, and that breakthroughs in nanotechnology have bestowed silver with newer applications in catalysis and biomedicines. In 2011, Nowack and co-workers described that nanosilver available in the form of colloidal silver for over 100 years is more efficient than the conventional bulk silver.[63] Bigioni and co-workers published an account, which depicted the synthesis,

structure, and reactivity along with origin and history of Ag molecular NPs.[64] Kang *et al.* reviewed the stabilization strategies employed for the stabilization of gold and silver NPs and their application in enhancing the plasmonic properties.[65] In another overview, He *et al.* focused the thermodynamic and kinetic perspectives for the formation and transformation of silver sulfide NPs along with their toxicity aspects.[66] Generally, batch reactors are utilized for the synthesis of Ag NMs, however due to improper mixing and in view of the difference in reaction conditions, spatial variation occurs in Ag NMs. In this regard, He *et al.* reviewed the importance of flow microreactors and various synthesis strategies adopted for the preparation of Ag NMs under flow reaction conditions.[67]

To date several reviews have been published in the field of synthesis strategies and applications of Ag NPs in antimicrobial activity and catalysis. Among them some instructive reviews summarized the progress on fabrication methodologies of silver-based NMs.[2,66,68–75] Cinelli and co-workers demonstrated the classification model based on green chemistry principles for the syntheses of Ag NMs.[76] Xue *et al.* reviewed the synthesis methodologies for Ag_2S quantum dots and their applications in solar cells.[77] Some appraisals only summarized the individual application of Ag-based nanocomposites in organic transformations,[48,78–81] electrochemical reactions,[82–85] and photocatalysis;[86–95] He *et al.* highlighted the chemical and biological synthesis of silver graphene-based nanocatalysts and their applications as antibacterial agents, catalysts, and sensors in biomedicine.[72] Tang and co-workers described the progress on the synthesis and photocatalytic applications of Ag_2S-based heterostructures.[87] Liao *et al.* summarized the fabrication strategies of Ag-based nanocomposites and their application in catalysis *i.e.* oxidation and reduction reactions, photo- and electrocatalysis.[31] Recently, Xu and co-workers highlighted the basics and mechanism of localized surface plasmon resonance (LSPR) in photocatalysis and the organic reaction catalyzed by plasmonic Ag nanocatalysts.[79] However, as per our perceptions, to date this is the first comprehensive review on Ag NMs that covers the advanced fabrication strategies for Ag NMs and their critical assessment including Ag NPs, supported Ag-NMs, silver single-atom catalysts, Ag-based bimetallic, Ag alloys, janus NPs and silver oxides, and their catalytic applications in liquid phase organic catalysis, photocatalysis and electrocatalysis along with mechanistic aspects. Also, we briefly discussed the positive role of the catalytic reactions excited by Ag NMs, culminating in perspectives for future research efforts in the field of engineering of Ag NMs and their applications in catalysis. We ardently believe that the in-depth discussion on the versatile synthetic procedures described herein for the synthesis of supported Ag catalysts and their effective use in a myriad of applications will be beneficial to a broad readership.

2. Scope of the review

Numerous review articles in the literature specifically deal with the medicinal use of Ag; however, none of the reviews comprehensively highlight the substantial progress made on Ag NMs in the field of organic catalysis, electrocatalysis, and photocatalysis. To date and to the best of our knowledge, there has been no comprehensive review focused on Ag NMs compiling their competent synthetic strategies exploited for the fabrication of Ag-based catalysts with a special emphasis on modern techniques such as continuous flow

and microwave reactors. Their structural modifications result in fine tuning for assorted catalytic applications in reactions such as photocatalysis for hydrogen evolution, CO_2 reduction, degradation of organic pollutants, electrocatalysis, liquid-phase catalysis, *etc.* The mechanistic aspects of Ag NP-catalyzed reactions have yet to be explored since the conclusions will certainly help to design potent catalysts. This review provides a broad overview of the tremendous progress in the use of nanostructured Ag in liquid-phase catalysis, electrocatalysis, and photocatalysis (Fig. 1). Additionally, we have discussed the synthetic methodologies that are employed for the preparation of bare or independent Ag NPs, mixed Ag NPs, and silver oxide NPs. Finally, we offer a new perspective on the design and synthesis of nanosilver-based structures for use in diverse applications. We anticipate that this review will inspire a broad community of scientists who are involved in the design and development of noble metal Ag-based nanostructures.

Since the discovery of Ag NPs, incredible research progress has been achieved not only in the field of nanomedicine, where they act as antibacterial agents, but also in photo- and electrocatalysis. Over the last decade, there has been an exponential increase in the number of articles in the field of catalysis reporting the utilization of Ag NPs as a key material. Fig. 2, clearly indicates the growth and importance of the research in the field of Ag NMs. This citation index figure is taken from the web of science with the keyword search "silver nanoparticles".

3. Synthetic strategies

In order to simplify the overview, the synthetic methodologies for nanostructured Ag are classified into four groups: (i) Ag NPs, (ii) supported Ag NPs, (iii) mixed Ag NPs, and (iv) AgO and Ag_2O NPs (Fig. 3). The prime intention of including this section is to summarize the synthetic procedures that have been employed until now for the preparation of Ag NMs with a special emphasis on a couple of recent examples.

3.1 Basic principles of Ag nanomaterial synthesis

As far as synthesis of Ag NPs is concerned, two approaches are commonly employed, namely top-down and bottom-up approaches (Fig. 4). As the name suggests, top-down approaches involve breaking down of larger substructures into nano-sized materials with the aid of physical or mechanical processes. The bulk metal is either mechanically ground or broken down into fine particles using diverse techniques such as laser ablation, grinding, milling, etching or cutting and subsequently stabilized with the aid of suitable protecting agents. The prime benefit of employing this approach is that a substantial amount of Ag NPs can be prepared within a very short time period. However, a major setback of this method involves the generation of imperfections in the surface structure of metallic Ag NPs which then substantially affect their physico-chemical and surface chemistry properties. This technique is particularly not useful for synthesizing high surface finished Ag NPs of anisotropic morphologies and narrow size distribution. Furthermore, this technique involves longer etching times and massive consumption of energy required to regulate high temperature and pressure conditions.[96] Employing the top-down nanosphere lithographic practice, Duyne and co-workers were able to synthesize solution phase Ag

nanotriangles;[97] their procedure led to the production of uniform and tunable silver nanoparticles demonstrating high economic viability. Bottom-up approaches in contrast entail building up or self-assembling atoms or small clusters into larger nanostructures in a stepwise or in a one-pot procedure. This strategy offers a propitious opportunity of attaining metallic Ag NPs with minimal surface imperfections and superior homogeneous chemical composition wherein certain criterions such as Gibbs free energy, thermodynamic equilibrium and kinetic parameters play a vital role during Ag NP fabrication. Besides, this process efficiently controls the physico-chemical properties of NPs by easy manipulation of thermodynamic and kinetic factors during synthesis.[98,99] Some of the most common bottom-up approaches that have been utilized for the fabrication of Ag NPs include chemical reduction, vapour deposition, atomic compression, sol–gel progression, electrochemical, polyol reduction and greener synthesis using biological materials. Recently, a two-step bottom-up strategy, fundamentally based on a melting-quenching technique and a post-annealing method has been employed for Ag NP synthesis wherein borophosphate glass was used as the reaction medium for nanoparticle growth.[100] This protocol displayed notable advantages including uniform nanoparticle clusters, ease of fabrication, low growth temperature *etc.* Another interesting example of the bottom-up approach mediated by *Garcinia atroviridis* leaf extract was reported by Kamal *et al.*[101] wherein rich bioactive constituents in the extract functioned as an efficient bioreducing agent for the reduction of the silver salt. The ability to produce Ag NPs with the desired size-and shape-dependent properties represents a huge milestone. Consequently, advanced and modified methods are incessantly being designed and tailored for Ag NPs.[102] The methods for fabricating Ag NPs can be broadly classified into eight groups: wet chemical reduction, sonochemical methods, microwave (MW)-assisted synthesis, greener techniques, thermal treatment, continuous and MW flow methods, seed mediated methods and atomic layer deposition (Fig. 5).

3.1.1. Chemical reduction method.—Among all these strategies, chemical reduction represents one of the widely employed methodologies for the preparation of nanostructured Ag. The three major components that direct or control the growth of NPs are the precursor Ag salt, reducing agents, and stabilizing or capping agents. A rigorous and extensive literature survey was conducted into various methods or techniques including the wet chemical method deployed to date, these being summarized in Table S1 (ESI†).

The most commonly employed precursor salt of Ag is $AgNO_3$, which can be reduced to Ag NPs in the presence of diverse reducing agents such as sodium citrate, sodium borohydride ($NaBH_4$), ascorbic acid, alcohols, hydrazines, hydroqui-none, glucose, *N,N*-dimethylformamide (DMF), and so on.[103–113] $NaBH_4$, which is a stronger reducing agent, results in NPs of smaller size. Suitable stabilizing or capping agents that include surfactants, ligands, or polymers such as polyethylene glycol (PEG), polyvinyl-pyrrolidone (PVP), polymethacrylic acid (PMAA), sodium oleate and collagen are added to control the growth of the NPs and to form the desired shapes.[114,115]

After the initial seminal report by Lee and Meisel in 1982, the citrate reduction method has been the most frequently utilized approach for the reduction of $AgNO_3$ to colloidal Ag. Here, citrate ions play the role of a reducing as well as stabilizing agent.[116,117] Furthermore, this synthetic methodology leads to Ag NPs with a variety of shapes and sizes. Since

then, a broad range of synthetic approaches that make use of hydrogen, dextrose, and ascorbic acid as reducing agents have been reported for the synthesis of Ag NPs.[118,119] In this context, Puntes and co-workers introduced an efficient and kinetically controlled seeded synthetic approach that involves the fusion of two reducing agents, namely sodium citrate and tannic acid, to produce monodisperse Ag NPs in the size range from 10 to 200 nm.[120] This procedure also lead to stable Ag NPs with narrow size distribution, which can be further functionalized with various groups, making them suitable for use in biomedicine and catalysis.[121,122] Another durable method developed by Creighton *et al.* has been frequently employed for the fabrication of nanosilver using $NaBH_4$ as a reducing agent.[123] The elucidation of the mechanistic route for the synthesis of Ag NPs by $NaBH_4$ is accredited to Van Hyning and Zukoski.[124] $NaBH_4$ as the reducing agent generated Ag NPs with narrow size distribution. In this context, Emmerling and co-workers illustrated a wet chemical approach for the size-controlled synthesis of Ag NPs whereby silver perchlorate $(AgClO_4)$ was reduced by $NaBH_4$ with various kinetically controlled reaction parameters that eventually affected the growth mechanism of the Ag NPs.[125] This profound mechanistic understanding enabled the authors to produce, for the first time, well directed and size-controlled Ag NPs with the radius ranging from 4 to 8 nm, this being carried out without the inclusion of any stabilizing agents.

Varma and co-workers utilized the wet chemical synthesis approach to obtain Ag nanocables wrapped with polypyrrole.[126] This synthetic approach employed direct polymerization of pyrrole involving silver nitrate as the oxidant. The major advantage of this method is that it does not require any external surfactant or template. The scope of this technique could be further extended to several other monomers such as aniline and *N*-methyl-aniline (NMA) which furnish silver nanostructures with diverse morphologies.

The polyol synthetic process is an alternative approach for synthesizing Ag NPs. This process involves the reduction of Ag salts at an increased temperature in the presence of diol solvents such as ethylene glycol or propylene glycol, which also serve as the reducing agent.[127,128] Upon closely evaluating the reaction mechanism, glycolaldehyde (formed after heating ethylene glycol in the presence of oxygen or air) was found to be the primary reducing agent involved in the reduction of Ag. Additionally, this process employs a capping agent that can help to gain precise control over the shape and growth of the resulting nanostructures.[129] Schlücker and co-workers developed an approach that was an effective extension of the conventional Lee and Meisel synthesis.[130] This method involves the incorporation of an auxiliary viscous compound possessing abundant hydroxyl groups such as glycerol, which not only increases the monodispersity of the resulting Ag NPs multiple-fold, but also provides added stability towards oxidation. On a similar basis, Varma and co-workers reported an MW-assisted protocol for the synthesis of Ag nanowires by utilizing glycerol as a reducing agent and solvent.[131]

It was Justus von Liebig that first invented a silver glass mirror, popularly known as Tollen's reaction, in 1835.

$$RCHO + 2[Ag(NH_3)_2]^+ + 2OH^- \rightarrow RCOOH + 2Ag + 4NH_3 + H_2O$$
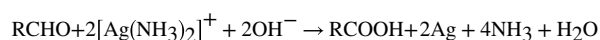
Since then, a modified Tollen's reaction employing aldehydes or sugars as reducing agents has been most commonly employed for synthesizing Ag nanostructures.[132,133] Nevertheless, it is difficult to obtain Ag NPs of high quality *via* this approach, which further limits their practical applicability in industrial applications.

Apart from the conventional reducing agents, TEM grids comprising Cu have also been employed for the purpose of reducing Ag^+ to metallic Ag. Following this approach, Nadagouda *et al.* accomplished the synthesis of tree-like Ag dendrites, which could be leveraged in diverse technological fields.[134] Notably, in addition to copper, the TEM grid comprised carbon, which played a vital role in controlling the dendritic growth.

3.1.2. Sonochemical mediated synthesis.—Another novel approach that has recently captured the attention of the scientific community is the sonochemical or ultrasound-mediated synthesis of Ag NPs. This technique involves the use of strong, powerful and non-hazardous ultrasonic irradiations ranging from 20 KHz to 10 MHz, for the synthesis of a multitude of nanomaterials having diverse morphologies. Sonochemistry arises as a consequence of extreme transient conditions created by ultrasound which then generate unique hot spots capable of achieving localized temperatures and pressures ~5000 K and 1000 atmospheres, respectively. In a sonochemical procedure, no direct interaction between ultrasonic waves and the chemical species occurs. Once the liquid is exposed to high intensity ultrasound, it generates alternating expansive and compressive acoustic waves which causes a change in the density of the liquid layer at the surface of the vibrating material. Thus, the sonication mechanism entails acoustic cavitation as the prime source of generating gas bubbles in the solution. These bubbles then undergo rapid inertial overgrowth during expansion, oscillate with respect to the applied sound field and upon reaching the critical size they collapse to produce pre-requisite conditions such as localized high temperature and pressure for the formation of desired products. These conditions are sufficient to break the chemical bonds, which was explored by researchers working in the field of NP synthesis.[135,136] From the perspective of sustainable chemistry, a sonochemical-mediated synthesis heavily relies on water, which is an environmentally benign solvent. Moreover, these reactions incredibly reduce the reaction time and energy, along with circumventing the use of a reducing agent, and produce materials with high selectivity and yield, which further distinguishes them from conventional techniques.[137,138] Substantial advancement has been made in the sonochemical synthesis of Ag NPs, which provides diverse shapes such as nanorods, nanotriangles, and nanowires,[139–143] alongside fascinating fluorescent characteristics.[144] For instance, Zhou *et al.* reported a facile preparative route involving ultrasonic irradiations and glutathione as a stabilizing agent for fabricating blue-emitting Ag nanoclusters.[145] It is worth noting that Suslick and co-workers reported a sonochemical scheme for fabricating fluorescent Ag nanoclusters using polymethylacrylic acid (PMAA) as a capping agent; these were found to be highly stable and retained their fluorescence properties even under aqueous conditions.[146]

3.1.3. Microwave-assisted synthesis.—MW-aided synthesis utilizing MW irradiations for synthesizing Ag-nanostructured materials is a promising synthetic approach, which has aroused interest among both the academic and industrial community.[147,148] It

was Gedye *et al.* who in 1986 first attempted to synthesize organic compounds using MW radiation; since then, it has been frequently employed for NP synthesis.[149] MW chemistry is based on the direct interaction of electromagnetic irradiation with the molecules present in reaction media through a dielectric heating mechanism including dipolar polarization and ionic conduction processes. MW irradiations heat materials possessing mobile electric charges like polar molecules or conducting ions. On being exposed to MW irradiations, polar molecules because of their inherent dipolar character get excited. Simultaneously, the oscillating electromagnetic field realigns the polar molecules and ions with the electric field. The re-orientation process causes rotation, collision of molecules, molecular friction and dielectric loss which finally produces a rapid internal heating phenomenon. While in the case of ionic conduction processes, ions oscillate back and forth, moving through the solution under the influence of an electric field, which then causes constant fluctuation due to friction and collision leading to overall increase in temperature. Further, MW dielectric heating can be classified on the basis of thermal and non-thermal effects. Thermal effects are the primary reason behind the rapid heating of the reaction mixture. In contrast, non-thermal effects are rather hypothetical and extend from reducing the Gibbs activation energy to increasing the collision efficiency of polar molecules.[150] MWs enable intense and rapid heating within a short time, which makes this technique much faster and easier in comparison with traditional methods for synthesizing NPs.[131] In fact, the heating effect produced from microwaves leads to the formation of high-quality crystalline NPs allowing pronounced control over the uniform size and morphology.[147,151,152] High product yields, selectivity, reduced energy consumption, or mild reaction conditions are examples of some intriguing attributes of these protocols, which make MW-aided synthesis of NPs fall under the banner of benign chemistry.[138,153,154] Numerous studies describe the use of microwaves in the facile synthesis of Ag NPs.[155–164] Recently, MW-assisted polyol method employing ethylene glycol as the solvent has been demonstrated by Saloga *et al.* for the synthesis of polyacrylic acid (PAA)—stabilized ultrasmall Ag NPs at 200 °C with a 3 nm radius.[165] The adjustable heating rate and longer reaction time offer another route for manoeuvring the particle growth and size. In another study, Baker and co-workers introduced an eco-friendly wet-chemical reduction path coupled with MW heating at 100 °C to synthesize organo-soluble Ag NPs.[166] Here, a halide-free deep eutectic solvent (DES) having a 1 : 2 molar ratio of choline nitrate and glycerol was deployed along with oleylamine, which functioned as a surfactant and reducing agent. This MW-mediated route was found to be energy efficient and expeditious as it resulted in uniform Ag NPs of an average diameter ranging from 6 to 25 nm.

3.1.4. Green synthetic approaches.—The synthetic methodologies discussed so far are energy and capital intensive and utilize strong reducing agents such as NaBH$_4$ and hydrazine hydrate, among others. Besides, they also employ various additives and stabilizing agents, which further hinders their use in biomedical and medicinal fields. The continuously increasing societal and environmental concerns have stimulated scientists to switch from conventional modus operandi to green approaches, and inspired them to develop clean, biocompatible, cost-effective, and eco-friendly routes for Ag NP synthesis.[167–169] Considerable efforts have been invested in this direction, including the assessment of greener strategies.[76,170–172] In general, greener synthetic approaches involve the use of appropriate

reductants in the form of plant extracts comprising a variety of flavonoids/alkanoids/ polyphenols that essentially reduce the metallic salts into lower oxidation state aiding in the formation of NPs and also serve as suitable capping agents/stabilizers that fundamentally help in not only controlling the particle size, but also imparting protection to the synthesized NPs. Recently, biomimetic approaches that employ living microorganisms have provided a prominent and sustainable platform for NP synthesis. For the microbial-assisted synthesis of NPs, microorganisms such as bacteria, yeast, or fungi function as a reducing agent, thus avoiding, to a large extent, the use of hazardous chemicals and subsidiary capping and stabilizing agents. Furthermore, these microbes and genetically engineered organisms are considered innate bio-factories for preparing NPs.[173] Furthermore, working with microbes is quite flexible; thanks to their ability to sustain harsh pH, temperature, and pressure conditions.[174,175] Driven by the capacity of *Chlorella pyrenoidosa* to survive extreme reaction conditions, Prasad and co-workers recently investigated this microbe as an algal platform for designing Ag NPs; the formation of size controlled and crystalline Ag NPs ranging from 5 to 15 nm was then stabilized by intrinsic capping agents.[176]

However, a microbial-assisted synthesis involves additional processing steps such as microbial isolation and requires specialized and expensive culture maintenance. To circumvent the aforementioned challenges, chemists have proposed the idea of using plant extracts as an eco-friendly and sustainable pathway. Plant-mediated synthesis or phytosynthesis involving extracts from different parts of the plant (such as leaves, seeds, fruits, stems, roots, *etc.*) as a reducing agent has recently been recognized as a promising strategy for NP fabrication.[96,177,178] Furthermore, these plant-assisted protocols chiefly employ water as a green solvent for preparing the extract solution along with deployment of ambient temperature and pressure conditions, thereby resulting in energy savings. To date, various synthetic methods that rely or incorporate the principles of green chemistry have been reported for the bio fabrication of Ag NPs.[167,179–183] The salient feature of phytosynthesis is that plant extracts contain numerous natural biomolecules and antioxidant secondary metabolites like alkaloids, flavonoids, phenolic groups, terpenoids, and proteins, which simultaneously serve as a safer form of reducing and stabilizing agents.[171] It is worth mentioning here that Xue *et al.* successfully synthesized Ag NPs (17–27 nm) from alkali lignin—a renewable source produced from pulp mill that acts as a reducing and stabilizing agent.[184] The authors used silver oxide instead of AgNO$_3$, which functioned, due to the strong metal–metal oxide interactions, as both the precursor salt of Ag and catalyst for the reduction of Ag ions. There are analogous reports in the literature where a cell free extract of *Pseudomonas aeruginosa* M6 from mangrove and an aqueous leaf extract from *Alysicarpus monilifer* were used to reduce AgNO$_3$ to Ag NPs, having a size of approximately 15 nm.[185,186] Similar synthetic protocols were reported by Varma and co-workers, where they utilized blueberry, blackberry, turmeric, tea and pomegranate extracts to reduce AgNO$_3$ to Ag NPs.[187] Furthermore, antioxidants present in the extracts such as flavonoids, anthocyanins, polyphenols, or curcumin played a key role in the reduction process. Notably, the extract obtained from pomegranate resulted in more uniform-sized Ag NPs, compared to the other green sources. A recent report described the fabrication of Ag NPs in the size from 40 to 80 nm using aqueous extracts from the bark of *Salacia chinensis*

(SC), the family of Celastraceae, which contained an array of antioxidants comprising phenolic and flavonoid compounds with reducing power strong enough for NP synthesis.[188]

3.1.5. Thermal treatment method.—Among other methods, thermal decomposition of solid precursors to fabricate NPs has achieved great success. Thermal decomposition, also referred to as thermolysis, is a heat driven process that involves chemical decomposition of a precursor material to form nanoparticles at a specific temperature most commonly known as the decomposition temperature. Thermal decomposition of solids is essentially controlled by the reaction geometry, nature of metallic ions and various physico-chemical processes that occur at the reaction interface. These processes include ruination of the crystal lattice of the reactant molecule, nucleation and growth, elimination of gaseous products *via* diffusion as well as related mass and heat transfer phenomena which are known to regulate the overall kinetics of the reaction.[189] It is a classical method, which is facile, economical and renders stable, monodispersed nanometric-sized particles in large amounts through a single heating process.[190] Besides, this approach smartly overcomes the hurdles associated with the controlled shape and size of the resulting NPs by merely regulating the annealing temperature, heating time, heating rate, and concentration of reactants, as shown by Koga and co-workers in a thermal decomposition route to Ag NPs from silver acetate, including the kinetic measurements and morphological studies.[191] Gharibshahi *et al.* adopted an improved thermal treatment approach in which $AgNO_3$ and PVP were employed for synthesizing pure Ag NPs with narrow size distribution; the calcination process alternating between O_2 and N_2 flow was carried out from 400 °C to 800 °C, which resulted in a decrease in the NP's size from 7.88 nm to 3.29 nm, based on a TEM analysis.[192] Goudarzi *et al.* reported a greener thermal treatment path employing two natural sources, namely a pomegranate peel extract and cochineal dye, for the synthesis of Ag NPs. A solution phase route using water was employed in the case of pomegranate peel extract wherein $AgNO_3$ transformed into Ag NPs at 300 °C.[193] On the other hand, a solid state approach was utilized in the case of cochineal dye obtained from insects in which masses of cochineal dye were ground with $AgNO_3$, followed by heat treatment at 600 °C that generated homogeneous as well as dispersed spherical Ag NPs.

3.1.6. Continuous flow and microwave flow assisted synthesis.—The advent of flow chemistry has completely revolutionized the scope of materials and synthetic organic chemistry.[194,195] Flow chemistry offers the opportunity to perform reactions with more intensity and efficient mixing, thus enabling researchers to have better control over the reaction parameters that can yield NPs of varied shapes, sizes, and superior properties. Continuous flow reactors are apparatus or devices in which synthesis experiments are performed in a continuously flowing stream. Flow reactors can be tubular-, tank- or disk-type reactors which are commercially available and can even be customized depending upon the desired application. In a continuous flow reactor assembly, reagents are separately pumped *via* a micromixer into the reaction compartment or microreactor which is temperature controlled, thereby allowing to attain superior optimized reaction conditions. The reaction compartment is further connected with a back pressure regulator that allows monitoring of reaction pressure. Such reaction conditions facilitate heating of solvents above their boiling point, a process also termed as superheating which further increases the

reaction kinetics and produces ultra-speedy reaction conditions. Besides, the residence time of the mixture in the reactor (total time that reactants spent inside the control volume), and flow rate of reactants are some of the additional parameters that affect the size, shape and physico-chemical properties of the ensuing Ag NPs.[196] In addition, flow reactors also offer striking benefits of easy scalability, good product quality, safety with upgraded thermal management and ability to withstand extreme reaction conditions.[197] In this context, Lin *et al.* successfully demonstrated the fabrication of monodispersed Ag NPs through a continuous flow tubular microreactor where silver pentafluoropropionate was employed as a single phase precursor of Ag, and its thermal reduction in isoamyl ether in the presence of the surfactant called trioctylamine (TOA) resulted in the generation of Ag NPs with narrow size distribution.[198] Similarly, Kulkarni and co-workers described a continuous flow production for Ag NPs using two different bio-surfactants—oleic acid sophorolipid (OASL) and stearic acid sophorolipid (SASL), which worked both as a stabilizing and reducing agent.[199] Dynamic light scattering (DLS) studies revealed that kinetic parameters such as temperature and time have a profound influence on the size and growth of NPs. Furthermore, the high temperature and higher residence time led to the formation of small and monodispersed spherical Ag NPs. A greener biogenic protocol coupled with continuous-flow tubular microreactors was disclosed by Huang *et al.*, wherein polyols present in the *Cinnamomum camphora* leaf lixivium were chiefly responsible for the reduction of Ag ions to Ag NPs.[200] However, Torrente-Murciano and co-workers reported the use of two continuous flow reactors connected in series to synthesize tuneable Ag NPs, the average size of which ranged from 5 to 10 nm. Additionally, the use of two separate flow reactors allowed the spatial separation of nucleation and growth of the NPs.[201]

Recently, the integration of the continuous flow strategy with MW-assisted chemistry has completely metamorphosed the manner in which research is conducted in academic and industrial sectors. The most frequently encountered problems such as low penetration depth, non-uniformity in temperature and difficulty in scaling up to an industrial level can be easily overcome in a continuous flow MW system wherein large quantities of NPs are synthesized thus allowing the upscaling of the manufacturing process while reducing overall cost. In a continuous flow MW reactor, the reaction mixture flows through the MW cavity under suitable temperature, pressure and MW power conditions. The overall assembly involves a Teflon coil (has exceptional resistance towards high temperature, chemical reactions, corrosion) kept in a commercial microwave oven. Thus, homogeneous MW heating and fine temperature and pressure control are easily achievable, which further helps in designing well-defined nanomaterials.[202] For instance, Gedanken and co-workers were the first to design a continuous circulating flow MW system by connecting a MW oven with a circulating pump for the synthesis of nanosized Ag NPs.[203] Horikoshi *et al.* employed a diamminesilver(I) complex $[Ag (NH_3)_2]^+$ as the precursor salt of Ag in the presence of carboxymethylcellulose (CMC) for the MW continuous flow mediated synthesis of Ag NPs, while Jarz bski and co-workers synthesized Ag NPs in a continuous flow MW system through a polyol method using $AgNO_3$ and silver acetate as precursors and ethylene glycol functioning as a solvent as well as reducing agent.[204,205] However, reaction studies revealed that silver acetate was a more efficient reagent as it resulted in the faster production of 10–20 nm spherical Ag NPs.

3.1.7. Seed-mediated growth.—Seed-mediated growth of Ag NPs is another synthetic strategy, which has recently gained popularity as a highly efficient process for producing Ag NPs with astonishing degree of control over size, morphology, structure and composition.[206,207] This technique is a classic example of a heterogeneous nucleation process involving two steps. In this methodology, firstly seed nanoparticles are synthesized and they are consequently added into growth solution containing metal precursor *i.e.* Ag salt, reducing agent and stabilizing or shape directing agents. By simply adding preformed metal seeds into the growth solution, the two most significant phenomena *i.e.* nucleation and growth are efficiently isolated as two disparate synthetic steps that allow superior control over the size, shape and morphology of the ensuing nanostructures. It has been witnessed that the activation energy for reduction of metal salt *i.e.* in the second step is significantly lower as compared to nucleation of seed particles thereby facilitating autocatalytic formation of metal atoms on pre-formed seeds. Furthermore, by judiciously selecting the seed nanoparticles and carefully maneuvering the crystal growth conditions, thoughtful design of metal NPs possessing varying shapes can be achieved.[208,209] Seed-mediated approaches can be further divided into two categories of growth: homoepitaxial and heteroepitaxial. Homoepitaxial growth is when a seed crystal bears a metal that is the same as the metal deposited on the seed; for example, the growth of Ag atoms on Ag seeds. In contrast, heteroepitaxial growth entails the deposition of metal which is different from the metal that comprises the seed crystal, *i.e.* the growth of Ag atoms on Au seeds or *vice versa*. One of the most important criteria that needs to be fulfilled in the case of heteroepitaxial-seeded growth is that there should be a small difference in the lattice constant of the seed and the deposited metal.[116] Recent reports demonstrated that this versatile approach could be successfully utilized for preparing excellent silver nanostructures including nanospheres, nanocubes, and octahedrons.[207,210] Wang and co-workers described a novel homoepitaxial seed-mediated approach in conjunction with oxidative etching for the synthesis of monodispersed and spherical Ag nanospheres (tunable diameter ranging from 37 to 68 nm) from Ag nanocubes.[211] Firstly, a seed solution was prepared using $AgNO_3$, $NaBH_4$ (reducing agent), and cetyltrimethylammonium chloride (CTAC) as a surfactant. This seed solution was then added to an aqueous solution of CTAC, $AgNO_3$, and ascorbic acid, and was constantly stirred at 60 °C for 3 h to form Ag nanocube seeds. Afterwards, these Ag nanocubes were successfully transformed into Ag nanospheres through a facile injection of Cu^{2+} using an aqueous solution of $Cu(NO_3)_2$, which is used as an etchant for the morphological modification process. Jabbari and co-workers devised a seed-mediated strategy for the fabrication of Ag NPs, where citrate-stabilized Ag nanoclusters were employed as seeds for the subsequent growth of Ag NPs.[212] Furthermore, a redox reaction between Ag^+ ions and ascorbic acid in the presence of CTAB led to the deposition of newly formed Ag atoms on the surface of the Ag seeds. Wang *et al.* exemplified a seed-mediated growth of Ag octahedra using silver trifluoroacetate, ascorbic acid, and sodium citrate, wherein nanocubes and quasispheres of Ag served the purpose of presynthesized seeds.[213] In another report, Zhu and co-workers illustrated a simple heteroepitaxial method employing a Au solution of seeds to grow Ag NPs.[214] Additionally, the silver mirror reaction utilizing glucose as a weaker reducing agent was employed to obtain dispersed Ag NPs with sizes ranging from 20 to 120 nm.

3.1.8.   Atomic layer deposition.—Atomic layer deposition (ALD) is one of the most important methods for the synthesis of supported Ag NPs. ALD is a surface dependent approach that entails construction of a thin film on a substrate through successive gaseous phase chemical reactions. For accomplishing the desired synthesis, precursors are allowed to undergo reaction with the substrate in a sequential alternating pulse manner. These individual gas surface reactions are referred to as half reactions and contribute to overall material synthesis. During each half reaction, precursor is pulsed into a reactor or chamber kept at designated temperature and pressure for a specified period of time so as to ensure that the precursor reacts completely with the substrate and forms only a monolayer at the surface. The subsequent step involves the purging of the chamber with an inert carrier gas (either nitrogen or argon) to eradicate any unreacted precursor or any by-product formed during the process. Furthermore, in the case of bimetallic NPs synthesis, this step is accompanied by a second reactant precursor pulse and purge. The process is then cycled for achieving desired film thickness. One of the most crucial aspects of this technique is that by using layer-by-layer deposition, film thickness can be altered by varying the number of ALD cycles. The temperature range at which growth is saturated is termed as the ALD temperature window.[215] The ability to produce well-defined materials with the anticipated film composition and tuneable thickness, along with homogeneous and conformal growth, is a beneficial feature of this methodology, compared to conventional chemical vapour deposition (CVD) and physical vapour deposition (PVD) techniques. There are two types of ALD techniques: plasma-enhanced atomic layer deposition (PEALD) and thermal ALD. Thermal ALD operating at higher temperatures around 150–350 °C is a surface driven phenomenon which proceeds *via* surface reactions and allows precise thickness control of the film regardless of the geometry of the substrate. On the other hand, PEALD by exploiting the high reactivity of plasma species successfully reduces the deposition temperature without hampering the quality of the films. This technique is particularly useful while working with temperature or heat sensitive materials and for producing high quality pure films. Additionally, the enhanced reactivity of plasma not only permits the utilization of a wide range of precursors or substrates but also simultaneously facilitates the deposition of substrates that are often not possible through thermal ALD. PEALD is preferable, in comparison with the thermal method, as it leads to continuous thin films with greater coverage. The growth formation for most of the noble metals takes place *via* cluster formation, which is also denoted as islands or 'Volmer–Weber (VW) growth mode'. For example, Kariniemi *et al.* employed a PEALD tactic for depositing thin films of Ag up to 200 mm of wafer size.[216] For this synthesis, Ag(fod)(PEt$_3$) (fod = 2,2-dimethyl-6,6,7,7,8,8,8-heptafluorooctane-3,5-dionato) and H$_2$ were utilized as starting reagents and the saturated growth was attained at 120–140 °C. Similarly, another research group explored the possibility of synthesizing polycrystalline Ag NPs, where Ag(fod) (PEt$_3$) along with plasma activated H$_2$ was used as a progenitor reagent.[217] For a better understanding of the growth mechanism, meticulous examination of ALD parameters such as alteration in the number of ALD cycles, further influencing the deposition of particles and material transfer *via* Ostwald ripening, was carried out.

3.1.9.   Critical assessment of various synthetic methodologies frequently employed for fabricating Ag NPs.—Since the first report on Ag nanoparticles,

researchers have been continuously exploring advanced and neoteric methods that could readily generate Ag nanostructures of desired size, shape and morphology. However, selecting a suitable and precise preparative method is equally important for engineering or fabricating ideal and high-quality Ag nanoparticles for assorted scientific and technological fields, since the experimental technique employed has a profound effect on the morphology, stability and physico-chemical properties of the ensuing nanoparticles. Each of the synthesis techniques employed has its own advantages and limitations. Table 1 succinctly summarizes the key benefits and limitations associated with various synthesis techniques.

In view of sustainability, it is imperative for the chemical sector to redirect all the synthetic approaches towards a greener pathway by reducing waste, and recycling catalysts and solvents, while simultaneously sustaining the production quality. In light of sustainable synthesis, traditional chemical reduction methods have lost their due credibility. Accomplishment of the dual goal of activity and sustainability in the real sense will require establishment of a strong networking between the research chemists and the process engineers. Nevertheless, major improvements have been witnessed through the utilization of the latest innovative tools such as continuous flow, MW- and ultrasonic irradiation *etc.* that have played a key role in transforming the chemical synthesis sector drastically from both an environmental as well as economic perspective. However, a number of challenges still remain to be tackled especially those associated specifically with the solvent and catalyst recovery while employing the continuous flow methodology to harness the true benefits of this approach. As already highlighted in Table 1, due consideration needs to be given to the monitoring of reaction temperature, manipulation of slurries and sustainable reactor design. In the case of MW-assisted manufacturing technology, advantages such as reduced energy consumption, less chemical waste generation, shorter reaction times, exceptional reproducibility and environmental safety renders this method suitable from a large scale industrial synthesis perspective. Nonetheless, future efforts of the researchers need to be dedicated towards recognizing the essentials of the mechanism of the chemical reactions employing MW irradiations, conducting *in situ* characterization and theoretical simulation for analyzing the impact of MWs on the crystal morphology to completely comprehend the nucleation and development process incurring under the influence of MWs. Additionally, it will be important to ensure that all the innovations involving MW-assisted synthesis lie within the premises of economic viability and high productivity in addition to being sustainable, clean, and green. The bulk chemical processing *i.e.* industrial scale-up, and the role of MWs in continuous flow needs to be completely understood and profitably utilized. Besides, emphasis should also be placed towards the fruitful design of reaction parameters for the synthesis of the nanomaterials in the solid phase system where a mechan-ochemical approach may be exploited.

3.2 Supported Ag-based NPs

The area of supported Ag NPs is another distinctive segment that is of fundamental interest to both the industrial and academic sector. It is well documented that bare Ag NPs readily undergo agglomeration and aggregation, which impedes their complete utilization in potential applications.[221–223] Moreover, the catalytic properties of Ag NPs strongly rely on the uniform dispersion and distribution of the active metal species. Consequently, the dual

quandaries of agglomeration and separation related to Ag NPs can be surmounted by fixing the particles onto appropriate engineered supports. The extraordinary characteristics arising from the synergistic integration of Ag NPs and the support material are worth highlighting. To date, numerous support materials such as graphene oxide, carbon nanotubes, metal oxides, boron nitrides, MOF, silica, and polymers have been effectively used for the synthesis of supported Ag NPs (Fig. 6). In this section, various support materials employed for preparing Ag-based composites have been categorized and subcategorized on the basis of the chemical composition and the functionalities involved. An exhaustive list of support materials reported in the literature has been presented in Table S2 (ESI†).

3.2.1. Carbon-supported Ag NPs.—Currently, the use of carbon as a support material for anchoring metal NPs has gained wide recognition as it provides a sufficient surface area for the complete dispersion of NPs.[227–232] Guo *et al.* reported the synthesis of four different (10, 20, 40, and 60 wt%) Ag-loaded carbon particles, whereby citrate was utilized as the stabilizing agent.[233] TEM images revealed that the mean size of the particles was 15 nm. In another report, Ag NPs supported on carbon microspheres were synthesized using *Brassica oleracea*, biomass pollen grains, as a precursor of carbon, which, after the treatment with $AgNO_3$ followed by successive preoxidization at 300 °C and carbonization at 600 °C, resulted in the formation of carbon-supported Ag nanocomposites.[234] Besides, the average size along with the distribution of the resulting Ag NPs could be easily regulated by altering the concentration and treatment time of $AgNO_3$.

Among the carbon-supported materials, graphene represents one of the most promising contenders for a broad spectrum of functional uses because of its extremely high surface area and outstanding mechanical, thermal, and chemical stability. The presence of oxygen functionalities makes graphene's surface hydrophilic, rendering it an exceptional building block for the attachment of NPs; thanks to the strong metal–support interactions.[235–237] In view of its facile delamination and easy functionalization, various groups have delineated the synthesis of graphene supported Ag NPs.[181,238–244] For example, Perdikaki *et al.* designed an *in situ* sequential approach for the growth of (Ag, Cu) monometallic and Ag/Cu bimetallic NPs on the graphene surface, whereby Ag ions were first adhered onto the surface of graphene through electrostatic interactions and further reduced with the successive addition of DMF.[245] Similarly, Jana and co-workers demonstrated the synthesis of reduced graphene oxide (rGO)-supported Ag NPs for the photocatalytic degradation of organic pollutants (Fig. 7a).[246] In this report, positively charged silica coated Ag NPs were electrostatically bonded onto the negatively charged GO surface owing to the presence of carboxylate groups. Furthermore, the addition of hydrazine hydrate resulted in the formation of rGO from GO. By varying the amount of aqueous silica-coated Ag nanoparticle solution and GO; different rGO-Ag nanocomposite materials with weight ratios of 1 : 0.5, 1 : 0.25, and 1 : 0.12 can be synthesized.

Wang and co-workers efficiently utilized GO nanosheets as substrates for preparing Ag nanoparticle films whereby it is easier to coat Ag NP thin films onto carbon nanosheets, just by simply dipping GO sheets into the precursor salts of Ag solution.[247] The presence of hydroxyl, epoxy, carbonyl, and carboxyl groups on the exposed sheets of GO readily initiated the adsorption of positive ion $Ag(NH_3)^{2+}$ *via* electrostatic interactions.

Furthermore, the addition of glucose afforded *in situ* reduction of $Ag(NH_3)^{2+}$ to metallic Ag NPs.

Over the past few years, carbon nanotubes (CNTs) have been extensively exploited as a support material for developing advanced catalytic processes.[248–250] Besides, CNTs also offer additional advantages of chemical modification of the surface through a variety of amination and acid treatment procedures, which makes them suitable for anchoring Ag NPs. This was exemplified by a simple templated approach for the synthesis of Ag-modified multi walled carbon nanotubes (MWCNTs) where the surface of these MWCNTs was initially covalently modified using adenine motifs that encouraged the formation of Ag NPs *via* metal-adenine coordination.[251] Recently, Pan and co-workers demonstrated an intricately designed electron-assisted reduction (EAR) and a thermal calcination method for the development of amine functionalized CNT-supported Ag NPs.[252] The first step entailed the oxidation of CNTs followed by amine functionalization using 1,6-hexamethylenediamine (HDA) and dicyclohexyl-carbodiimide (DCC). Then, a wet impregnation approach was utilized to load Ag NPs onto the surface of the modified CNTs. This was very well accomplished by thermal calcination in N_2 at 400 °C and by an electron-assisted reduction process where the electrons were produced by radio frequency (RF) plasma. The designed EAR strategy led to the production of Ag NPs with an average diameter of 3.8 nm, which was found to be much smaller than the diameter attainable by a thermal calcination process (25.5 nm).

Recent advancements in the field of photo- and electrocatalytic reactions suggested that carbon nitride (C_3N_4) can be successfully used as a support material to develop heterogeneous catalytic systems. One of the striking features of carbon nitride is that the existence of a N-atom in the structure of C_3N_4 allows ready coordination with the metal NPs.[253–256] Patel *et al.* described the fabrication of C_3N_4-supported Ag NPs for the MW-assisted synthesis of propargylamines and 1,3-diynes.[257] SEM images of C_3N_4 revealed an aggregated yet smoothly layered structure, while SEM images of AgNPs@g-C_3N_4 showed that the surface of C_3N_4 roughened due to the presence of Ag NPs on the surface of the material.

Diamond is another allotrope of carbon that has been identified as a neoteric support material for anchoring Ag NPs. Furthermore, the occurrence of inert and stable sp^3 carbon in diamond makes it suitable as a host material for supporting active metal species.[258] In this regard, Hamers and co-workers established a facile and sequential route to synthesizing Ag NPs embedded in diamond films.[259] The fabrication process initially involved the seeding growth of another layer of diamond thin films on a Si substrate through a MW plasma-enhanced CVD technique followed by the deposition of Ag on a diamond film *via* an electron beam evaporator. It was further validated that once a thin layer of Ag is deposited onto the surface of diamond, simultaneous growth of another diamond occurs, forming a diamond-Ag-diamond sandwich-like structure in which the Ag NPs are completely embedded within the diamond films. On a similar basis, Navalon *et al.* formulated a diamond NP supported Ag NP-based Fenton-photocatalytic system for the natural sunlight mediated degradation of phenol.[260]

3.2.2. Silica-supported Ag NPs.—Silica has provided an unprecedented platform for the development of nanoscale functional materials that have proven their utility in diverse fields of catalysis, magnetism, optics, sensors, medicine, and electrochemistry.[261,262] The presence of silanol groups makes the surface of silica more hydrophilic, thus facilitating the attachment of metal NPs. Mesoporous silica with a large surface area has attained wide recognition as a support material for anchoring Ag NPs, which is evidenced by recent advancements in the field of supported Ag NPs.[263–267] In this context, Lykakis and co-workers reported an efficient synthesis of hollow mesoporous silica (HMS)-supported Ag NPs.[268] To synthesize HMS support material, dodecylamine (DDA) was employed as a mesostructure template-directing agent. In the next step, TEOS (as silica source) was added to the ethanolic-water solution of DDA, which subsequently underwent hydrothermal aging at 65 °C in a shaker bath for 24 h. The calcination of the material at 600 °C resulted in the removal of the organic template. Afterwards, Ag NPs of diverse sizes were loaded onto the HMS *via* efficient exploitation of two methods: (i) a wet impregnation method with a subsequent reduction using H_2 at 350 °C, and (ii) an *in situ* deposition and reduction using ethanolamine and ethylenediamine followed by calcination. In another report by He *et al.*, a divergent approach was employed to impregnate Ag NPs into a silica support material following a wet chemical reduction route.[269] This strategy entailed the use of cationic polysaccharide and chitosan with hydroxyl and amino groups, which not only worked as a suitable ligand for the coordination of Ag ions, but also displayed significant affinity towards the silica surface. In order to synthesize the overall composite, the key step involved the deprotonation of silica to its nucleophilic form, which further bound with an electrophilic Ag(I) complex. Once coordinated, these Ag ions were further reduced to Ag NPs on the silica surface either by using glucose or $NaBH_4$ as reducing agents.

Although various research groups have focused on loading Ag NPs onto the silica surface, this approach shows one major drawback. Owing to the weak binding forces and chemical erosion, the loaded Ag NPs are consumed very promptly. In order to combat this complexity, Shen and his group adopted a unique engineered style for loading Ag NPs onto the interior walls of a microporous silica shell.[270] To this end, Ag NPs were used as the inner core material, and the coating of silica onto these Ag NPs was achieved by the well-known Stöber method. The synthesis of the overall composite involved two steps. The initial step involved the adsorption of Ag ions *via* electrostatic interactions onto the surface of sulfonated polystyrene (PS) beads, followed by a subsequent reduction and protection by PVP in order to generate the PS–Ag composites. In the next step, the hydrolysis and polymerization of TEOS formed silica colloids, which then assembled as a shell of silica on the sulfonated PS–Ag composites *via* H-bonding interactions. The unique core–shell structure protected the active inner Ag NPs from undergoing aggregation and oxidation and imparted high chemical stability. Besides, the presence of the mesoporous shell of silica allowed a facile and slow release of Ag ions. A more sophisticated method was reported by Chen *et al.*, whereby the authors illustrated a distinct template-based strategy for the growth of Ag NPs in the channels of mesoporous silica (MCM-41).[271] To synthesize the mesoporous support, CTAB was used as a templating agent. The reaction mixture containing CTAB, TEOS, NaOH, and H_2O was kept in a Parr reactor at 110 °C for 96 h. The resulting material was filtered, washed, dried and finally calcined at 550 °C for 24 h, which yielded the desired MCM-41.

The Ag NPs were further supported onto the formed MCM-41 by deploying $AgNO_3$ and PVP as the precursor salt and the reducing agent, respectively, in the presence of ethylene glycol as the solvent. TEM images clearly showed that active Ag NPs were present not only on the surface but also within the channels of the MCM-41.

3.2.3. Metal oxide-supported Ag NPs.—Metal oxide supported NPs have gained full recognition among the scientific fraternity. The increasing interest has been attributed to their unique features including controlled size and shape, which make them excellent candidates for various industrial applications such as catalysis, adsorption, electronics, optics, or sensors. Apart from this, the surface of metal oxide NPs also offers additional benefits of surface modifications for various functional applications. Thus, the choice of a support material is crucial as it largely influences the properties of the resulting composite materials.[272–275]

Alumina (Al_2O_3) is a kind of support that has attracted the interest of academic as well as industrial researchers since diverse synthetic routes have been established for immobilizing Ag NPs onto this support.[276] For instance, Yamashita and co-workers employed a distinguishing pH-dependent approach for the controlled synthesis of Al_2O_3-supported Ag NPs.[277] 3-Mercaptopropionic acid was used as a surface protecting agent to produce Ag NPs as the thiol groups easily formed a strong metal-sulfur bond. Apart from this, zeta electric potential studies have been carried out for Ag NPs and an Al_2O_3 support. At high pH values, a negative electric potential surface of Ag NPs formed due to carboxylate anions (present in 3-mercaptopropionic acid), which were readily deposited onto the positively charged surface of the Al_2O_3 support *via* electrostatic interactions. Highly dispersed Ag NPs with an average diameter of 10 nm were formed onto the surface of Al_2O_3. In another report, Poreddy *et al.* employed an incipient wetness impregnation method for the preparation of Ag NPs supported on Al_2O_3 scaffolds where the support material was impregnated with the aqueous solution of precursor metal salt ($AgNO_3$); Ag NPs were homogeneously distributed onto the solid Al_2O_3, as affirmed by TEM images.[278] The Stamplekoskie research group exploited a successive ion layer adsorption and reaction (SILAR) to synthesize Ag NPs films onto Al_2O_3.[279] Al_2O_3 films were synthesized first by drying and annealing a reaction mixture containing α-terpinol, ethyl cellulose, benzyl alcohol, and Al_2O_3 at 80 °C and 500 °C, respectively. In the next step, films of alumina were alternately dipped into an aqueous solution of $AgNO_3$, followed by rinsing with water. Further treatment with a $NaBH_4$ solution was necessary to reduce the metallic Ag ions to Ag NPs. This yielded Al_2O_3 films decorated with Ag NPs.

Recent development in the field of supercapacitors has prompted researchers to explore manganese dioxide (MnO_2) as a unique support material. Three-dimensional (3-D) mesoporous MnO_2 having an ultra-high surface area was recently identified by Bai *et al.* as a superior support material for immobilizing Ag NPs.[280] The authors used an impregnation method to produce a Ag/MnO_2 composite material, in which Ag NPs were uniformly distributed on mesoporous MnO_2. Xie and co-workers designed a facile route to hierarchical one-dimensional Ag NP-decorated MnO_2 nanowires (Fig. 7b).[281] The overall hybrid composite material was synthesized by dipping a Ag foil into a solution containing $KMnO_4$ and H_2SO_4. An insight into the morphological picture was acquired through a

TEM analysis which revealed the monodispersity of the Ag NPs and their attachment onto the surface of MnO_2 nanowires. Strong interactions between the surface atoms of Ag NPs and the oxygen atoms of MnO_2 were found to be the driving force for fabricating these hierarchical heterostructures.

Copper oxide is another metal oxide that has been widely used as a support material for the decoration of NPs.[282] For example, Chen *et al.* designed a facile scheme to synthesize porous CuO microspheres decorated with Ag NPs.[283] In this synthesis, CuO microspheres were first synthesized *via* a hydrothermal approach by mixing copper nitrate in ethanol, followed by the addition of ammonium hydroxide and NaOH. Such synthesized microspheres were then dispersed in an aqueous solution of $AgNO_3$ and further stirred for 5 h. Next, a galvanic replacement reaction was used to decorate the Ag NPs onto the porous surface of the CuO microspheres.

Another interesting support material that has recently captured attention of the scientific community regarding the development of efficient photocatalysts is zinc oxide (ZnO)—a semiconductor with a band gap of 3.37 eV. Various synthetic approaches have been designed for constructing ZnO-supported Ag NPs.[284] Wang and co-workers reported the synthesis of ZnO micrometre rods decorated with Ag NPs for photocatalytic applications.[285] Herein, ZnO NPs were synthesized by a solvothermal-assisted heat treatment technique and the deposition of Ag NPs *via* the reduction of Ag ions was carried out by using a solar light photoreduction technique. On the other hand, a surfactant-assisted method has been reported for the construction of ZnO/Ag nanoflowers, wherein ZnO NPs were synthesized by a solution-based approach and in the next step, Ag NPs were further deposited on a ZnO nanoflower using hydrazine hydrate as the reducing agent.[286]

Similarly, various research groups have explored the possibility of using nanostructured ceria (CeO_2), zirconia (ZrO_2), and tungsten oxide (WO_3) as effectual catalyst supports for immobilizing the Ag NPs.[287–289] Titanium dioxide (titania or TiO_2) has emerged as a popular support material for NPs since it exhibits fundamental applicability in diverse areas including photocatalysis, solar energy conversion, and gas sensing.[290] Amongst several TiO_2 based supports, TiO_2 nanotubes have gained prominence due to their exceptional electronic and optical properties coupled with high surface area, chemical inertness, and physical and thermal stability. For instance, Liang *et al.* reported a facile reduction method for the preparation of a Ag/TiO_2 composite *via* a polyol process.[291] For this, TiO_2 nanotubes were added to a reaction mixture containing an aqueous $AgNO_3$ solution, $NaBH_4$, ethylene glycol, and PVP where $NaBH_4$ worked as the reductant, ethylene glycol served the dual role of a reductant and solvent, and PVP functioned as the surfactant that directed the growth of the resulting Ag NPs on the TiO_2 nanotubes. The reduction in the band gap for TiO_2 by dopants has been explored in conjunction with Ag NPs for photochemical enhancement in the visible light region;[292] both nitrogen and sulfur[293] were incorporated along with Ag NPs. In another report, He and co-workers reported the synthesis of three Ag-based catalysts *via* an impregnation technique employing TiO_2, γ-Al_2O_3, and CeO_2 as the support materials; which were subsequently investigated in the oxidation of formaldehyde.[294] Indeed, these support materials considerably altered the dispersion and particle size of the Ag NPs and therefore had a profound effect on the overall catalytic performance.

Over the past few decades, abundant iron oxides have also been gaining immense popularity as a recoverable and reusable support for developing metal NP-immobilized catalysts. The increase in the interest has been attributed to the presence of a magnetic core, which allows facile removal of the catalyst *via* an external magnet. This magnetic field-assisted separation is benign, economic, and expeditious, compared to the traditional centrifugation and filtration techniques, which frequently suffer from a catalyst loss and are not energy efficient.[295–297] It is worth mentioning here that Chiou *et al.* utilized a one-pot green method for the synthesis of Ag/iron-oxide nanocomposites, whereby arginine was successfully used as a reducing and capping agent.[298] Ferrous sulphate was used as the precursor salt of iron, which, along with $AgNO_3$ and arginine after stirring at 70 °C for 1 h, resulted in the formation of silver/iron oxide nanocomposite used in the reduction of 4-nitro phenol to 4-amino phenol.

3.2.4. Boron nitride supported Ag NPs.—Incredible advancements over the last few years have completely transformed the outlook on NPs and nanotechnology in general. Specifically, 2-dimensional hexagonal boron nitride (h-BN) nanosheets comprising sp^2 conjugated boron and nitrogen atoms have gained wide recognition as support materials for various catalytic and adsorption-based appliances. These BN nanosheets are thermally and chemically stable, resistant to oxidation, have extremely high surface area and good mechanical strength, and are electrical insulators with a band gap of 6 eV.[299–301] However, the synthesis of chemically exfoliated h-BN is quite challenging. In this perspective, Gao *et al.* have adopted a facile one-pot MW-mediated methodology for the synthesis of h-BN supported Ag NPs.[302] For the synthesis of the overall composite, the use of DMF was crucial as it not only served as a reducing agent, but also functioned as a solvent and a pre-requisite reagent for the dispersion of h-BN. Furthermore, the h-BN nanosheets, when dissolved in a solution containing DMF and $AgNO_3$, acted as a template for the consequent growth of Ag NPs. Besides, the MW-assisted technique, which is devoid of surfactants and stabilizing agents with localized heating at reaction sites, is very expeditious compared to conventional systems and plays a decisive role in determining the size of the resulting NPs; SEM images revealed that numerous Ag NPs were embedded in the edges of the sheets.[302] The results were accredited to the presence of sp^2 hybridized h-BN, which expedited the growth of Ag NPs *via* adsorption and electrostatic interactions. Pang *et al.* adopted a one-pot pyrolysis scheme for the fabrication of a Ag nanoparticle-BN hybrid composite material, where an *in situ* approach was employed to load tuneable amounts of Ag NPs onto the BN nanosheets.[303] Recent reports suggest that the hybrid composites of Ag NPs with BN nanosheets have been effectively employed as fillers in polymers to improve their thermal properties. This has been recently very well demonstrated when a simple liquid exfoliation strategy was adopted for the preparation of a Ag nanoparticle-BN nanosheet hybrid composite.[304] The use of advanced microscopic techniques such as HRTEM disclosed that the Ag NPs were uniformly decorated/incorporated on the surface of the BN nanosheets.[304] Apart from this, the synthesized nanocomposite was used as a filler in a poly (methyl methacrylate) (PMMA) matrix. Furthermore, the use of an elemental mapping technique validated the homogeneous dispersion and distribution of the filler inside the PMMA polymer matrix.

3.2.5. Polymer-supported Ag NPs.—Considerable effort devoted to the design and fabrication of advanced nano-functional materials has enabled the exploration of polymers as a key ingredient for developing supported catalysts. Polymers with excellent thermal and chemical stability, high surface area, and outstanding mechanical strength have generally proven beneficial as a support matrix for stabilizing Ag NPs.[305–307] Cao *et al.* fabricated a conjugated 2D microporous polymer (CMP) *via* a condensation reaction between aminoacrylonitrile and phthalaldehyde, which generated exposed cyano and pyridyl groups as potentially interacting sites for Ag^+ ions (Fig. 8a).[308] Thus, the loading of Ag ions onto the CMP support material was achieved through a liquid impregnation method. Light induced reduction of Ag ions produced spherical Ag NPs having a mean diameter of 3.9 nm, as shown by SEM and TEM analysis. Yu *et al.* delineated the construction of N-heterocyclic carbene (NHC) polymer-supported Ag NPs of 3–5 nm in size for the carboxylation of terminal alkynes with carbon dioxide, while Eisa *et al.* synthesized spherical Ag NPs of 15 nm in size supported on a PVA (polyvinyl alcohol)/PVP (polyvinyl pyrrolidone) nanocomposite film by a facile casting approach utilizing $NaBH_4$ as a reducing agent which was further applied in the degradation of 4-nitrophenol.[309,310] Varma and co-workers utilized a unique approach in which chitosan-poly(3-hydroxybutyrate) polymer (Chit-PHB) was employed as a capping and reducing agent for Ag NPs.[311] Chit-PHB was initially synthesized by simply mixing chitosan and PHB in acidified water under constant stirring overnight at 80 °C. The final nAg-Chit-PHB composite was prepared by dropwise addition of aqueous $AgNO_3$ to Chit-PHB under dynamic stirring conditions at 90 °C.

3.2.6. Zeolite-supported Ag NPs.—Zeolites were first discovered by the Swedish mineralogist Cronstedt in 1756. They are a class of porous scaffolds that have been extensively employed as supports for immobilizing metallic Ag NPs.[312] Many of them have a crystalline cage-like framework of aluminosilicates containing SiO_4 and AlO_4 tetrahedra units. One of the most untypical features of zeolites is that they simply enable the exchange of Ag ions with the native cations of zeolites, which can be further reduced by successive addition of reducing agents.[313–315] Mintova and co-workers reported a simple protocol using an ion exchange method followed by a photochemical reduction approach for the synthesis of Faujasite (FAU) type zeolite-supported Ag NPs.[316] Once a Ag^+ ion-exchanged FAU zeolite was synthesized, it was further irradiated with a Xe–Hg lamp in the presence of 2-hydroxy-2-methylpropiophenone, which acted as a photoactive reducing agent. Special features of the protocol included a fast reduction rate and short irradiation time. A similar protocol has been demonstrated by Liu *et al.* in which mineral chabazite (MC)—an aluminium silicate zeolite obtained from the deposit in Arizona—was used as the support to immobilize Ag NPs. Specifically, the mineral chabazite with the level of 50–100 mesh was being dispersed in a solution containing $AgNO_3$ under constant stirring at 80 °C for 16 h; it was then filtered, washed, and dried.[317] The product was heated at 110 °C under 40 mL/min flow of argon followed by calcination at 400 °C for 1 h, in the presence of argon. Thermal induced reduction of Ag NPs proceeded in several steps involving the reduction of Ag ions first to a Ag cluster and then to metallic Ag NPs, which were then ultimately grown on the external surfaces of chabazite.

3.2.7. MOF-supported Ag NPs.—Rapid progress has been made over the past three decades on the design and formulation of porous 3-dimensional crystalline polymers-metal organic frameworks (MOFs), which comprise metal clusters linked by organic linkers through strong coordination bonds.[318–320] MOFs exhibit many unique features such as high porosity, crystallinity, or ultra-high surface area, making them excellent candidates for various functional applications such as catalysis, sensing, drug delivery, adsorption, and degradation. Besides, the structure and coordination modes of MOFs can be tuned and tailored for specific purposes. Inspired by their unique features, various groups have explored the use of MOFs as a support material for the immobilization of metal NPs.[321] For instance, Natarajan and co-workers reported the synthesis of an amine functionalized porphyrin-based MOF $[Zn_3(C_{40}H_{24}N_8)(C_{20}H_8N_2O_4)_2(DEF)_2](DEF)_3$ encapsulated with Ag NPs.[322] A one-pot solvothermal approach was employed for the synthesis of the desired MOF by taking Zn^{2+} salt and 5,10,15,20-tetrakis(4-pyridyl)porphyrin along with 1,2-diamino-3,6-bis(4-carboxyphenyl)benzene as the organic ligands. The presence of free amine groups in the structure of the MOF served as the anchoring point for the immobilization of Ag ions, which were reduced *in situ* by $NaBH_4$ to Ag NPs having an average diameter of 3.83 nm. Another report by Yang and co-workers clearly illustrated the fabrication of a Ag@MIL-100(Fe) composite for CO_2 capture and conversion *via* a facile liquid impregnation technique, whereby the synthesized MIL-100(Fe) was being dispersed into acetonitrile and $AgNO_3$ under continuous stirring at room temperature for 12 h and reduced by $NaBH_4$ to generate the desired Ag@MIL-100(Fe) composite.[323] Similarly, Chang *et al.* also proposed an effective strategy for embedding Ag NPs within the pores of Fe_3O_4@MIL-100(Fe) (Fig. 8b).[324] During the first step, carboxyl-modified Fe_3O_4 NPs were prepared, and, subsequently, a layer-by-layer approach was adopted, leading to the formation of a MIL-100(Fe) around the Fe_3O_4 core. In the final step, uniform Ag NPs of 20 nm size were first successfully synthesized *via* a radiation-mediated reduction technique and finally homogeneously dispersed and embedded in the MOF shell.

3.2.8. Cellulose-supported Ag NPs.—Naturally occurring renewable and abundant biopolymers such as cellulose have gained significant prominence as a lucrative and biodegradable support matrix for anchoring metal NPs. Additionally, copious hydroxyl and ether functionalities present in the macromolecular chains of cellulose make it structurally suitable as a promising support matrix and stabilizer for the resulting NPs. In this context, Eisa *et al.* utilized a facile greener solvent free strategy for cellulose nanocrystal (CNC)-supported Ag NPs.[325] The exploitation of advanced microscopic tools revealed that hexagonal shaped Ag NPs of 6–35 nm in size were formed on the surface of CNC. Apart from this, an FTIR analysis revealed that strong hydrogen bonds developed between the hydroxyl groups of CNC, and the metal ions initiated the anchoring process. Further, experimental observations revealed that the addition of ascorbic acid reduced Ag ions to Ag NPs. Das and co-workers explored the possibility of using a stem extract of *Hibiscus sabdariffa* to produce cellulose polymer, which acted as a support material and stabilizing agent for the production of Ag NPs having an average size of 4 nm.[326] On a similar basis, Heidari *et al.* utilized ultrasonic irradiations for transforming microcrystalline cellulose into rod-shaped nanocrystalline cellulose with an average diameter and length ranging from 30 to 50 nm and 500 to 700 nm, respectively.[327] The resulting nanocrystalline cellulose was

successfully exploited as a favourable support, in addition to being a reducing and capping agent for the preparation of Ag NPs. TEM analysis revealed that spherical Ag NPs of 20 nm size were homogeneously distributed on the surface of nanocrystalline cellulose.

3.3. Mixed Ag NPs (bimetallic alloys, core–shell and Janus NPs)

The ability to control and manipulate matter at the nanoscale has opened up new and exciting opportunities for the construction of unique and specific architectures. In particular, the synthesis of nanocomposites including alloys and bimetallics has captured incredible attention. These multimetallic composite materials including bimetallic alloys, core–shell, and Janus NPs exhibit superior thermal, electrical, optical, and catalytic properties, compared to their monometallic counterparts.[328,329] Various synthetic methodologies including MW, sonochemical, wet-chemical reduction, and greener protocols have been described for diverse Ag-based nanocomposites.[153] Table S3 (ESI†) summarizes all the recently synthesized nanocomposites of Ag along with the primarily involved reaction conditions.

Bimetallic NPs are a unique class of materials, which has aroused interest across the different fields of science and technology during the past few decades. Thanks to the strong synergism that exists between the two metals and their excellent redox chemistry, promising results have been yielded in the area of catalysis, particularly in terms of their superior activity and selectivity. These bimetallic composites can be further segregated into three types: bimetallic alloys, bimetallic core–shell composites, and Janus NPs.[330–333] An example of bimetallic alloy was reported by Sharma *et al.*[334] They synthesized multipode Au/Ag bimetallic multispiked NPs with high monodispersity using a co-reduction method in which PVP served as the stabilizer and ascorbic acid as the reducing agent. During the material fabrication process, PVP was added to an aqueous $AgNO_3$ solution while stirring at room temperature followed by the addition of ammonia, which prevented the precipitation of silver chloride. Next, a $AuCl_3$ solution along with KI was added under constant stirring, followed by the successive addition of ascorbic acid. This protocol resulted in the production of stable Au/Ag bimetallic nanocomposites for enhanced photovoltaic applications. Similarly, the synthesis of Ag/Ni binary NPs showing a core–shell and snowman morphology was illustrated by Kim *et al.*, starting with a reduction of Ag NPs and following with the subsequent reduction and growth of Ni NPs on the surface of Ag.[335]

With the progress in benign and sustainable technologies, there has been a paradigm shift towards developing facile and greener protocols. In this context, Li and co-workers exemplified an economic route to synthesizing Au/Ag bimetallic NPs, in which degraded pueraria starch (DPS) was utilized as the reducing and stabilizing agent (Fig. 9a).[336] To obtain the desired results, the authors utilized a replacement reaction to substitute gold ions with Ag NP seeds. Successive addition of DPS in the above-mentioned mixture resulted in the formation of DPS-coated metallic NPs. Similarly, Abdel-Mottaleb reported a facile approach for Au, Ag, and Au–Ag bimetallic NPs from an aqueous extract of sago pondweed (*Potamogeton pectinatus L.*).[337] In addition to hexagonal and triangular shapes, the adopted method led to the production of spherical shaped NPs.

Roy and co-workers developed a one-pot strategy for the fabrication of Cu/Ag alloy NPs using glucose as an eco-friendly reducing agent and hexadecylamine (HDA) as a stabilizing and capping agent (Fig. 9b).[338] Alloyed bimetallic NPs were obtained using a one-pot reduction method where $AgNO_3$ and $CuCl_2$ were chosen as the Ag and Cu precursors, respectively. Mechanistically, a ring opening process for glucose led to the formation of aldehyde, which reduced Ag^+ to $Ag(0)$, while the reaction of Cu^{2+} with glucose led to the formation of Cu NPs and, consequently, owing to a galvanic replacement reaction ($Cu + 2Ag^+ = Cu^{2+} + 2Ag$), bimetallic NPs were created.

Zhang *et al.* adopted a radiolytic scheme in which γ radiations were used for the concomitant reduction of Ag^+ and Ni^{2+} ions to form Ag–Ni bimetallic alloy NPs, while Kleinermanns and co-workers employed a laser-assisted approach for the synthesis of Au–Ag bimetallic nanoalloys.[339,340]

Core–shell bimetallic NMs are another class of materials that have gained recognition from the scientific and technological point of view. Here, the metal that acts as the core forms the basis of many functional applications, while the metal that acts as the shell influences the surface properties of the resulting hybrid nanocomposite.[341–343] A representative example of bimetallic core–shell NPs has been demonstrated by Samal *et al.* when the authors prepared size-controlled as well as citrate capped Au@Ag NPs.[344] Furthermore, the authors showed that a stepwise reduction of Ag^+ ions on the presynthesized citrate-capped Au NPs could be efficiently achieved by the gradual addition of $AgNO_3$ in the presence of ascorbic acid. The pH of the solution plays a pivotal role as it largely affects the reducing power of ascorbic acid; it was found that a pH value of 8.5 was necessary for the controlled reduction of Ag^+ ions to generate bimetallic core–shell Au@Ag NPs. A sonochemical assisted co-reduction approach was used for the preparation of Au-Ag core–shell NPs, while in another protocol, a MW-polyol method was used for Au@Ag core–shell nanocrystals where ethylene glycol acted as a reducing agent and PVP as a surfactant or surface protecting agent.[345,346] Nazir *et al.* designed a galvanic exchange method to synthesize AgPt, AgPd, and AgAu bimetallic NPs supported on a graphitic carbon nitride (C_3N_4) surface (Fig. 9c). Initially, bare Ag NPs were decorated on C_3N_4 using $NaBH_4$.[347] The lower reduction potential of Ag^+, in comparison with Pt^{2+}, Pd^{2+}, and Au^{3+}, favoured a facile galvanic exchange of Ag to generate C_3N_4 supported AgPt, AgPd, and AgAu bimetallic nanocomposite materials. Similarly, Zhu *et al.* reported the synthesis of C_3N_4 nanotube-supported Ag–Cu bimetallic NPs, whereby bare C_3N_4 was fabricated *via* a modified water-induced morphological method.[348] Successive addition of $AgNO_3$ and $CuNO_3$, followed by a chemical reduction using $NaBH_4$, led to the formation of the desired photocatalyst for effective hydrogen production.

Mori *et al.* developed a scheme for a carbon supported uniform-sized bimetallic alloy of Pd–Ag NPs, in which bimetallic NPs were initially synthesized through a polyol method employing ethylene glycol as a reducing agent.[349] Later on, an impregnation technique has been used for loading the synthesized NPs onto the carbon support. Another report by Yang and co-workers described the fabrication of graphene paper-supported bimetallic Cu/Ag dendrites *via* an electrodeposition technique.[350] On similar grounds, Kuang and co-workers described the synthesis of r-GO supported Pd-Ag bimetallic NPs *via* a wet-

chemical route.[351] Greener strategies have also been explored using plant-based extraction for generating core–shell entities.[352]

As a significant category of mixed NPs, Janus NPs have also transformed the outlook on catalysis, in addition to influencing other interfacial biomedical applications. Similar to heterodimers, these NPs simultaneously show the presence of two different regions having rich diverse surface chemistry, which allows the integration of widely diverse chemical or physical properties in a single entity.[353] As a result of these superior attributes, 'Janus' has found wider applicability based on its molecular asymmetry, which can be profitably employed for designing assorted systems with different architectures, shapes (ranging from spherical to dumbbell to vesicles/capsules to cylinders or disk), and dispositions of the separate entities inside the particle.[354] Incorporating the amalgamation of galvanic exchange and Langmuir methodology, Song *et al.* accomplished the synthesis of bimetallic AgAu Janus NPs which were utilized as a electrocatalyst for an oxygen reduction in an alkaline medium.[355] For fabricating Janus NPs, hexanethiolate-passivated silver (AgC6) NPs were employed as the starting precursor (Fig. 9d). Following the Langmuir–Blodgett method, a single layer of the AgC6 NPs was deposited on the surface of a glass slide, which was subsequently immersed into a gold solution containing gold(I)-mercapto-propanediol (AuI-MPD) complex. As a result of the galvanic exchange process between the AgC6 NPs and the Au^I-MPD, some of the Ag atoms were displaced on the NPs' cores with Au and, simultaneously, the original hydrophobic hexanethiolates were replaced with the hydrophilic MPD ligands. In comparison with the bulk counterpart, which exhibited homogeneous distribution of the capping ligands within the NPs, the core and the surface displayed an asymmetrical distribution, as evidenced by contact angle measurements, UV-vis, XPS, and TEM.

On a similar basis, but exploiting a chemical etching methodology at the air/water interface, Chen and his research team also fabricated gold core@silver semishell Janus NPs.[356] The NPs were synthesized *via* the chemical deposition of the Ag shell onto the Au seed colloids, which was followed by the self-assembly of 1-dodecanethiol onto the NP surface. Using a one-pot controllable thermal decomposition method, Jiang *et al.* produced eggplant shaped Ag–Ag_2S Janus particles that exhibited high photocatalytic efficiency.[357] Morphological analyses revealed that the Janus particles, of an eggplant shape (15–25 nm), can be coupled with commercial P25 Degussa. Dutta *et al.* also synthesized Ag–Ag_2S Janus NPs (JNP) but adopted a one-step co-precipitation technique and immobilized the JNPs onto an eco-friendly cellulose support, which functioned as a template for promoting the growth of the NPs.[358] A locally available bamboo species named as '*Bambusa tulda*' was used for the extraction of cellulose *via* the right interplay of chemical and biochemical treatment.

Researchers have been channelling their creativity and energy into utilizing polymeric shells for the creation of novel hybrid Janus catalysts since polymers show high contrast in hydrophobicity on the opposite sides of the Janus NPs, which intensifies their affinity towards diverse phases in an emulsion, enabling greater stability. Inspired by these attributes, Synytska and co-workers designed an advanced hairy Janus catalyst consisting of silica as the core material and two polymeric shells—hydrophobic and hydrophilic.[359] The hydrophilic end consisted of large Janus particles with polyacrylic acid, which

showed catalytically active Ag species immobilized on it, while the hydrophobic end comprised polystyrene. An integrated Pickering emulsion and 'grafting from/grafting to' was incorporated for the synthesis of polymeric-encapsulated Janus NP approaches. The combination of TEM and cryo-TEM techniques divulged the selective localization of the incorporated Ag NPs on the polyacrylic end of the Janus particles.

3.4. AgO and Ag_2O NPs

Silver oxide NPs (both AgO as well as Ag_2O) are a rapidly evolving class of silver nanostructures, which has found commercial applicability in a large number of fields including catalysis, sensors, photovoltaic cells, fuel cells, *etc.*[360] Table S4 in the ESI† collates the recent representative examples for the synthesis of AgO and Ag_2O NPs.

Nasab *et al.* described a facile precipitation technique for synthesizing AgO nanostructures using $AgNO_3$ as the precursor.[361] For this, an equimolar concentration of $AgNO_3$ and surfactants were mixed under constant stirring at 50 °C, followed by the addition of $K_2S_2O_8$ and KOH. The obtained powder was thoroughly washed with water and ethanol, dried to generate nanocrystalline AgO, and used as a photocatalyst in the degradation of rhodamine-B. Besides this, the effect of various stabilizing agents or surfactants such as glucose, CTAB, sodium dodecyl benzene sulfonate, and sodium dodecyl sulfate has been studied in the synthetic processes. Akbari *et al.* reported a simple method for the fabrication of AgO–TiO_2 nanocomposites where TiO_2 NPs were synthesized separately using tetra-*n*-butyl titanate and were incrementally added under continuous stirring at 50 °C for 1 h to a reaction mixture containing $K_2S_2O_8$, NaOH, and an equimolar concentration of $AgNO_3$ and TiO_2.[362]

Owing to their unique catalytic, optoelectronic, pyroelectronic, and piezoelectric properties, Ag_2O NPs have caught widespread interest among the research community. Vinay *et al.* designed a unique protocol in which a cantaloupe (*Cucumis melo*) seed extract acted as a reducing agent for the eco-friendly synthesis of spherical Ag_2O NPs having a diameter of 20 nm.[363] The fabrication was carried out in a muffle furnace operating at 500 °C wherein a combustion phenomenon led to the production of nanocrystalline Ag_2O NPs. Similarly, Rashmi *et al.* adopted a greener combustion-based methodology in which *Centella Asiatica* and *Tridax* plant powders were utilized for synthesizing Ag_2O NPs.[364] Another study uncovered the preparation of a p–n junction type Ag_2O/TiO_2 nanocomposite using a hydrothermal approach accompanied by a UV light-assisted photochemical reduction strategy.[365] Microscopic analyses revealed the uniform deposition of Ag_2O NPs on the nanorod surface of 3D TiO_2 microspheres, thereby yielding multitudinous p–n heterojunctions. Similarly, successful fabrication of cubic Ag_2O incorporated within mesoporous silica and Ag_2O anchored onto $Mg(OH)_2$ nanoplates have been described.[366,367] Li *et al.* demonstrated an out-of-the-box approach in which a photochemical technique was employed for growing Ag–Ag_2O nanoplates on the ZnO substrate.[368] For this, smaller Ag–Ag_2O nanoplates of varied morphologies were initially synthesized and structurally converted into larger and smoother plates through a photoinduction mechanism and a layer-by-layer crystallization phenomenon.

4. Application in catalysis

Catalysis is a primary technology for the green chemistry approach due to the increasing focus on the development of sustainable manufacturing processes.[369] Currently, the main challenge faced by researchers is to develop a catalyst that will combine the benefits of high activity, selectivity, and recyclability. Nanotechnology offers a unique route to achieving these goals as it enables a rational synthesis of such types of catalysts.[370,371] As a result of the nanosized dimensions, there is a drastic increase in the surface area to volume ratio, which results in enhancing the catalytic activity.

Over the last decade, the synthesis and application of Ag NPs (often termed as the magical NPs) have attracted incredible attention, which results from their potential to offer the ideal green catalysts, along with the integrated benefits of activity, selectivity, stability, and recovery within a single platform.[31] Moreover, they ensure economic viability owing to their low cost; for example, the price is reduced by 1/50 compared to gold (Au) or platinum (Pt) and about 1/25 compared to palladium (Pd). Recently, nanosilver catalysts have also proven to be very promising in total synthesis of natural products and pharmaceutical molecules because of their powerful analgesic and antipyretic activities.[78]

In this review, we will highlight some of the promising activities of nanosilver-based catalysts in industrially significant organic transformations such as coupling, oxidation, reduction, multicomponent, condensation, CO_2 capturing, *etc.* Also, a special emphasis will be placed on the application of advanced heterogeneous catalytic systems whereby silver NPs are supported/immobilized on different solid matrices and such surface engineered catalysts are employed for expediting numerous reactions. The anchoring of such active catalytic species on a support prevents the product stream from getting contaminated with the catalyst residues.

4.1. Liquid phase catalysis

4.1.1. Coupling reactions.—The breakthrough discovery of cross coupling reactions that enable the formation of new C–C and C–heteroatom bonds has completely transformed the landscape of preparative organic chemistry.[372,373] However, the use of traditional homogeneous metal catalysts for coupling reactions hampers their large-scale industrial utility and therefore creates a need for developing competent catalytic systems. Ag-based nanocatalysts have overcome the challenges associated with conventional catalytic protocols. The following sections will shed light on the different cross-coupling reactions achieved with the help of silver nanocatalysts. The reasons behind the wide-scale utility of silver in the design of catalysts based on nanosupports will be thus elucidated.

4.1.1.1.   Suzuki Miyaura coupling reactions (SMCRs).: Over the past 40 years of their rich history, Suzuki Miyaura coupling reactions (SMCRs) have provided a practical route to direct C–C bond formation *via* the reaction between aryl halides and organic boron compounds.[374] Over the last decade, they have gained wide recognition, thanks to their efficiency. In addition to total synthesis and pharmaceuticals, these reactions have been profitably used for the large-scale production of polymers and fine chemicals. With the increasing emphasis on environmental sustainability, several Ag-based monometallic

and bimetallic nanocomposites have been reported for catalyzing the Suzuki–Miyaura reaction. Radhakrishnan and co-workers demonstrated that the combination of Ag and Pd can efficiently catalyse the Suzuki–Miyaura reaction of iodobenzene with phenylboronic acid.[375] Recently, Gorji *et al*. designed a novel and reusable catalyst comprising Ag NPs (BF@Propyl/DETA/Ag) stabilized on the thermally and chemically resistant basalt fibres for expediting the Suzuki Miyaura reaction.[376] The catalyst was prepared by the reaction of basalt fibres with (3-chloropropyl) triethoxysilane, followed by the addition of diethylenetriamine (DETA) and consequently by metalation using $AgNO_3$. Using this catalyst, aryl halides possessing either electron donating or electron-withdrawing groups reacted satisfactorily with the phenylboronic acid, generating the desired biaryl products with excellent yields (Fig. 10). Mechanistically, the protocol involved oxidative addition, transmetallation, and reductive elimination steps. The catalyst was reused six times, showing no appreciable loss in its activity.

4.1.1.2.   Sonogashira coupling reactions (SCRs).: Discovered by Sonogashira, Tohda, and Hagihara in 1975, the palladium catalysed sp^2–sp coupling reaction between aryl halides or alkenyl halides and terminal alkynes using copper as the co-catalyst, which is commonly known as the Sonogashira coupling reaction, has drawn considerable attention of chemists in the field of organic synthesis.[377] It leads to the synthesis of aryl alkynes and conjugated enynes, which are active components of natural products, pharmaceuticals, and organic materials. Since the pioneering report on SCRs, remarkable progress has been made on the enhancement of their overall utility.[378] For instance, copper-free Sonogashira reactions have been reported.[379] Also, replacement of Pd has been explored as it is expensive, sensitive to air and moisture, can get easily poisoned, and requires the incorporation of organic ligands such as triphenyl phosphines, which not only adds to the pollution but also involves intensive product purification steps. Gao and team developed ultrafine Ag–Pd bimetallic NPs decorated on the surface of reduced graphene oxide (rGO) nanosheets and employed them for the SCR.[380] The experimental observations revealed interesting facts; for instance, this catalytic protocol yielded two different products in the presence or absence of oxygen, meaning that oxygen could be utilized as a switch to control the product formation.

Furthermore, in view of maximizing the 'atom economy', the synthesis of core–shell NPs comprising a cheap metal core and a noble shell material is gaining significance. As evident from the published reports, a couple of palladium-containing bi- and trimetallic NPs including core/shell structures were synthesized in a way that Pd occupied the core and the other metal species, such as Au or Ag, covered the surface of Pd.[381] Venkatesan *et al*.have designed a Au/Ag/Pd trimetallic-based nanocatalyst containing Au-Ag in the core and Pd as the shell material, employing a chemical method whereby cetyltrimethylammonium bromide (CTAB) was used as the capping agent and applied for the Sonogashira coupling reaction (Fig. 11a).[382] In comparison with monometallic and bimetallic Pd catalysts, trimetallic NPs exhibited superior activity, which could be attributed to the concerted electronic effects of the Au–Ag core in the Pd shell atoms.

4.1.1.3.   Heck coupling reactions (HCRs).: Heck reactions that involve the cross-coupling between alkenes and aryl/vinyl halides/triflates hold a special place in the list of most

efficient coupling reactions, also taking on immense industrial significance.[383] Thanks to the remarkable versatility and potential, Heck chemistry has been able to find novel applications. Thus, it is not surprising that extensive coverage has been given to Heck reactions in the form of reviews that highlight the various aspects of this unique reaction.

Trimetallic NPs comprising three different metal NPs, as discussed in the previous section, have been explored to improve the yield and selectivity of these types of reactions. A series of colloidal dispersions of trimetallic Au–Ag–Pd nanocatalysts were prepared using a surfactant-mediated chemical method and were applied for the HCR (Fig. 11b).[384] The developed trimetallic Au–Ag–Pd NPs were used in the catalysis of HCRs, and they showed enhanced performance in comparison with the monometallic and bimetallic counterparts. In this report, the authors have highlighted that such a metal NP-mediated catalytic protocol eliminates the need for toxic bases, which are often used in this reaction.

4.1.2. Oxidation reactions.—Oxidation reactions lie at the heart of industrial chemical synthesis, contributing to almost 30% of the total production. The enormous significance of these reactions arises from the fact that the products derived from the oxidative processes such as alcohols, epoxides, aldehydes, ketones, and organic acids are utilized as key intermediates and are further deployed for manufacturing a large number of value-added agrochemicals and pharmaceuticals.[385]

However, from the viewpoint of benign and sustainable chemistry, selective oxidation still remains a challenge. A number of factors such as the type of support matrix, concentration of active surface functional groups, distribution of the active component along the support surface, presence of impurities, thermal conductivity and stability, or physical-mechanical properties need to be effectively considered while trying to develop a new generation of highly effective catalysts for different oxidative processes.

In order to achieve selective oxidation of alcohols, a variety of heterogeneous metal catalysts including supported copper (Cu), Au, Pt, and ruthenium (Ru) NPs in the presence of green oxidants (ambient air/oxygen) have been explored so far as sustainable technologies.[386] However, the catalytic activity of Ag-based alloys or nanosilver-based catalytic systems is found to be highly impressive, which may be attributed to the increased affinity of oxygen towards silver.

4.1.2.1. Alcohol (methanol and ethanol) oxidation.: Gas phase oxidation of methanol has been recognized as one of the key oxidative industrial processes that leads to the production of formaldehyde and can be further efficiently catalysed by polycrystalline or supported Ag under alcohol rich conditions.[387,388] However, the selectivity % was found to be higher in the case of the polycrystalline Ag in comparison with the supported one. Also, the activity was compared with Fe-Mo based oxide catalysts and, as expected, the Ag catalyst was much more productive. In an attempt to develop novel catalytic systems that would incorporate a support not traditionally used in the process of selectively oxidizing methanol to formaldehyde, Aouat *et al.* succeeded in designing a hybrid catalyst by which thermally activated Congo red (CR) NPs were entrapped within Ag deposited on titania nanofibers (TiO$_2$ NFs).[389] Owing to the structural and morphological benefits of TiO$_2$, the

developed catalyst showed unprecedented activity in boosting this reaction, compared to the unsupported CR@Ag powder and supported undoped Ag/TiO$_2$-NF catalysts. Besides, the organic dopant molecules played an indispensable role in serving as a barrier for the sintering of Ag and in preventing the formation of large aggregate clusters, which could be the primary reason for the higher specific surface and porous morphology of the nanocomposites. Carbon has also proven to be a support material of choice for the immobilization of Ag, as evident from the work carried out by Grader and co-workers, who developed Ag/C fibres *via* an electrospinning technology and utilized the composite material in the selective oxidation of methanol to formaldehyde.[390] In order to demonstrate the significance of the support, the reaction was also carried out in the presence of unsupported uniform Ag fibre mats, and from the results, it was inferred that the supported analogue was far more efficient in boosting the oxidative transformation. The report revealed that carbon, near the Ag grains, participated in this catalytic process through an 'adsorb and shuttle' of the 'spillover' mechanism.

In pursuit of getting promising results, Sobczak *et al.* took advantage of the synergistic benefits of using two different metals (Au and Ag) and reported a bimetallic catalyst comprising Au–Ag bimetallic NPs supported on mesostructured cellular foams (MCF) and NbMCF.[391] Interestingly, it should be noted that the Au–Ag alloy was found to be growing on the surface of the AuAg–MCF and the AuAg–NbMCF. The combination of the extraordinary features of each of these metals in the alloy was responsible for the high activity of the catalysts. It is worth mentioning that the presence of Nb species on the MCF support had a positive influence on both the catalytic activity and selectivity towards formaldehyde.[391] Recently, a research group highlighted the significance of a well-defined structural hierarchy in the process under consideration. They synthesized bimetallic Ag–Au NPs with controlled size and composition which were then embedded within a porous silica matrix (SiO$_2$–Ag$_x$Au$_y$).[392] This methodology helped to gain control over the particle composition, morphology, distribution, *etc.*, which was beneficial for obtaining promising results for the ester production from selective oxidation of methanol and ethanol.

Regardless of the efforts directed towards selective methanol oxidation, a number of impediments still remain to be tackled. For instance, without the addition of a second metal, a satisfactory reduction in the process temperature for the Ag catalysts would not be achieved. Weak adsorption of methanol over the surface of Ag and extreme difficulty with the cleavage of the C–H bond in the methanol molecule, compared to other alcohols, could be the complicating factors. Moreover, deactivation of the catalyst as a result of sintering and the loss of active species hinders the large-scale utility of some of these processes.

Recently, the research community is showing a growing interest in ethanol conversion as it provides an economic gateway to the synthesis of crucial organic moieties including acetaldehyde, butadiene, acetone, *etc.*[393,394] Over the past few years, various nanocatalysts such as Ag and Au supported on ceria,[395,396] Au–Ir catalysts,[397] vanadium oxides,[398] *etc.* have been documented in the literature for ethanol oxidation as potent catalytic materials. On the grounds of achieving selective oxidation of ethanol, a study focussing on the critical comparison of Group 11 transition metals—Ag, Cu, and Au—supported on Li$_2$O/γ-Al$_2$O$_3$ was reported by a research team.[399] Notably, when Ag–Li$_2$O/γ-Al$_2$O$_3$ was used as the

catalyst a complete conversion of ethanol occurred at 350 °C with high selectivity towards acetaldehyde up to 100% at 100–300 °C, while the use of only support material (γ-Al_2O_3) led to the dehydration of ethanol into diethyl ether. In contrast to the results obtained by Lippits *et al.*, who detected ethylene oxide formation in ethanol oxidation in the presence of Au and Ag-supported Al_2O_3 catalysts doped with CeO_x and Li_2O, no ethylene oxide was formed in this catalytic protocol.[400]

4.1.2.2.   Alkene oxidation.: Olefins stand out as one of the most important synthetic organic intermediates because of their easy availability and ability to undergo a wide range of transformations into functional compounds, such as epoxides and other oxygen containing products.[78] Purcar *et al.* have developed a novel nanosilver catalyst containing different amounts of Ag NPs (0.5, 1 and 2.5 wt%) supported on hybrid films comprising methyltrimethoxysilane (Ag-MeTMS), which was eventually employed for the oxidative transformation of styrene.[401] The use of 1% Ag-MeTMS yielded the desired styrene oxide product with excellent selectivity (>99%) and promising conversion (60%) at 96 °C under microwave irradiation (Fig. 12a).

Lately, a research study by Chen and Luck, offered new insights into the technique of oxygen activation that allows the transfer of an oxygen atom from the atmosphere onto an olefin, presumably *via* the formation of a peroxide radical.[271] In this work, Ag NPs were grown on the surface and within the channels of mesoporous silica 'MCM-41' by mixing $AgNO_3$ and PVP in a 1 : 20 ratio with MCM-41 using ethylene glycol as the solvent for about 1 h. The developed material successfully catalysed the oxidation of a variety of olefins including (*Z*)-cyclooctene, cyclohexene, styrene, and indene. It is noteworthy that the catalyst was recycled for at least five sequential cycles without any appreciable loss in its activity. A radical mechanism was proposed for this reaction (Fig. 12b). Interestingly, it was found that right after the first cycle, H_2O_2 worked as the radical initiator instead of TBHP as the Ag NPs were passivated due to the formation of AgCl on the surface. Cheng and co-workers demonstrated that the dual promoter *i.e.* synergism of Cu + Re, Cs + Re, and Cs + Cu and Ag(111) and (110) surfaces enhanced the adsorption strength of oxygen and oxametallacycle intermediates in ethylene epoxidation on the basis of computational study.[402] Very recently, Tian *et al.* reported a single Ag site catalyst supported on mesoporous graphitic carbon nitride (Ag_1/mpg-C_3N_4) for the epoxidation of styrene;[403] Ag_1–C_2N_1 structures in Ag_1/mpg-C_3N_4 exhibited higher catalytic efficiency for styrene epoxidation with 96% conversion and 81% selectivity.

In addition to the above-mentioned strategies, oxidation/epoxidation reactions are well reported on Ag-based nanocatalysts, for example a Ag-LDH catalyst, a Ag NP cage, and water-compatible Ag/Au NPs, which have shown high catalytic activity and selectivity.[404–406]

4.1.2.3.   Oxidative processes involving conversion of silanes.: Silanes have long been recognized as vital building blocks for the generation of organosilane-based polymeric materials and valuable synthons for a variety of organic reactions.[407] To date, several methodologies have been reported for providing rapid access to silanols; however, from the viewpoint of green and sustainable chemistry, the development of environmentally

benign protocols continues to attract the synthetic pursuit of industrial as well as academic researchers. Within this perspective, an efficient strategy for the green synthesis of silanols from hydrosilane precursors was elucidated by Kaneda *et al.* in 2008.[408] In this work, Ag NPs were firstly supported on a hydroxyapatite (HAP) support, and the developed catalyst was used for the selective oxidation of hydrosilanes. Interestingly, water was used as a green oxidant in this case, thus eliminating the need for any other solvents (Fig. 13).

Notably, the catalyst could be readily recovered from the reaction media simply *via* filtration, and could be reused continually for four runs showing consistent activity. On a similar basis, several other research groups have fabricated Ag-based NMs and investigated their activity in the oxidation of hydrosilanes.[409] They found that an efficient conversion of both aromatic and aliphatic silanes could be achieved by using water or alcohol as oxidants.

Furthermore, in an attempt to accomplish the polymerization of an alkylsilane for the production of silanol/siloxane composite microspheres, Li and Wang synthesized an active catalyst comprising halloysite nanotube supported Ag NPs.[410]

4.1.3. Reduction reactions.—Various synthetic industrial processes rely on the reduction of materials to oxidation states lower than those occurring in nature primarily for two reasons: (i) the chemical products obtained as a result of the reductive transformations have interesting pharmacological utility, apart from serving as precursors and intermediates in total organic synthesis. (ii) When not employed as structural materials, these products create an excellent opportunity for being reoxidized for different commercial applications.[411,412] The commonly employed catalytic strategies for reduction/hydrogenation include (i) direct reduction with a pressure of hydrogen (H_2) gas;[413] and (ii) transfer hydrogenation (TH), which involves the addition of hydrogen to a molecule from a non-H_2 source.[414] In this context, it is worth mentioning that Ag NPs or bimetallic Ag-based NPs have drawn special attention from chemists working in this area of reduction of various nitroaromatics, carbonyls, and reductive amination or its related transformations.[338,415–420]

The catalytic reduction of nitroarenes has recently gained prominence as a key reaction owing to its utility in remediation applications, eradicating toxic and carcinogenic nitro compounds from environmental matrices, as well as in the efficient production of corresponding amino aromatics.[421–423] Apparently, amino compounds acquired special significance as crucial intermediates in the chemistry of dyes, pigments, agrochemicals and herbicides, pharmaceuticals, *etc.* Thus, extra effort has been devoted to improving the selectivity of the hydrogenation processes with a focus on elimination of by-products formed *via* the hydrogenolysis of other carbon–heteroatom (C–X where X = O, N, S) bonds present in the nitroarene structure. These unwanted by-products not only hamper the selectivity, but also restrain the rate of hydrogenation reactions, causing difficulty in separation of the final pure products. To further add to the complexity associated with hydrogenation of nitroarenes, the presence of other sensitive functional groups including nitriles, alkenes, halogens, and ketones, which are reduced faster than the nitro compounds, make selective hydrogenation rather difficult. To deal with such complexities, three major approaches have been explored, which can be divided into three major categories: nature of catalysts, reaction conditions, and additives (Fig. 14).[424]

Amongst the different strategies, modification of the catalyst structure, which may be morphological changing allowing the use of different support materials such as polyelectrolyte brushes, polyionic liquids, micelles, or dendrimers is widely exploited to enhance the activity and selectivity. A few interesting examples are highlighted to illustrate that the engineering of catalysts can result in confined catalytic activity with improved selectivity. Li and co-workers designed ultrafine Ag NPs supported on a covalent carbazole framework to accomplish the reduction of 4-nitrophenol (4-NP) to 4-aminophenol (4-AP) (Fig. 15).[425] Ag NPs were immobilized onto the CZ–TEB (carbazole analogue and 1,3,5-triethynylbenzene) support to obtain a new Ag catalyst, *i.e.* Ag^0@CZ–TEB. This Ag^0@CZ–TEB nanocomposite exhibited superior catalytic efficiency towards a nitrophenol reduction with a high-rate constant of 21.49 $mmol^{-1} s^{-1}$.

COFs (covalent organic frameworks) are a new class of porous crystalline polymers possessing a wide range of properties such as good crystallinity, ultrahigh surface area, and chemical/thermal stability.[426] Thanks to their versatile nature, COFs can be utilized as a support for the adsorption of metal atoms because of the enhanced electronic conductivity during the catalytic transformation. A spherical covalent organic framework (SCOF) was synthesized to provide adsorption sites for Ag ions by which Ag NPs were decorated onto the SCOF to obtain AgNPs@SCOF microspheres.[427] The Ag NPs, through a strong interaction between the abundant nitrogen functional groups of the SCOF and Ag NPs, manifested higher catalytic activity for a 4-NP reduction under continuous flow conditions. Product 4-AP facilitated the acceleration of the catalytic reduction reaction and the detachment of 4-AP from the surface of the catalysts to refresh the free active sites for the continuous flow reaction. SEM and high-resolution transmission electron microscopy (HRTEM) images verified that the Ag NPs (yellow dots) were evenly distributed on the surface of the SCOF, showing spherical morphology of the AgNPs@SCOF nanostructures (Fig. 16). The superlative stability of the Ag NPs@SCOF microspheres amid the continuous catalytic process can be accredited to the strong interactions between the Ag NPs and the SCOF, and the large size of the catalyst prevented the leaching of the active catalytic species. Similarly, Wang *et al.* have synthesized Ag NPs@SCOF microspheres with superior catalytic activity towards the reduction of 4-NP to 4-AP.[428] Recently Ag NPs embedded on aluminium MOF *i.e.* NOTT-300(Al) were used for catalytic reduction of 4-NP,[429] wherein nanosize Ag^0 NPs and porous NOTT-300(Al) supports synergistically enhanced the reduction reaction *via* diffusion of reactants. Very recently, MW-assisted synthesis of Ag NPs supported on SBA-15,[430] Ag NPs on A4 zeolite (Ag/ZA4-MW) catalyst,[431] and Ag enclosed dendritic mesoporous silica nanospheres synthesized *via* a chemical reduction method,[432] have been reported for the reduction of 4-NP. In another report, a multifunctional Ag catalyst was fabricated by Reddy *et al.*[433] They synthesized Ag NPs supported on a nitrogen-doped carbon dot (AgNPs/NCD) nanocomposite for the reduction of methyl red (97.14% yield), rhodamine B (RhB) (98.83% yield), and 4-NP (99.95% yield) at ambient temperature.[433] The AgNP/NCD catalyst was synthesized *via* a microwave-assisted method without the use of any stabilizing or reducing agents. Furthermore, the AgNP/NCD nanocomposite is a stable and reusable catalyst for the reduction reactions as it can be continually reused for five cycles without a loss of catalytic activity. As described in the synthesis section, silica is a good support for the adsorption of Ag NPs, synergistically

enhancing the catalytic efficiency. Shabir *et al.* have reported the reduction of nitroarenes and degradation of organic dyes over Ag NPs immobilized on core–shell fibrous silica particles (cSiO$_2$@DFNS@Ag) in the presence of NaBH$_4$ as a reducing agent.[434] In another study, Ding *et al.* demonstrated that the PdAg alloy NPs supported on –NH$_2$ surface modified silica *i.e.* a PdAg/SiO$_2$–NH$_2$ catalyst is useful for catalytic reduction of nitrate in the presence of formic acid as a reducing agent.[435] Very recently, Coeck *et al.* reported the reductive amination of benzoic acid to benzylamine *via* Ag NP supported TiO$_2$ catalysts.[436]

The application of Ag-based nanocatalysts is not limited only to the nitro reduction; they are also employed in other reduction processes such as chemo-selective reduction of imines to *N*-alkylated amines.[278] In recent studies, Wang *et al.* reported that a single Ag atom could be uniformly anchored on the surface of nanosized γ-Al$_2$O$_3$ (Ag/γ-Al$_2$O$_3$) *via* terminal hydroxyl groups present on the γ-Al$_2$O$_3$;[437] dispersed single-atom Ag/γ-Al$_2$O$_3$ exhibited higher performance for selective catalytic reduction of NO.

4.1.4.   Addition reactions.—Addition reactions are one of the most common chemical transformations whereby two or more molecules are combined to form a larger one. Silver has remained the salt of choice for catalysing addition reactions. A number of reviews have given extensive coverage of its role in boosting diverse reactions based on intramolecular addition of O–H to unsaturated bonds, intramolecular haloamination, and intramolecular addition of N–H.[438,439] The reaction of allenic systems has been widely studied as they provide direct access to an array of heterocycles, and it is here where coinage metals such as silver step in since they enable to control the regiochemistry of such systems. In 2012, for the very first time, a report was published on the 1,2-addition of alkynes to aldehydes catalyzed by TiO$_2$-supported Ag NPs, which provided ready access to propargylamines (Fig. 17).[440] The catalyst exhibited good activity in terms of reaction yields and excellent reusability without any appreciable loss in its performance.

Regarding the wide range of addition reactions, cycloadditions hold a special place since they lead to the formation of cyclic adducts. Typically, cycloadditions allow two reaction partners containing a total of four or six electrons to react and form a new ring either *via* an intra or intermolecular process.[441] Diels–Alder (DA) reactions have emerged as one of the most powerful cycloaddition reactions utilized for the design of drug delivery systems and important bioactive products as they offer a promising 100% theoretical yield. For instance, panduratin A is a Diels Alder natural product derived from highly oxygenated 2′-hydroxychalcone dienophiles that show a broad spectrum of biological activities including anticancer, anti-HIV, and anti-inflammatory.[442] Although the synthetic approach seems straightforward, it actually poses a number of challenges since the dienophile '2′-hydroxychalcone' is not reactive enough, resisting the conventional Lewis acid promoted conditions, and the diene '*trans*-β-ocimene' undergoes olefin isomerization and polymerization only under acidic conditions, further complicating the reaction. To combat the challenges associated with the traditional approaches, a silica supported Ag NP catalyst was designed and utilized for Diels–Alder cycloadditions of 2′-hydroxychalcones to obtain cyclohexenyl chalcones (active component of a couple of biologically active 'Diels–Alder' natural products).[442] An insight into the reaction mechanism with the help of electron paramagnetic resonance (EPR) spin trapping experiments indicated that the Ag

NPs worked as a redox catalyst and mediated the cycloaddition process. Similarly, Okamoto and co-workers have reported a [3+2]-cycloaddition reaction of azomethine ylides with 2′-hydroxychalcone derivatives using silica supported Ag NPs (Fig. 18).[443]

4.1.5. C–H activation reactions.—Transition metal-catalyzed C–H activation reactions involving the cleavage of the C–H bond and formation of new C–X (where X = O, S, N) bonds have aroused interest of researchers as they offer a sustainable pathway to the construction of an extensive range of organic molecules using inexpensive, readily available precursors.[444,445] Although different metals have been exploited for this transformation,[446] Ag has received particular attention as Ag catalysed/mediated reactions have been reported,[447] including a review on Ag catalysed C–H and C–C bond functionalization.[448] However, the use of nanosilver catalysts started gaining momentum as soon as there were reports on bare Ag NPs, mixed silver oxide NPs, or supported Ag NPs developed and subsequently applied to a broad spectrum of C–H functionalization reactions (this review exemplifies a few pertinent ones). Yu *et al.* designed a novel, durable and recyclable catalytic system based on N-heterocyclic carbene polymer-supported Ag NPs that exhibited promising activity (good yield and wide substrate scope) in the carboxylation of terminal alkynes involving the cleavage of the C–H bond using CO_2 as the reaction precursor (Fig. 19).[309] The authors shed light on the reason behind the excellent results, attributing it to the unique synergism exhibited by the composite materials, *i.e.* between the Ag NPs and the polymeric support. The mechanistic aspects were paid attention to in this article, revealing that the Ag ions played a key role in activating the terminal alkynes in the presence of a base to form a metal acetylide intermediate, which was followed by CO_2 insertion into the metal carbon bond for the generation of the final carboxylic acid product.

Very recently, Tang and co-workers demonstrated the carboxylation of terminal alkynes with CO_2 *via* direct C–H bond activation by the molecular architecture of graphene oxide-supported Ag NPs (Ag/*tert*-GO).[449] The catalyst was simply prepared through the introduction of *p-tert*-butylaniline into graphene oxide powder, followed by localized growth of Ag NPs. Importantly, Ag/*tert*-GO shows superlative catalytic activity for the conversion of alkynes regardless of the presence of electron-withdrawing or donating groups under mild reaction conditions. The theoretical calculation indicates that the introduced amides around the Ag NPs can effectually capture CO_2 and provide an appropriate microenvironment for enabling carboxylation reactions. This facile, green, efficient, and inexpensive synthesis method brings a new perspective on designing this type of efficient two-dimensional material-supported catalyst at a molecular level. In another study, Biswas *et al.* developed AgNPs immobilized over functionalized 2D hexagonal SBA-15 and Dehghani and co-workers reported ternary Ag/AgBr/TiO_2 nanotubes for the catalytic activation of C–H bonds of hydrocarbons with molecular oxygen under solvent-free conditions.[450,451] The immobilization of Ag NPs on the surface of ordered mesoporous silica offers a very efficient pathway to designing an easily reusable, separable, and robust catalyst for the activation of the C–H bond under eco-friendly reaction conditions. Chang *et al.* reported a Ag cluster-based framework as a π-activation catalyst for the cycloaddition of propargylamines with CO_2 to produce oxazolidinone derivatives at room temperature and atmospheric pressure.[452]

4.1.6. Multicomponent reactions.—Multicomponent reactions (MCRs) have proven their utility in medicinal chemistry and drug discovery by providing ready access to more than five hundred different organic scaffolds.[453] They allow performing the subsequent transformations in a single pot, showing high compatibility with a broad spectrum of unprotected orthogonal functional groups. Ever since the pioneering work on the silver-catalysed three component coupling reaction of aldehyde, alkynes and amines,[454] silver has been extensively deployed for boosting such multicomponent reactions. Since the advent of the buzz-word 'nano', different types of nanosilver catalysts have been fabricated, proving their widespread utility in these reactions. Lykakis and team developed metallic silver (Ag^0) supported on hollow mesoporous silica NPs-and scrutinized their catalytic efficiency in the multicomponent synthesis of heterocyclic amines and dihydroquinoxalin-2-ones.[455] This work demonstrated the use of three variants of well-established isocyanide-based MCRs, namely (i) Ugi-Smiles, (ii) Ugi-tetrazole (UT-4CR), and (iii) classical Ugi reaction (Fig. 20a). The results revealed that the catalyst with an average size of the Ag NPs below 15 nm displayed the most promising activity in terms of the conversion and selectivity of the amine formation, leading to the synthesis of inhibitors for therapies for hypertension or inflammation.

Recently, bimetallic NPs have drawn particular attention of the scientific community; thanks to their effective activity resulting from the synergism of two different metals. Among the various combinations, silver remains the material of choice owing to its exceptional catalytic and bioactive properties. For instance: Sapkota *et al.* have fabricated Au–Ag@AgCl nanocomposites using a plant-mediated green approach to catalyzing multicomponent domino annulation-aromatization to obtain quinolines (Fig. 20b).[456] The preparation method primarily comprised the reduction of cationic Ag and Au, followed by the simultaneous generation of AgCl in the presence of a plant material (tuber extract of *Nephrolepis cordifolia*). In order to confirm the formation of the nanocomposites, the UV-visible spectrum of the synthesized Au–Ag@AgCl NPs was obtained, verifying the characteristic surface plasmon resonance peak of metallic Ag and Au in the applied electromagnetic field. The developed nanomaterial showed impressive catalytic activity in terms of good yield, substrate scope, and reusability.

Magnetic recovery has lately aroused interest of researchers in the field of catalysis science and technology. Therefore, magnetite NPs are being increasingly employed as support materials for the fabrication of catalysts. This concept was utilized by Veisi and co-workers, who fabricated ultrasmall iron oxide NPs and managed to immobilize Ag NPs *in situ* using a *Rubia tinctorum* extract.[457] The final nanocatalyst was used for the synthesis of propargylamines by an A^3 coupling reaction. The idea behind the use of the extract was modifying the magnetite NPs employing plentiful carbonyl and phenolic hydroxyl functional groups of the extract, which would assist in increasing the adsorption of metals and chelate silver ions and decreasing the adsorption of silver by the Ag NPs. As evident from TEM studies, this extract-mediated method resulted in the reduction of the size of the magnetite NPs from 15–20 to 2–5 nm. The catalytic activity was, undeniably, very promising in this multicomponent reaction that involved the use of aldehydes, amines and alkynes as precursors for the preparation of propargylamines.

Apart from this, Ag_2S NPs,[458] AgO NPs,[459] TiO_2-supported Ag NPs,[460] carbon nitride-supported Ag NPs,[257] and modified montmorillonite clay-stabilized Ag NPs[461] have also been employed as catalysts for the A^3-coupling (aldehyde–amine–alkyne) reaction. For the preparation of the carbon nitride-supported Ag NPs, microwave irradiation methodology was incorporated.[257] Excellent yield (up to 97%), high TON and TOF (72932 and 3636 min^{-1}), E-factor (0.27), and atom economy (94%) were the fundamental aspects of this protocol.

Mesoporous silica-based materials are also emerging as great catalytic materials.[262] Making use of the advantages that these materials could offer, Yong *et al.* fabricated mesoporous SBA-15 supported Ag NPs with a highly ordered hexagonal mesostructure (average 8 nm), which readily allowed the A^3 coupling reaction to proceed at a faster rate, thus forming the desired products with moderate to excellent yields.[462] However, a noticeable steric factor played a key role in this synthetic protocol and limited the substrate scope. The reason behind this phenomenon was the unfavourable effect of the SBA-15 channels upon the addition of iminium ions to activated alkynes. Similarly, another research group has reported the immobilization of silver on surface-modified ZnO NPs, which provided a good example of the one-pot three-component A^3 condensation of aldehydes, amines, and alkynes.[463]

Recently Praveena *et al.* synthesized heterogeneous Ag NPs using isolated strains of *Streptomyces* sp. RAB (Ras-related protein)10 which were used as a catalyst in a three-component reaction of 5-amino-3-methyl pyrazole, aryl aldehydes, and b-naphthol for the synthesis of naphthalene-2-derivatives in aqueous media.[464] The main advantages of using the multicomponent one-pot protocol in the study included good yield, shorter reaction time, reuse, and ease of recoverability of the Ag NPs as catalysts. The most important feature of this methodology is that it leads to the generation of a novel product with two reactive functional groups (free amine and a hydroxyl group), which opens up new opportunities in the field of medicinal chemistry. Also a Ag/sodium borosilicate nanocomposite has been reported for 1-substituted 1H-1,2,3,4-tetrazole synthesis under solvent free conditions.[465]

4.1.7. Hydrogenation–dehydrogenation reactions.

—Hydrogen is widely considered to be an ideal energy source from the viewpoint of sustainability.[466–468] Hydrogen is a gas under ambient conditions and needs to be handled with care; therefore the development of safe and efficient hydrogen storage methods is indispensable for realizing advanced hydrogen technologies. In this section, Ag NP-based catalytic studies of hydrogenation reactions and dehydrogenation reactions using organic hydrogen carriers will be studied.

4.1.7.1. Hydrogenation.:

As mentioned above, hydrogenation by Ag-based nanocomposites is a relatively well-documented transformation even in the field of homogeneous catalysis.[469,470] The design of a facile green synthesis of supported metal-engineered NPs with efficient catalytic activity is of significant industrial importance. In this regard, Das *et al.* have demonstrated an intricate design of Ag NPs supported on nanosilica (Ag@nanosilica), which was the first report regarding the protein-mediated *in vitro* synthesis of nanosilica-supported Ag NPs.[471] Nanosilica-supported Ag NPs (average size of 21 ± 3 nm) were synthesized using a single step bio-inspired synthetic route

involving protein extract of *Rhizopus oryzae*. The synthesized Ag@nanosilica exhibited high catalytic reactivity and reusability for the hydrogenation reaction of a model compound of 4-NP to 4-AP, likely due to favourable mass transfer and the synergistic effect.

Shimizu *et al.* reported that Ag clusters supported on Al_2O_3 selectively catalyzed the hydrogenation of the nitro group in the presence of C=C, C=O, or CN groups.[472] The Ag catalyst could be applied for the chemoselective hydrogenation of substituted nitroaromatic compounds including nitrostyrene to the corresponding anilines. These catalysts demonstrated higher catalytic activity and selectivity than other metals such as platinum-group metal-based heterogeneous catalysts. The acid–base bifunctional supports such as (θ-Al_2O_3, SnO_2, sepiolite, CeO_2, WO_3, ZrO_2, TiO_2, MgO) exhibited higher catalytic activity than other acidic or basic supports. These supports used for the catalytic hydrogenation of 4-nitrostyrene to 4-aminostyrene with different selectivity are listed in Fig. 21. The initial rate of 4-aminostyrene was below 40%; however, the Ag-supported catalysts produced 4-aminostyrene, *i.e.* b as the main product and a trace amount of c.

Another important investigation was made by Wang and co-workers.[473] They developed an N-doped porous carbon (denoted as N-doped-MOF-C) support for adsorption of Ag ions. It was prepared *via* one-step carbonization of MOFs, *i.e.* NH_2-MIL-125. The Ag and Pd NPs were immobilized on the N-doped-MOF-C through a co-reduction reaction with $NaBH_4$ as a reducing agent. The Pd_9Ag_1-N-doped-MOF-C catalyst exhibited excellent catalytic selectivity and activity for the catalytic hydrogenation of nitroarenes using formic acid as the hydrogen source. The use of N-doped-MOF-C as a catalyst support might bring new opportunities for the development of efficient heterogeneous catalysts, thanks to the synergistic effect of a MOF precursor and metal atom.

In another study, Zhang and co-workers developed silica-supported Ag–Ni bimetallic catalysts for the selective semi-hydrogenation of acetylene in an ethylene-rich stream.[474] Herein, a series of Ag–Ni/SiO_2 bimetallic catalysts with varied Ni/Ag atomic ratios ($AgNi_1$/SiO_2, $AgNi_{0.5}$/SiO_2, $AgNi_{0.25}$/SiO_2, $AgNi_{0.125}$/SiO_2) were prepared by a wetness co-impregnation method. The ethylene selectivity over the $AgNi_{0.25}$/SiO_2 catalyst increased by >600%, compared to the $Ni_{0.25}$/SiO_2 catalyst. The selectivity of ethylene is highly dependent on the bimetallic (Ni/Ag) atomic ratio. A bimetallic Ag–Au NPs nanocatalyst expedited the hydrogenation of anthracene in the presence of sodium borohydride as the hydrogen source.[475] The Ag and Au NP catalysts played a crucial role in acting as a nanoelectrode for storing electrons from hydride, and the resulting hydrogen radical reacted with anthracene to form the desired product exclusively (9,10-dihydroanthracene) obtained from the reaction. The hydrogenation of acrolein to *n*-propanol has been reported by Aich *et al.* over a Pd–Ag alloy nanocatalyst.[476] The 0.01% Pd and 8% Ag alloy NPs demonstrated high catalytic efficiency for hydrogenation as compared with their monometallic counterparts.

4.1.7.2.   Dehydrogenation.: Formic acid (FA) has great potential as a safe and convenient hydrogen carrier for fuel cell applications.[477] The efficient and CO-free hydrogen production through the decomposition of formic acid at low temperatures (<363 K) in the absence of additives constitutes a major challenge. In this context, Liu *et al.* have

developed surface Pd-rich PdAg nanowires (NWs) as highly efficient catalysts for the dehydrogenation of formic acid and subsequent hydrogenation of adiponitrile (ADN).[478] The diffusing strategy has been demonstrated to prepare Pd-rich D-Pd_5Ag_5 NWs *via* seed-mediated growth in a polyol solution for an efficient dehydrogenation catalysis of formic acid and subsequent hydrogenation of ADN by using FA as an *in situ* hydrogen source. The one-pot protocol diffused the newly reduced Pd atoms into Ag NPs, yielding surface Pd-rich PdAg NWs (D-PdAg NWs) in the polyol solution, which efficiently catalyzed the dehydrogenation of FA and subsequently hydrogenated ADN to 1,6-hexanediamine (HDA), achieving 99% selectivity and 99% conversion at 50 °C by using FA as an *in situ* hydrogen source.

The selective FA dehydrogenation using a robust solid catalyst at room temperature is very attractive for the fuel-cell-based hydrogen economy, yet quite challenging to accomplish.[479] Another important investigation was made by Wang and co-workers, they integrated AgPd NPs on a N-decorated nanoporous carbon (NPC) derived from a zeolitic imidazolate framework (ZIF/($Zn(MeIM)_2$, (MeIM = 2-methylimidazole))) to yield AgPd@NPC.[480] This was the first time that such a composite was fabricated and used as an efficient FA decomposition catalyst. The synergistic effect between the AgPd NPs and the NPC greatly enhanced the performance of the catalyst, depicted in Fig. 22a. The AgPd@NPC exhibited high catalytic activity (TOF = 936 h^{-1}) and 100% H_2 selectivity towards the dehydrogenation of FA at 353 K. Recently, Gao and co-workers reported boron-doped PdAg alloy immobilized on reduced graphene oxide (PdAgB/rGO) catalysts through a chemical reduction method.[481] This catalyst was used for the dehydrogenation of FA with sodium formate as the additive for hydrogen production with TOF of up to 480 h^{-1} at 323 K.

An analogous report by Sun and co-workers demonstrated a facile approach to a composition-controlled synthesis of monodisperse 2.2 nm AgPd NPs.[482] The synthesized NPs worked as highly durable and active catalysts for FA dehydrogenation and for hydrogen generation without requiring any additive. Another publication by Sun and his research team reported a nanocomposite of AgPd NPs anchored on $WO_{2.72}$ nanorods (NRs) (denoted as AgPd/$WO_{2.72}$) as a general catalyst for the dehydrogenation of FA and hydrogen transfer from Ar–NO_2 to Ar–NH_2, which further reacted with aldehydes to form benzene fused heterocyclic compounds.[483]

Another report by Shimizu *et al.* highlighted the fabrication of a γ-alumina-supported Ag cluster catalyst (Ag/Al_2O_3) for oxidant-free alcohol dehydrogenation to carbonyl compounds at 373K.[484] Notably, the developed catalyst exhibited higher activity than conventional heterogeneous catalysts based on platinum group metals and also showed potential for excellent recyclability. The activity of the Ag/Al_2O_3 strongly depends on the size and charge of the silver species. The silver clusters, possibly having a slightly cationic nature, show higher rates per surface Ag site than monomeric Ag$^+$ ions and bulk Ag particles. Amongst the several fabricated catalysts, Ag/Al_2O_3-5 (2.0 mol% of Ag) worked as a standard catalyst in the oxidant-free oxidation of various alcohols, as shown in Fig. 22b. 4-Methylbenzyl alcohol was treated in the presence of Ag/Al_2O_3-5 at 373 K in toluene for 24 h; 4-methyl aldehyde was produced in a 93% yield and selectivity at a level of alcohol conversion of 99% (Fig. 22b, entry 5).

Similarly, several other Ag-supported catalysts have been explored for ethanol oxidation and the role of the support material has been studied in detail. For instance, Vodyankina and co-workers developed Ag NPs in the size of less than 7 nm supported on silica as well as on silica modified with CeO_2 *via* the impregnation method.[485] The catalyst (Ag–CeO_2/ SiO_2) was used for the dehydrogenation of ethanol into acetaldehyde with >95% selectivity under both aerobic and anaerobic conditions. Similarly, Janlamool *et al.*[486] demonstrated that the support matrix, *i.e.* mixed γ–χ alumina in the supported Ag–Li catalyst greatly influenced the interaction with the Ag^+ species, and a weaker interaction led to a facilitated reduction of the Ag^+ species into $Ag^{n\delta+}$ clusters. According to the opinion of the authors, the $Ag^{n\delta+}$ clusters were far more active in the dehydrogenation of ethanol to acetaldehyde in comparison with the Ag^+ and Ag^0 species.

4.1.8.   Miscellaneous reactions.—Phthalides such as isobenzo-furan-1(3*H*)-one and isocoumarins like 1*H*-2-benzopyran-1-one constitute integral building blocks of many natural products with astounding bioactivities—anti-HIV, antidiabetic, antispasmodic, antiallergic, antifungal, *etc.*[487,488] In view of their significance, several synthetic methodologies have been reported, amongst which metal-catalyzed 5-*exo*-dig and 6-*endo*-dig cyclization of 2-alkynylbenzoic acid/esters that can be generated *in situ* by employing the Sonogashira-type coupling reaction, has gained profound significance.[489–491] However, achieving enhanced regioselectivity has remained a real challenge for chemists from the field of organic synthesis. Chaudhary *et al.* gave the first example of direct regioselective synthesis of 3-ylidenephthalides and isocoumarins using silver oxide NPs as the catalyst with an excellent yield of up to 95% (Fig. 23a and b).[488] Ag_2O NPs facilitated the catalytic process by coordinating simultaneously with the triple bond as well as with the electron-rich substituents that underwent the cyclization process in a regioselective manner.

Chadha *et al.* demonstrated the oxidation of 3-hydroxy anthranilic acid (HAA) to its azo derivatives using Ag NPs, thus excluding the use of any laser excitation or heat (Fig. 23c), as evidenced by time-dependent surface-enhanced Raman scattering (TDSERS).[492] The SERS measurements were recorded under different environmental conditions. The studies revealed that intramolecular hydrogen bonding in HAA led to a net weakening of the N–H bond, sequentially resulting in the formation of an azo derivative of HAA. Moreover, it was revealed that thermal electrons from the metallic surface of the Ag NPs played an indispensable role in the surface-catalyzed azo formation.

Metal-assisted reduction of GO has attracted immense interest of materials chemists and other scientists in this area since it complies with all the requirements of sustainable catalysis. As for the mechanistic role, not all metals have been found to serve this purpose. Rodil and his team reported a highly efficient Ag NP-assisted reduction of aqueous graphene oxide dispersions using $NaBH_4$ as a reductant.[493] The Ag NP catalyst was generated *in situ* from the $AgNO_3$ precursor added into the aqueous GO dispersion. A deep insight into the reaction mechanism revealed the charging of the Ag NPs with the excess electrons that were obtained from the oxidation of the product of spontaneous hydrolysis of $NaBH_4$ in an aqueous medium. The excess electrons were then transferred to the GO nanosheets which triggered their reduction (Fig. 24a).

In recent years, with respect to the increasing production of fatty acids and biodiesels, there has been a growing interest in the utilization of glycerol, especially in view of its great tendency to be converted into various value-added chemicals.[494] Yadav *et al.* described a novel process for the selective hydrogenolysis of glycerol to 1,2-propanediol (1,2-PDO) over a silver-incorporated octahedral molecular sieve (OMS-2) catalyst.[495] The catalyst— Ag-doped manganese oxide OMS-2—was synthesized by a precipitation method. It is worth highlighting that this was the first time, a silver-based catalyst had been utilized in the hydrogenolysis of glycerol. The major products of glycerol hydrogenolysis were 1,2-PDO and ethylene glycol (EG); however, acetol was produced in minor quantities, as shown in Fig. 24b.

On a similar basis, Zhang and co-workers prepared γ-Al_2O_3-supported silver catalysts (Ag/Al_2O_3) with various Ag loadings and calcination temperatures *via* an incipient wetness impregnation method for glycerol to (1,2-PDO) conversion.[496] Another publication by Sato and co-workers revealed the construction of Ag loading on a Cu/Al_2O_3 catalyst in the production of 1,2-PDO from glycerol.[497] The addition of Ag to the Cu/Al_2O_3 catalysts was found to be beneficial to inhibiting the decomposition of glycerol to produce EG, thereby generating 1,2-PDO in higher yields, compared to the original Cu/Al_2O_3 without Ag. Very recently, Koley *et al.* reported the Ag–Co core–shell nanoalloy catalyst for the production of g-valerolactone from levulinic acid;[498] Ag–Co core–shell nanoalloy was synthesized *via* a simple wet impregnation process. In another protocol, Liu and co-workers reported nitrous oxide (N_2O) production *via* nitrification by using Ag NPs.[499] Isotopomer analysis proved that the hydroxylamine oxidation was the primary pathway for the production of N_2O, and this pathway contributed more to N_2O emission when exposed to low-dose Ag NPs.

4.2 Photocatalysis

Photocatalysis is a light driven process that transforms solar energy into chemical, and is currently a hot topic for scientists as it holds the potential for tackling societal problems.[500,501] Since its historic discovery in 1972 by Fujishima and Honda, who demonstrated photo-assisted electrochemical splitting of water into H_2 and O_2 by a TiO_2 electrode, the field of semiconductor photocatalysis has aroused considerable interest as it enables the devising of new photocatalysts that have splendid visible light response and could mimic photosynthesis.[502,503] Ever since this pioneering discovery, the range of semiconductor photocatalysis has expanded immensely and industrial researchers have endeavoured to make the most of the copious solar energy. To date, numerous semiconductor photocatalysts that effectively make use of the solar spectrum have been reported, finding extensive applications in various fields.[504–506] Within this context, it should be noted that semiconductors incorporated/doped with noble metal NPs such as Ag, Au, and Pt have gained wide recognition.

Among them, silver, which shows high conductivity and encouraging photocatalytic activity coupled with low cost and non-toxicity, is the most profusely used noble metal in semiconductors[507] that finds extensive applications in industry. The possibility of smartly altering the resonance wavelength by varying the size and shape of these Ag NPs by means of the surface plasmon resonance effect represents a viable strategy through which

the whole solar spectrum can be exploited. Ag NPs, due to their unique physico-chemical characteristics when used in combination with semiconductor substrates, can be effectively used as a plasmonic photocatalyst.[508–511] The following section will summarize the recent development in the design and fabrication of Ag-based photocatalytic systems and their applications in the hydrogen evolution reactions, CO_2 reduction reactions, photocatalytic degradation of organic pollutants, and photocatalyzed organic transformations.

4.2.1.   Hydrogen evolution reactions (HERs).—In a typical photocatalytic HER, when photons of adequate energy are irradiated on a semiconductor, electrons are excited from the valence to conduction band. As a result, the excess electrons get accumulated in the conduction band, leaving behind the electron holes in the valence band. The electrons then reduce water to hydrogen and the holes oxidize water to form oxygen. As mentioned earlier, for efficient photocatalytic water splitting, three challenges need to be overcome including the narrowing of the band gap for harvesting visible light, boosting the efficiency of charge separation, and minimizing the recombination of hydrogen and oxygen, *i.e.* back reaction to water. The photogenerated electrons and holes may recombine when there is a dearth of active sites on the surface. This is when cocatalysts and sacrificial agents come into play. The presence of a cocatalyst, which simultaneously introduces active sites on the surface of the semiconductor while suppressing the charge recombination, is imperative. On the other hand, sacrificial agents as organic/inorganic electron donors also play a dominant role in enhancing the overall photocatalytic performance for water splitting reactions.[512] Recent studies prove that semiconductor photocatalysts coupled with a suitable doping material like Ag, which has exceptional visible light-responsive photochemical properties, are worth designing. Since the Fermi level of Ag NPs is lower than that of the conduction band of TiO_2, on UV irradiation, electrons of TiO_2 are excited from the valence to the conduction band and then move to the Ag NPs.[513] This is how the photogenerated electrons and holes get elegantly separated by simply integrating Ag NPs as the functional composite, while their surfaces also function as an active site for the photocatalytic water splitting process.[514–516]

It is worth mentioning here that Alenzi *et al.* fabricated Ag/TiO_2 nanocomposite films for the production of hydrogen under UV light, whereby methanol was employed as a hole scavenging agent.[517] It should be noted that the anatase crystal structure of TiO_2 is more stable and photocatalytically active in comparison with the rutile and brookite form, while TiO_2 films are more suitable than powders in terms of recyclability. The photochemical reactions were performed in a pyrex flask that was transparent in the near UV region. Methanol was used as a strong oxidizing agent, *i.e.* the electron donor and hole scavenging agent, which reduced the possibility of electron hole recombination. Besides playing the role of the hole scavenger, methanol also promoted the hydrogen generation through a decomposition mechanism. Thus, the water/methanol system contributed to the production of hydrogen. The feasibility of photoelectrochemical hydrogen production was tested not only in the presence of Ag/TiO_2 anatase films, but also in the presence of bare anatase TiO_2 films and amorphous TiO_2 films. The rate of H_2 production in the case of Ag/TiO_2 anatase films was determined to be 147.9 ± 35.5 μmol h^{-1} g^{-1}, which was found to be much higher than for the anatase TiO_2 films (4.65 ± 0.39 μmol h^{-1} g^{-1}) and amor phous TiO_2 films (0.46

± 0.66 μmol h^{-1} g^{-1}). The study carried out by Cheng and his research group led to the development of a photocatalytic route by which an ultralow amount of photocatalyst can be used as a high through-put screening process.

The work conducted by Zhang *et al.* and Iwase *et al.* where they synthesized ternary graphene based nanocomposites proved to be the stepping stone to the discovery of efficient photocatalysts.[518,519] Their findings led to the conclusion that ternary graphene nanocomposites exhibit a distinguished photocatalytic performance in comparison with binary composites. Following these findings, Fan and his research group constructed a ternary Ag-P25-GR (APG) composite as a photocatalyst for the hydrogen production and methylene blue degradation.[520] The high loading of Ag NPs significantly improved the suppression of the photo-generated electron hole pairs. Furthermore, the ternary composite, due to the concurrent existence of graphene and Ag NPs, which contributes to the surface plasmon resonance (SPR) effect, demonstrated high photocatalytic activity towards the hydrogen evolution in comparison with bare TiO$_2$ (P25) and TiO$_2$ graphene (PG) composites. The reason behind this observation could be attributed to the extended light absorption range, prolonged lifetime of photo-generated electron–hole pairs, and faster interfacial charge transfer rate.

In view of the structural benefits offered by TiO$_2$ nanotubes (NTs), Wu *et al.* followed an anodic oxidation process for the synthesis of nanotube arrays of TiO$_2$, which were utilized as a photocatalyst for the HER.[521] Since Ag NPs extend the overall visible light absorption, a microwave-assisted chemical reduction strategy was employed for loading the metallic Ag NPs into TiO$_2$ NTs. A plausible mechanistic justification involving a surface plasmon resonance effect was also proposed for the HER. The electrons of TiO$_2$ are excited to the conduction band upon light irradiation, while the holes remain in the valence band. The electrons then move to the Ag NPs and accumulate there. The unification of TiO$_2$ with Ag NPs forms a Schottky barrier, which further behaves as an electron trapper, thereby inhibiting the electron hole recombination process. During water splitting, the holes undergo a reaction with water to form $^\bullet$OH and H$^+$. At the same time, visible light drives the SPR phenomenon by enhancing the energy of the trapped electrons. These energetic electrons combine with H$^+$ at the surface of the Ag NPs to form hydrogen atoms. Thus, two hydrogen atoms combine to form a H$_2$ molecule. Moreover, the presence of ethanol as a sacrificial agent hastens the water decomposition process (as the produced $^\bullet$OH is consumed while oxidizing ethanol to acetic acid). It was observed that Ag/TiO$_2$ NTs exhibited superior photocatalytic HER performance in this reaction at a rate 3.3 times higher than that of pure TiO$_2$ NTs.

According to the volcano plot of H$_2$ evolution on metal catalysts, the silver catalyst's efficiency for H$_2$ production is limited by its lower binding energy (bonding in M–H) and slower electron transfer than that of Pt, which reduces the effectiveness of silver as a hydrogen evolving catalyst.[522,523] In short, the electrons injected into the Ag phase accumulate due to the delayed interfacial transfer. In this regard, Choi *et al.* demonstrated the surface modification of Ag with a thiocyanate (SCN$^-$) group, which allowed proton binding and electron transfer, further improving Ag's cocatalytic activity.[524] The Ag NPs were deposited on a TiO$_2$ (P25) support (Ag/TiO$_2$) *via* a photodeposition process

for photocatalytic H_2 production by forming a simple SCN^- surface complex of silver. The bright spots of Ag uniformly deposited on TiO_2 particles were verified through the dark-field STEM images. The photocatalytic H_2 evolution activity was enhanced fourfold when thiocyanate adsorbed on the Ag/TiO_2 catalyst in the presence of methanol as the electron sacrificing agent (Fig. 25a–d). Among these three catalysts (Pt/TiO_2, Ag/TiO_2, and Au/TiO_2), only the Ag/TiO_2 with thiocyanate demonstrated higher H_2 generation in the presence of methanol, compared with other hydrogen donors like ethanol and ethylenediaminetetraacetic acid (EDTA). The maximum H_2 production rate was observed at the saturation point of [KSCN] >0.1 mM thiocyanate and >3.0 wt% of Ag loading. The synergistic effect of S and CN in thiocyanate helped to transfer the stored electrons in Ag through the Ag-SCN ad-layer (the inner Helmholtz layer) to enhance the overall proton reduction to molecular hydrogen. The H_2 production overpotential and electron transfer resistance decreased due to the interfacial electron transfer of thiocyanate on the Ag/TiO_2 electrode (Fig. 25e).[524]

Thanks to their tunable electronic and optical properties, inorganic semiconductors have always been at the forefront of photocatalytic transformations of solar energy into a greener and renewable fuel – hydrogen.[525] Graphitic carbon nitride (g-C_3N_4) has aroused intense interest as it works as a metal free n-type semiconductor showing different qualities such as low toxicity, appropriate bandgap, low cost, high thermal and chemical stability, facile preparation due to its unique two dimensional (2D) layered structures, and visible light response.[526–528] Thus, several strategies such as the loading of co-catalyst, doping, and integrating g-C_3N_4 with noble metals have been explored by various research groups, all enhancing the resulting composite's photocatalytic activity and conductivity.[505,529]

A significant advancement in this direction was made by Li and co-workers when they integrated plasmonic Ag NPs with g-C_3N_4[530]. For this, the surface of g-C_3N_4 was loaded with different weight ratios of Ag NPs *via* a simple heating method. The synthesized Ag/g-C_3N_4 photocatalyst displayed a remarkable photocatalytic performance for hydrogen evolution, *i.e.* 10.105 μmol h^{-1}, which was 11.7 times higher than the performance of the pure g-C_3N_4. Such astonishing results were accredited to the synergistic effect, which occurred between the Ag NPs and the g-C_3N_4.

Another important investigation was made by Zeng and co-workers. They integrated plasmonic Ag NPs onto g-C_3N_4 for the HER.[531] The g-C_3N_4 was synthesized directly by calcining urea at 520 °C for 2 h. After that, Ag NPs of varying weight ratios, *i.e.* 1 to 9 wt%, were introduced on carbon nitride using a facile ultrasonic assisted chemical reduction method whereby $NaBH_4$ was added as a reducing agent along with PEG-600 performing the role of both a dispersant and protective agent. Among them, the sample having 3 wt% Ag/g-C_3N_4 displayed superlative photocatalytic activity in the presence of triethanolamine (TEOA) and fluorescein in comparison with the reported composites. TEOA as a sacrificial agent hampers the electron hole recombination phenomenon by consuming the generated holes of carbon nitride, while fluorescein, after getting adsorbed on the surface of carbon nitride, amplifies the visible light harvesting process and increases the electron transfer rate from fluorescein to carbon nitride, thereby acting as a photosensitizer in the catalytic process.

Single-atom catalysts (SACs) are highly desirable because they maximise the use of metallic catalysts by deploying nearly all atoms, which results in high catalytic efficiency and selectivity. However, the decoration of isolated atoms on an ideal support with a good coordination environment is crucial to stabilizing the single atoms.[532,533] The nanosized Ag-based cocatalysts, *i.e.* ultra-small Ag nanoclusters (Ag_{24}) and its monoplatinum-tailored analogue (Pt_1Ag_{24}) supported on g-C_3N_4 (Ag_{24} and Pt_1Ag_{24}/g-C_3N_4), have been reported for photocatalytic HER.[534] The single Pt atom embedded into the Ag_{25} nanoclusters gave a better photocatalytic performance in the HER due to the interfacial electron transfer of the catalyst, compared with the bare g-C_3N_4 (330 times) and Ag_{25}/g-C_3N_4 (4 times). The Pt_1Ag_{24}/g-C_3N_4 showed the highest rate of hydrogen evolution, *i.e.* 39.7 µmol h^{-1}, in the presence of 10 vol% TEOA as a hydrogen donor under visible light irradiation of λ   420 nm with long-term operational stability (Fig. 26).

Recently, Chen and co-workers have demonstrated a super-molecular method for decoration of individual Ag atoms on a carbon nitride (CN) supporting medium *via* M-N_2C_2 configuration (Ag–N_2C_2/CN).[535] Such a Ag–N_2C_2/CN catalyst exhibited maximum Ag-metal loading, good stability, and excellent photocatalytic activity for the production of hydrogen. HRTEM and aberration corrected high-angle annular dark-field scanning transmission electron microscopy (AC-HAADF-STEM) images revealed that the Ag single atoms were uniformly dispersed on the CN surface and coordinated with N_2C_2 (Fig. 27a and b). The Ag–N_2C_2/CN exhibited high photocatalytic H_2 production efficiency and stability for more than 15 cycles, compared to Ag_{NP}/CN and Ag–N_4/CN. DFT and experimental results proved that the Ag coordinated with C and N was responsible for the decrease in the overpotential of the H_2 evolution along with enhancing the visible light absorption range and promoting the charge separation and migration of carbon nitride, which ultimately resulted in higher photocatalytic H_2 evolution (Fig. 27c–e).[535]

Bimetallic NPs have gained an important position in the field of materials chemistry owing to their distinctive electronic and catalytic properties suitable for developing photocatalysts. Reports in the literature clearly document the significant enhancement in the photocatalytic activity of TiO_2 when intermixed with an appropriate combination of bimetallic NPs such as Au/Pd and Cu/Ni. Keeping this in mind, Stride and his research group adopted a chemical reduction strategy for decorating bimetallic Pd-Ag NPs on g-C_3N_4.[536] The resulting composite showed a high rate of hydrogen production, which was then attributed to the positive synergistic effect that exist between Ag and the Pd metals. The innate ability of the palladium metal to decrease the rate of the electron–hole recombination process by forming the Schottky barrier and the strong visible light absorption capacity of Ag NPs due to the SPR effect greatly contributes to escalating the H_2 generation.

Recently, Jiang and his research group also successfully explored the possibility of using bimetallic Ag–Cu NPs on g-C_3N_4 as an efficient photocatalyst for the hydrogen evolution phenomenon.[348] It was the first time that a modified water-induced morphological transformation had been employed for preparing bare carbon nitride nanotubes (C_3N_4 NTs). After that, a chemical reduction approach was exploited for introducing Ag–Cu bimetallic NPs on carbon nitride nanotubes. Besides, triethylamine (TEA) as a sacrificial agent beats most other commonly employed amine substrates like TEOA and methanol. In support of

the above-mentioned result, suitable mechanistic studies were carried out, also disclosing the superiority of triethylamine. It was revealed that the photodegradation of TEA resulted in the formation of diethylamine and acetaldehyde, which further enhanced the yield of hydrogen production. By contrast, TEOA was oxidized to diethanolamine and glycolaldehyde, while methanol, due to its low oxidation potential, was incompetent to react with the photoinduced holes. Experimental studies led to the conclusion that Ag–Cu NPs on carbon nitride nanotubes doubled the rate of hydrogen evolution. The inimitable tubular nanostructured morphology of the C_3N_4 NTs, strong Ag–Cu nanoparticle–(C_3N_4 NTs) interaction, and effective separation of the electron-holes in the Ag–Cu C_3N_4 nanocomposite significantly ameliorated the rate of hydrogen production.

Over the past few years, quasi-spherical classes of nanocarbon particles, known as carbon quantum dots (CQDs), have been scrutinized as promising materials applicable in the fields of sensing, fluorescence, and photoelectrochemistry.[537] Zeng and co-workers reported a novel and promising Ag/CQDs/g-C_3N_4 composite with ameliorated broad spectrum absorption.[538] Carbon quantum dots synthesized by an alkali-auxiliary sonication approach were added to an aqueous solution containing urea; then, they were sonicated and dehydrated, followed by heat treatment at 500 °C for 1 h. Once the CQDs/g-C_3N_4 composite was synthesized, the loading of Ag NPs was carried out following a chemical reduction method. An amine substrate like TEOA was added as a hydrogen sacrificial agent during the photocatalytic experiment because of the active interaction of the lone pair present on the nitrogen atom with the holes of carbon nitride. The synchronous existence of the Ag NPs and the CQDs, which promoted quick photoelectron generation, transfer, and separation, was found to noticeably improve the photocatalytic activity of graphitic carbon nitride, with the Ag/CQD-modified g-C_3N_4 showing about 6.7 and 2.8 times higher activity than the pure g-C_3N_4 and CQDs/g-C_3N_4 composites. The hydrogen evolution rate of the Ag/CQD-modified g-C_3N_4 was found to be 626.93 μmol g^{-1} h^{-1}.

The bimetallic core–shell NPs with an Au core and Ag shell have recently been fabricated by Bardhan and co-workers.[539] The unique and untypical core–shell architecture of Au–Ag NPs appears to be very promising for developing efficient photocatalysts showing potential for water splitting applications. The presence of dual metal nanoparticles in the photocatalyst not only extends the visible light absorption range and facilitates greater light capturing capacity, but also smartly modulates the electronic properties without varying the size. In order to enhance the photocatalytic activity of mesoporous TiO_2, a seed-mediated approach has been employed for preparing Au-Ag core shell NPs with Au seeds, which are then coated with a silica layer that acts as a protective agent and also reduces the electron–hole recombination process.

Tantalates, owing to their admirable optical and electronic properties, have been identified as superb photocatalytic materials for converting solar energy into renewable fuels of global interest. Despite their unique features, there are still several limitations that restrain a wider use of tantalates. The low quantum efficiency, high band gap ranging between 3.0 and 4.7 eV, and fairly high reduction potential are some of the challenges associated with tantalates that need to be overcome. With this intention, Shi and his research group adopted a facile and straightforward approach by dispersing Ag NPs on $KTaO_3$ and $NaTaO_3$ nanocubes.[540]

For this, $KTaO_3$ and $NaTaO_3$ nanocubes were first synthesized *via* a hydrothermal route, and a varying amount of Ag NPs were then deposited on them following an *in situ* photodeposition method. The Ag-decorated $KTaO_3$ and $NaTaO_3$ nanocubes in the presence of stimulated light displayed remarkable efficiency in the hydrogen evolution reaction, showing high evolution rates of 185.60 and 3.54 µmol h^{-1} g^{-1}, respectively, from methanol, *i.e.* photocatalytic activity increased twice in comparison with the pure $KTaO_3$ and $NaTaO_3$ nanocubes.

In addition to Ag NPs, the photocatalytic activity of P-doped Ag NPs embedded in a N-doped carbon nanoflake (P-Ag@NC) has been recently explored.[541] The P-Ag@NC composite has been synthesized by thermally annealing silver nitrate, glucose, and urea in the presence of sodium hypophosphite. The resulting composite was not only electrochemically stable and durable; it also showed high activity towards hydrogen evolution when tested in the presence of sulfuric acid. The high thermo-neutral hydrogen adsorption free energy is a remarkable aspect of this composite that distinguishes it from conventional Ag-based photocatalysts.

Most of the hydrogen currently used in the world comes from natural gas reforming, which leads to increased emission of carbon. The photocatalytic H_2 evolution is an emerging technology that offers a solution to environmental issues and global energy demands.[542] For enhancing the photocatalytic water oxidation, Ag(I) is typically used as an electron scavenger as it can capture holes to form high-valent Ag-species in addition to functioning as an electron acceptor.[543] To this end, it is essential to produce highly stable, efficient, and nonprecious photocatalysts.

4.2.2. CO$_2$ reduction reactions.—Undeniably, the significant progress achieved worldwide over the past few centuries has been attributed to hydrocarbon fuels such as coal, oil, and gas. However, excessive use of these hydrocarbon fuels with the mounting world population is a dystopian vision, eventually leading to an environmental and economic catastrophe. Combustion of fossil fuels releases 30 billion tonnes of CO_2 into the atmosphere and is thus a major contributor to the global greenhouse effect. Therefore, the recent climate agreements have bound countries to take necessary action needed for a sustainable future.[544–546] In this context, solar energy driven photocatalytic transformation of CO_2 into valuable chemicals and fuels such as hydrocarbons, alcohols, or formic acid is an attractive twofold approach that not only mitigates the rising CO_2 level by closing the anthropogenic carbon circle, but simultaneously provides an economically viable pathway to renewable energy storage and utilization.[547,548] Despite several decades of research devoted to this area, the industrial utilization of CO_2 suffers from major technological drawbacks because of its high thermodynamic stability and inertness. Therefore, designing a suitable catalyst that will thermodynamically and kinetically drive the CO_2 conversion reaction remains a challenge. In this regard, considerable attention has been paid to photocatalytic CO_2 reduction over the past few years.[549] The photocatalytic CO_2 processing technology, devoid of any external thermal and electrical energy, smoothly proceeds under ambient reaction conditions and atmospheric pressure. Several semiconductor photocatalysts including TiO_2, ZrO_2, $SrTiO_3$, metal nitride, and metal sulfide have been intensely scrutinized. In addition to this, the inherent use of Ag NPs as cocatalysts improving the

photocatalytic activity of numerous semiconductors in the CO_2 reduction has recently been investigated by various research groups. For example, in a recent publication, the authors have adopted a sol–gel processing technique in the reverse micellar environment for the fabrication of Ag doped TiO_2 powders.[550] The effect of Ag as a dopant for enhancing the activity of TiO_2 in both the liquid and gas phase was closely studied. During the photocatalytic CO_2 reduction process, methane and methanol were found to be the major products. The Ag-modified TiO_2 composite substantially increased the yield of the CO_2 photocatalytic reduction in comparison to pure TiO_2. This remarkable improvement has been primarily attributed to the doping mechanism. Firstly, the decrease and shifting of the absorption edge towards visible light increases the photogeneration of electron–hole pairs, which ultimately increases the CO_2 photoreduction phenomenon. Secondly, the Fermi level of TiO_2 lies higher than that of Ag NPs, which then forms the Schottky barrier. Both of the factors decrease the rate of the electron–hole recombination process, along with increasing the charge separation and eventually the photocatalytic activity of TiO_2.

Several research groups have explored the possibility of using $CaFe_2O_4$, $LaCoO_3$, $BiVO_4$, $InTaO_4$, and Zn_2GeO_4 as materials that can substitute TiO_2 as a semiconductor photocatalyst. Therefore, a great deal of scientific effort over the past few years has been devoted to preparing d^0 type highly active metal oxide photocatalysts for CO_2 reduction. In this context, Kudo and his colleagues constructed a novel Ag cocatalyst-loaded $ALa_4Ti_4O_{15}$ (A = Ca, Sr and Ba) photocatalyst with perovskite structure that could significantly convert CO_2 to formic acid and carbon monoxide, without any sacrificial agent.[551] The $ALa_4Ti_4O_{15}$ (A = Ca, Sr and Ba) photocatalyst was synthesized by a polymerizable complex method. The loading of Ag on the photocatalyst was conducted *via* various routes including impregnation, photo-deposition, and the liquid phase chemical reduction technique. Among all the prepared composites, a Ag cocatalyst-loaded $BaLa_4Ti_4O_{15}$ plate-shaped composite synthesized by a liquid phase chemical reduction method, with the Ag NPs having a diameter smaller than 10 nm, showed the highest activity towards the CO_2 photoreduction. The spatial and ordered distribution of alkali earth metal and lanthanum cations in $BaLa_4Ti_4O_{15}$ leads to its higher anisotropy, which finally affects the photocatalytic activity. Moreover, the separation reaction sites in a plate-shaped $BaLa_4Ti_4O_{15}$, where the edge of the plate represents the reduction site and the basal plane signifies the oxidation site, terminates the back reactions during the photocatalytic reduction process. The uphill reaction of the CO_2 reduction not only generates carbon monoxide as the major product but simultaneously produces oxygen (Fig. 28a).

Another major development in the field of semiconductor photocatalysis has been made by integrating Ag NPs with carbon fibres (CFs). Carbon fibres (CFs), due to their superior electron conductivity property, have been highly exploited in catalytic and electronic applications. An innovative approach for the fabrication of Ag NP-decorated carbon fibres has been adopted by Ding *et al.*, achieving efficient photocatalytic CO_2 reduction.[552] The synthesis of carbon fibres implementing an electrospinning technique was the first step towards accomplishing the desired goal. After that, the loading of Ag NPs onto the carbon fibres was conducted utilizing a facile solution dipping technique accompanied by ultrasonic treatment. The photocatalytic activity of this Ag NP/carbon fibre composite towards methanol formation increased fourfold compared to that of the pure Ag NPs (Fig.

28b). Such a pronounced increase in the photocatalytic activity was ascribed to the SPR phenomenon exhibited by the Ag NPs, generation of plasmon excited electrons on the Ag NPs, increased electron transfer process by the interface from the Ag NPs to carbon fibres, decreased rate of electron–hole combination, increased charge separation, and increased CO_2 adsorption. In addition, the nanoscale morphology of carbon fibres, which allows competent dispersion of nanometric size Ag NPs, also provides an added advantage to the extensive light absorption range.

Another publication was reported on the photochemical generation of hydrogen and simultaneous reduction of CO_2 to form CO using a Ag NP-modified TiO_2 composite.[553] The photocatalytic hydrogen evolution experiments were performed deploying a water/methanol mixture with N_2 as the carrier gas, while the CO_2 reduction experiments were conducted using CO_2 as the carrier gas in a methanol/water mixture. It was found that a 2% Ag/TiO_2 composite synthesized *via* spray pyrolysis displayed six-fold H_2 production activity, *i.e.* 1130 μmol g^{-1} h^{-1}, compared to the composite prepared *via* the wet impregnation method, because a high Ag content favours the electron hole recombination process. Similarly, the rate of CO production *via* the photocatalytic reduction of CO_2 was 87 μmol g^{-1} h^{-1} *i.e.* 50% higher in the case of the 2% Ag/TiO_2 composite (the spray pyrolysis method) in comparison with the wet impregnation method. It was revealed that a higher fraction and better dispersion of the metallic Ag species on the TiO_2 prepared *via* the spray pyrolysis route enabled a fast rate of charge transfer alongside marked enhancement in the photocatalytic activity. After carrying out a deep mechanistic analysis, the authors stated that the H_2 evolution and the CO_2 reduction processes competed with each other. Partial pressure of the CO_2 and the concentration of the hole scavenger, *i.e.* methanol, are two determining factors that need to be finely tuned for the syngas (H_2 and CO) production from CO_2, H_2O and methanol.

The feedstock utilization of CO_2, which is a major constituent of flue gas that is responsible for global warming, stands out as an environmentally benign method for chemical transformations.[554–556] It is an abundant, nontoxic, and cost-effective one-carbon building block for the chemical production of fuels. The non-catalytic industrial use of the CO_2 feedstock leads to the effective syntheses of salicylic acid, urea, and carbonates of groups 1 and 2 elements. For instance, recently, Mallouk and co-workers developed a molecularly thin layer of 2-aminobenzenethiol (2-ABT) that was adsorbed onto the nanoporous p-type silicon (b-Si) photocathodes decorated with Ag NPs (p-type b-Si/Ag).[557] The addition of 2-ABT alters the balance of the hydrogen evolution and CO_2 reduction reactions and consequently more selective reduction of CO_2 to CO could be accomplished. The conclusion is that the molecule attached to the surface of Ag through its amino and the thiol group in the ortho position plays a crucial role in facilitating the transport of CO_2 and protons to the surface of the metal. Otgonbayar *et al.* have developed a novel-structured CuCaAg$_2$Se-graphene–TiO_2 ternary nanocomposite for the photocatalytic reduction of CO_2 to methanol.[558] The catalyst CuCaAg$_2$Se was prepared *via* the muffle-assisted hydrothermal method, and the powder was calcined at 700 °C for 2 h in order to obtain the desired product. A solution precursor was synthesized using the Pechini-method, which depends on the metallic citrate polymerization by using chelating cations such as citric acid ($C_6H_8O_7$) and ethylene glycol ($C_2H_6O_2$). The structure, morphology, and charge-

carrier separation confirmed that the combination of graphene, TiO_2, and $CuCaAg_2Se$ increased the photocatalytic activity of the synthesized nanocomposite. Significantly, such a nanocomposite exhibited greater stability during the recyclability with no evident loss in the production of methanol from CO_2 photoreduction. Another report by Oh and co-workers describes the novel micro and nanostructure of a $AgCuInS_2$–graphene–TiO_2 for the photocatalytic reduction of CO_2 to methanol fuel.[559] Recently, Baldi and co-workers proved that under reducing gas conditions, intermittent Stokes emission from Ag NPs revealed a dynamic surface structure of Ag photocatalysts, resulting in the formation of nanoscopic and highly active Ag clusters for photocatalytic reduction of CO_2.[560]

4.2.3.   Degradation of organic pollutants.—It has been rightly said that *"Water is life's matter and matrix, mother and medium. There is no life without water".* Since the dawn of the 21st century, access to clean and fresh water has remained a subject of utmost importance. Moreover, the rapid growth of the economy and industrialization coupled with unparalleled consumption of resources has added fuel to it. Industrial effluents containing certain carcinogenic and mutagenic compounds are a major source of organic water pollution that are not only toxic to human health, but also hazardous to aquatic life. Mounting concerns associated with these toxic organic substances such as dyes, pesticides, and phenols have facilitated the implementation of stricter rules and regulations. Thus, rapid and convenient elimination of pollutants is a challenge that scientists across the globe are attempting to solve. As a consequence, tremendous endeavour is made towards redesigning and developing newer technologies that will eradicate recalcitrant pollutants directly rather than by transformations triggering unnecessary damage to the environment.[561–563] In this regard, photocatalytic degradation of organic pollutants by harnessing the solar UV and visible light spectrum has emerged as a promising technique for combating this problem. Besides, photocatalytic degradation involves oxygen as an eco-friendly oxidant for the oxidation of organic compounds at low concentrations and ambient reaction conditions. For this, metal oxide semiconducting materials having the desired band gap for capturing solar light energy are receiving increasing attention as photocatalysts. Nonetheless, the inability of TiO_2 and ZnO to absorb major components of solar light, *i.e.* visible region, has prompted researchers to incorporate Ag NPs (due to their SPR phenomenon) while designing suitable photocatalysts. So far, significant advancements have been made in the design and fabrication of these semiconductor-based heterostructures.[564–569]

Within this context, Zheng and his research group adopted three different research methodologies, namely deposition precipitation, co-precipitation, and a solvothermal technique assisted with chemical reduction and photolysis for fabricating Ag/ZnO heterostructures.[570] The resulting Ag/ZnO composite is further used in the degradation of methyl orange (MO). During the photocatalytic experiments, the transfer of photogenerated electrons from ZnO to Ag NPs occurs through the Ag-ZnO interface. The key role of Ag NPs is to trap the photogenerated electrons, thereby producing holes to form hydroxyl radicals, which ultimately degrades the organic pollutants. Moreover, the oxygen vacancy defects on the surface of ZnO substantially maintain the separation of photogenerated electron–hole pairs. Experimental results reveal that the photocatalytic performance of a hybrid nanocomposite relies on the extent of the dispersion of Ag NPs in the catalyst—the

better the dispersion, the higher the light utilizing efficiency and the photocatalytic activity towards MO degradation.

Literature reports clearly document the fabrication of several titania-Ag composites for degradation purposes. Chen and co-workers reported a S-doped Ag_2O/TiO_2 composite, *i.e.* $Ag_2O/Ag_2S_2O_7/TiO_2$, as a stable photocatalyst for the degradation of methyl orange.[571] The presence of $Ag_2S_2O_7$ on Ag_2O sufficiently protects the silver oxide NPs from undergoing reduction to Ag NPs. Furthermore, Ag_2O and $Ag_2S_2O_7$ behave as efficient visible light sensitizers, thereby boosting the photocatalytic activity of TiO_2 nanobelts. In another report, the authors employed bismuth based materials, *i.e.* $Ag/Bi_2O_2CO_3$ nanocomposites, for the photodegradation of methyl orange.[572] The high photocatalytic activity of these composites is further attributed to the high surface area of $Bi_2O_2CO_3$ and the ability of Ag NPs to act as electron trapping agents.

The photocatalytic properties of Ag NPs are highly dependent on the overall plasmonic architecture. It has been reported that core–shell heterostructures with a metal core and a semiconductor shell prevent Ag NPs from undergoing corrosion and expedite the energy transfer process through a direct contact between the Ag NPs and the semiconductor shell, thus improving the overall photocatalytic performance. Within this context, work carried out by Li *et al.* as part of which they constructed a $Ag@Cu_2O$ core–shell photocatalyst for the degradation of methyl orange is worth highlighting.[573] Moreover, the ability to finely tune the shell thickness allows visible light absorption over a large spectrum.

Indeed, it has been widely accepted that the adsorption capability of photocatalysts is a vital prerequisite for an enhanced performance. In this regard, Zhu *et al.* reported a plasmonic photocatalyst based on a Ag/AgCl/GO nanocomposite for the degradation of methyl orange.[574] The non-covalent π–π interactions between the dye molecule and the graphene oxide-Ag hybrid composites, along with the reinforced charge transfer and the minimized recombination of photo-generated electron–hole pairs, are the major factors responsible for the superior photocatalytic activity. Similarly, several other research groups have also reported Ag-doped ZnO NPs and Ag@AgCl NPs for the degradation of methyl orange.[575,576]

However, it has been frequently observed that the nanosized ZnO materials are more prone to photocorrosion owing to their poor structural stability, which ultimately impedes their photocatalytic performance. In an attempt to overcome the drawbacks associated with nanosized ZnO, materials chemists endorsed the use of microstructured ZnO particles. In this regard, Wang and his research group fabricated Ag NP-decorated nanoporous ZnO micrometre rods using a solvothermal method supported by a photoreduction technique.[577] The resulting composite was highly photostable, along with exhibiting a superb degradation efficiency of 98% for the degradation of methylene blue dye under both UV and solar light irradiation. Moreover, the composite revealed high photocatalytic efficiency for five consecutive cycles without any discernible loss in its activity. The inimitable nano/microconfigured assembly of the heterostructure coupled with the higher crystallinity of the ZnO rods were the major factors responsible for enhancing the overall photocatalytic performance (Fig. 29a).

Chen *et al.* established, for the very first time, the preparation of Ag nanoparticle-decorated SiO_2 nanospheres as a visible light photocatalyst for the degradation of methylene blue.[578] A seed-mediated approach by which SiO_2 nanospheres reacted with $AgNO_3$ was employed to enable the growth of Ag NPs. The photocatalytic degradation studies were investigated under a 500 W xenon lamp having a light intensity of 175 mW cm^{-2}. The SPR phenomenon exhibited by the Ag NPs generated plentiful charge carriers in the Ag/SiO_2 composite, as a result of which the developed composite revealed high photocatalytic activity towards the degradation of methylene blue. Besides, the existence of the silica shell enabled facile recovery *via* filtration and centrifugation alongside reusability for multiple runs.

Wei *et al.* reported that photocatalytic performance relies on extensive charge separation and is highly dependent on the structure and morphology of the overall photocatalyst.[579] Therefore, they synthesized one-dimensional $AgVO_3$ nanoribbons incorporated with Ag NPs as a plasmonic photocatalyst for the degradation of crystal violet dye. High conductivity along with Ag NP's superior electron storage capability and SPR phenomenon significantly boosted the photocatalytic activity of the $Ag/AgVO_3$ composite.

Among other metal oxides, bismuth tungstate (Bi_2WO_6), which has varying morphologies such as NPs, nanoplates, nanocages, and nanoflowers, is a type of material that has been frequently employed for the degradation of water pollutants under visible light irradiation. For example, Wang *et al.* prepared a Ag-deposited spherical Bi_2WO_6 nanocomposite for the degradation of RhB and desulfurization of thiophene.[580] In a quest to obtain the anticipated composite, Bi_2WO_6 was synthesized *via* a hydrothermal strategy using bismuth nitrate and ammonium tungstate, followed by the deposition of Ag NPs utilizing a photoreduction technique.

In another report, the authors fabricated ternary nanocomposites of TiO_2–SiO_2–Ag by a biomimetic technique.[581] The material achieved high degradation efficiency for RhB. The enhanced photocatalytic performance was accredited to the presence of both Ag NPs and SiO_2 layers. On one hand, because of the SPR phenomenon, the Ag NPs increased the visible light absorption, while the SiO_2, owing to its large surface area, increased the adsorption of positively charged rhodamine through electrostatic interactions with the negatively charged Si–OH moieties. A similar ternary plasmonic photocatalyst comprising graphitic carbon nitride/Ag NPs/MoS_2 having flowerlike morphology was synthesized for the degradation of RhB by Fang and co-workers.[582] Molybdenum disulphide (MoS_2), due to its optimum band gap of 1.75 eV, is capable of absorbing light in both the UV and visible regions. Moreover, the existence of a flowerlike morphology due to the controllable mesopores and macropores allow greater interfacial transfer and a lower rate of recombination of the photo-generated electron and holes. Thus, the ternary g-C_3N_4/Ag/MoS_2 composite achieved 9.43 times higher photocatalytic activity for the degradation of RhB than Ag/MoS_2 and 3.56 times than the g-C_3N_4/MoS_2 composite.

Several reports in the literature clearly established that Ag NPs, when coupled with metal oxide semiconductors such as TiO_2, ZnO and CeO_2, can be used for the simultaneous degradation of more than one organic pollutant. For instance, Liang and his research group synthesized Ag/TiO_2 nanotubes using electrochemical anodization followed by

a wetting-thermal decomposition method for the degradation of methylene blue and pentachlorophenol, while Shao *et al.* fabricated ternary core–shell TiO_2@carbon/Ag nanofibres for the photocatalytic degradation of methyl orange and RhB.[583,584] The ternary photocatalyst exhibited higher rates of degradation, which were then attributed to the photosynergistic effects that occurred between the TiO_2 nanofibers, carbon and the Ag NPs. Besides, the developed photocatalyst was found to be easily recycled owing to its one-dimensional nanostructural characteristics. On similar grounds, Park and his research group fabricated a ternary hybrid composite consisting of graphene oxide nanosheet wrapped Ag@$Ag_2Mo_3O_{10}$ in order to achieve the concomitant degradation of RhB and 4-chlorophenol.[585] In this work, Ag NPs acted as an electron mediator by bridging the graphene oxide and the $Ag_2Mo_3O_{10}$ wires in order to achieve better degradation efficiency. Similarly, Cho and co-workers fabricated a coupled photoactive Ag–ZnO nanocomposite using a biogenic protocol for the photocatalytic degradation of methylene blue (MB), methyl orange (MO), and 4-NP.[284] The combination of Ag NPs with ZnO led to enhanced photocatalytic degradation because of the extended visible light absorption spectrum and the reduced electron–hole recombination process (Fig. 29b). Another publication by Bettini and co-workers mentioned the preparation of the ZnO@Ag patchy-nanostructured composite for the degradation of MB and 2,4-dichlorophenol (a pesticide) under light irradiation in the wavelength range from 370 to 800 nm.[586] The rapid photoinduced charge transfer from ZnO to Ag NPs, the increased charge separation at the metal-semiconductor interface, and the stabilization of holes in the valence band of ZnO enhanced the photocatalytic efficiency of the ZnO@Ag composite towards the degradation of organic pollutants.

Thanks to their microporous/mesoporous nature, large surface area, high mechanical strength and adsorption capacity, graphene oxide aerogels have been recently used as a promising candidate for water treatment applications. Besides, its wonderful superhydrophobic and superoleophilic features facilitate faster adsorption of organic pollutants from water. Considering the properties of graphene oxide-based composites, a research group recently fabricated reduced graphene oxide/polyethyleneimine/Ag hydrogels for the photocatalytic-assisted degradation of MB and RhB.[587] Both graphene oxide and silver ions were reduced *in situ* using vitamin C as an environmentally benign reducing agent. The photocatalytic mechanism revealed that the dye molecules were efficiently adsorbed onto the surface of the hybrid composite *via* π–π conjugation interactions that developed between the aromatic regions of the dye and graphene. Furthermore, upon light irradiation, photoexcited electrons were transferred onto graphene and reacted with oxygen molecules to produce superoxide and peroxide radicals, which eventually cleaved dye molecules into CO_2 and H_2O. On similar grounds, Tao *et al.* also reported the preparation of Ag NPs/CeO_2/Graphene aerogels for the bifunctional degradation of MB and bisphenol A.[588] It was observed that the synergistic integration of hierarchical graphene aerogels, CeO_2, and Ag NPs in the hybrid composite resulted in an enhanced performance and enabled 100% degradation of MB and 81.8% degradation of bisphenol A within 12 min and 4 h of the start of the experiment.

Another publication by Zeng and co-workers revealed the construction of Ag/AgCl NPs decorated on the surface of $SrTiO_3$ nanocubes using a facile ultrasonic mediated precipitation-photoreduction route to the photocatalytic degradation of numerous organic

water pollutants such as MO, MB, RhB, phenol, and bisphenol A.[589] Furthermore, Ag NPs supported on ZrO_2, zeolite Y, and SiO_2 have been reported for the photocatalytic-assisted degradation of phenol by Chen *et al.*, while a ternary Fe_3O_4–TiO_2–Ag composite synthesized by a ultrasonic-mediated hydrothermal method has been described in the literature for the photocatalytic degradation of 4-chlorophenol by Ghasemi and co-workers.[510,590] Another report by Cai and his colleagues demonstrates the photocatalytic degradation of pentachlorophenol by a Ag cluster-TiO_2 hybrid composite under UV light irradiation.[591]

The photocatalytic technology utilizing solar power is a suitable method for handling the energy crisis in the near future; it is widely applied for hydrogen production from water splitting and degradation of organic pollutants.[592] Liu and his group reported Ag/AgCl-based plasmonic photocatalysts with a controlled size and shape deploying GO as a catalyst promoter as well as a capping agent. Muthuraj and co-workers synthesized silver molybdate (Ag_2MoO_4) embedded with a polypyrrole (PPy) polymer α-Ag_2MoO_4/Ppy nanocatalyst for the photodegradation of MO pollutants.[593,594] The catalyst was synthesized by a one-pot approach *via* a precipitation reaction between $Ag(NH_3)_2NO_3$ or $AgNO_3$ and NaCl. It was observed that the near-spherical and cube-like nanostructure of Ag/AgCl in the size of 500 nm was fabricated at lower and higher temperatures, respectively. After the addition of GO nanosheets into the synthesis medium, the size of the prepared near-spherical and cube-like nanostructures of Ag/AgCl/GO reduced to *ca.* 200 and 100 nm, respectively, when $Ag(NH_3)_2NO_3$ and $AgNO_3$ were employed as the silver source. The cube-like Ag/AgCl/GO nanoarchitectures of 100 nm displayed the highest catalytic activity for the degradation of MO pollutants in comparison with the near-spherical ones. In an analogous study, Kulkarni *et al.* reported a fast green additive-free synthesis method at low temperature for the preparation of Ag@AgCl plasmonic NPs in a size smaller than 50 nm (average size 37 nm and the discerned particle size smaller than 10 nm) employing sugar cane juice as the only reagent.[595] Additionally, this process is eco-friendly, fast, and economically favourable, avoiding the use of additional solvents, external halide, external reducing agents, templates, and external ion sources. Ag@AgCl NPs are highly efficient photocatalysts for fast degradation of MO and MB[596] azo dyes, which are environmental pollutants in water under visible light. Similarly, Jiang and co-workers developed Ag/AgCl@MIL-53-Fe photocatalysts and described the efficient integration of plasmonic Ag/AgCl with a typical photoactive metal–organic framework (MOF, MIL-53-Fe) to increase the visible light photoreactivity of MOFs.[597] The Ag/AgCl@MIL-53-Fe photocatalysts were successfully synthesized and designed *via* a facile one-pot solvothermal method, whereby the Ag/AgCl NPs were placed on the surface of the MIL-53-Fe micro-rods. The synthesized catalyst was highly efficient for dye degradation and Cr(VI) reduction under visible light irradiation. Ag/AgCl NPs were firmly, uniformly, and densely anchored on the surfaces of the MIL-53-Fe micro-rods, while the final Ag/AgCl@MIL-53-Fe microstructures exhibited a rod-like morphology. Fig. 30a illustrates the photocatalytic mechanism for the Ag/AgCl@MIL-53-Fe system, in which the valence band (VB) and conduction band (CB) energy levels of MIL-53-Fe are 2.09 eV and −0.50 eV *vs.* NHE (*vs.* normal hydrogen electrode), respectively. It can be excited under visible light due to the suitable bandgap energy of 2.64 eV. Significantly, the MIL-53-Fe not only readily oxidizes OH^- to $^\bullet OH$ radicals, but also assists in the direct

hole oxidation of RhB under visible light irradiation conditions because the VB value of the redox potential of $^\bullet$OH/OH$^-$ (2.38 V *vs.* NHE) is lower than the redox potential of RhB (1.43 V *vs.* NHE). This observation justifies the plasmonic Z-scheme photocatalytic process in Ag/AgCl@MIL-53-Fe. The Ag is SPR-excited and the SPR-electron is injected into the CB of AgCl to reduce Cr(VI) to Cr(III) under visible light irradiation.

Jiang and co-workers have synthesized a green and efficient photocatalyst comprising a Ag-supported carbon nitride (Ag/C$_3$N$_4$) nanocomposite with 0.048% of Ag content for the degradation of organic pollutants under visible light irradiation.[598] The Ag NPs were synthesized using a squeezed-out liquid (SOL) of plant biomass in the presence of NaBH$_4$ as the reducing agent; the obtained Ag NPs were loaded onto carbon nitride (C$_3$N$_4$) in order to form synthesized Ag/C$_3$N$_4$ nanocomposites, which exhibited superior catalytic reactivity for the reduction of RhB under visible light. Finally, it was concluded that the biogenically prepared Ag/C$_3$N$_4$ nanocomposites demonstrated good photocatalytic reactivity compared to the synthesized nanocomposite obtained *via* a chemical transformation. Mechanistically, the photoexcited electrons in C$_3$N$_4$ are transferred to Ag NPs, which react with water to produce O$_2$$^{\bullet-}$ ions. The O$_2$$^{\bullet-}$ ions diffuse into the bulk solution and react with the RhB molecules under visible light illumination (Fig. 30b). The nanostructured Ag/C$_3$N$_4$ photocatalyst exhibits excellent photocatalytic activity under visible light irradiation, leading to the 60% mineralization of RhB within 2 h. Similarly, Cai *et al.* reported the Ag immobilized on ultrathin g-C$_3$N$_4$ nanosheets (Ag@U-g-C$_3$N$_4$-NS) for the degradation of organic pollutants as well as hydrogen peroxide production.[599]

Chen *et al.* reported a green synthetic route to the preparation of Ag–TiO$_2$ supported on porous glass (PG), which was utilized for the catalytic degradation of organic dyes and photocatalytic desulfurization under visible light irradiation.[600] The TiO$_2$ composites in the Ag–TiO$_2$/PG were prepared by an *in situ* reduction methodology at room temperature without any hydrogen atmosphere or severe conditions. PG was chosen as a support, and Ag–TiO$_2$/PG (as-prepared) showed remarkable merits of effective separation of electron–hole pairs, intense visible light absorbance, abundant reactive sites, and high surface areas for the photocatalytic oxidation. The microcrystalline structures of the catalyst showed that the Ag NPs were monodispersed on the TiO$_2$/PG surface. The Ag–TiO$_2$/PG also showed great photocatalytic activity in the removal of methylene orange (MO), RhB, and MB with different rate constants 0.18, 0.14, and 0.055 min^{-1}, respectively (Fig. 31A). Using Ag–TiO$_2$/PG, the catalytic conversion of dibenzothiophene was observed to be 83.5%, while that of benzothiophene was 80.1% under the irradiation of visible light in 80 min. On a similar line of application, Saarinen and co-workers reported the flame spray technique to deposit Ag NPs on TiO$_2$ inverse opal (TIO) for the photocatalytic degradation of organic pollutants and hydrogen evolution.[601]

Zhu and co-workers synthesized ZnAlTi-layered double oxide (ZnAlTi-LDO)-supported C$_{60}$@AgCl NPs using a coprecipitation light-induced method for the photocatalytic degradation of Bisphenol A (BPA).[603] The C$_{60}$@AgCl-LDO catalyst containing the photoinduced electron–hole pairs was greatly inhibited due to greater electrical conductivity of C$_{60}$ and strong coupling between ZnAlTi-LDO and C$_{60}$@AgCl. The C$_{60}$ was used as a support material for enhancing the stability of Ag-based photocatalysts. The C$_{60}$@AgCl-

LDO catalyst was beneficial for the fast charge separation and electron transfer as well. The C_{60}@AgCl-LDO photocatalyst showed a 90% photocatalytic degradation rate of the BPA under visible light irradiation. Sattari and co-workers have reported a Ag_2S–ZnO@rGO core–shell micro-sphere photocatalyst for the degradation of acetaminophen (ACT) under visible light irradiation.[604] In this catalyst, Ag_2S played a crucial role as the synergism between the rGO and the Ag_2S led not only to increased efficiency in the light process, but also to overcoming the recombination of the charge. The synthesized catalyst was prepared *via* a novel green one-step *in situ* wet chemical method using dimethyl sulfoxide (DMSO) as a solvent and sulfur (S^{-2}) as a reducing agent at 140 °C. Trang *et al.* demonstrated the photocatalytic degradation of RhB and hydrogen evolution using Ag@ZnO nanostructures under UV and visible light irradiation.[602] Green nanoengineering and concerted catalysis were combined for the synthesis of ZnO-based composite photocatalysts while the decoration with Ag was conducted by the method of radio frequency (RF) sputtering at room temperature. The synthesized Al-doped ZnO (AZO) nanostructure showed a photocurrent density of 2.5 mA cm^{-2} *vs.* Ag/AgCl, which increased 12-folds compared to bare ZnO, which exhibited a value of 0.2 mA cm^{-2}. Under visible light and UV exposure, the H_2 evolution rates of AZO-20 were found to be ~24 and ~38 μmol h^{-1}, respectively, these being much higher than those of pristine ZnO. Also, quite appreciably, the degradation efficiency of AZO-20 under these conditions was found to be 82% and 97%, respectively. Notably, the highest RhB decomposition and the H_2 evolution performance were accomplished with the quantum yields of 4.9 and 2.7% under UV or visible light irradiation. The photocatalytic enhancement mechanism involving a charge-transfer pathway of the AZO photocatalyst under UV and visible light is demonstrated in Fig. 31B.

4.2.4.   Organic transformations.—Photocatalytically driven conversion of organic compounds into fine and commodity chemicals is considered a major step towards the orientation of solar energy dependent 'green' chemistry.[605,606] Giacomo Ciamician, the father of organic photochemistry, during his lecture in the 8th International Congress of Applied Chemistry in 1912, stated that thermally activated processes can be effectively transformed into cost-effective and more selective photochemical reactions.[607] Moreover, sunlight as an inexhaustible and sustainable resource of clean chemical potential has also the power to drive synthesis of complicated molecules. Surprisingly, the photochemical technique for catalyzing organic reactions has not gained much momentum in the chemical field. However, with the collaborative effort of chemists and materials scientists, this technique has started acquiring great prominence amongst the research fraternity for organic synthesis. Moreover, the incorporation of plasmonic metal NPs such as Ag simultaneously couples the thermal energy with low intensity visible photons, driving commercially and industrially significant organic reactions.[608–613] Nevertheless, there have been only few reports where plasmonic activities of Ag NPs were exploited to carry out catalytic reactions.

Aniline—one of the most highly demanding intermediates in the agrochemical and the pharmaceutical industry—is frequently synthesized by the reduction of nitrobenzene. Generally, the hydrogenation of nitrobenzene takes longer reaction times and is performed at high reaction temperatures and high hydrogen gas pressure. It is worth mentioning here that Tada *et al.* reported the fabrication of a Ag/TiO$_2$ composite for the photocatalytic reduction

of nitrobenzene to aniline in the presence of methanol.[614] The composite not only achieved 84% conversion of nitrobenzene within 1 h of irradiation, but also demonstrated 100% selectivity towards the formation of aniline. The density functional theory (DFT) along with structural studies indicated that once nitrobenzene is adsorbed onto the surface of Ag/TiO_2, Ag NPs play the key role of reduction sites in transferring electrons to nitrobenzene. In the developed photocatalyst, the suppression of electron-holes, increased charge separation efficiency, and careful adsorption of reactant molecules sufficiently increased the overall activity and selectivity in the hydrogenation reaction.

Similarly, Ibrahim and co-workers prepared a Ag/Bi_2MoO_6 composite for the photocatalytic reduction of nitrobenzene to aniline using a xenon lamp.[615] A hydrothermal technique followed by a photo-assisted deposition method was employed for doping Ag NPs on Bi_2MoO_6. The Ag/Bi_2MoO_6 composite resulted in 100% photocatalytic reduction of nitrobenzene within 120 min of irradiation. Besides, the photocatalyst was easily recycled and reused for five consecutive runs, without any noticeable change in its activity. Similarly, Zheng and his research group synthesized a hybrid WO_3–Ag nanowire composite for the photocatalytic degradation of nitrobenzene to aniline.[616] The synthesized composite, due to its porous nature and high surface area, not only revealed enriched photocatalytic performance, but also showed outstanding reusability towards the hydrogenation of nitrobenzene.

Kominami along with his research group reported a Ag-deposited TiO_2 photocatalytic redox system for the chemoselective reduction of epoxides to alkenes and oxidation of alcohols to ketones.[617] 2,3-Epoxypropyl benzene was selectively reduced to allylbenzene, while alcohols were oxidized to ketones at room temperature without the addition of any reducing agent. The most fascinating feature of the protocol was that the C=C bond of allylbenzene remained intact, *i.e.* it was not further reduced to propyl benzene. Besides, a diverse range of epoxides was found to be efficiently converted into corresponding alkene molecules in the presence of a Ag-based photocatalyst.

Another publication by Yang *et al.* reported in the literature mentioned the bifunctional role of a heterostructured $MIL-125/Ag/g-C_3N_4$ composite for the photocatalytic reduction of nitro compounds to amine and oxidation of alcohols to aldehydes.[618] The combination of advanced microscopic techniques such as TEM and SEM revealed the uniform photodeposition of Ag NPs on MIL-125, followed by adhering $g-C_3N_4$ on the Ag/MIL-125 composite. The resulting composite exhibited enhanced photocatalytic efficiency because of extended visible light absorption and increased charge separation efficiency of the photogenerated holes and electrons (Fig. 32a). Besides, the Ag NPs, by acting as an electron conduction bridge between the MIL-125 and the $g-C_3N_4$, enabled an uninterrupted transfer of electrons from the C_3N_4 to the MIL-125 while simultaneously suppressing the electron–hole recombination process. The designed photocatalyst not only exhibited better results in terms of conversion and selectivity, but could also be reused for four consecutive cycles. Jain and co-workers demonstrated the one-step preparation of a ternary hybrid $Ag–rGO/g-C_3N_4$ through hydrothermal process for photocatalytic reduction of nitrobenzene to aniline in the presence of hydrazine hydrate as a reducing agent where methanol acts as a hole scavenger as well as proton donor in the reaction.[619]

Hydrogen peroxide, regarded as a clean oxidant, is of great importance in organic synthesis from a commercial standpoint and finds extensive applications in pulp bleaching industries and waste water treatment techniques. On an industrial scale, hydrogen peroxide is produced by an anthraquinone method, which involves numerous hydrogenation and oxidation steps. In this regard, Tsukamoto *et al.* employed a sufficiently green route to the production of hydrogen peroxide.[620] In this report, the authors synthesized a Au/Ag bimetallic alloy NP-system deposited on TiO_2 for the generation of hydrogen peroxide. In this, an oxygen saturated ethanol/water solution is irradiated by a 450 W high pressure mercury lamp. The existence of Au/Ag bimetallic alloy leads to a double effect phenomenon, which reduces oxygen for stimulating the production of H_2O_2 and also inhibits the photocatalytic decomposition of hydrogen peroxide by decreasing the rate at which H_2O_2 molecules are adsorbed on the surface of Au atoms, thereby enhancing the rate of the formation of hydrogen peroxide.

Another research group led by Xiao *et al.* also fabricated an Ag–Cu alloy NP system for the production of azoxy compounds from nitro groups.[621] The selective hydrogenation of aromatic nitro moieties to azoxybenzene rather than to aniline is a challenging route in organic synthetic chemistry. However, this exacting route appeared easy with the use of an Ag–Cu alloy system having a molar ratio of 4 : 1. The generation of hot excited electrons by localized surface plasmon resonance effect triggered the adsorption of reactant groups on the nanoparticle system. Besides, the ability to finely tune the wavelength of incident light offered a perfect opportunity for tailoring the selectivity towards the product formation, *i.e.* azoxybenzene and aniline.

The epoxidation of ethylene to ethylene oxide, a major feedstock and key intermediate for producing plastics in chemical manufacturing industries, is a highly substantial organic transformation.[622] This reaction is generally carried out under high temperature and pressure conditions. Silver is a well-proven ethylene epoxidation catalyst that is widely utilized in industry.[623] However, the involvement of a graphene/Ag/α-Al_2O_3 photocatalyst significantly lowered the harsh reaction conditions associated with this process, making it a greener synthetic route. The photocatalytic mechanism of this reaction initiated with the photosynthesis of graphene after irradiation with a laser light having a wavelength of around 514 nm. Air was employed as the major source of oxygen. Density functional studies revealed that the epoxidation of ethylene was activated by the photogenerated graphene, which acted as the major site for the chemisorption of ethylene and oxygen. The fabricated graphene/Ag/α-Al_2O_3 composite exhibited enhanced photocatalytic performance towards this epoxidation reaction in comparison with the traditional Ag/α-Al_2O_3 system.

Varma and co-workers have synthesized a reusable bimetallic AgPd@g-C_3N_4 catalyst by reducing Ag and Pd salts supported on photo active g-C_3N_4.[624] This catalyst was used for the amino formylation of a nitro-aromatic compound under photochemical conditions deploying visible light as an energy source and formic acid as a formylating as well as reducing agent. Firstly, 5 mol% of Pd was immobilized on the g-C_3N_4 and tested for the reductive formylation of the nitro group using formic acid as a hydrogen donor agent and the formation of the desired product occurred with 31% yield within 12 hours under visible light (Fig. 32b, entry 1). While the increase in the Pd loading did not improve the catalytic

activity, decreasing the loading of Pd also resulted in a net decrease in the product yield. Hence, the Pd@g-C_3N_4 catalyst was not very effective for this transformation. However, the activity improved after adding a catalytic promoter, preferably an abundant material such as Cu and Ag. Accordingly, the bimetallic copper–palladium CuPd@g-C_3N_4 catalysts afforded a 55% yield of the desired product (Fig. 32b, entry 2). The CuPd@g-C_3N_4 catalyst with 5% Cu and 10% Pd gave a 69% yield of the desired product (Fig. 32b, entry 3). The catalytic activity was enhanced due to the use of silver as a co-catalyst,[625] and, therefore the synthesized AgPd@g-C_3N_4 framework used for the reaction of nitrobenzene with formic acid gave a greater yield of *N*-formyl aniline (Fig. 32b, entries 4–6). The variation between the Ag and the Pd concentrations in the AgPd@g-C_3N_4 played a crucial role in the formylation of aromatic nitro groups. The nitro-aromatic compounds were subjected to the optimized reductive formylation conditions and, strikingly, all the substrates containing electron donating or withdrawing groups were rapidly converted to the corresponding amino formyl derivatives with impressive yields within just 2 hours.

Similarly, Verma *et al.* exploited the idea of using C–H activation for the conversion of benzene to phenol (a crucial organic intermediate utilized mostly for the sustainable production of pharmaceuticals, polymer resins, fungicides, preservatives, *etc.*) under visible light irradiation.[626] In order to achieve it, they designed a bimetallic catalyst based on inherently photoactive graphitic carbon nitride (g-C_3N_4) as the support material and thereafter incorporated the combinations of Ag and Cu onto the support. The graphitic nitride was prepared by calcining urea at 500 °C and by dispersing in water using an ultrasonicator for about 30 min. Cu and Ag salts were sequentially added and reduced to Cu(0) and Ag(0) using $NaBH_4$ as the reductant. Close introspection into the reaction mechanism revealed that the hydroxyl radicals were generated *via* the degradation of hydrogen peroxide over the bimetallic surface. The non-covalent interaction of molecular benzene with the support, followed by the activation of the C–H bond through CuAg@g-C_3N_4 catalyst and the reaction of hydroxyl radicals with benzene, led to the formation of phenol. This C–H bond activation-hydroxylation of benzene was facilitated by the rich nitrogenous surface of graphitic carbon nitride, which not only ensured an electron rich environment for keeping the copper and Ag NPs intact, but also played a crucial role in absorbing the visible light and dissipating it into the reaction media. Wang *et al.* have demonstrated the visible light mediated oxidative amidation of aromatic aldehydes *via* Ag supported g-C_3N_4 nanosheets.[627] The synthesized catalyst was prepared through a modified solvothermal-roasting process by using melamine and cyanuric chloride as precursors. In the context of Ag SACs, Wang and co-workers reported the single-atom silver(0) catalyst generated from AgF that exhibited excellent catalytic activity for the dehalogenation–arylation and the hydrodehalogenation reaction under visible light irradiation.[628]

Another work on styrene oxidation reported polyacrylonitrile nanofiber (PAN NF) supported by Ag NPs/g-C_3N_4 nanostructures that was used for the oxidation of organic substrates such as styrene, benzene, and –CH_2 bonded molecules under photocatalytic conditions.[629] This PAN/Ag NP/g-C_3N_4 NF catalyst showed good selectivity towards epoxide formation with a 98% conversion rate in the case of styrene oxidation (Fig. 33b). The electron donating substituted styrene derivatives showed greater conversion rate and selectivity for epoxide conversion. However, the electron withdrawing substituent displayed lower

conversion and selectivity in the presence of substituted styrene derivatives. Furthermore, the PAN/Ag NPs/g-C_3N_4 NFs catalyst exhibited excellent performance in the C–H oxidation of benzene, leading to 99% conversion to phenol with superior selectivity, (Fig. 33a) as well as oxidation of ethylbenzene to acetophenone with 99% conversion using H_2O_2 as an oxidising agent (Fig. 33c). The substituted ethylbenzene samples were tested and from the results it was concluded that the electron donating substituent exhibited impressive selectivity, compared to the electron withdrawing substituent. Additionally, the oxidation of some −CH_2 bonded molecules such as halogen-based derivatives, except fluorene and indene, also yielded higher conversion with selectivity under similar reaction conditions. The catalyst possessed mesoporous properties with superb absorptive activity; thanks to the NFs exhibiting increased activity, recyclability, and excellent stabilization.

With the aim to further improve the efficiency of the DA reaction for the construction of synthetically and biologically important [4+2] cycloadducts, Bhalla and co-workers designed an innovative and efficient Ag NP-based photocatalytic system for which pentacenequinone derivatives comprising 4-formylphenyl groups at the 2,9 or 2,10 positions were synthesized.[630] One of the derivatives served as an excellent reactor and stabilizer for the preparation of spherical Ag NPs, and the final nanomaterial served as a photocatalyst for the DA reaction (Fig. 33d). Landry *et al.* reported plasmonic Ag nanocages for the catalytic hydrogenation of aldehydes and ketones to corresponding alcohols under visible light irradiation.[631] Huang and co-workers demonstrated the photoinduced electron transfer (PET) mechanism for the conversion of *p*-aminothiophenol to 4,4′-dimercaptoazobenzene over a single Ag NP, which is useful for prediction of surface-enhanced Raman spectroscopy (SERS) behaviour.[632]

4.3. Electrocatalysis

The excessive use of non-renewable energy sources, especially the heavy reliance on fossil fuels, has resulted not only in the depletion of such resources, but also in a severe energy crisis. In order to overcome this catastrophe and fulfil the energy demands for a sustainable environment, the design and development of renewable energy sources from sun, wind, and tides has become a necessity of today's world.[633] To date, several transition metal-based nanocatalysts have shown high catalytic performance in the electroreduction of CO_2, oxygen reduction reaction, nitrogen reduction reaction, hydrogen evolution reaction and the electro-oxidation of methanol.[329,634] But, due to the competitive co-evolution of hydrogen, these catalysts exhibited low faradaic efficiency (FE), large overpotential, and poor product selectivity during the electrochemical conversion.[635] Among the wide-ranging non-noble metal nanocomposites, Ag NMs exhibit fascinating physicochemical properties like tuneable size and shape, electronic behaviour, low toxicity, and long-term operational stability, as well as being relatively lower cost, in comparison with Pd, Pt, and Au, which increased their value for applications in electrocatalysis and several other fields.[31,78,636] Ag has a similar mechanism and kinetics for electrochemical conversions to Pt, along with showing high tolerance towards methanol poisoning and membrane degradation, *i.e.* rapid decomposition of hydroxide ions to hydrogen peroxide.[637] Therefore, Ag NMs are highly exploited for electrochemical conversion of fuels and chemicals as an energy feedstock. The electrocatalytic efficiency of these NMs can be easily tuned by controlling their morphology,

size, and composition.[638] Dispersed Ag NPs provide more active sites for the catalytic transformation, compared to its aggregates.[639] Over the last two decades, several types of Ag NMs have been explored for electrocatalytic applications including the hydrogen evolution reaction (HER), oxygen evolution reaction (OER), oxygen reduction reaction (ORR), carbon dioxide reduction reaction (CO_2RR), nitrogen reduction reaction (NRR), and alcohol oxidation reaction, *i.e.* the methanol oxidation reaction (MOR) and ethanol oxidation reaction (EOR) (Fig. 34).[82–84,640–643] Along with these uses, Ag NMs have also been employed in formate oxidation reactions,[644] electrooxidation of hydrogen peroxide (H_2O_2),[645], or in electrochemical sensors.[646,647] In this section, applications of advanced Ag NMs in electrocatalysis have been briefly summarized for clean fuel production while considering the environmental sustainability.

4.3.1. Hydrogen evolution reactions (HERs).—Hydrogen, which is regarded as the most promising alternative to traditional fossil fuels in the 21st century, has gained considerable attention over the recent decades as a clean, renewable, and sustainable resource with high energy density. One of the most promising ways to meet the ever-increasing demand for renewable electricity storage is to generate sustainable hydrogen with water electrolyzers.[648,649] Sustainable hydrogen production is a prerequisite for realizing the hydrogen economy, *i.e.* hydrogen fuel cells and hydrogen energy of the near future.[650] A HER is a process of electrochemical reduction of protons at the metal electrode surface resulting in the production of hydrogen fuels. Platinum and platinum-based catalysts are widely regarded as the most effective electrocatalysts for HERs, OERs, and ORRs, but their high cost and scarcity prevent widespread use.[651] In search of efficient electrocatalysts for hydrogen production, a number of inexpensive and earth-abundant metal-based or metal-free or noble metal-free catalytic systems have been designed by several research groups to date.[649,652–655] In comparison with other Pt-group metals, Ag has high electrical and thermal conductivity and is relatively low cost and abundant; therefore, nanostructured Ag and Ag-based catalysts are efficiently utilized for electrocatalytic hydrogen evolution.[640,656–661] Campbell *et al.* have reported a Ag NP array for electrochemical hydrogen evolution.[640] They synthesized Ag NPs *via* a citric acid reduction of $AgNO_3$ followed by an array that was constructed on a basal plane pyrolytic electrode through colloidal suspension. The shape of the NPs helped to boost the electrocatalytic efficiency. Lee and co-workers have synthesized hexagonal, circular, and triangular Ag–Pt nanoplates by a simple galvanic displacement process.[662] The Ag–Pt nanoplates were employed for electrocatalytic HER. Among these diverse morphologies, the triangular Ag–Pt nanoplates exhibited the highest hydrogen evolution efficiency.

Ag_2O has garnered particular attention due to its high catalytic performance as well as selectivity as a catalyst.[663–665] Wang and co-workers have reported a dendritic MoO_3/Ag catalyst with good crystallinity for the electrochemical evolution of hydrogen.[666] The heterojunction of Ag_2O and MoO_3 synergistically enhanced the crystallinity of the composite and ultimately increased the HER efficiency. Improved electrocatalytic efficiency was achieved using composite catalysts such as binary and ternary systems. Solomon *et al.* have reported a one-pot synthesis of a ternary composite of Ag_2S, MoS_2, and reduced graphene oxide (RGO) flakes (Ag_2S/MoS_2/RGO) for the HER.[667] The ternary

$Ag_2S/MoS_2/RGO$ system was prepared *via* a hydrothermal method whereby the Ag_2S NPs were uniformly distributed on the surface of the MoS_2 nanosheets supported by RGO. The $Ag_2S/MoS_2/RGO$ sample exhibited appreciable electrocatalytic HER activity with a current density of -10 mA cm^{-2} at -190 mV *vs.* RHE overpotential and Tafel slope of 56 mV dec^{-1}, which was higher than the activity of the bare binary MoS_2/RGO and MoS_2 composites.

In another protocol, Yao *et al.* have reported bimetallic Pt-free surface alloys of Pd and Ag catalysts for scalable and sustainable hydrogen production under acidic and alkaline conditions *via* electrochemical water splitting.[668] The hydrogen bonding energy of neighbouring surface Pd atoms was moderately weakened by Ag, which improved the HER intrinsic behaviour and the interconnective metal skeleton, which facilitated the electron transfer. The nanoporous Pd–Ag–Al electrodes exhibited low onset overpotentials and ultralow Tafel slopes, *i.e.* 26 and 56 mV dec^{-1}, as well as 63 and 108 mV overpotentials, respectively, in 0.5 M H_2SO_4 and 1 M KOH electrolytes. Based on previous protocols, it has been proved that the electrocatalytic activity is stimulated by the surface atoms on the top and bottom facets of the nanosheets, whereas the edge and corner sites of the electrocatalysts also show superior catalytic activity. Recently, Cheng and co-workers have prepared trimetallic dendritic PdAgPt nanoalloys through a one-pot chemical reduction process in the presence of octadecyltri-methylammonium chloride as surfactant templates and L-ascorbic acid as a reducing agent.[669] This ternary nanoalloy displayed superior HER efficiency thanks to several crystal defects such as twin boundary, steps, and atomic holes, which are capable of functioning as catalytically active-sites. TEM and HRTEM images revealed that such $Pd_{43}Ag_{21}Pt_{36}$ nanoalloys have several pores in the middle and nanodendrites at the edges (Fig. 35a–f). Based on the catalyst morphology, it was proved that the mass transport of the reactants takes place through the diffusion channels. The centre pores and nanodendrites of Ag nanocomposites are responsible for high specific area, and several step sites together enhanced the electrocatalytic performance.[670–672] Among the wide range of catalysts (binary $Pd_{68}Ag_{32}$ nanodendrites, $Pd_{62}Pt_{38}$ nanospheres, $Pd_{43}Ag_{21}Pt_{36}$ nanowheels, and Pt/C) the $Pd_{43}Ag_{21}Pt_{36}$ nanowheels manifested a high electrocatalytic hydrogen production performance and operational stability with a lower overpotential of 9 mV at 10 mA cm^{-2} of current density in an acidic electrolyte (Fig. 35g and h). The ternary $Pd_{43}Ag_{21}Pt_{36}$ nanowheels with optimised composition and morphology also demonstrated the best mass/specific activity and stability in the alcohol (methanol and ethanol) oxidation reaction.

It is a well-known fact that amongst several transition metals, Ag possesses the highest electrical conductivity[673–675] and exhibits low hydrogen adsorption energy as well as adequate HER efficiency because of the d^{10} electronic structure.[640,676,677] Notably, as evident from the literature, Ag NPs' small coordination numbers, surface structures, such as a corner, edge and step, and high surface strain have significantly contributed to the change in the adsorption capability and in the interactions between the catalyst and the intermediates.[381,678] Making use of the properties such as small coordination number and high surface strain, Li *et al.* have proposed that the behaviour of a Ag catalyst can be modified in order to enhance the HER performance.[659] They demonstrated that a laser ablation technique allows the formation of multiple stacking faults in the Ag NPs, whereby hot Ag nanodroplets are produced and then quenched to cool liquid (L-Ag NPs), resulting in

low CN and high tensile strain. The L-Ag NPs manifested a low overpotential of ~32 mV at a current density of 10 mA cm^{-2} and 31 mV per decade (dec) of Tafel slope in an aqueous acid electrolyte. Also, L-Ag NPs exhibited 160 h long-term operational stability. Similarly, Kang *et al.* have synthesized Ag NPs for HER with different sizes *via* laser ablation in a liquid process.[679] In another report, Ag NPs were deposited on a carbon fiber with higher purity, and a clean surface was prepared *via* the spark ablation in gas method for HER.[660]

Apart from these reports, some other interesting protocols such as nanoporous Ag foam,[661] Ag/WO$_{3-x}$ heterostructures,[680] Ag/Au NP-supported MoS$_2$ (1T-MoS$_2$@ Ag/AuNPs),[681] heterogeneous Ag$_x$Ni$_{1-x}$ alloy nanocrystal,[682] and SiO$_2$–Ag^0 NPs[683] have been also proposed for the electrochemical production of hydrogen. Based on the above-mentioned protocols, it can be concluded that the laser ablation technique is particularly useful for producing stacking faults in metal NPs. This strategy can be useful for preparing other transition metal-based NPs for various applications.

4.3.2. Oxygen evolution reactions (OER).—The OER is an anodic reaction that involves a four-electron/four-proton transfer pathway, which is a very energy-intensive step in the electrochemical water oxidation reaction.[677] In electrochemical energy conversion and storage devices like alkaline fuel cells and metal–air batteries, the OER plays a crucial role.[684,685] To date, several noble and non-noble metal-based electrocatalysts have been reported for the OER,[686–690] among which Ag NMs exhibited good electrocatalytic performance towards the electrochemical OER due to their high activity, better tolerance, long term operational stability, and longer performance.[691]

Ag nanocomposite catalysts have emerged as promising materials for the electrocatalytic OER owing to the synergistic benefits arising from the combination of two or more distinct materials. Hou *et al.* have reported a heterogeneous Ag@Co$_x$P core@shell-type nanoelectrocatalyst for the OER.[692] *In situ* growth of transition-metal phosphides on a Ag seed created Ag@Co$_x$P core–shell nanostructures, which involved the formation of Ag seeds, growth of the Co shell, and subsequent phosphating. TEM and HRTEM images revealed a spherical morphology of the NPs and lattice fringes of the (111) facets of the metallic Ag in the core. The surrounding Co$_x$P shell was built around the distinctive Ag core structure, which resulted in strong electronic interactions between the Co and the Ag (Fig. 36a–c). Such a nanostructured core–shell Ag@Co$_x$P electrocatalyst exhibited high electrocatalytic OER performance at a small overpotential of 310 mV with a current density of 10 mA cm^{-2} and long-term catalytic stability. Furthermore, Ag@Co$_x$P nanocomposites showed eight times higher catalytic activity than pure Co$_2$P NPs (Fig. 36d–g).

Multifunctional Ag NPs supported on a reduced graphene oxide (rGO)-coated MIL-88B(Fe) hybrid (AgNP@rGO/MIL-88B (Fe)) electrocatalyst was reported by Acharya and co-workers[693] exhibited lower overpotential along with improved activity and stability for the OER under environmentally benign conditions. The glassy carbon (GC) electrode modified with a Ag NPs@rGO/MIL-88B (Fe) hybrid manifested higher OER activity at ~395 mV of overpotential and 1 mA cm^{-2} of current density at neutral pH. Such a Ag catalyst exhibited 30-day operational stability with only 2.6% deviation, compared to the first run. The electric conductivity of the electrocatalyst successively boosted the OER

performance. Geng and co-workers have synthesized $Co(OH)_2$ nanosheets decorated with Ag NPs by a selective reduction–oxidation process for the OER.[694] The Ag NPs were uniformly dispersed on $Co(OH)_2$ nanosheets, as verified by TEM images (Fig. 37a and b). The doping of Ag into the $Co(OH)_2$ nanosheets enhanced the electrical conductivity. The $Co(OH)_2$ nanosheets were decorated with loadings of Ag ranging from 0 to 20%. A 10% Ag-decorated $Co(OH)_2$ nanocomposite exhibited a higher OER performance, as tested through linear sweep voltammetry (LSV) with the scan rate of 5 mV s^{-1}. Based on these results, it should be noted that higher Ag loadings decreased the catalyst performance, and after the addition of Ag, the overpotential decreased. The overpotential of the Ag-decorated $Co(OH)_2$ nanosheets was as low as 270 mV at current density of 10 mA/cm^2 due to the synergistic benefits of the high electrical conductivity and the catalytic active surfaces (Fig. 37c–f).

In addition, Yu *et al.* have reported a mesoporous Ag–Co oxide nanocomposite for the OER.[695] They demonstrated that the decoration of Ag on the Co_3O_4 matrix enhanced the OER performance two-fold. The mixture of 88 wt% Co_3O_4 and 12 wt% metallic Ag was used for the synthesis of Co_8Ag oxide. A hard templating technique, *i.e.* the nanocasting route, was employed for the incorporation of metallic Ag NPs and Ag_2O clusters into mesostructured Co_3O_4. The HR-SEM and elemental mapping revealed that Ag occurred in the form of metallic Ag NPs and well-dispersed Ag_2O nanoclusters within the ordered Co_3O_4 mesostructure (Fig. 38a and b). Due to the synergistic benefits of two different Ag species (metallic Ag NPs and Ag_2O clusters) in Ag–Co oxide, the electrocatalyst demonstrated high OER performance at a lower overpotential of 376 mV at a current density of 10 mA cm^{-2}, compared with pristine Co_3O_4. It was noted that the Fe impurities from the KOH electrolyte were absorbed by ultra-small Ag_2O clusters, which increased the catalytic ability of Co–Ag oxides as well as their electronic conductivity (Fig. 38c–e).

Recently, a very interesting protocol based on homogeneous dispersion of Ag NP clusters on metal oxide was reported by Zhang *et al.*[696] A spontaneous redox reaction was incorporated for the synthesis of $Co(OH)_2$ nanohybrid-supported Ag NPs (Ag@$Co(OH)_x$) at room temperature, which was subsequently employed for electrocatalytic OER. Experimental and theoretical studies proved that the catalytically active sites for the OER *i.e.* Ag clusters, were activated by a strong electronic interaction between Ag and $Co(OH)_2$, ultimately playing a key role in maximizing the binding energies with the reacted intermediates, which helped to increase the OER rate. Similarly, bifunctional Ag/Co_3O_4 electrocatalysts[697] have been reported for electrochemical OER and ORR. Herein, the electrochemical analysis proved that the synergic effect between Ag and Co enhanced the catalytic activity by improving the reduction mechanism *via* breaking the O–O bond in the molecular oxygen quickly. Working on a similar basis, Chala *et al.* have reported nickel–ruthenium layered double hydroxide (NiRu-LDH) nanosheets decorated with Ag NPs (Ag NP/NiRu-LDH) for the OER and ORR under electrochemical conditions.[698] From these protocols, it could be inferred that the addition of transition metals to the metal oxides nanostructures significantly enhanced the catalytic performance by tuning the surface properties, and the electronic conductivity also increased the kinetics of the reaction. Very recently, Zhang *et al.* reported the single Ag atoms enclosed in an IrO_2 matrix, *i.e.* an Ag_1/IrO_x single atom catalyst (SAC) for

electrochemical OER.[699] Ag-based SACs demonstrated the low overpotential of 224 mV at 10 mA cm^{-2} of current density with long term operational stability.

4.3.3. Oxygen reduction reaction (ORR).—The ORR has been recognized as one of the most important electrochemical transformations in electrochemistry, and is widely used in energy conversion and storage devices such as fuel cells and metal–air batteries.[82,700,701] In comparison with the well-known Pt-based catalysts, Ag-based catalysts have been identified over the last decade as one of the most promising candidates for ORR catalysis because of their low cost, abundance, and relatively high ORR stability in an alkaline environment.[702–706] Nanostructured Ag is a promising substitute for precious metals in electrocatalytic ORR because it has a similar mechanistic pathway and reaction kinetics.[637,701] Ag is more resistant to methanol poisoning than Pt, and it quickly decomposes hydroxide ions, forming peroxides, which can cause membrane degradation. Although no single metal can catalyze the ORR nor Pt, it has been proposed that by alloying Ag with other metals, Ag's high overpotential may be minimized.[637] Ag NPs demonstrated high catalytic efficiency and stability towards the electrochemical reduction of oxygen in the alkaline electrolyzer.[707–709] Ag-based catalytic systems are not only highly active towards ORR,[710] but also exhibit higher performance in anion exchange membrane fuel cells (AEMFCs).[701,711] In fact, the Ag-catalyzed electrochemical ORR testing started decades ago. Interestingly, a two-electron or four-electron transfer pathway to ORR regulated by the surface state, *i.e.* oxidation state and electrode potential, was demonstrated by Shumilova *et al.*[712] The oxygen adsorbed on the surface of Ag was directly converted to OH$^-$ as this reduces the formation of hydrogen peroxide at anodic polarization.[82] It is quite evident from literature that the structure, shape, and size of nanocomposites play a vital role in electrochemical ORR.[713,714] For instance, Cleve *et al.*[715] reported that cubical nanosilver had slightly higher catalytic efficiency than spherical NPs for ORR in an alkaline solution. Chen and co-workers have reported 'surface-clean' Ag nanoclusters supported on carbon nanodots for ORR through a four-electron pathway.[716] In comparison with carbon nanodots, the hybrid Ag nanoclusters showed blue fluorescence, which can be employed in fluorescence-related areas.

In recent years, metal oxides and carbon-supported transition metal oxides have been employed as electrocatalysts for the ORR.[717] Literature reports reveal that the incorporation of inexpensive metals into transition metal oxide-supported carbon carriers has significantly enhanced the electrocatalytic ORR performance.[233,718–720] It has been proved that the synergism between metal oxides and Ag NPs resulted in an efficient catalysis of the electrochemical ORR due to strong electronic conductivity and upshift of the d-band centre.[721–724] Liu *et al.* have reported a three-phase hybrid nanocomposite, *i.e.* Ag and trimanganese tetraoxide (Mn$_3$O$_4$), embedded on a carbon-supported (Ag–Mn$_3$O$_4$/C) nanocatalyst for the ORR.[725] AgNO$_3$ and Mn(NO$_3$)$_2$ were used as precursors for the synthesis of a nanostructured Ag–Mn$_3$O$_4$/C hybrid. At higher temperatures, Ag and Mn$_3$O$_4$ nanocrystals were covalently coupled with a carbon support through a thermal decomposition process. Ag and the Mn$_3$O$_4$ NPs, very closely situated on a carbon matrix, enhanced the 'particle-to-particle' electronic interactions over the supported conductive carbon channels.[725] From these catalysts Ag–Mn$_3$O$_4$/C, blend (obtained by simple mixing

of Ag/C and Mn_3O_4/C), and Ag/C, the Ag–Mn_3O_4/C hydride catalyst exhibited high ORR efficiency. An onset potential of –0.15 V and 0.445 mA cm^{-2} of the ORR current density was recorded using the hybrid Ag–Mn_3O_4/C catalyst, which was ~4 times higher than when the blend and Ag/C were used (Fig. 39). The enhancement in the ORR performance could be attributed to the particle-to-particle ligand and ensemble effects between the Ag and the Mn_3O_4 phases, which resulted in higher electrocatalytic activity and long-term operational stability of the catalyst. Apart from the electrocatalytic oxygen reduction applications, the Ag–Mn_3O_4/C hydride nanocomposite was also employed for H_2O_2 degradation. Similarly, Lee *et al.* have reported reduced graphene oxide (rGO)-supported Ag and manganese dioxide (MnO_2)-deposited porous-like (rGO/MnO_2/Ag) catalysts for the ORR in an alkaline fuel cell.[726] The rGO/MnO_2/Ag cathode catalyst was prepared by an electrochemical deposition method. The synthesized cathode catalyst exhibited 1.2 times higher current density as well as an excellent electron transfer rate at 0.3 V per O_2, compared with 20 wt% Pt/C. Ryu *et al.* reported the metal seed-mediated growth method for the synthesis of Ag NP-mediated Ag–MnO_x nanoplates *via* incorporation of Ag atom on a plate-like MnO_x for electrochemical ORR.[727]

To date, several bimetallic non-noble metal based catalysts have been reported for electrocatalytic ORR, showing high selectivity and activity.[728,729] Lee and co-workers have reported bimetallic Ag-doped Fe mesoporous carbon nanofibers (FeAg-CNFs) for the electrochemical reduction of oxygen.[730] The pore structure and electrical conductivity/ active sites of FeAg-CNFs were enhanced artificially *via* the activation of FeAg-CNFs with water vapour denoted as A-FeAg-CNFs. The FeAg-CNFs synthesized by a simple electrospinning method followed by pyrolysis manifested a quasispheroidal morphology. From these catalysts, *i.e.* Fe-CNF, Ag-CNF, 20% Pt/C, and the binary A-FeAg-CNF catalyst, the activated FeAg-CNF exhibited the highest oxygen reduction efficiency during electrochemical conversion. The cyclic voltammetry demonstrated that the scan rate of 5 mV s^{-1} in an alkaline electrolyzer along with the high current density and large surface area (529.21 m^2 g^{-1}) could be attributed to the improved pore structures. The enhancement in the pore structures and electronic conductivity was a result of the water vapour activation, which led to excellent electrocatalytic ORR efficiency along with long-term operational stability (10 000 cycles).[730]

Among the wide-ranging NMs, Janus NPs represent a class of materials having two distinct chemical hemispheres, which are utilized for directional functionalization and controlled assembly.[731] The availability of structurally asymmetric Janus particles offers a unique and effective platform for NP engineering and functionalization on such a large scale that was previously unimaginable. This was demonstrated by a recent study in which bimetallic Janus NPs were prepared using an interfacial engineering method, resulting in an exceptional oxygen reduction electrocatalytic operation.[732] Song *et al.* have reported bimetallic nanosized AgAu Janus particles for electrocatalytic ORR.[732] Hexanethiolate-passivated Ag NPs were used as a precursor for the synthesis of AgAu Janus NPs *via* a galvanic exchange reaction. Low Au loadings (5%) in nanosized Ag Janus NPs exhibited high performance for the electrocatalytic reduction of oxygen. The area-specific kinetic current density at +0.68 V *vs.* RHE was calculated to be 8.75 A m^{-2} for the evenly mixed particles and 40.64 A m^{-2} for the Janus NPs. In comparison with bulk Ag and

monometallic Ag NPs, bimetallic AgAu Janus NPs exhibited 7 and 6 times higher area and mass-specific current densities respectively. A polar hydrophobic hexanethiolate ligand enhanced the moment of electron transfer from Ag to Au, consequently improving the adsorption and reduction of oxygen. Similarly, Au core@Ag semishell Janus NPs obtained using chemical etching in air/water interface has also been utilized for ORR.[733] Herein, a Ag shell was chemically deposited on Au seed colloids, followed by the self-assembly of 1-dodecanethiol onto the NP's surface to produce Au@Ag core–shell NPs. The core–shell NPs were chemically etched by using a mixture of hydrogen peroxide (H_2O_2) and ammonia (NH_3) in the subphase of water, which selectively produced Au@Ag semishell Janus NPs. A value of 633 A g^{-1} as mass-specific kinetic current density was demonstrated by Au@Ag semishell Janus NPs, this being 4.8 and 45 times higher than the value of Au@Ag and Ag@Au core–shell NPs, respectively. These Ag/Au bimetallic Janus NPs exhibited a higher electrocatalytic ORR performance due to the synergistic effect of the Au cores and the Ag semi shells, which resulted in a number of electron transfers and optimized oxygen bindings.

The tuning of Ag with other transition metals such as Fe, Cu, and Co has been also manifested in higher ORR efficiency.[725,734] These binary Ag-based alloys exhibit excellent electronic properties, high stability, acceptable ORR performance under alkaline conditions, and are relatively low cost, which further enhance their use in metal–air batteries. Miller *et al.* have reported nanostructured Fe–Ag electrocatalysts for ORR in alkaline electrolyzer involving a 4-electron pathway.[735] The Fe(II) and Ag(II) phthalocyanines (Pc) were directly adsorbed on the obtained bimetallic FeAgPc/C on Ketjen Black (C), which was followed by heat treatment in an inert atmosphere. The FeAgPc/C(600) exhibited higher ORR activity with a limiting current at 0.88 V (*vs.* RHE) of *ca.* 18 A g_{cat}^{-1}, compared to the monometallic AgPc/C(600) and FePc/C(600) nanocomposites at room temperature. A specific nanostructure formed during the heat treatment, which consisted of very finely distributed Ag NPs and Fe–N_4 moieties, resulting in an improved ORR performance and stability thanks to the synergistic Ag–Fe interaction. It was stated that by forming alloys or bimetallic materials with cobalt (Co), the ORR behaviour of Ag-based electrocatalysts could be significantly improved.[706] Materials based on mixed Ag and Co can bind oxygen-containing species more strongly than only pure Ag because Co exhibits stronger binding affinity to oxygen.[736,737] Thus, the AgCo bimetallic composite nanotubes were employed for the ORR.[738] Electrospinning and subsequent thermal annealing in the air were used to make cobalt oxide (Co_3O_4) nanotubes. Subsequently, the AgCo composite nanotubes were formed by a galvanic replacement reaction (GRR) between the Co nanotubes and the Ag precursor. The binary Ag/Co nanotubes were prepared with varying reduction and GRR times. Among them, the AgCo composite nanotubes synthesized through 1 h reduction and 3 h GRR gave the best ORR performance, based on positive onset potential, the greatest limiting current density, and the highest number of electrons transferred. Also, this bimetallic composite manifested high ethanol tolerance, compared with a Pt/C catalyst.[738] Similarly, Ag–Co/C catalysts,[739] Ag/Co_3O_4 catalysts,[697] bimetallic Co@Ag NPs encapsulated in nitrogen-rich graphene layers,[740] and Co flower-decorated Ag nanotrees[741] have been reported to exhibit higher ORR performance in fuel cells and metal–air batteries. In addition to this, various Ag-based bimetallic NMs such as Pt–Ag nanocages,[742] Ag–Pt nanodisks,[734] or Ag–Cu electrocatalysts,[743] have been recently utilized

in the electrocatalytic ORR for the conversion of energy and storage devices such as alkaline fuel cells and metal–air batteries.[82,734,744–747]

Recently core–shell nanostructures with graphene and N-doped graphene have attracted considerable attention of the scientific community, thanks to their fascinating properties such as superior electronic conductivity, high stability at adverse reaction conditions or low cost for various organic, photo, and electrocatalytic applications.[329,748–751] In view of this, Sekol *et al.* have reported that the Ag–Pd core–shell catalysts assisted on multiwalled carbon nanotubes (Ag@Pd/MWNTs) are highly active for the ORR in alkaline media (Fig. 40a).[752] The Ag@Pd core–shell structures, uniformly dispersed on the surface of the MWNTs, were revealed by TEM images (Fig. 40b and c). The Ag@Pd/MWNTs demonstrated high tolerance to the presence of methanol and ethanol in the electrolyte. The Ag@Pd/MWNT current density decreased by 0.18 mA cm^{-2} and 0.12 mA cm^{-2} for methanol and ethanol respectively, as compared to Pt/C and Pd/C. After durability testing in ethanol, the Ag@Pd/MWNTs exhibited long-term operational stability and showed 3.5-fold enhancement in mass activity, compared to that of regular Pd/C (Fig. 40d and e).

In addition to this, Chen and co-workers have prepared Ag–Co NPs core and nitrogen (N)-doped carbon shells by encapsulating Co@Ag bimetallic NPs into a N-doped graphene (Co@Ag@NC) *via* Ag-doped metal–organic framework (MOF) pyrolysis.[740] Co@Ag@NCs were employed for the electrochemical reduction of oxygen under alkaline conditions. The core–shell nanostructures showed high methanol tolerance; it is also interesting to note that the carbon layers prevented the catalyst from being corroded, thus consequently enhancing the operational stability (up to 5000 cycles) of the electrolytic cell. Computational studies revealed that the Ag 'mantle'-tuned electronic structures of carbon atoms near to nitrogen dopants in Co@Ag@NC were accountable for the active catalytic sites, thus giving a high ORR performance.[740] Because of the weak adsorption of oxygenated species at the electroneutral carbon site, graphene with an intrinsic sp^2-conjugated carbon structure is inactive towards the ORR.[753] Over decades, extra effort has been invested in increasing the ORR activity. Heteroatom doping undeniably stands out as one of the most successful strategies reported for raising the electrocatalytic ORR performance in fuel cells and metal–air batteries.[701,740,753–755] Jin *et al.* have reported Ag nanoclusters anchored on N-doped graphene (AgNC/NG) for electrocatalytic ORR.[756] Single-stranded oligo-nucleotide sequences (ssDNA) were used as the template for the synthesis of AgNC/NG following an electrochemical reduction technique. AgNC/NG exhibited high electrocatalytic ORR efficiency due to the high onset potential, half-wave potential as well as mass activity, compared to Pt/C. AgNC/NG displayed high methanol tolerance and long-term operational stability (8000 cycles) in the electrochemical reduction of oxygen. The high electrocatalytic ORR performance was possible to achieve because of the Ag–N bonding,[757] where the Ag bonded with N-doped graphene altered the electronic structure of the N-doped graphene. Similarly, Lopes *et al.* have demonstrated the homogeneous deposition of Ag NPs on graphene (GRn/Ag) *via* a potentiostatic double-pulse technique.[758] The prepared GRn/Ag nanocatalyst exhibited high ORR performance thanks to the superior ionic and electronic conductivity. The electrochemical exfoliation of graphite yielded GRn sheets with high yield and purity as well as a low degree of oxidation, as a result of which these sheets were efficiently utilized as a support for the decoration of Ag

NPs. With the help of a potentiostatic double-pulse technique, a controllable size of Ag NPs was possible to prepare. In another report, Ag NPs embedded in N-doped graphitized carbon shells (Ag@NCs) were demonstrated for the electrocatalytic ORR.[753] A N-doped carbon-supported Ag core–shell catalyst exhibited high ORR activity with 906 mV of half-wave potential and a limited current density value of 6.10 mA cm^{-2} in the alkaline electrolyzer. Strikingly, this has been the highest catalytic performance reported for the ORR to date. According to a computational study, the Ag core transferred 0.0572 electrons to the carbon sites of Ag@4C, and these transferred electrons tuned the electron occupancy of carbon sites, further raising the catalytic activity. Apart from the above highly efficient protocols, there are many Ag-supported carbon materials reported for the electrocatalytic reduction of oxygen in alkaline media such as silver nanonet-supported graphene nanohybrid,[759] graphene supported Ag–Fe/C_3N_4,[760] *etc.*

Metal oxides such as manganese oxide (MnO_2) have gained significance as highly efficient electrocatalysts,[761] in view of their promising performance, environmental compatibility, and low cost. Further to this, the incorporation of transition metals like Ag into these oxides has been recognized as a key strategy for improving the electrocatalytic efficiency.[724,762] In view of the superb features of metal oxide-supported single-atom electrocatalysts, Sun and co-workers demonstrated the synthesis of atomically dispersed Ag atoms adsorbed on MnO_2 nanowires (Ag–MnO_2) *via* a single-step hydrothermal process.[763] Ag–MnO_2 SAC was simultaneously employed for the ORR and OER. The fascinating physicochemical properties of Ag–MnO_2 enhanced the electrocatalytic efficiency towards the ORR and OER. Ag–MnO_2 exhibited a higher ORR performance than α-MnO_2 with an onset potential of 0.95 V and 0.81 V *vs.* RHE, respectively. The OER polarization curves also revealed that Ag–MnO_2 displayed a higher overpotential of ~80 mV in order to achieve 10 mA cm^{-2} energy, compared with the commercial IrO_2 (Fig. 41a and b). Chronoamperometric tests also indicated that the Ag–MnO_2 showed greater operational durability for the OER than MnO_2. The Ag–MnO_2 based zinc air battery (ZAB) demonstrated an energy density value of 915.4 Wh kg$_{Zn}$$^{-1}$, a high discharge peak power of 273.2 mW cm^{-2}, and a higher rate performance. Ag–MnO_2 manifested 164.0 mA cm^{-2} of current density at 1 V (*vs.* Zn); however, 10 wt% Pt/C exhibited 133.2 mA cm^{-2} of current density at a similar voltage. The ZAB showed long-term operational stability for more than 3200 cycles of charge–discharge (Fig. 41c–f). The promoted crystal phase transition from α-MnO_2 to δ-MnO_2, which is advantageous for the OER due to the existence of atomic Ag, can be attributed to the excellent rechargeability. The isolated Ag atoms incorporated into MnO_2 surfaces increased the electrical conductivity, surface oxygen vacancies, and lattice distortion, which were altogether responsible for the high electrocatalytic activity of Ag–MnO_2.

Apart from the interesting above-mentioned Ag-based electrocatalyst, several other Ag NMs like bimetallic Ag–Co alloy catalysts,[764] silver-graphene nanoribbons,[765] Ag–Cu electrocatalyst,[743] AgCl nanowires,[766] and AgCl–Ag@AgCl NWs,[767] have been reported for the electrochemical ORR. In a recent study, Xu *et al.* demonstrated the solution-phase synthesis of bifunctional Ag-based multi-elemental NPs, *i.e.* Ag–Ni–Fe–P MENPs,[768] and Wang *et al.* prepared Ag/Ag_2O NPs supported on a metallo-covalent organic framework (Ag/Ag_2O@MCOF(Co)) *via* a simple encapsulation process,[769] for electrocatalytic OER and ORR.

4.3.4. CO_2 reduction reaction.

—Rising urbanization and industrial revolution with the ever-increasing global warming poses a serious threat to the environment. CO_2 has been identified as one of the major contributors to the greenhouse effect and therefore its sequestration has become a necessity. As a consequence, the scientific community has been directing its efforts towards the catalytic conversion of CO_2 to liquid fuels and chemical feedstock as a future energy source.[770,771] The utilization of renewable electricity for the electrochemical conversion of CO_2 to C_1/C_2 products such as carbon monoxide, formic acid, methanol, methane, ethanol, and ethylene is one of the thriving fields.[772–775] Silver is one of the interesting electrocatalysts, in view of its ability to stimulate electrochemical conversion of CO_2 to CO at room temperature.[85] Shao and colleagues recently revealed a rapid operando X-ray absorption spectroscopy (XAS) approach for tracking the composition and structure evolution of a Ag_2O precatalyst for electrochemical reduction of CO_2.[776] The prepared Ag-D (Ag nanocrystals with rich defects) catalyst exhibited a nearly 100% FE for conversion of CO_2 to CO at an overpotential of 0.7 V in an H-cell reactor along with a very trace amount of degradation efficiency in 120 h.

From all noble and non-noble metals, silver has been identified as the best metal for the CO production through electrocatalytic CO_2RR (EC-CO_2RR) with 81.5% of FE at −1.14 V in an aqueous medium, this being pioneered by Hori *et al.*[777] Tremendous development has been made over the past two decades in the arena of nano-Ag electrocatalysts as Ag NMs with high surface area provide abundant active sites and well-defined shapes, which further promotes the electrocatalytic efficiency to the maximum reported to date.[778] In this context, Masel and co-workers demonstrated that the electrocatalytic performance of a Ag catalyst directly depends on the size of the Ag NPs.[779] They reported a ten times higher electrochemical conversion of CO_2 to CO catalyzed by Ag NPs (5 nm) than by a bulk Ag catalyst. Kenis and co-workers have reported Ag NPs supported on titanium dioxide (Ag/TiO_2) for the electrocatalytic reduction of CO_2 to CO.[780] They prepared an array of Ag/TiO_2 catalysts with different % of Ag loadings on TiO_2 and 40% Ag supported on carbon black, among which the 40% Ag/TiO_2 catalyst exhibited higher CO production in an electrochemical flow reactor[781] through EC-CO_2RR.

Over the last decade, various methodologies have been developed for the synthesis of Ag NPs with reduced sizes as it plays a key role in the electrocatalytic CO_2 reduction.[782] Hwang and co-workers[783] have prepared three different sizes (3, 5, and 10 nm, respectively) of immobilized Ag NPs dispersed on carbon (nanosized Ag/C) *via* a direct one-pot synthesis process where cysteamine was utilized as an anchoring agent. The designed nanosized Ag/C showed good potential for CO production from electrochemical CO_2RR in an aqueous electrolyte. Among the prepared samples, 5 nm Ag particles exhibited high electrocatalytic activity and FE of 84.4% with long-term operational stability towards electrochemical CO_2 reduction. In comparison with Ag foil, nanosized Ag/C (5 nm) exhibited low overpotential, *i.e.* 300 mV, at a current density of 1 mA cm^{-2}. The interaction of Ag–S occurred due to the anchoring agent, *i.e.* cysteamine. Computational studies proved that the Ag–S interactions developed after anchoring cysteamine created surface localization of the unpaired electrons, which further stabilized the intermediates and helped to achieve high catalytic efficiency during the electrocatalytic CO_2 reduction process.

To overcome the hydrogen evolution side reaction during the CO_2 electrolysis, substantially high overpotential is required.[784] Thus, in order to reduce the co-evolution of hydrogen, Hsieh *et al.* have reported coral-like Ag nanostructures with high surface area for selective CO production from electrochemical CO_2 reduction at adequate overpotential.[785] A Ag nanocoral-based electrocatalyst was synthesized by the oxidation–reduction process in the presence of aqueous chloride anions, which exhibited 95% of current efficiency at 0.37 V of overpotential. Furthermore, this coral-like Ag nanostructure exhibited a 32 times higher catalytic efficiency related to a normalized surface area along with 0.49 V overpotential than its Ag metallic foil. The high electrocatalytic activity of Ag nanocorals was attributed to the adsorbed chloride ions on the surface of the catalyst, leading to higher surface area. The adsorbed chloride anions enhanced the electroreduction of CO_2 and reduced the hydrogen evolution. Apart from the above-mentioned protocol, several research groups proved that organic molecules adsorbed on Ag NPs significantly reduce hydrogen evolution and enhance CO production *via* the electrocatalytic reduction of CO_2.[783,786,787] In this context, Kim *et al.* have synthesized Ag NPs coated with organic molecules through a surface-capping precursor for the EC-CO_2RR.[787] Oleylamine, oleic acid, and dodecanethiol were the three different surface-capping agents used for the coating of Ag NPs with an amine, carboxyl, and thiol functionality, respectively.

Abeyweera *et al.* have reported porous Ag nanostructures with highly active surface area for the formation of CO *via* the EC-CO_2 RR.[788] Ag benzenethiolate nanoboxes, electrochemically reduced to porous Ag nanostructures, enhanced the electrocatalytic efficiency, *i.e.* nearly 100% FE for the CO production. Benzenethiolate ions readsorbed on the Ag surface enhanced the cathodic potentials and suppressed the hydrogen evolution pathway. SEM and TEM images revealed that the porous Ag nanostructures, having a box-like nanocage morphology in the pore size of 10 nm, were interconnected by ligaments (Fig. 42a and b). They demonstrated an electrocatalytic performance of a 3D porous Ag nanostructure in a H-type cell for the electrochemical reduction of CO_2, which showed high FE (96%) along with specific current density (6.0 mA cm^{-2}) at −1.03 V (*vs.* RHE) electrode potential (Fig. 42c). The large surface area of the porous Ag nanostructures was attributed to smaller pores and larger hollows, which enhanced the abundant active sites that were responsible for fast diffusion of the reactant and product during the electrochemical reduction of CO_2 from the surface of Ag. The Ag nanostructures exhibited a high mass-specific current density of 502 A g^{-1} for CO production at an increased cathodic potential (Fig. 42d).

Silver nanowires (Ag-NWs) synthesized in a polyol solution exhibited good conductivity and excellent film formability and were therefore used for the preparation of a Ag NW-based electrode *via* a simple drop-casting technique, which enhanced the surface area of the electrocatalyst.[789] A Ag NW-based electrode was employed for the electrochemical reduction of CO_2 to CO (FE = 80%) and formic acid (FE = 2.6–5.6%) with the low working potential of −0.9 V *vs.* reversible hydrogen electrode (*vs.* RHE). On a similar basis, Broekmann and co-workers have reported Ag-NWs for the production of CO from the electrochemical reduction of CO_2.[790] Ag-NWs were synthesized by a PVP-assisted polyol synthetic protocol, where PVP served the purpose of a capping agent. The Ag-NWs were further deposited on a glassy carbon support and highly porous carbon support, which

enhanced the electrocatalytic performance of the bare Ag NWs. SEM images demonstrated that the three dimensional and loosely packed Ag NWs were uniformly distributed and embedded in both of the supports (Fig. 43a–d).

The synthesized Ag-NWs pre-treated by electrochemical looping exhibited 94% FE for the CO production. The PVP removal efficiency was enhanced due to the electrochemical activation treatments applied to the Ag-NW catalysts. The studies proved that the surface without chemisorbed chloride and PVP exhibited a higher EC-CO_2RR performance than the surface with chloride and PVP, as the latter shifted the selectivity towards the HER (Fig. 43e).

Nanomorphology can form high-index facets or edge active sites, which are then responsible for the adsorption and activation of CO_2, thus electrochemically enhancing the CO_2RR. In this context, Fan *et al*. have synthesized a sponge-like nanomorphology of Ag nanostructures (SPC-Ag) for EC-CO_2RR to CO.[791] Compared with commercial Ag NPs, SPC-Ag exhibited 93% of FE at −0.9 V *vs*. RHE (*versus* reversible hydrogen electrode) for CO production due to the high surface area and large number of active sites. Along with high electrocatalytic activity, SPC-Ag manifested long-term operation stability, *i.e.* 24 h at 0.79 V overpotential. In the past few years, many researchers have adopted the biosynthetic pathway, inspired from nature, for the development of Ag NMs. In this context, Mauzeroll and co-workers reported the Ag nanoring as an electrocatalyst for reduction of CO_2 to CO in the presence of CO_2 saturated $KHCO_3$ electrolyzer;[792] Ag nanorings fabricated on tobacco mosaic virus coat protein *via* a chemical reduction method exhibited 95.0% of CO FE with an 910 mV of overpotential. Gao and co-workers prepared $Pd_{1−x}Ag_x$ alloy NPs supported on activated carbon *via* a modified wet reduction method for the electrochemical reduction of CO_2 to CO.[793]

When the structure, morphology, and composition of bimetallic electrocatalysts are finely tuned, they can outperform monometallic equivalents in terms of operation and selectivity.[31,85,794,795] Thus, in order to enhance the performance of the electrochemical CO_2RR, on introduction of a second metal atom in the outer layer, the outer layer expands significantly and that will increase the activity and selectivity of bimetallic nanocomposites. In this regard, Chang *et al*. have reported a structure-controlled model for the synthesis of bimetallic Ag@Cu NPs by a polyol method.[794] A binary Ag@Cu nanocomposite was employed for the electrocatalytic reduction of CO_2. The architectonic characterization of Ag@Cu NPs verified that the surface was composed of an inner Ag core and an outer Cu shell. By further regulating the heating duration from 0 to 25 min, time-dependent bimetallic Ag/Cu NP samples, such as Ag@Cu-5, Ag@Cu-7, Ag@Cu-10, Ag@Cu-15, Ag@Cu-20, and Ag@Cu-25, were prepared. From these samples, Ag@Cu-7 and Ag@Cu-20 exhibited higher FEs towards CO and hydrocarbon, *i.e.* ethylene production. The Ag dominant Ag@Cu-7 NPs and the Cu dominant Ag@Cu-20 NPs significantly suppressed the hydrogen evolution and increased the activities for CO_2RR at a potential of −0.5 V. The Ag-based electrocatalyst exhibited higher selectivity for the production of CO, while the addition of Cu shifted the selectivity towards the hydrocarbon because of the 'dilution' effects between Ag and Cu. For these AgCu bimetallic electrocatalysts, the synergistic or dilution effect between Cu and Ag stems primarily from the component mixing patterns, which

play a key role in determining each catalyst's activity and selectivity. Wang *et al.* also demonstrated the ethylene production from the electrochemical reduction of CO_2 over the Ag–Cu bimetallic catalyst.[796] The sharp interface of the Ag and Cu components in the nanocomposite enhanced the selective formation of ethylene. They reported 42% of FE for the ethylene production, which was two times higher than was achieved by the pure Cu catalyst. In another study, Yeo and co-workers described that the surfaces of Ag NPs and the Cu–Ag boundaries on the surface of Cu–Ag nanostructures were responsible for ethanol production from the electrochemical reduction of CO_2.[797] The C–C coupling on Cu was facilitated by the easy CO availability at the Cu− + Ag boundaries, allowing selective ethanol formation. Moreover, by forming an additional bond with Cu, the Ag adatom on the Cu surface reduced the charge density. As a consequence, the surface binding energy of the CO intermediate increased.[798] A large number of biphasic Cu–Ag boundaries enhanced the migration of CO from the Ag active sites to Cu, and multicarbon product formation occurred. Ag is a CO-selective cocatalyst,[799] which combines with Cu and shifts the EC-CO_2RR to C_{2+} products.[794,798,800,801] Yang and co-workers have designed a tandem Cu–Ag-based catalytic architecture for a fast electrochemical reduction of CO_2 to higher oxygenates, *i.e.* C_2H_4, C_2H_5OH, and CH_3COOH, respectively[801]. A tandem Cu-Ag catalyst was prepared by physically mixing Cu and Ag nanopowders on a carbon paper support and was thereafter employed in gas diffusion flow cells. A variety of Cu–Ag tandem catalysts were synthesized with metal compositions x mg cm^{-2} Cu and y mg cm^{-2} Ag denoted as Cu_xAg_y ($Cu_{500}Ag_{1000}$, Cu_{500}, Ag_{1000}, *etc.*). Among them, the $Cu_{500}Ag_{1000}$ catalyst exhibited high FEs, and the current density of C_2H_4, C_2H_5OH, and CH_3COO^- product formation increased from 37 to 160 mA cm^{-2} at –0.70 V vs RHE after the addition of Ag to the Cu matrix (Fig. 44).[801] Chang *et al.* illustrated a two-step process for the preparation of a Ag nanowire coated CuO_x layer with varying thicknesses for ethanol production *via* EC-CO_2RR.[802]

Working on a similar basis, other Ag-based bimetallic NMs such as AgIn dendrites,[803] Cu dots on Ag,[804] a AgCo surface alloy,[805] Ag-decorated Cu,[806] a bifunctional Cu/Ag layered catalyst,[798] Cu–Ag core–shell NPs,[807] a mixed-metal oxide catalyst, *i.e.* $Ag_2Cu_2O_3$,[808] and Ag@ZnO@rGO electrocatalysts,[809] were also reported for the production of hydrocarbons and liquid fuels from the CO_2RR. From the above-reported protocols, it can be predicted that the synergistic effects between the Ag NPs and the other components can be used to tailor and boost the activity, stability, and selectivity of the active catalysts while simultaneously lowering the overall cost. Besides, the size, shape, and physico-chemical properties of Ag-based nanocomposites are also important for tuning and promoting their catalytic properties.

Investigations on Ag-based nanocatalysts, have revealed that on decreasing the size of NPs to isolated single atoms (below 5 nm), described as single-atom catalysts (SACs), considerable enhancement in surface area is observed which further raises the maximum atom utilization efficiency.[532,810] However, due to the low stability of Ag SACs, very few atomically dispersed Ag-supported metal oxide catalysts have been reported to date.[437,763,811–814] Under these circumstances, Zhou and co-workers demonstrated an electrochemical reduction approach for the synthesis of single atoms and dual Ag atoms immobilized on graphene, *i.e.* a Ag_1 or a Ag_2-graphene (Ag_1 or Ag_2-G) catalyst.[815] Such

an atomically dispersed Ag-G catalyst was employed for the production of CO from the electrochemical reduction of CO_2. TEM and AC and enlarged high-angle annular dark-field scanning transmission electron microscopy (HAADF STEM) images revealed that the isolated monoatomic and diatomic Ag ions were uniformly dispersed on graphene surfaces (Fig. 45a–d). These findings indicated that the dual Ag atoms in the Ag_2-G catalyst and the single Ag atom in the Ag_1-G catalyst came from the initial binuclear and mononuclear Ag complexes, respectively, rather than from aggregation or separation during the preparation phase. Out of the two catalysts, Ag_2-G exhibited high electrocatalytic efficiency at −0.7 V potential for the electroreduction of CO_2 to CO with up to 90% FE with an 11.87 mA cm^{-2} current density in 36 h (Fig. 45e–g). The active site was made up of two neighbouring silver atoms, which coordinated with three nitrogen atoms each, and the AgN_3–AgN_3 sites were securely anchored on the graphene matrix thanks to the formation of Ag–C bonds. Computational studies revealed that the two adjacent Ag atoms bound with C and O and enhanced the adsorption of CO_2 by reducing the energy barrier to the formation of an *COOH intermediate, which subsequently reduced to CO (Fig. 45h).

Very recently, more than 90% FE for the CO production (FE_{CO}) was achieved from the electrochemical reduction of CO_2, as reported by Zhang *et al.*[816] The isolated Ag_1 atom supported on a MnO_2 catalyst (Ag_1/MnO_2) was employed for the electrocatalytic CO_2RR. A simple thermal conversion of Ag NPs and a surface reconstruction of MnO_2 were performed to make a single-atom Ag catalyst. Among the prepared $AgNP/MnO_2$ and other Ag-based electrocatalysts, the atomically dispersed Ag_1/MnO_2 catalyst demonstrated superior CO_2RR catalytic efficiency, with 95.7% FE_{CO} at a potential of 0.85 V *vs.* RHE.[816] This catalyst showed long-term operation stability during the electrolysis of CO_2. DFT studies showed that only Ag_1 was the active site in Ag_1/MnO_2 for the CO_2RR. Furthermore, Ag_1 had high electronic density, which was similar to the Fermi level, resulting in lower energy barriers for the CO_2 adsorption and activation to form *COOH intermediates.

Apart from CO, formate or formic acid ($HCOO^-/HCOOH$) is also produced from the electrochemical reduction of CO_2, which is further deployed as a hydrogen carrier in fuel cells.[817] Formic acid is also used in direct formic acid fuel cells (DFAFC) as a clean and portable power source of energy *via* the electrooxidation of formic acid.[818] The Ag doping in transition metals such as Cu assists in achieving high selectivity for the production of C_2 liquid fuels from the $EC-CO_2RR$ by tuning the binding strength of reaction intermediates on the Cu surface.[819–821] In this regard, a Ag–Cu bimetallic nanocatalyst has been employed for the production of CO and formate from the electrocatalytical reduction of CO_2.[822] The Ag–Cu bimetallic sponge-like and coral-like bicontinuous porous structures with a change in composition (spongeous $Ag_{91}Cu_9$ and coralline $Ag_{65}Cu_{35}$, respectively) were synthesized by an electrochemical anodizing and a dealloying technique. Among them, spongeous $Ag_{91}Cu_9$ exhibited high selectivity for CO formation at 80.6% of FE and current density of 5.6 mA cm^{-2}, while coralline $Ag_{65}Cu_{35}$ yielded opposite results. The coralline $Ag_{65}Cu_{35}$ exhibited high selectivity for the production of formate with 91.8% of FE at a current density of 16.79 mA cm^{-2} (Fig. 46a–c). The Cu and Ag alloying enhanced the electronic properties thanks to the adsorbate–metal interaction,[823] compared with metallic Ag observed in calculated projected density of states. It has been revealed that as the Ag content decreases, the d-band centre moves upwards steadily, resulting in lowering the

efficiency of the CO_2 reduction (Fig. 46d). The large number of Ag–Cu (111) facets in the coralline $Ag_{65}Cu_{35}$ directed the most significant formate pathway, which was attributed to the synergistic effect of Ag and Cu, compared with spongeous $Ag_{91}Cu_9$ (Fig. 46e).

Over the last few decades, heteroatom-doped carbon nanomaterials have aroused great interest in the area of electrocatalytic reduction of CO_2 thanks to their low cost, high surface areas, reasonable chemical stability, and controllable doping of heteroatoms.[426,824,825] Among the range of heteroatoms embedded in N-doped graphene, carbon nitride has been employed in the EC-CO_2RR for the production of liquid fuels and hydrocarbons.[826,827] For the transformation of CO_2 to C_{2+} products, especially ethanol high overpotential and multiple proton-electron transfers are required. Ethanol has a higher industrial value since it is used as a transportation fuel and an alternative energy source in a fuel cell. The production of ethanol from the electroreduction of CO_2 with an inexpensive catalyst, *i.e.* Ag supported on a graphene-embedded N-doped carbon foam (Ag-G-NCF), was reported by Zhang and co-workers.[828] Among various catalysts such as NCF, G-NCF, Ag-NCF, and Ag-G-NCF, the Ag-G-NCF catalyst efficiently reduced CO_2 to ethanol with a maximum 85.2% FE of ethanol at an overpotential of −0.6 V (*vs.* RHE). Computational studies proved that the pyridinic N species of the Ag-G-NCF catalyst had a higher binding capacity against CO* intermediates than against other N species, and the Ag NPs eventually converted CO* to the OC–COH intermediate of ethanol. The high N content in the pyridinic architecture and the Ag NPs synergistically enhanced the electrocatalytic performance for CO_2RR to ethanol because of the hierarchical porous structure and good electronic conductivity.

Apart from the EC-CO_2RR, Wang *et al.* have reported CuAg electrocatalysts for acetaldehyde production from electrochemical CO reduction.[829] Along with the above-mentioned protocols for the CO_2RR, there are several Ag-based NMs such as TiO_2 supported Ag NPs,[780] $(Cu)_m(Ag)_n$ NPs,[830] sponge-like porous Ag nanocubes,[831] Ag NPs encapsulated MOFs,[832] MnO_2/Ag(111) nanocatalysts,[833] heterogeneous Ag/*tert*-GO catalysts,[449] Ag-alloyed Zn dendritic electrodes,[834] or nanoporous Ag electrocatalysts[835] which have demonstrated good potential for the production of liquid fuels and hydrocarbons from the EC-CO_2RR.

4.3.5.   Nitrogen reduction reaction (NRR).—Electrochemical NRR under an ambient atmosphere provides a novel route to producing carbon-free hydrogen sources.[836] Production of ammonia from NRR is a clean and sustainable approach that has received particular attention as a possible energy storage source and alternative vehicle fuel.[837,838] However, the catalytic selectivity and activity of NRR is still hampered by the slow reaction rate.[839] Electrocatalysts must be rationally designed in order to optimize the mass transport and to tune the chemical and physical properties alongside the proton/electron transfer, thus achieving a high electrochemical NRR performance and selectivity.[840] Among the range of non-noble metal-based electrocatalysts reported for the production of ammonia,[841] a Ag electrode catalyst demonstrated a high catalytic activity.[842,843] Sun and co-workers proved that Ag nanosheets exhibited high NRR activity for ammonia production under room temperature and pressure.[843] Such a Ag-based electrocatalyst demonstrated 4.8% of FE with an NH_3 yield rate of 4.62×10^{-11} mol s^{-1} cm^{-2} at an overpotential of −0.60 V *vs.* RHE. To overcome the sluggish kinetics of the NRR, Nazemi *et al.* have reported bimetallic Au–Ag

nanocages with tuneable localized surface plasmon resonance (LSPR) peak positions for ammonia production *via* an electrocatalytic NRR.[643] The addition of Ag NPs alters the size and density of the pores in the walls, the corners of porous Au–Ag nanocages, and the position of the LSPR peak from 635 to 715 nm is redshifted. The galvanic replacement process was utilized for the synthesis of porous Au–Ag bimetallic nanocages, followed by oxygen treatment at 644 and 719 nm of the LSPR peak positions, as a result of which the nanocages transformed into Ag_2O–Au nanocages (Ag_2O–Au-644 and Ag_2O–Au-719) (Fig. 47a–d). Out of the two bimetallic nanocages, Ag_2O–Au-719 demonstrated slightly higher electrocatalytic NRR efficiency with a NH_3 yield rate of 2.14 µg cm^{-2} h^{-1}, and 23.4% of FE was obtained at −0.4 V *vs.* RHE (Fig. 47e and f). In another report, Li *et al.* prepared boron-doped Ag nanosponges (B-Ag NSs) *via* a reduction reaction for electrocatalytic nitrogen reduction to ammonia.[844]

4.3.6.   Miscellaneous reactions.—Alcohol oxidation reactions consisting of electrocatalytic methanol and ethanol oxidation reactions (MOR and EOR) are widely utilized in fuel cells for the production of energy.[845–848] Tao and co-workers have synthesized open-mouthed yolk–shell Au@AgPd NPs (OM-YS Au@AgPd NPs) for electrocatalytic EOR through a galvanic replacement process at room temperature.[849] In this yolk–shell catalyst, Au cores were encapsulated in a AgPd NP shell with a single opening. The OM-YS Au@AgPd NPs demonstrated high EOR efficiency with a 1.25 A mg_{Pd}^{-1} of mass activity and 87.8 m^2 g^{-1} of the electrochemically active surface area along with long-term stability. Zhang *et al.* reported BH_4^--capped Pd_xAg_y NPs for the EOR.[850] The colloidally prepared Pd_xAg_y NPs reduced the energy barrier during the electro-oxidation of ethanol and enhanced the electrocatalytic activity of the catalyst; however, the surface ligands reduced the oxidation potentials and increased the exchange current densities. Very recently, Zhang *et al.* reported the Pd-rich phase on Au–Ag alloy NWs *i.e.* Au–Ag–Pd alloy NWs for the electrochemical oxidation of biomass-derived alcohols such as ethanol, glycerol, and ethylene glycol.[851]

A Au/Ag NP system was prepared for the electro-oxidation of methanol *via* microwave-assisted irradiation at two hydrothermal temperatures (120 and 160 °C).[852] Interestingly, it was observed that at 120 °C, the Au/Ag NPs converted into their core–shell structure while the core/alloy nature was obtained at 160 °C. Out of both nanocomposites, the core/shell Au/Ag electrocatalyst showed higher current density for the electrocatalytic MOR. Similarly, bimetallic PdAg NPs supported on a carbon nanotube were also employed for the electro-oxidation of methanol.[853] Recently, Yao *et al.* have reported hollow porous platinum-silver double-shelled nanocages (Pt–Ag DSNCs) for the electro-oxidation of methanol.[642] A one-pot hydrothermal process was utilized for the synthesis of Pt–Ag DSNCs in the presence of *N,N*-methylenebisacrylamide (MBAA). The morphologies of Pt–Ag nanocomposites can be modified from single-shelled to double-shelled Pt–Ag nanocages with the assistance of MBAA. SEM and TEM images revealed that double shelled nanocages were obtained, consisting of spherical particles with a high morphology yield, rough surface, and uniform particle-size distribution (Fig. 48a and b). Electrochemical measurements depicted that the Pt–Ag DSNCs exhibited increased electrocatalytic activity for the MOR and long-term operational stability without CO poisoning. Computational

studies showed that the MOR undergoes a bifunctional mechanism in which adsorbed CO_{ads} are removed with the help of adsorbed OH, resulting in excellent MOR performance. The surface defects in the double-shell nanocage structures provide several catalytically active sites for the MOR, allowing Pt atoms in the Pt–Ag DSNCs to be used more efficiently (Fig. 48c–f). The Ag_2S–Pt nanocomposites have been also reported for electrocatalytic MOR.[854] Xiong *et al.* prepared ultrathin octahedral Au_3Ag nanoframes *via* a one-step process for the electro-oxidation of methanol.[855] The Au_3Ag nanoframes demonstrated higher electrocatalytic MOR performance with a large specific activity of 3.38 mA cm^{-2}, as well as 3.9 times higher than the commercial Pt/C.

Alkaline direct formate fuel cells (ADFFC) are rapidly growing as a viable alternative to sustainable energy conversion devices.[856] Chen and co-workers have reported nanoassemblies of Pt–Ag alloy nanoballoons (ANBNSs) for the formate oxidation reaction (FOR).[857] Compared with commercial Pt NPs, ANBNSs exhibited a 19.3 times higher electrocatalytic performance towards the FOR under alkaline conditions.

Plant-derived NPs, which are bio-renewable and sustainable, find a number of applications in the field of catalysis and electrocatalysis, along with their widespread use in the medicinal, pharmaceutical, and agricultural sector.[858] Sethuraman and co-workers have reported a green method for the preparation of Ag NPs, which were further utilized in the electrocatalytic reduction of benzyl chloride.[859] An aqueous extract of *A. nilotica pods* was utilized for the synthesis of Ag NPs. Cyclic voltammetry results demonstrated that the Ag NPs exhibited higher electrocatalytic performance towards benzyl chloride reduction when compared with bulk Ag and inert glassy carbon electrodes.

Yao and co-workers demonstrated the synthesis of Cu–Ag NPs supported on reduced graphene (rGO), *i.e.* (Cu–Ag NP/rGO) nanocomposites, by a wet chemical method whereby $NaBH_4$ was used as a reducing agent.[860] Furthermore, the synthesized Cu–Ag NPs/rGO nanocatalyst exhibited high catalytic activity for electrochemical H_2O_2 reduction.

Along with the above-mentioned protocols, several other Ag NM-based electrocatalysts have been reported for chloride evolution reaction,[861] hydrogen peroxide reduction,[862] glycerol oxidation,[863,864] or the oxidation of glucose,[865] along with showing a high catalytic performance in electrolytic fuel cells.

5. Positive role of the catalytic reactions excited by silver-based nanomaterials in various fields

From the preceding sections highlighting the various multi-faceted catalytic applications (liquid phase, photo and electrocatalysis) of Ag-based NMs, it is quite apparent that silver has played a remarkable role in improving the existing catalytic processes, rephasing them towards sustainability and transforming the outlook of the chemical industries. Undeniably, nanosilver has emerged as the catalyst of choice in view of its notable interaction with various organic (ethylene and methanol) as well as inorganic molecules (oxygen, water, carbon dioxide *etc.*) and proven its superiority to the conventional catalysts. Quite appreciably, nanosilver has spread its catalytic essence in every dynamic field,

right from environmental remediation, and waste-water purification, combatting global warming through CO_2 fixation to the synthesis of valuable pharmaceuticals. Through excellent examples, Ag-supported nanocatalysts have shown their proficiency in numerous industrially significant organic reactions, allowing the ready transformation of diverse moieties possessing either electron donating or withdrawing groups, generating the targeted products in high yields, whilst simultaneously displaying exceptional reusability (often up-to even 10 times), thus rendering the protocols economically viable. The interest in synthesizing novel Ag-based nanocatalysts has compounded in light of the fact that they enable unprecedented or rather less selective transformations to occur with greater selectivity (examples on chemoselective catalysis have been discussed previously). For instance, the kinetically challenging reduction of *p*-nitrophenol which is difficult to be achieved even in the presence of very strong reducing agents such as sodium borohydride becomes easily achievable with the aid of Ag NPs.[866] The potentiality of Ag NMs in the field of total synthesis of natural products and pharmaceutical molecules is amply well established. The discussion would remain incomplete if we do not ponder upon the role of nanostructured silver in the degradation of noxious contaminants and effective disinfection of drinking water. It is quite evident from the examples presented previously that Ag NPs have functioned as efficient photocatalysts in degrading a rather expansive range of contaminants by virtue of trapping the photogenerated electrons, producing holes to form OH^-, thereby helping in the degradation.[867] For example, the $AgCl_x^{(x-1)-}$ species of dissolved AgCl in surface water acts as a precursor for formation of Ag NPs in the presence of sunlight irradiation, which subsequently reduced the bacterial contamination in water.[868,869] Additionally, the high conductivity, photocatalytic properties, low cost, durability and tunable morphology of nanosilver have been effectively exploited in highly important hydrogen evolution, CO_2 reduction and photocatalytic organic transformations, demonstrating a notable enhancement in reaction rates. In certain cases, the morphological change in architecture of nano Ag has fuelled the catalytic degradation rate drastically. Not only as catalysts, Ag NPs have entranced the field of drug discovery with their outstanding and broad-ranging antibacterial/antiviral properties. It is certain that nanocatalytic silver has acquired commercial significance as antibacterial agents for food storage, the health industry and textile coatings, yet the molecular mechanisms influencing the Ag-bacteria interactions and toxicity need to be thoroughly investigated; due to the likelihood of their release, NPs might have a detrimental impact on the functioning of living organisms;[870–872] their trace level abundance in environmental matrices might pose severe problems. Therefore, it is imperative to develop techniques that can monitor potential risks. For complete investigation of fate and transport of Ag NPs in the environmental compartments, more competent methods for preconcentration, separation and speciation of Ag NPs along with development of analytical tools for detecting these NPs would be essential. Moreover, there is a need to comprehensively understand the positive as well as negative impacts of Ag-based NMs while fully exploiting them in various applications (especially environmental).[873–875] So far, although considerable efforts have been directed towards elucidation of the mechanism behind the biocidal action of Ag NPs, as yet no general conclusion could be drawn. Henceforth, the pre-requisite of the hour is to conduct long-term exploratory research on the safety of Ag-based NPs so that definite answers can be found. Fortunately, one can take a sigh of relief that the boons of science have helped in the development of techniques for

controlling environmental pollution with the aid of Ag-based NMs, yet these need to be verified thoroughly as per the current state of development. Once complete and satisfactory toxicity results are accomplished and methods to overcome any toxicity risk are developed, the day is not far off when these Ag NMs will rule the nano market.

6. Conclusions and future outlook

This review aims to describe the recent developments in the fabrication of Ag and Ag-based NMs and their significant contribution in advancing the bourgeoning fields of catalysis, photocatalysis, and electrocatalysis. The synthetic section delivered an exclusive conspectus of several vital preparative methods such as chemical reduction and sonochemical; microwave; and thermal treatment. In a painstaking effort to develop sustainable protocols, greener methodologies as well as continuous flow techniques are incessantly being innovated and subsequently incorporated for the preparation of Ag NPs. Additionally, the current state-of-the-art of Ag-based nanomaterials for catalyzing a broad array of industrially demanding organic reactions has also been reflected, including oxidation, hydrogenation, coupling (Heck, Suzuki–Miyaura, Sonogashira, *etc.*), addition, and C–H activation along with the flourishing field of photocatalysis (H_2 evolution, CO_2 reduction, organic pollutants degradation) and electrocatalysis (fuel cell reactions, N_2 reduction). The integration of Ag NPs with additional functionalities (stable support material) or coupling with other metals generates a new class of hybrid materials with enhanced properties for various chemical transformations.

Despite witnessing an immense success in this field, some of the major challenges remain to be faced by the scientific fraternity. Towards swift progress in a nanomaterial synthesis, the potential of neoteric fabrication strategies is being investigated in order to render more stable Ag NPs. Firstly, crucial control over the size at the atomic level and the geometry of the resulting Ag NPs remains a bottleneck for materials chemists. The resourceful modulation of the structures and morphologies, which further influences the physical and chemical properties is highly advantageous for improving the catalytic performance. Accomplishing the key goals of catalysis, high activity, good selectivity and simultaneously exceptional recyclability by ensuring a consistency in the catalyst nanostructure remain highly challenging and calls for a deep understanding of the correlation between the statics and dynamics of the active catalytic centres at a nanoscale. In particular, special emphasis needs to be put on a fundamental understanding of the mechanistic aspects, which can aptly be achieved with the utilization of modern molecular modelling tools, careful introspection and determination of reaction intermediates, and a directed analysis devoted to the individual elementary catalytic steps. This is possible only with the fruitful collaboration between theoretical and experimental chemists.

The current challenges of energy and sustainability have now compelled researchers to shift from material-driven to application-based approaches in catalysis, by which, based on the knowledge gained through surface science and quantum mechanistic studies, shape-selective catalysts or carve-specific catalytic sites can be explicitly designed for targeted purposes. When deliberating the organic synthesis for medicinal and pharmaceutical sectors, it is

imperative to synthesize catalysts possessing great stability and selectivity, *i.e.* enantio-, chemo- or regio-selectivity for the production of value added chemicals.

Recent advancements in the burgeoning field of Ag based-photocatalytic and electrocatalytic systems have also been appraised. There is significant room for further opportunities along with overcoming various challenges in this fervent research area. Furthermore, an effective photocatalyst ought to be selective in action as poor selectivity can be problematic especially in water treatment applications.

There is an upsurge in environmental concern because of rising energy demands and globalization. We need to establish an effective and safe protocol to produce a large amount of energy, without further damaging and contaminating the environment, thus satisfying the energy demand and achieving environmental remediation. The conversion of CO_2, H_2O, and N_2 into chemical sources of energy and raw materials with electrochemical techniques is the prerequisite for securing a sustainable development of 'green' energy supply. Silver is a promising candidate as well as an alternative to Pt thanks to its similar kind of mechanisms and kinetics for electrocatalytic transformations. Additionally, silver shows more resistivity to methanol poisoning, compared to Pt. Moreover, Ag NMs are able to strongly decompose hydroxide ions, which produces hydrogen peroxide responsible for the degradation of the proton exchange membrane used in fuel cells. Owing to their unprecedented catalytic activity and sustainability for various electrocatalytic reactions in fuel cells and electrolyzers, silver-based nanocatalysts appear absolutely necessary for electrochemical reactions. Despite the fact that Ag NPs constitute an ideal catalyst, single Ag NPs have a number of disadvantages, including fast oxidation and agglomeration, poor stability, and low catalytic activity, compared to other metal NPs such as Ni, Ru, Co, Cu, and Au. Therefore, it is necessary to tune the morphology of silver with other metal atoms and a supporting medium to enhance its electronic conductivity, catalytic selectivity, and stability for long-term operations. The synergistic effect between Ag NPs and other transition metals, metal oxides, or carbon supports should be considered to escalate the electrocatalytic activity, selectivity, and stability of Ag-based nanocomposites for major electrochemical reactions like the HER, ORR, OER, CO_2RR and NRR. Furthermore, the competitive co-evolution of hydrogen and low CO_2 solubility are also of major concern in electrocatalytic CO_2RR. To overcome these drawbacks, other new solvent-electrolytes, such as deep eutectic solvents and ionic liquids need to be developed. These solvent systems can become more appealing as their costs will fall in the future, but, in order to be successful CO_2RR electrolytes, their viscosity would need to be regulated, for example by combining with a co-solvent like water.[876]

Notably, two very different electrochemical and material characterization strategies still have their pitfalls, which prevent accurate evaluation of important kinetic parameters and material properties, as well as complex physicochemical phenomena under specific experimental parameters. Designing experimental and theoretical models that will enable the capture of the complex existence of catalysts under specific reaction conditions, as well as the related tandem processes in the electrochemical double layer, are necessary for further progress in this field. The electrochemical double layer and the transient nature of electrocatalysts are

needed for a thorough understanding of the reaction mechanisms and the development of better catalysts and electrochemical interfaces.[877]

Also, further improvements need to be made to today's *operando* characterization techniques, such as near ambient XPS, electrochemistry coupled with Raman, liquid cell electrochemical TEM, surface enhanced Raman, X-ray absorption spectroscopy, and ATR-FTIR spectroscopy, with respect to their response time, sensitivity, and data acquisition pace. These *operando* characterization methods can be utilized for monitoring not only the steady state of electrochemical reactions, but also for the transient existence of electrified materials, *i.e.* the interplay between the precursor, structure, composition, active sites, and catalytic properties of electrocatalysts.

New experimental perspectives and benchmarks for activity, stability, and selectivity of product formation *via* Ag-based nanocatalysts must be established under conditions that realistically reflect those required in industrial applications in order to facilitate the implementation of critical breakthroughs in technical applications. The coordination of electrochemical devices with electricity generated through renewable energy sources is another important step towards a greener future; however, when measuring the carbon footprint, the cost of renewable energy production must be taken into account. In this review, several electrocatalytic applications such as CO_2RR, HER, NRR, OER, and ORR of Ag NMs have been briefly summarized. With respect to their diverse catalytic features, such as high electronic conductivity, low overpotential, and high methanol tolerance, Ag-based NMs have emerged as an inexpensive catalytic system for the production of energy for a sustainable future.

Lastly, deeper insights/more research into the mechanistic role of Ag species in photocatalysis is necessary. Moreover, continuous and automatic scalable synthetic design is highly imperative for promoting the industrial implementation of Ag nanomaterials. We envisage that this review will not only provide new directions to the scientific fraternity but will also serve as a promising learning guide for stimulating all forthcoming developments in this prosperous field.

Supplementary Material

Refer to Web version on PubMed Central for supplementary material.

Acknowledgements

Biographies

Rakesh Kumar Sharma

Prof. R. K. Sharma is the Coordinator of Green Chemistry Network Centre and Professor at the Department of Chemistry, University of Delhi, India. He is also Honorary Professor of Deakin University, Australia. He is a fellow of the Royal Society of Chemistry (RSC) and the Honorary Secretary of RSC London (North India Section). Prof. Sharma worked on JSPS PDF at University of Tokyo and Kumamoto University. He has published about 200 research as well as review articles in renowned international journals which include the top cited articles of Green Chemistry, Materials Horizons and Nature Scientific Reports. Currently he is the series advisor of the RSC Green Chemistry Book Series and a member of the editorial board of Current Research in Green and Sustainable Chemistry. He has edited and authored several books on Green Chemistry published by the RSC green chemistry series, Stanford, Wiley and World Scientific Publications.

Sneha Yadav

Sneha Yadav is an active member of the Green Chemistry Network Centre and is currently pursuing a PhD under the supervision of Prof. R. K. Sharma from Department of Chemistry, University of Delhi (D. U.). She completed her graduation from Hindu College in 2014 and post-graduation from Department of Chemistry, D. U. India in 2016. She was conferred the meritorious award by Hindu College for being the topper of MSc Chemistry. Her research work includes design and development of magnetic metal organic framework composites and their application in the field of catalysis. She has numerous publications in renowned international journals including Inorganic Chemistry, ACS Omega, Material Chemistry Frontiers and Molecular Catalysis, and has also authored a chapter entitled "Gold Nanoparticles by Green Chemistry" in the 21st Century Nanoscience – A Handbook edited by Klaus D. Sattler.

Sriparna Dutta

Dr Sriparna Dutta is a CSIR Research Associate at University of Delhi (D. U.) and an active member of the Green Chemistry Network Centre India. She is also the secretary of ACS International Student Chapter, Delhi University. She completed her doctoral studies under the supervision of Prof. R. K. Sharma from Department of Chemistry, University of Delhi in 2019. Sriparna was awarded the Prof. K. N. Johri Memorial Gold Medal by Delhi University in 2014 for being the university topper with inorganic specialization. Her research efforts are directed towards the fabrication of magnetically retrievable core–shell structured nanocatalysts and their use in various organic transformations. She has over 30 international publications in reputed high impact factor journals and has also co-authored various book chapters in Stanford Publishing, RSC Green Chemistry Series and World Scientific Publications. She was conferred a Young Scientist Award at various national as well as international platforms for her research work.

Hanumant B. Kale

Hanumant B. Kale did his Master of Science in organic chemistry from the Savitribai Phule Pune University (2014–2016). He is a recipient of "The Late Smt. Rukminibai Alias Tai Kshirsagar Prize" for securing the highest number of marks in organic chemistry. Later, he worked in industry as a Research Associate at Lupin Research Park, Lupin Ltd., Pune (2016–2018) and Junior Research Fellow on SERB Funded Project in an institute affiliated to Mumbai University. Currently, he is pursuing his PhD under the supervision of Prof. Manoj B. Gawande at Institute of Chemical Technology, Mumbai-Marathwada Campus, Jalna, India. He is currently working on the research topic "Utilization of carbon dioxide with the purpose of transforming it into a fuels and chemicals by using single-atom catalysts".

Indrajeet R. Warkad

Indrajeet R. Warkad studied chemistry at the Dr B. A. M. University, Aurangabad where he received his bachelor's degree (BSc) in 2015 and master's degree in organic chemistry (MSc) in 2017. Later on he qualified in NET-LS, SET, and GATE exams in chemical sciences subjects. Currently, he is pursuing his doctoral studies under the supervision of Prof. Manoj B. Gawande at Institute of Chemical Technology, Mumbai-Marathwada

Campus, Jalna. His research interests include synthesis of nanomaterials, and single-atom catalysts for organic transformations as well as biomass valorisation.

Radek Zbo il

Radek Zbo il (*1973) was a former Director of Regional Centre of Advanced Technologies and Materials at Palacky University in Olomouc, Czech Republic (www.rcptm.com). After finishing his PhD study (2000), he underwent several short-term stays e.g. at University of Delaware and University of Tokyo. Currently, he works as the head of the group at VSB Technical University Ostrava. He is a co-author of more than 500 publications and many books published by Springer, Wiley and American Chemical Society. His current h-index is 81/95 and he has a total number of citations over 32 000/45 000 (Web of Science/Google Scholar; July 2021). Professor Zbo il was awarded as a Highly Cited Researcher in 2018, 2019, and 2020 as announced annually by Clarivate Analytics, US. He is a member of the editorial boards of many journals published by the Nature family, Elsevier and Wiley.

Rajender S. Varma

Prof. Rajender S. Varma (H-Index 114, Highly Cited Researchers 2016, 2018, 2019, 2020; Publons Awardee 2018, 2019) was born in India (PhD, Delhi University 1976). After postdoctoral research at Robert Robinson Laboratories, Liverpool, UK, he was a faculty member at Baylor College of Medicine and Sam Houston State University prior to joining the Sustainable Technology Division at the US-EPA in 1999. He has a visiting scientist's position at the RCPTM-CATRIN, Palacky University, Czech Republic. He has over 48 years of research experience in management of multidisciplinary technical programs ranging from natural products chemistry to development of more environmentally friendly synthetic methods using microwaves, ultrasound, etc. He is a member of the editorial advisory board of several international journals, has published over 715 papers, and has been awarded 17 U.S. Patents and has written six books, 26 book chapters, and three encyclopaedia contributions with 49 400 citations.

Manoj B. Gawande

Prof. Manoj B. Gawande received his PhD in 2008 from the Institute of Chemical Technology, Mumbai, India, and then undertook several research stints in Germany, South Korea, Portugal, Czech Republic, USA, and UK. He also worked as a Visiting Professor at CBC-SPMS, Nanyang Technological University, Singapore, in 2013. Presently, he is an Associate Professor at the Institute of Chemical Technology, Mumbai-Marathwada Campus, Jalna, India. Recently, he has been invited as visiting professor in chemistry at RCPTM-CATRIN, Palacky University, Czech Republic. His research interests focus on single-atom catalysts, advanced nanomaterials, and sustainable technologies, as well as cutting-edge catalysis and energy applications. He is an editor and an editorial board member of several reputed journals including guest editor of Small, Advanced Materials Interfaces and ACS Sustainable Chemistry and Engineering. He has published over 135 research as well as review articles. He is also included in the global list of the top 2% of scientists in the chemistry field: Stanford University, US, 2019. Currently, he is supervising several doctoral students and postdoctoral co-workers.

References

1. Lea MC, Am. J. Sci, 1889, 37, 476–491.

2. Beyene HD, Werkneh AA, Bezabh HK and Ambaye TG, Sustainable Mater. Technol, 2017, 13, 18–23.

3. Natsuki J, Natsuki T and Hashimoto Y, Int. J. Mater. Sci. Appl, 2015, 4, 325–332.

4. Gunawan C, Marquis CP, Amal R, Sotiriou GA, Rice SA and Harry EJ, ACS Nano, 2017, 11, 3438–3445. [PubMed: 28339182]

5. Rizzello L and Pompa PP, Chem. Soc. Rev, 2014, 43, 1501–1518. [PubMed: 24292075]

6. Fernando A, Weerawardene KDM, Karimova NV and Aikens CM, Chem. Rev, 2015, 115, 6112–6216. [PubMed: 25898274]

7. Calderón-Jiménez B, Johnson ME, Montoro Bustos AR, Murphy KE, Winchester MR and Vega Baudrit JR, Front. Chem, 2017, 5, 6. [PubMed: 28271059]

8. Zhang XF, Liu ZG, Shen W and Gurunathan S, Int. J. Mol. Sci, 2016, 17, 1534.

9. Fraser JA, Kemp S, Young L, Ross M, Prach M, Hutchison GR and Malone E, Sci. Rep, 2018, 8, 1–14. [PubMed: 29311619]

10. Jana NR, Gearheart L and Murphy CJ, Chem. Commun, 2001, 617–618.

11. Wiley B, Herricks T, Sun Y and Xia Y, Nano Lett, 2004, 4, 1733–1739.

12. Personick ML, Langille MR, Zhang J, Wu J, Li S and Mirkin CA, Small, 2013, 9, 1947–1953. [PubMed: 23292747]

13. Im SH, Lee YT, Wiley B and Xia Y, Angew. Chem., Int. Ed, 2005, 44, 2154–2157.

14. Wiley B, Sun Y and Xia Y, Acc. Chem. Res, 2007, 40, 1067–1076. [PubMed: 17616165]

15. Pastoriza-Santos I and Liz-Marzán LM, Nano Lett, 2002, 2, 903–905.

16. Zhang SH, Xie ZX, Jiang ZY, Xu X, Xiang J, Huang RB and Zheng LS, Chem. Commun, 2004, 1106–1107.

17. Korte KE, Skrabalak SE and Xia Y, J. Mater. Chem, 2008, 18, 437–441.

18. Li B, Wen X, Li R, Wang Z, Clem PG and Fan H, Nat. Commun, 2014, 5, 1–7.

19. Wijaya YN, Kim J, Choi WM, Park SH and Kim MH, Nanoscale, 2017, 9, 11705–11712. [PubMed: 28776049]

20. Gao Y, Jiang P, Song L, Wang J, Liu L, Liu D, Xiang Y, Zhang Z, Zhao X and Dou X, J. Cryst. Growth, 2006, 289, 376–380.

21. Elsner C, Prager A, Sobottka A, Lotnyk A and Abel B, Anal. Methods, 2017, 9, 4663–4672.

22. Tang S, Vongehr S, Wan N and Meng X, Mater. Chem. Phys, 2013, 142, 17–26.

23. Wiley BJ, Chen Y, McLellan JM, Xiong Y, Li ZY, Ginger D and Xia Y, Nano Lett, 2007, 7, 1032–1036. [PubMed: 17343425]

24. Rycenga M, McLellan JM and Xia Y, Adv. Mater, 2008, 20, 2416–2420.

25. Wiley BJ, Xiong Y, Li ZY, Yin Y and Xia Y, Nano Lett, 2006, 6, 765–768. [PubMed: 16608280]

26. González A, Noguez C, Beránek J and Barnard A, J. Phys. Chem. C, 2014, 118, 9128–9136.

27. Ross MB, Mirkin CA and Schatz GC, J. Phys. Chem. C, 2016, 120, 816–830.

28. Bilankohi SM, Orient. J. Chem, 2015, 31, 2259–2263.

29. Heiligtag FJ and Niederberger M, Mater. Today, 2013, 16, 262–271.

30. Brust M and Kiely CJ, Colloids Surf., A, 2002, 202, 175–186.

31. Liao G, Fang J, Li Q, Li S, Xu Z and Fang B, Nanoscale, 2019, 11, 7062–7096. [PubMed: 30931457]

32. Wang H, Qiao X, Chen J, Wang X and Ding S, Mater. Chem. Phys, 2005, 94, 449–453.

33. Desireddy A, Conn BE, Guo J, Yoon B, Barnett RN, Monahan BM, Kirschbaum K, Griffith WP, Whetten RL and Landman U, Nature, 2013, 501, 399–402. [PubMed: 24005327]

34. Joshi CP, Bootharaju MS, Alhilaly MJ and Bakr OM, J. Am. Chem. Soc, 2015, 137, 11578–11581. [PubMed: 26322865]

35. Naik RR, Stringer SJ, Agarwal G, Jones SE and Stone MO, Nat. Mater, 2002, 1, 169–172. [PubMed: 12618805]

36. Lamoth M, Jones T, Plodinec M, Machoke AGF, Wrabetz S, Krämer M, Karpov A, Rosowski F, Piccinin S and Schlögl R, ChemCatChem, 2020, 12, 1–13.

37. Pandey S, Do JY, Kim J and Kang M, Carbohydr. Polym, 2020, 230, 115597. [PubMed: 31887912]

38. Liu H, Feng Y, Chen D, Li C, Cui P and Yang J, J. Mater. Chem. A, 2015, 3, 3182–3223.

39. Shahi PK, Prakash R and Rai SB, AIP Adv, 2018, 8, 065117.

40. Divya KP, Miroshnikov M, Dutta D, Vemula PK, Ajayan PM and John G, Acc. Chem. Res, 2016, 49, 1671–1680. [PubMed: 27552443]

41. Samanta A and Medintz IL, Nanoscale, 2016, 8, 9037–9095. [PubMed: 27080924]

42. Wu M, Li Y, Yue R, Zhang X and Huang Y, Sci. Rep, 2017, 7, 42773. [PubMed: 28202922]

43. Liu Y, Goebl J and Yin Y, Chem. Soc. Rev, 2013, 42, 2610–2653. [PubMed: 23093173]

44. Patel AC, Li S, Wang C, Zhang W and Wei Y, Chem. Mater, 2007, 19, 1231–1238.

45. Lu Y, Mei Y, Drechsler M and Ballauff M, Angew. Chem., Int. Ed, 2006, 45, 813–816.

46. Edison TJI and Sethuraman M, Process Biochem, 2012, 47, 1351–1357.

47. Tsujino K and Matsumura M, Adv. Mater, 2005, 17, 1045–1047.

48. Fang G and Bi X, Chem. Soc. Rev, 2015, 44, 8124–8173. [PubMed: 26222839]

49. Sekine K and Yamada T, Chem. Soc. Rev, 2016, 45, 4524–4532. [PubMed: 26888406]

50. Pellissier H, Chem. Rev, 2016, 116, 14868–14917. [PubMed: 27960274]

51. Zhu QL and Xu Q, Chem, 2016, 1, 220–245.

52. Pal J and Pal T, Nanoscale, 2015, 7, 14159–14190. [PubMed: 26255749]

53. Song H, Rioux RM, Hoefelmeyer JD, Komor R, Niesz K, Grass M, Yang P and Somorjai GA, J. Am. Chem. Soc, 2006, 128, 3027–3037. [PubMed: 16506784]

54. Navalón S and García H, Nanomaterials, 2016, 6, 123.

55. Liu J, ACS Catal, 2017, 7, 34–59.

56. Bu Y and Lee S, ACS Appl. Mater. Interfaces, 2012, 4, 3923–3931. [PubMed: 22833686]

57. Thanh NTK and Green LAW, Nano Today, 2010, 5, 213–230.

58. Zhang W, Liu J, Niu W, Yan H, Lu X and Liu B, ACS Appl. Mater. Interfaces, 2018, 10, 14850–14856. [PubMed: 29569899]

59. Das D, Senapati S and Nanda KK, ACS Sustainable Chem. Eng, 2019, 7, 14089–14101.

60. Carlson C, Hussain SM, Schrand AM, Braydich-Stolle LK, Hess KL, Jones RL and Schlager JJ, J. Phys. Chem. B, 2008, 112, 13608–13619. [PubMed: 18831567]

61. Li Y, Zhao J, Shang E, Xia X, Niu J and Crittenden J, Environ. Sci. Technol, 2018, 52, 4842–4849. [PubMed: 29260863]

62. Li Y, Zhang W, Niu J and Chen Y, Environ. Sci. Technol, 2013, 47, 10293–10301. [PubMed: 23952964]

63. Nowack B, Krug HF and Height M, Environ. Sci. Technol, 2011, 45, 1177–1183. [PubMed: 21218770]

64. Bhattarai B, Zaker Y, Atnagulov A, Yoon B, Landman U and Bigioni TP, Acc. Chem. Res, 2018, 51, 3104–3113. [PubMed: 30462479]

65. Kang H, Buchman JT, Rodriguez RS, Ring HL, He J, Bantz KC and Haynes CL, Chem. Rev, 2019, 119, 664–699. [PubMed: 30346757]

66. He D, Garg S, Wang Z, Li L, Rong H, Ma X, Li G, An T and Waite TD, Environ. Sci.: Nano, 2019, 6, 1674–1687.

67. He X, Lu A, Cheng J, Chen J, Song Q, Liu W and Chen C, Nano, 2017, 12, 1730002.

68. Guo Z, Cui K, Zeng G, Wang J and Guo X, Sci. Total Environ, 2018, 643, 1325–1336. [PubMed: 30189549]

69. Zhang P, Wyman I, Hu J, Lin S, Zhong Z, Tu Y, Huang Z and Wei Y, Mater. Sci. Eng., B, 2017, 223, 1–23.

70. Sadovnikov SI and Gusev AI, J. Mater. Chem. A, 2017, 5, 17676–17704.

71. Bhattarai B, Zaker Y and Bigioni TP, Curr. Opin. Green Sustainable Chem, 2018, 12, 91–100.

72. He K, Zeng Z, Chen A, Zeng G, Xiao R, Xu P, Huang Z, Shi J, Hu L and Chen G, Small, 2018, 14, 1800871.

73. Zhang Z, Shen W, Xue J, Liu Y, Liu Y, Yan P, Liu J and Tang J, Nanoscale Res. Lett, 2018, 13, 54. [PubMed: 29457198]

74. Nasrollahzadeh M, Mahmoudi-Gom Yek S, Motahharifar N and Ghafori Gorab M, Chem. Rec, 2019, 19, 2436–2479. [PubMed: 31021524]

75. Heinemann MG, Rosa CH, Rosa GR and Dias D, Trends Environ. Anal. Chem, 2021, 30, e00129.

76. Cinelli M, Coles SR, Nadagouda MN, Błaszczy ski J, Słowi ski R, Varma RS and Kirwan K, Green Chem, 2015, 17, 2825–2839.

77. Xue J, Liu J, Mao S, Wang Y, Shen W, Wang W, Huang L, Li H and Tang J, Mater. Res. Bull, 2018, 106, 113–123.

78. Dong XY, Gao ZW, Yang KF, Zhang WQ and Xu LW, Catal. Sci. Technol, 2015, 5, 2554–2574.

79. Liang C, Lu ZA, Wu J, Chen MX, Zhang Y, Zhang B, Gao GL, Li S and Xu P, ACS Appl. Mater. Interfaces, 2020, 12, 54266–54284. [PubMed: 33226767]

80. Tarannum N, Divya D and Gautam YK, RSC Adv, 2019, 9, 34926–34948.

81. Pellissier H, Chem. Rev, 2016, 116, 14868–14917. [PubMed: 27960274]

82. Qaseem A, Chen F, Wu X and Johnston RL, Catal. Sci. Technol, 2016, 6, 3317–3340.

83. Zhao Q, Zhao M, Qiu J, Lai WY, Pang H and Huang W, Small, 2017, 13, 1701091.

84. Zhao S, Jin R and Jin R, ACS Energy Lett, 2018, 3, 452–462.

85. Sun D, Xu X, Qin Y, Jiang SP and Shao Z, ChemSusChem, 2020, 13, 39–58. [PubMed: 31696641]

86. Li G, Wang Y and Mao L, RSC Adv, 2014, 4, 53649–53661.

87. Xue J, Liu J, Liu Y, Li H, Wang Y, Sun D, Wang W, Huang L and Tang J, J. Mater. Chem. C, 2019, 7, 3988–4003.

88. An C, Wang S, Sun Y, Zhang Q, Zhang J, Wang C and Fang J, J. Mater. Chem. A, 2016, 4, 4336–4352.

89. Marimuthu S, Antonisamy AJ, Malayandi S, Rajendran K, Tsai PC, Pugazhendhi A and Ponnusamy VK, J. Photochem. Photobiol., B, 2020, 205, 111823. [PubMed: 32120184]

90. Tsvetkov M, Zaharieva J and Milanova M, Catal. Today, 2020, 357, 453–459.

91. Xue W, Huang D, Wen X, Chen S, Cheng M, Deng R, Li B, Yang Y and Liu X, J. Hazard. Mater, 2020, 390, 122128. [PubMed: 32006844]

92. Wang L and Wu J, Inorg. Chem. Commun, 2021, 129, 108619.

93. Sharma S, Dutta V, Raizada P, Hosseini-Bandegharaei A, Thakur VK, Kalia S, Nguyen VH and Singh P, J. Environ. Chem. Eng, 2021, 9, 105157.

94. Wen XJ, Shen CH, Fei ZH, Fang D, Liu ZT, Dai JT and Niu CG, Chem. Eng. Sci, 2020, 383, 123083.

95. Li X, Xu P, Chen M, Zeng G, Wang D, Chen F, Tang W, Chen C, Zhang C and Tan X, Chem. Eng. J, 2019, 366, 339–357.

96. Dauthal P and Mukhopadhyay M, Ind. Eng. Chem. Res, 2016, 55, 9557–9577.

97. Haes AJ, Zhao J, Zou S, Own CS, Marks LD, Schatz GC and Van Duyne RP, J. Phys. Chem. B, 2005, 109, 11158–11162. [PubMed: 16852361]

98. Bhatia S, Natural polymer drug delivery systems, Springer, 2016, pp. 33–93.

99. Pacioni NL, Borsarelli CD, Rey V and Veglia AV, Silver nanoparticle applications, Springer, 2015, pp. 13–46.

100. Belusso LCS, Lenz GF, Fiorini EE, Pereira AJ, Sequinel R, Bini RA, Felix JF and Schneider R, Appl. Surf. Sci, 2019, 473, 303–312.

101. Zulkifli NI, Muhamad M, Mohamad Zain NN, Tan WN, Yahaya N, Bustami Y, Abdul Aziz A and Nik Mohamed Kamal NNS, Molecules, 2020, 25, 4332.

102. Xia X, Zeng J, Zhang Q, Moran CH and Xia Y, J. Phys. Chem. C, 2012, 116, 21647–21656.

103. Caswell K, Bender CM and Murphy CJ, Nano Lett, 2003, 3, 667–669.

104. Ben Moshe A and Markovich G, Chem. Mater, 2011, 23, 1239–1245.

105. Métraux GS and Mirkin CA, Adv. Mater, 2005, 17, 412–415.

106. Zhang D, Qi L, Yang J, Ma J, Cheng H and Huang L, Chem. Mater, 2004, 16, 872–876.

107. Pérez M, Moiraghi R, Coronado E and Macagno V, Cryst. Growth Des, 2008, 8, 1377–1383.

108. Banerjee S, Loza K, Meyer-Zaika W, Prymak O and Epple M, Chem. Mater, 2014, 26, 951–957.

109. Sahoo P, Kamal S, Kumar TJ, Sreedhar B, Singh A and Srivastava S, Def. Sci. J, 2009, 59, 447–455.

110. Shameli K, Bin Ahmad M, Jazayeri SD, Sedaghat S, Shabanzadeh P, Jahangirian H, Mahdavi M and Abdollahi Y, Int. J. Mol. Sci, 2012, 13, 6639–6650. [PubMed: 22837654]

111. Yang Y, Matsubara S, Xiong L, Hayakawa T and Nogami M, J. Phys. Chem. C, 2007, 111, 9095–9104.

112. Nickel U, Zu Castell A, Pöppl K and Schneider S, Langmuir, 2000, 16, 9087–9091.

113. Raza MA, Kanwal Z, Rauf A, Sabri AN, Riaz S and Naseem S, Nanomaterials, 2016, 6, 74.

114. Ge L, Li Q, Wang M, Ouyang J, Li X and Xing MM, Int. J. Nanomed, 2014, 9, 2399–2407.

115. Washio I, Xiong Y, Yin Y and Xia Y, Adv. Mater, 2006, 18, 1745–1749.

116. Rycenga M, Cobley CM, Zeng J, Li W, Moran CH, Zhang Q, Qin D and Xia Y, Chem. Rev, 2011, 111, 3669–3712. [PubMed: 21395318]

117. Pillai ZS and Kamat PV, J. Phys. Chem. B, 2004, 108, 945–951.

118. Nadagouda MN and Varma RS, Cryst. Growth Des, 2007, 7, 2582–2587.

119. Han C, Nagendra V, Baig R, Varma RS and Nadagouda MN, Appl. Sci, 2015, 5, 415–426.

120. Bastús NG, Merkoçi F, Piella J and Puntes V, Chem. Mater, 2014, 26, 2836–2846.

121. Chen S, Wang G, Sui W, Parvez AM and Si C, Green Chem, 2020, 22, 2879–2888.

122. Giner-Casares JJ, Henriksen-Lacey M, Coronado-Puchau M and Liz-Marzán LM, Mater. Today, 2016, 19, 19–28.

123. Creighton JA, Blatchford CG and Albrecht MG, J. Chem. Soc., Faraday Trans. 2, 1979, 75, 790–798.

124. Van Hyning DL and Zukoski CF, Langmuir, 1998, 14, 7034–7046.

125. Wuithschick M, Paul B, Bienert R, Sarfraz A, Vainio U, Sztucki M, Kraehnert R, Strasser P, Rademann K and Emmerling F, Chem. Mater, 2013, 25, 4679–4689.

126. Nadagouda MN and Varma RS, Macromol. Rapid Commun, 2007, 28, 2106–2111.

EPA Author Manuscript

EPA Author Manuscript

EPA Author Manuscript

127. Sun Y, Mayers B, Herricks T and Xia Y, Nano Lett, 2003, 3, 955–960.

128. Sun Y and Xia Y, Adv. Mater, 2002, 14, 833–837.

129. Arvizo RR, Bhattacharyya S, Kudgus RA, Giri K, Bhattacharya R and Mukherjee P, Chem. Soc. Rev, 2012, 41, 2943–2970. [PubMed: 22388295]

130. Steinigeweg D and Schluecker S, Chem. Commun, 2012, 48, 8682–8684.

131. Kou J and Varma RS, Chem. Commun, 2013, 49, 692–694.

132. Yin Y, Li ZY, Zhong Z, Gates B, Xia Y and Venkateswaran S, J. Mater. Chem, 2002, 12, 522–527.

133. Yu D and Yam VWW, J. Am. Chem. Soc, 2004, 126, 13200–13201. [PubMed: 15479055]

134. Nadagouda MN and Varma RS, Aust. J. Chem, 2009, 62, 260–264.

135. Xu H, Zeiger BW and Suslick KS, Chem. Soc. Rev, 2013, 42, 2555–2567. [PubMed: 23165883]

136. Bang JH and Suslick KS, Adv. Mater, 2010, 22, 1039–1059. [PubMed: 20401929]

137. Duan H, Wang D and Li Y, Chem. Soc. Rev, 2015, 44, 5778–5792. [PubMed: 25615873]

138. Chatel G and Varma RS, Green Chem, 2019, 21, 6043–6050.

139. Salkar R, Jeevanandam P, Aruna S, Koltypin Y and Gedanken A, J. Mater. Chem, 1999, 9, 1333–1335.

140. Jiang LP, Xu S, Zhu JM, Zhang JR, Zhu JJ and Chen HY, Inorg. Chem, 2004, 43, 5877–5883. [PubMed: 15360236]

141. Zhang M, Zhao A, Sun H, Guo H, Wang D, Li D, Gan Z and Tao W, J. Mater. Chem, 2011, 21, 18817–18824.

142. Zhang J. p., Chen P, Sun C. h. and Hu X. j., Appl. Catal., A, 2004, 266, 49–54.

143. Zhu Y. p., Wang X. k., Guo W. l., Wang J. g. and Wang C, Ultrason. Sonochem, 2010, 17, 675–679. [PubMed: 20149712]

144. El-Dessouky R, Georges M and Azzazy HM, Functional Nanoparticles for Bioanalysis, Nanomedicine, and Bioelectronic Devices, ACS Publications, 2012, vol. 1, pp. 359–404.

145. Zhou T, Rong M, Cai Z, Yang CJ and Chen X, Nanoscale, 2012, 4, 4103–4106. [PubMed: 22635158]

146. Xu H and Suslick KS, ACS Nano, 2010, 4, 3209–3214. [PubMed: 20507161]

147. Gawande MB, Shelke SN, Zboril R and Varma RS, Acc. Chem. Res, 2014, 47, 1338–1348. [PubMed: 24666323]

148. Rathi AK, Gawande MB, Zboril R and Varma RS, Coord. Chem. Rev, 2015, 291, 68–94.

149. Gedye R, Smith F, Westaway K, Ali H, Baldisera L, Laberge L and Rousell J, Tetrahedron Lett, 1986, 27, 279–282.

150. Kumar A, Kuang Y, Liang Z and Sun X, Mater. Today Nano, 2020, 11, 100076.

151. Polshettiwar V, Baruwati B and Varma RS, ACS Nano, 2009, 3, 728–736. [PubMed: 19209927]

152. Bilecka I and Niederberger M, Nanoscale, 2010, 2, 1358–1374. [PubMed: 20845524]

153. Nadagouda MN, Speth TF and Varma RS, Acc. Chem. Res, 2011, 44, 469–478. [PubMed: 21526846]

154. Magalhães Sousa D, Chiappim W, Leitão JP, Lima JOC and Ferreira I, ACS Omega, 2020, 5, 12877–12881. [PubMed: 32548471]

155. Kundu S, Wang K and Liang H, J. Phys. Chem. C, 2009, 113, 134–141.

156. Hu B, Wang SB, Wang K, Zhang M and Yu S-H, J. Phys. Chem. C, 2008, 112, 11169–11174.

157. Gou L, Chipara M and Zaleski JM, Chem. Mater, 2007, 19, 1755–1760.

158. Nadagouda MN and Varma RS, Cryst. Growth Des, 2008, 8, 291–295.

159. Mallikarjuna NN and Varma RS, Cryst. Growth Des, 2007, 7, 686–690.

160. Baruwati B, Polshettiwar V and Varma RS, Green Chem, 2009, 11, 926–930.

161. Cai Y, Piao X, Gao W, Zhang Z, Nie E and Sun Z, RSC Adv, 2017, 7, 34041–34048.

162. Seku K, Gangapuram BR, Pejjai B, Kadimpati KK and Golla N, J. Nanostruct. Chem, 2018, 8, 179–188.

163. Özkar S and Finke RG, J. Phys. Chem. C, 2017, 121, 27643–27654.

164. Kahrilas GA, Wally LM, Fredrick SJ, Hiskey M, Prieto AL and Owens JE, ACS Sustainable Chem. Eng, 2014, 2, 367–376.

165. Saloga PE, Kästner C and Thünemann AF, Langmuir, 2018, 34, 147–153. [PubMed: 29215896]

166. Adhikari L, Larm NE, Bhawawet N and Baker GA, ACS Sustainable Chem. Eng, 2018, 6, 5725–5731.

167. Nadagouda MN and Varma RS, Green Chem, 2008, 10, 859–862.

168. Kou J and Varma RS, ChemSusChem, 2012, 5, 2435–2441. [PubMed: 22945662]

169. Virkutyte J and Varma RS, Chem. Sci, 2011, 2, 837–846.

170. Moulton MC, Braydich-Stolle LK, Nadagouda MN, Kunzelman S, Hussain SM and Varma RS, Nanoscale, 2010, 2, 763–770. [PubMed: 20648322]

171. Hebbalalu D, Lalley J, Nadagouda MN and Varma RS, ACS Sustainable Chem. Eng, 2013, 1, 703–712.

172. Cinelli M, Coles SR, Nadagouda MN, Błaszczy ski J, Słowi ski R, Varma RS and Kirwan K, J. Cleaner Prod, 2017, 162, 938–948.

173. Iravani S and Varma RS, Green Chem, 2019, 21, 4583–4603.

174. Das RK, Pachapur VL, Lonappan L, Naghdi M, Pulicharla R, Maiti S, Cledon M, Dalila LMA, Sarma SJ and Brar SK, Nanotechnol. Environ. Eng, 2017, 2, 18, DOI: 10.1007/s41204-017-0029-4.

175. Patete JM, Peng X, Koenigsmann C, Xu Y, Karn B and Wong SS, Green Chem, 2011, 13, 482–519.

176. Aziz N, Faraz M, Pandey R, Shakir M, Fatma T, Varma A, Barman I and Prasad R, Langmuir, 2015, 31, 11605–11612. [PubMed: 26447769]

177. Akhtar MS, Panwar J and Yun YS, ACS Sustainable Chem. Eng, 2013, 1, 591–602.

178. Alavi M and Varma RS, Sustainable Chem. Pharm, 2021, 21, 100412.

179. Raveendran P, Fu J and Wallen SL, J. Am. Chem. Soc, 2003, 125, 13940–13941. [PubMed: 14611213]

180. Gardea-Torresdey JL, Gomez E, Peralta-Videa JR, Parsons JG, Troiani H and Jose-Yacaman M, Langmuir, 2003, 19, 1357–1361.

181. Sutradhar P and Saha M, J. Phys. Chem. C, 2016, 120, 8941–8949.

182. Ashraf JM, Ansari MA, Khan HM, Alzohairy MA and Choi I, Sci. Rep, 2016, 6, 20414, DOI: 10.1038/srep20414. [PubMed: 26829907]

183. Rheder DT, Guilger M, Bilesky-José N, Germano-Costa T, Pasquoto-Stigliani T, Gallep TBB, Grillo R, dos Santos Carvalho C, Fraceto LF and Lima R, Sci. Rep, 2018, 8, 1–11. [PubMed: 29311619]

184. Xue Y, Qiu X, Liu Z and Li Y, ACS Sustainable Chem. Eng, 2018, 6, 7695–7703.

185. Boopathi S, Gopinath S, Boopathi T, Balamurugan V, Rajeshkumar R and Sundararaman M, Ind. Eng. Chem. Res, 2012, 51, 5976–5985.

186. Kasithevar M, Saravanan M, Prakash P, Kumar H, Ovais M, Barabadi H and Shinwari ZK, J. Interdiscip. Nanomed, 2017, 2, 131–141.

187. Nadagouda MN, Iyanna N, Lalley J, Han C, Dionysiou DD and Varma RS, ACS Sustainable Chem. Eng, 2014, 2, 1717–1723.

188. Jadhav K, Deore S, Dhamecha D, Hr R, Jagwani S, Jalalpure S and Bohara R, ACS Biomater. Sci. Eng, 2018, 4, 892–899. [PubMed: 33418773]

189. Koga N and Tanaka H, Thermochim. Acta, 2002, 388, 41–61.

190. Hosseinpour-Mashkani SM and Ramezani M, Mater. Lett, 2014, 130, 259–262.

191. Nakano M, Fujiwara T and Koga N, J. Phys. Chem. C, 2016, 120, 8841–8854.

192. Gharibshahi L, Saion E, Gharibshahi E, Shaari AH and Matori KA, Materials, 2017, 10, 402.

193. Goudarzi M, Mir N, Mousavi-Kamazani M, Bagheri S and Salavati-Niasari M, Sci. Rep, 2016, 6, 32539. [PubMed: 27581681]

194. Gutmann B, Cantillo D and Kappe CO, Angew. Chem., Int. Ed, 2015, 54, 6688–6728.

195. Pastre JC, Browne DL and Ley SV, Chem. Soc. Rev, 2013, 42, 8849–8869. [PubMed: 23999700]

196. Długosz O and Banach M, React. Chem. Eng, 2020, 5, 1619–1641.

197. Wiles C and Watts P, Green Chem, 2012, 14, 38–54.

198. Lin XZ, Terepka AD and Yang H, Nano Lett, 2004, 4, 2227–2232.

199. Kumar DR, Kasture M, Prabhune A, Ramana C, Prasad B and Kulkarni A, Green Chem, 2010, 12, 609–615.

200. Huang J, Lin L, Li Q, Sun D, Wang Y, Lu Y, He N, Yang K, Yang X and Wang H, Ind. Eng. Chem. Res, 2008, 47, 6081–6090.

201. Wu KJ and Torrente-Murciano L, React. Chem. Eng, 2018, 3, 267–276.

202. Ching Lau C, Kemal Bayazit M, Reardon PJT and Tang J, Chem. Rec, 2019, 19, 172–187. [PubMed: 30525292]

203. Groisman Y and Gedanken A, J. Phys. Chem. C, 2008, 112, 8802–8808.

204. Horikoshi S, Abe H, Torigoe K, Abe M and Serpone N, Nanoscale, 2010, 2, 1441–1447. [PubMed: 20820732]

205. Dzido G, Markowski P, Małachowska-Jutsz A, Prusik K and Jarz bski AB, J. Nanopart. Res, 2015, 17, 27. [PubMed: 25620882]

206. Zhang Q, Li W, Moran C, Zeng J, Chen J, Wen LP and Xia Y, J. Am. Chem. Soc, 2010, 132, 11372–11378. [PubMed: 20698704]

207. Zhang L, Wang Y, Tong L and Xia Y, Langmuir, 2013, 29, 15719–15725. [PubMed: 24308796]

208. Niu W, Zhang L and Xu G, Nanoscale, 2013, 5, 3172–3181. [PubMed: 23467455]

209. Xia Y, Gilroy KD, Peng HC and Xia X, Angew. Chem., Int. Ed, 2017, 56, 60–95.

210. Lin ZW, Tsao YC, Yang MY and Huang MH, Chem. – Eur. J, 2016, 22, 2326–2332. [PubMed: 26756437]

211. Lin X, Lin S, Liu Y, Gao M, Zhao H, Liu B, Hasi W and Wang L, Langmuir, 2018, 34, 6077–6084. [PubMed: 29747504]

212. Rostami S, Mehdinia A and Jabbari A, Spectrochim. Acta, Part A, 2017, 180, 204–210.

213. Wang Y, Wan D, Xie S, Xia X, Huang CZ and Xia Y, ACS Nano, 2013, 7, 4586–4594. [PubMed: 23631674]

214. Zong R, Wang X, Shi S and Zhu Y, Phys. Chem. Chem. Phys, 2014, 16, 4236–4241. [PubMed: 24452515]

215. Johnson RW, Hultqvist A and Bent SF, Mater. Today, 2014, 17, 236–246.

216. Kariniemi M, Niinistö J, Hatanpää T, Kemell M, Sajavaara T, Ritala M and Leskelä M, Chem. Mater, 2011, 23, 2901–2907.

217. Wack S, Lunca Popa P, Adjeroud N, Guillot J, Pistillo BR and Leturcq R, J. Phys. Chem. C, 2019, 123, 27196–27206.

218. Faramarzi MA and Sadighi A, Adv. Colloid Interface Sci, 2013, 189–190, 1–20.

219. Horikoshi S and Serpone N, Chem. Rec, 2019, 19, 118–139. [PubMed: 30277645]

220. Vijayaraghavan K and Ashokkumar T, J. Environ. Chem. Eng, 2017, 5, 4866–4883.

221. Sokolov SV, Tschulik K, Batchelor-McAuley C, Jurkschat K and Compton RG, Anal. Chem, 2015, 87, 10033–10039. [PubMed: 26352558]

222. Levard C, Hotze EM, Lowry GV and Brown GE Jr, Environ. Sci. Technol, 2012, 46, 6900–6914. [PubMed: 22339502]

223. Wang Z, Zhai S, Zhai B, Xiao Z, Zhang F and An Q, New J. Chem, 2014, 38, 3999–4006.

224. Gokarna A, Parize R, Kadiri H, Nomenyo K, Patriarche G, Miska P and Lerondel G, RSC Adv, 2014, 4, 47234–47239.

225. Sun P, Zhang K, Shang S, Song J and Wang D, RSC Adv, 2016, 6, 95656–95662.

226. Sadeghzadeh SM, Green Chem, 2015, 17, 3059–3066.

227. Zhang P, Shao C, Zhang Z, Zhang M, Mu J, Guo Z and Liu Y, Nanoscale, 2011, 3, 3357–3363. [PubMed: 21761072]

228. Garcia AC, Gasparotto LH, Gomes JF and Tremiliosi-Filho G, Electrocatalysis, 2012, 3, 147–152.

229. Guo S, Zhang Q, Li H, Guo H and He W, Nano Res, 2017, 10, 3261–3267.

230. Wang Z, Xin L, Zhao X, Qiu Y, Zhang Z, Baturina OA and Li W, Renew. Energy, 2014, 62, 556–562.

231. Ji T, Chen L, Schmitz M, Bao FS and Zhu J, Green Chem, 2015, 17, 2515–2523.

232. Varma RS, ACS Sustainable Chem. Eng, 2019, 7, 6458–6470.

233. Guo J, Hsu A, Chu D and Chen R, J. Phys. Chem. C, 2010, 114, 4324–4330.

234. Wang Y, Liu Z, Han B, Huang Y and Yang G, Langmuir, 2005, 21, 10846–10849. [PubMed: 16262361]

235. Lu X, Qi H, Zhang X, Xue Z, Jin J, Zhou X and Liu X, Chem. Commun, 2011, 47, 12494–12496.

236. Tang XZ, Cao Z, Zhang HB, Liu J and Yu ZZ, Chem. Commun, 2011, 47, 3084–3086.

237. Zhang H, Fu Q, Yao Y, Zhang Z, Ma T, Tan D and Bao X, Langmuir, 2008, 24, 10874–10878. [PubMed: 18729334]

238. Bao Q, Zhang D and Qi P, J. Colloid Interface Sci, 2011, 360, 463–470. [PubMed: 21628064]

239. Li Y, Cao Y, Xie J, Jia D, Qin H and Liang Z, Catal. Commun, 2015, 58, 21–25.

240. Liu S, Tian J, Wang L and Sun X, Carbon, 2011, 49, 3158–3164.

241. Zhang Y, Yuan X, Wang Y and Chen Y, J. Mater. Chem, 2012, 22, 7245–7251.

242. Shao W, Liu X, Min H, Dong G, Feng Q and Zuo S, ACS Appl. Mater. Interfaces, 2015, 7, 6966–6973. [PubMed: 25762191]

243. Jeon EK, Seo E, Lee E, Lee W, Um MK and Kim BS, Chem. Commun, 2013, 49, 3392–3394.

244. Golsheikh AM, Huang N, Lim H and Zakaria R, RSC Adv, 2014, 4, 36401–36411.

245. Perdikaki A, Galeou A, Pilatos G, Karatasios I, Kanellopoulos NK, Prombona A and Karanikolos GN, ACS Appl. Mater. Interfaces, 2016, 8, 27498–27510. [PubMed: 27680975]

246. Bhunia SK and Jana NR, ACS Appl. Mater. Interfaces, 2014, 6, 20085–20092. [PubMed: 25296393]

247. Xu C and Wang X, Small, 2009, 5, 2212–2217. [PubMed: 19662647]

248. Prasek J, Drbohlavova J, Chomoucka J, Hubalek J, Jasek O, Adam V and Kizek R, J. Mater. Chem, 2011, 21, 15872–15884.

249. Krainoi A, Kummerlöwe C, Vennemann N, Nakaramontri Y, Pichaiyut S and Nakason C, J. Appl. Polym. Sci, 2019, 136, 47281.

250. Zheng J, Duan X, Lin H, Gu Z, Fang H, Li J and Yuan Y, Nanoscale, 2016, 8, 5959–5967. [PubMed: 26924186]

251. Singh P, Lamanna G, Ménard-Moyon C, Toma FM, Magnano E, Bondino F, Prato M, Verma S and Bianco A, Angew. Chem., Int. Ed, 2011, 50, 9893–9897.

252. Yan X, Li S, Bao J, Zhang N, Fan B, Li R, Liu X and Pan YX, ACS Appl. Mater. Interfaces, 2016, 8, 17060–17067. [PubMed: 27327238]

253. Liu J, Wang H and Antonietti M, Chem. Soc. Rev, 2016, 45, 2308–2326. [PubMed: 26864963]

254. Gong Y, Li M, Li H and Wang Y, Green Chem, 2015, 17, 715–736.

255. Kundu MK, Sadhukhan M and Barman S, J. Mater. Chem. B, 2015, 3, 1289–1300. [PubMed: 32264480]

256. Veerakumar P, Rajkumar C, Chen SM, Thirumalraj B and Lin KC, J. Electroanal. Chem, 2018, 826, 207–216.

257. Patel SB and Vasava DV, ChemistrySelect, 2018, 3, 471–480.

258. Espinosa JC, Navalón S, Álvaro M and García H, Catal. Sci. Technol, 2016, 6, 7077–7085.

259. Li S, Bandy JA and Hamers RJ, ACS Appl. Mater. Interfaces, 2018, 10, 5395–5403. [PubMed: 29286230]

260. Espinosa JC, Navalón S, Álvaro M and García H, ChemCatChem, 2015, 7, 2682–2688.

261. Caltagirone C, Bettoschi A, Garau A and Montis R, Chem. Soc. Rev, 2015, 44, 4645–4671. [PubMed: 25406516]

262. Singh B, Na J, Konarova M, Wakihara T, Yamauchi Y, Salomon C and Gawande MB, Bull. Chem. Soc. Jpn, 2020, 93, 1459–1496.

263. Sharma R, Sharma S, Dutta S, Zboril R and Gawande MB, Green Chem, 2015, 17, 3207–3230.

264. Jiang ZJ, Liu CY and Sun LW, J. Phys. Chem. B, 2005, 109, 1730–1735. [PubMed: 16851151]

265. Raji V, Chakraborty M and Parikh PA, Ind. Eng. Chem. Res, 2012, 51, 5691–5698.

266. Steffan M, Jakob A, Claus P and Lang H, Catal. Commun, 2009, 10, 437–441.

267. Naik B, Hazra S, Prasad VS and Ghosh NN, Catal. Commun, 2011, 12, 1104–1108.

268. Charistoudi E, Kallitsakis MG, Charisteidis I, Triantafyllidis KS and Lykakis IN, Adv. Synth. Catal, 2017, 359, 2949–2960.

269. He D, Kacopieros M, Ikeda-Ohno A and Waite TD, Environ. Sci. Technol, 2014, 48, 12320–12326. [PubMed: 25272282]

270. Yang H, Liu Y, Shen Q, Chen L, You W, Wang X and Sheng J, J. Mater. Chem, 2012, 22, 24132–24138.

271. Chen Z and Luck RL, Green Chem, 2016, 18, 3354–3359.

272. Campelo JM, Luna D, Luque R, Marinas JM and Romero AA, ChemSusChem, 2009, 2, 18–45. [PubMed: 19142903]

273. Zheng N and Stucky GD, J. Am. Chem. Soc, 2006, 128, 14278–14280. [PubMed: 17076500]

274. Gawande MB, Branco PS and Varma RS, Chem. Soc. Rev, 2013, 42, 3371–3393. [PubMed: 23420127]

275. Gawande MB, Pandey RK and Jayaram RV, Catal. Sci. Technol, 2012, 2, 1113–1125.

276. Trueba M and Trasatti SP, Eur. J. Inorg. Chem, 2005, 3393–3403.

277. Mori K, Kumami A, Tomonari M and Yamashita H, J. Phys. Chem. C, 2009, 113, 16850–16854.

278. Poreddy R, García-Suárez EJ, Riisager A and Kegnæs S, Dalton Trans, 2014, 43, 4255–4259. [PubMed: 24323249]

279. Stamplecoskie KG and Manser JS, ACS Appl. Mater. Interfaces, 2014, 6, 17489–17495. [PubMed: 25243827]

280. Bai B, Qiao Q, Arandiyan H, Li J and Hao J, Environ. Sci. Technol, 2016, 50, 2635–2640. [PubMed: 26629972]

281. Xia H, Hong C, Shi X, Li B, Yuan G, Yao Q and Xie J, J. Mater. Chem. A, 2015, 3, 1216–1221.

282. Bouazizi N, Vieillard J, Thebault P, Desriac F, Clamens T, Bargougui R, Couvrat N, Thoumire O, Brun N and Ladam G, Dalton Trans, 2018, 47, 9143–9155. [PubMed: 29946586]

283. Chen X, Ku S, Weibel JA, Ximenes E, Liu X, Ladisch M and Garimella SV, ACS Appl. Mater. Interfaces, 2017, 9, 39165–39173. [PubMed: 29059530]

284. Ansari SA, Khan MM, Ansari MO, Lee J and Cho MH, J. Phys. Chem. C, 2013, 117, 27023–27030.

285. Deng Q, Duan X, Ng DH, Tang H, Yang Y, Kong M, Wu Z, Cai W and Wang G, ACS Appl. Mater. Interfaces, 2012, 4, 6030–6037. [PubMed: 23092309]

286. Fageria P, Gangopadhyay S and Pande S, RSC Adv, 2014, 4, 24962–24972.

287. Qu Z, Yu F, Zhang X, Wang Y and Gao J, Chem. Eng. J, 2013, 229, 522–532.

288. Kundakovic L and Flytzani-Stephanopoulos M, Appl. Catal., A, 1999, 183, 35–51.

289. Ghosh S, Acharyya SS, Sasaki T and Bal R, Green Chem, 2015, 17, 1867–1876.

290. Zou X, Silva R, Huang X, Al-Sharab JF and Asefa T, Chem. Commun, 2013, 49, 382–384.

291. Liang Y, Cui Z, Zhu S, Liu Y and Yang X, J. Catal, 2011, 278, 276–287.

292. Virkutyte J and Varma RS, New J. Chem, 2010, 34, 1094–1096.

293. Virkutyte J and Varma RS, RSC Adv, 2012, 2, 2399–2407.

294. Zhang J, Li Y, Zhang Y, Chen M, Wang L, Zhang C and He H, Sci. Rep, 2015, 5, 12950. [PubMed: 26263506]

295. Sharma RK, Dutta S, Sharma S, Zboril R, Varma RS and Gawande MB, Green Chem, 2016, 18, 3184–3209.

296. Gawande MB, Monga Y, Zboril R and Sharma R, Coord. Chem. Rev, 2015, 288, 118–143.

297. Tang D, Yuan R and Chai Y, J. Phys. Chem. B, 2006, 110, 11640–11646. [PubMed: 16800458]

298. Chiou JR, Lai BH, Hsu KC and Chen DH, J. Hazard. Mater, 2013, 248, 394–400. [PubMed: 23416483]

299. Sun W, Meng Y, Fu Q, Wang F, Wang G, Gao W, Huang X and Lu F, ACS Appl. Mater. Interfaces, 2016, 8, 9881–9888. [PubMed: 27023711]

300. Wu J, Qin L, Wang C, Lv B, Wang L, Chen J and Xu Y, RSC Adv, 2016, 6, 38356–38364.

301. Lin Y, Bunker CE, Fernando KS and Connell JW, ACS Appl. Mater. Interfaces, 2012, 4, 1110–1117. [PubMed: 22280102]

302. Gao G, Mathkar A, Martins EP, Galvão DS, Gao D, da Silva Autreto PA, Sun C, Cai L and Ajayan PM, J. Mater. Chem. A, 2014, 2, 3148–3154.

303. Pang J, Chao Y, Chang H, Li H, Xiong J, Zhang Q, Chen G, Qian J, Zhu W and Li H, ACS Sustainable Chem. Eng, 2018, 6, 4948–4957.

304. Pullanchiyodan A, Nair KS and Surendran KP, ACS Omega, 2017, 2, 8825–8835. [PubMed: 31457413]

305. Benaglia M, Puglisi A and Cozzi F, Chem. Rev, 2003, 103, 3401–3430. [PubMed: 12964876]

306. Mbhele Z, Salemane M, Van Sittert C, Nedeljkovi J, Djokovi V and Luyt A, Chem. Mater, 2003, 15, 5019–5024.

307. Zhu JF and Zhu YJ, J. Phys. Chem. B, 2006, 110, 8593–8597. [PubMed: 16640412]

308. Cao HL, Huang HB, Chen Z, Karadeniz B, Lü J and Cao R, ACS Appl. Mater. Interfaces, 2017, 9, 5231–5236. [PubMed: 28165717]

309. Yu D, Tan MX and Zhang Y, Adv. Synth. Catal, 2012, 354, 969–974.

310. Eisa WH, Abdel-Baset T, Mohamed EM and Mahrous S, J. Inorg. Organomet. Polym. Mater, 2017, 27, 1703–1711.

311. Silvestri D, Wacławek S, Venkateshaiah A, Krawczyk K, Sobel B, Padil VV, erník M and Varma RS, Carbohydr. Polym, 2020, 232, 115806. [PubMed: 31952605]

312. Colella C and Gualtieri AF, Microporous Mesoporous Mater, 2007, 105, 213–221.

313. Johnson E and Arshad SE, Appl. Clay Sci, 2014, 97, 215–221.

314. Farrusseng D and Tuel A, New J. Chem, 2016, 40, 3933–3949.

315. Wu Y, Li C, Bai J and Wang J, Results Phys, 2017, 7, 1616–1622.

316. Zaarour M, El Roz M, Dong B, Retoux R, Aad R, Cardin J, Dufour C, Gourbilleau F, Gilson JP and Mintova S, Langmuir, 2014, 30, 6250–6256. [PubMed: 24810992]

317. Liu Y, Zhu Z, Liu G, Xu Z, Kuznicki SM and Zhang H, J. Phys. Chem. C, 2011, 115, 14591–14597.

318. Guillerm V, Kim D, Eubank JF, Luebke R, Liu X, Adil K, Lah MS and Eddaoudi M, Chem. Soc. Rev, 2014, 43, 6141–6172. [PubMed: 25009001]

319. Czaja AU, Trukhan N, and Müller U, Chem. Soc. Rev, 2009, 38, 1284–1293. [PubMed: 19384438]

320. Zhu QL and Xu Q, Chem. Soc. Rev, 2014, 43, 5468–5512. [PubMed: 24638055]

321. Xu GW, Wu YP, Dong WW, Zhao J, Wu XQ, Li DS and Zhang Q, Small, 2017, 13, 1602996.

322. Dutta G, Jana AK, Singh DK, Eswaramoorthy M and Natarajan S, Chem. – Asian J, 2018, 13, 2677–2684. [PubMed: 29923682]

323. Zhu NN, Liu XH, Li T, Ma JG, Cheng P and Yang GM, Inorg. Chem, 2017, 56, 3414–3420. [PubMed: 28263612]

324. Chang S, Liu C, Sun Y, Yan Z, Zhang X, Hu X and Zhang H, ACS Appl. Nano Mater, 2020, 3, 2302–2309.

325. Eisa WH, Abdelgawad AM and Rojas OJ, ACS Sustainable Chem. Eng, 2018, 6, 3974–3983.

326. Goswami M, Baruah D and Das AM, New J. Chem, 2018, 42, 10868–10878.

327. Heidari H and Karbalaee M, Appl. Organomet. Chem, 2019, 33, e5070.

328. Goswami A, Rathi AK, Aparicio C, Tomanec O, Petr M, Pocklanova R, Gawande MB, Varma RS and Zboril R, ACS Appl. Mater. Interfaces, 2017, 9, 2815–2824. [PubMed: 28035800]

329. Gawande MB, Goswami A, Asefa T, Guo H, Biradar AV, Peng DL, Zboril R and Varma RS, Chem. Soc. Rev, 2015, 44, 7540–7590. [PubMed: 26288197]

330. Sankar M, Dimitratos N, Miedziak PJ, Wells PP, Kiely CJ and Hutchings GJ, Chem. Soc. Rev, 2012, 41, 8099–8139. [PubMed: 23093051]

331. Chen T and Rodionov VO, ACS Catal, 2016, 6, 4025–4033.

332. Jia K, Yuan L, Zhou X, Pan L, Wang P, Chen W and Liu X, RSC Adv, 2015, 5, 58163–58170.

333. Karatok M, Duanmu K, O'Connor CR, Boscoboinik JA, Sautet P, Madix RJ and Friend CM, Chem. Sci, 2020, 11, 6492–6499. [PubMed: 34094115]

334. Sharma M, Pudasaini PR, Ruiz-Zepeda F, Vinogradova E and Ayon AA, ACS Appl. Mater. Interfaces, 2014, 6, 15472–15479. [PubMed: 25137194]

335. Kim C, Suh BL, Yun H, Kim J and Lee H, ACS Catal, 2017, 7, 2294–2302.

336. Xia B, He F and Li L, Langmuir, 2013, 29, 4901–4907. [PubMed: 23517530]

337. AbdelHamid AA, Al-Ghobashy MA, Fawzy M, Mohamed MB and Abdel-Mottaleb MM, ACS Sustainable Chem. Eng, 2013, 1, 1520–1529.

338. Wu W, Lei M, Yang S, Zhou L, Liu L, Xiao X, Jiang C and Roy VA, J. Mater. Chem. A, 2015, 3, 3450–3455.

339. Zhang Z, Nenoff TM, Leung K, Ferreira SR, Huang JY, Berry DT, Provencio PP and Stumpf R, J. Phys. Chem. C, 2010, 114, 14309–14318.

340. Peng Z, Spliethoff B, Tesche B, Walther T and Kleinermanns K, J. Phys. Chem. B, 2006, 110, 2549–2554. [PubMed: 16471854]

341. Ghosh Chaudhuri R and Paria S, Chem. Rev, 2012, 112, 2373–2433. [PubMed: 22204603]

342. Karam TE, Smith HT and Haber LH, J. Phys. Chem. C, 2015, 119, 18573–18580.

343. Carroll KJ, Hudgins DM, Spurgeon S, Kemner KM, Mishra B, Boyanov MI, Brown III LW, Taheri ML and Carpenter EE, Chem. Mater, 2010, 22, 6291–6296.

344. Samal AK, Polavarapu L, Rodal-Cedeira S, Liz-Marzán LM, Pérez-Juste J and Pastoriza-SantoI s., Langmuir, 2013, 29, 15076–15082. [PubMed: 24261458]

345. Anandan S, Grieser F and Ashokkumar M, J. Phys. Chem. C, 2008, 112, 15102–15105.

346. Tsuji M, Miyamae N, Lim S, Kimura K, Zhang X, Hikino S and Nishio M, Cryst. Growth Des, 2006, 6, 1801–1807.

347. Nazir R, Fageria P, Basu M and Pande S, J. Phys. Chem. C, 2017, 121, 19548–19558.

348. Zhu Y, Marianov A, Xu H, Lang C and Jiang Y, ACS Appl. Mater. Interfaces, 2018, 10, 9468–9477. [PubMed: 29465987]

349. Navlani-García M, Mori K, Nozaki A, Kuwahara Y and Yamashita H, Ind. Eng. Chem. Res, 2016, 55, 7612–7620.

350. Li D, Liu J, Wang H, Barrow CJ and Yang W, Chem. Commun, 2016, 52, 10968–10971.

351. Liu J, Zhou H, Wang Q, Zeng F and Kuang Y, J. Mater. Sci, 2012, 47, 2188–2194.

352. Khatami M, Alijani HQ, Nejad MS and Varma RS, Appl. Sci, 2018, 8, 411.

353. Yang Z, Muller AH, Xu C, Doyle PS, DeSimone JM, Lahann J, Sciortino F, Glotzer S, Hong L and Aarts DA, Janus particle synthesis, self-assembly and applications, Royal Society of Chemistry, 2012, DOI: 10.1039/9781849735100.

354. Poggi E and Gohy JF, Colloid Polym. Sci, 2017, 295, 2083–2108.

355. Song Y, Liu K and Chen S, Langmuir, 2012, 28, 17143–17152. [PubMed: 23163535]

356. Chen L, Deming CP, Peng Y, Hu P, Stofan J and Chen S, Nanoscale, 2016, 8, 14565–14572. [PubMed: 27417026]

357. Jiang F, Tian Q, Tang M, Chen Z, Yang J and Hu J, CrystEngComm, 2011, 13, 7189–7193.

358. Dutta D, Hazarika R, Dutta PD, Goswami T, Sengupta P and Dutta DK, RSC Adv, 2016, 6, 85173–85181.

359. Kirillova A, Schliebe C, Stoychev G, Jakob A, Lang H and Synytska A, ACS Appl. Mater. Interfaces, 2015, 7, 21218–21225. [PubMed: 26357969]

360. Kaviyarasu K, Manikandan E, Kennedy J and Maaza M, RSC Adv, 2015, 5, 82421–82428.

361. Sobhani-Nasab A and Behpour M, J. Mater. Sci.: Mater. Electron, 2016, 27, 1191–1196.

362. Akbari M, Aetemady A, Firoozeh F and Yaseliani M, J. Mater. Sci.: Mater. Electron, 2017, 28, 10245–10249.

363. Vinay S, Sumedha H, Nagaraju G, Harishkumar S and Chandrasekhar N, Appl. Organomet. Chem, 2020, 34, e5830.

364. Rashmi B, Harlapur SF, Avinash B, Ravikumar C, Nagaswarupa H, Kumar MA, Gurushantha K and Santosh M, Inorg. Chem. Commun, 2020, 111, 107580.

365. Sarkar D, Ghosh CK, Mukherjee S and Chattopadhyay KK, ACS Appl. Mater. Interfaces, 2013, 5, 331–337. [PubMed: 23245288]

366. Das P, Ray S, Bhaumik A, Banerjee B and Mukhopadhyay C, RSC Adv, 2015, 5, 6323–6331.

367. Chen YY, Yu SH, Yao QZ, Fu SQ and Zhou GT, J. Colloid Interface Sci, 2018, 510, 280–291. [PubMed: 28957744]

368. Li MY, Mao YQ, Yang SK, Dai TT, Yang H, Feng F, Wu T, Chen M, Xu GQ and Wu JH, ACS Omega, 2016, 1, 696–705. [PubMed: 31457157]

369. Sheldon RA, J. R. Soc., Interface, 2016, 13, 20160087. [PubMed: 27009181]

370. Yan N, Nanotechnol. Rev, 2013, 2, 485–486.

371. Polshettiwar V and Varma RS, Green Chem, 2010, 12, 743–754.

372. Biffis A, Centomo P, Del Zotto A and Zecca M, Chem. Rev, 2018, 118, 2249–2295. [PubMed: 29460627]

373. Cahiez G and Moyeux A, Chem. Rev, 2010, 110, 1435–1462. [PubMed: 20148539]

374. Martin R and Buchwald SL, Acc. Chem. Res, 2008, 41, 1461–1473. [PubMed: 18620434]

375. Rao VK and Radhakrishnan T, J. Mater. Chem. A, 2013, 1, 13612–13618.

376. Gorji S and Ghorbani-Vaghei R, Appl. Organomet. Chem, 2021, 35, e6018.

377. Chinchilla R and Nájera C, Chem. Rev, 2007, 107, 874–922. [PubMed: 17305399]

378. Chinchilla R and Nájera C, Chem. Soc. Rev, 2011, 40, 5084–5121. [PubMed: 21655588]

379. Mohajer F, Heravi MM, Zadsirjan V and Poormohammad N, RSC Adv, 2021, 11, 6885–6925.

380. Chen M, Zhang Z, Li L, Liu Y, Wang W and Gao J, RSC Adv, 2014, 4, 30914–30922.

381. Tedsree K, Li T, Jones S, Chan CWA, Yu KMK, Bagot PAJ, Marquis EA, Smith GDW and Tsang SCE, Nat. Nanotechnol, 2011, 6, 302–307. [PubMed: 21478867]

382. Venkatesan P and Santhanalakshmi J, Langmuir, 2010, 26, 12225–12229. [PubMed: 20462280]

383. Beletskaya IP and Cheprakov AV, Chem. Rev, 2000, 100, 3009–3066. [PubMed: 11749313]

384. Venkatesan P and Santhanalakshmi J, Phys. Chem, 2012, 2, 12–15.

385. Hruszkewycz D, McCann S and Stahl S, Liquid Phase Aerobic Oxidation Catalysis, Wiley-VCH, Weinheim, 2016, pp. 67–83.

386. Besson M and Gallezot P, Catal. Today, 2000, 57, 127–141.

387. Waters T, O'Hair RA and Wedd AG, J. Am. Chem. Soc, 2003, 125, 3384–3396. [PubMed: 12630894]

388. Velasquez Ochoa and J Cavani F, Transition Metal Catalysis in Aerobic Alcohol Oxidation, 2015, pp. 203–230, DOI: 10.1039/9781782621652-00203.

389. Aouat Y, Azan Y, Marom G and Avnir D, Sci. Adv. Mater, 2013, 5, 598–605.

390. Halperin V, Shter G, Gelman V, Peselev D, Mann-Lahav M and Grader G, Catal. Sci. Technol, 2015, 5, 1153–1162.

391. Sobczak I, Kozlowska M and Ziolek M, J. Mol. Catal. A: Chem, 2014, 390, 114–124.

392. Shirman T, Lattimer J, Luneau M, Shirman E, Reece C, Aizenberg M, Madix RJ, Aizenberg J and Friend CM, Chem. – Eur. J, 2018, 24, 1833–1837. [PubMed: 28960528]

393. Zhu Q, Wang B and Tan T, ACS Sustainable Chem. Eng, 2017, 5, 722–733.

394. Pomalaza G, Capron M, Ordomsky V and Dumeignil F, Catalysts, 2016, 6, 203.

395. Mamontov G, Grabchenko M, Sobolev V, Zaikovskii V and Vodyankina O, Appl. Catal., A, 2016, 528, 161–167.

396. Ciftci A, Ligthart DM, Pastorino P and Hensen EJ, Appl. Catal., B, 2013, 130, 325–335.

397. Guan Y and Hensen EJ, J. Catal, 2013, 305, 135–145.

398. Oyama ST and Somorjai GA, J. Phys. Chem, 1990, 94, 5022–5028.

399. Silbaugh TL, Devlaminck P, Sofranko JA and Barteau MA, J. Catal, 2018, 364, 40–47.

400. Lippits M and Nieuwenhuys B, Catal. Today, 2010, 154, 127–132.

401. Purcar V, Donescu D, Petcu C, Luque R and Macquarrie DJ, Appl. Catal., A, 2009, 363, 122–128.

402. Li Z, Zhu L, Chen JF and Cheng D, Ind. Eng. Chem. Res, 2018, 57, 4180–4185.

403. Tian S, Peng C, Dong J, Xu Q, Chen Z, Zhai D, Wang Y, Gu L, Hu P, Duan H, Wang D and Li Y, ACS Catal, 2021, 11, 4946–4954.

404. Wang X, Liang Z, Zhang F, Yang L and Xu S, J. Mater. Sci, 2013, 48, 5899–5903.

405. Anandhakumar S, Sasidharan M, Tsao CW and Raichur AM, ACS Appl. Mater. Interfaces, 2014, 6, 3275–3281. [PubMed: 24552178]

406. Fisher E, Kenisgberg L, Carreira M, Fernández-Gallardo J, Baldwin R and Contel M, Polyhedron, 2016, 120, 82–87.

407. Xu LW, Li L, Lai GQ and Jiang JX, Chem. Soc. Rev, 2011, 40, 1777–1790. [PubMed: 21088772]

408. Mitsudome T, Arita S, Mori H, Mizugaki T, Jitsukawa K and Kaneda K, Angew. Chem., Int. Ed, 2008, 47, 7938–7940.

409. Mikami Y, Noujima A, Mitsudome T, Mizugaki T, Jitsukawa K and Kaneda K, Tetrahedron Lett, 2010, 51, 5466–5468.

410. Li C, Li X, Duan X, Li G and Wang J, J. Colloid Interface Sci, 2014, 436, 70–76. [PubMed: 25268813]

411. Cho BT, Chem. Soc. Rev, 2009, 38, 443–452. [PubMed: 19169459]

412. Shao M, Chang Q, Dodelet JP and Chenitz R, Chem. Rev, 2016, 116, 3594–3657. [PubMed: 26886420]

413. Dub PA and Ikariya T, ACS Catal, 2012, 2, 1718–1741.

414. Brieger G and Nestrick TJ, Chem. Rev, 1974, 74, 567–580.

415. Jia Z, Zhou F, Liu M, Li X, Chan AS and Li CJ, Angew. Chem., Int. Ed, 2013, 52, 11871–11874.

416. Jia Z, Liu M, Li X, Chan AS and Li CJ, Synlett, 2013, 2049–2056.

417. Gawande MB, Guo H, Rathi AK, Branco PS, Chen Y, Varma RS and Peng DL, RSC Adv, 2013, 3, 1050–1054.

418. Mitsudome T, Matoba M, Mizugaki T, Jitsukawa K and Kaneda K, Chem. – Eur. J, 2013, 19, 5255–5258. [PubMed: 23504913]

419. Cui G, Sun Z, Li H, Liu X, Liu Y, Tian Y and Yan S, J. Mater. Chem. A, 2016, 4, 1771–1783.

420. Silvestri D, Wacławek S, Venkateshaiah A, Krawczyk K, Sobel B, Padil VVT, erník M and Varma RS, Carbohydr. Polym, 2020, 232, 115806. [PubMed: 31952605]

421. Agrawal A and Tratnyek PG, Environ. Sci. Technol, 1995, 30, 153–160.

422. Formenti D, Ferretti F, Scharnagl FK and Beller M, Chem. Rev, 2018, 119, 2611–2680. [PubMed: 30516963]

423. Xu Y, Zhou F, Chen M, Hu H, Lin L, Wu J and Zhang M, New J. Chem, 2020, 44, 9793–9801.

424. Mali M, Synth. Catal, 2017, 2, 1–8.

425. Gong W, Wu Q, Jiang G and Li G, J. Mater. Chem. A, 2019, 7, 13449–13454.

426. Sharma RK, Yadav P, Yadav M, Gupta R, Rana P, Srivastava A, Zbo il R, Varma RS, Antonietti M and Gawande MB, Mater. Horiz, 2020, 7, 411–454.

427. Ma W, Zheng Q, He Y, Li G, Guo W, Lin Z and Zhang L, J. Am. Chem. Soc, 2019, 141, 18271–18277. [PubMed: 31656073]

428. Wang N, Wang F, Pan F, Yu S and Pan D, ACS Appl. Mater. Interfaces, 2021, 13, 3209–3220. [PubMed: 33404207]

429. Liu GF, Qiao XX, Cai YL, Xu JY, Yan Y, Karadeniz B, Lü J and Cao R, ACS Appl. Nano Mater, 2020, 3, 11426–11433.

430. Manno R, Sebastian V, Irusta S, Mallada R and Santamaria J, Catal. Today, 2021, 362, 81–89.

431. Horta-Fraijo P, Smolentseva E, Simakov A, José-Yacaman M and Acosta B, Microporous Mesoporous Mater, 2021, 312, 110707.

432. Hu XD, Shan BQ, Tao R, Yang TQ and Zhang K, J. Phys. Chem. C, 2021, 125, 2446–2453.

433. Bhagavanth Reddy G, Dadigala R, Bandi R, Seku K, Koteswararao D, Mangatayaru K G and Shalan AE, RSC Adv, 2021, 11, 5139–5148.

434. Shabir J, Rani S, Sharma M, Garkoti C, Surabhi and Mozumdar S, RSC Adv, 2020, 10, 8140–8151.

435. Ding Y, Sun W, Yang W and Li Q, Appl. Catal., B, 2017, 203, 372–380.

436. Coeck R, Meeprasert J, Li G, Altantzis T, Bals S, Pidko EA and De Vos DE, ACS Catal, 2021, 7672–7684, DOI: 10.1021/acscatal.1c01693.

437. Wang F, Ma J, Xin S, Wang Q, Xu J, Zhang C, He H and Cheng X, Zeng, Nat. Commun, 2020, 11, 529. [PubMed: 31988282]

438. Barreiro EM, Adrio LA, Hii KK and Brazier JB, Eur. J. Org. Chem, 2013, 1027–1039.

439. Muñoz MP, Chem. Soc. Rev, 2014, 43, 3164–3183. [PubMed: 24668233]

440. Yu M, Wang Y, Sun W and Yao X, Adv. Synth. Catal, 2012, 354, 71–76.

441. Jewett JC and Bertozzi CR, Chem. Soc. Rev, 2010, 39, 1272–1279. [PubMed: 20349533]

442. Cong H, Becker CF, Elliott SJ, Grinstaff MW and Porco JA, J. Am. Chem. Soc, 2010, 132, 7514–7518. [PubMed: 20443601]

443. Madhavan S and Okamoto S, ChemCatChem, 2018, 10, 2014–2018.

444. Gandeepan P, Müller T, Zell D, Cera G, Warratz S and Ackermann L, Chem. Rev, 2018, 119, 2192–2452. [PubMed: 30480438]

445. Tzouras NV, Stamatopoulos IK, Papastavrou AT, Liori AA and Vougioukalakis GC, Coord. Chem. Rev, 2017, 343, 25–138.

446. Wan JP, Gan L and Liu Y, Org. Biomol. Chem, 2017, 15, 9031–9043. [PubMed: 29075706]

447. Weibel JM, Blanc A and Pale P, Chem. Rev, 2008, 108, 3149–3173. [PubMed: 18616324]

448. Zheng QZ and Jiao N, Chem. Soc. Rev, 2016, 45, 4590–4627. [PubMed: 27056573]

449. Zhang X, Liu H, Shi Y, Han J, Yang Z, Zhang Y, Long C, Guo J, Zhu Y, Qiu X, Xue G, Zhang L, Zhang B, Chang L and Tang Z, Matter, 2020, 3, 558–570.

450. Biswas R, Das SK, Bhaduri SN, Bhaumik A and Biswas P, ACS Sustainable Chem. Eng, 2020, 8, 5856–5867.

451. Hosseini-Sarvari M and Dehghani A, New J. Chem, 2020, 44, 16776–16785.

452. Chang Z, Jing X, He C, Liu X and Duan C, ACS Catal, 2018, 8, 1384–1391.

453. Hulme C, Akritopoulou-Zanze I, Dai WM, Beck B, Srivastava S, Wang W, Wang K, Czarna A, Holak TA and Meireles L, MCR 2009, Springer, 2011, pp. 75–106.

454. Wei C, Li Z and Li CJ, Org. Lett, 2003, 5, 4473–4475. [PubMed: 14602028]

455. Iordanidou D, Zarganes-Tzitzikas T, Neochoritis CG, Dömling A and Lykakis IN, ACS Omega, 2018, 3, 16005–16013. [PubMed: 30533584]

456. Sapkota K and Han SS, New J. Chem, 2017, 41, 5395–5402.

457. Veisi H, Mohammadi L, Hemmati S, Tamoradi T and Mohammadi P, ACS Omega, 2019, 4, 13991–14003. [PubMed: 31497717]

458. Torabi P and Moradian M, J. Nanostruct, 2019, 9, 478–488.

459. Zhou X, Lu Y, Zhai LL, Zhao Y, Liu Q and Sun WY, RSC Adv, 2013, 3, 1732–1734.

460. Mohamed YM, El Nazer HA and Solum EJ, Chem. Pap, 2019, 73, 435–445.

461. Borah SJ and Das DK, Catal. Lett, 2016, 146, 656–665.

462. Yong GP, Tian D, Tong HW and Liu SM, J. Mol. Catal. A: Chem, 2010, 323, 40–44.

463. Movahedi F, Masrouri H and Kassaee M, J. Mol. Catal. A: Chem, 2014, 395, 52–57.

464. Praveena G, Yagnam S, Banoth L, Trivedi R and Prakasham RS, New J. Chem, 2020, 44, 13046–13061.

465. Nasrollahzadeh M, Sajjadi M, Tahsili MR, Shokouhimehr M and Varma RS, ACS Omega, 2019, 4, 8985–9000. [PubMed: 31459987]

466. Johnson TC, Morris DJ and Wills M, Chem. Soc. Rev, 2010, 39, 81–88. [PubMed: 20023839]

467. Joó F, ChemSusChem, 2008, 1, 805–808. [PubMed: 18781551]

468. Enthaler S, ChemSusChem, 2008, 1, 801–804. [PubMed: 18781550]

469. Shimbayashi T and Fujita K-I, Tetrahedron, 2020, 76, 130946.

470. Yadav GD and Mewada RK, Catal. Today, 2012, 198, 330–337.

471. Das SK, Khan MMR, Guha AK and Naskar N, Green Chem, 2013, 15, 2548–2557.

472. Shimizu KI, Miyamoto Y and Satsuma A, J. Catal, 2010, 270, 86–94.

473. Liu Z, Dong W, Cheng S, Guo S, Shang N, Gao S, Feng C, Wang C and Wang Z, Catal. Commun, 2017, 95, 50–53.

474. Pei G, Liu X, Wang A, Su Y, Li L and Zhang T, Appl. Catal., A, 2017, 545, 90–96.

475. Deng JP, Shih WC and Mou CY, J. Phys. Chem. C, 2007, 111, 9723–9728.

476. Aich P, Wei H, Basan B, Kropf AJ, Schweitzer NM, Marshall CL, Miller JT and Meyer R, J. Phys. Chem. C, 2015, 119, 18140–18148.

477. Bulut A, Yurderi M, Karatas Y, Say Z, Kivrak H, Kaya M, Gulcan M, Ozensoy E and Zahmakiran M, ACS Catal, 2015, 5, 6099–6110.

478. Liu H, Guo Y, Yu Y, Yang W, Shen M, Liu X, Geng S, Li J, Yu C, Yin Z and Li H, J. Mater. Chem. A, 2018, 6, 17323–17328.

479. Zhang Z, Luo Y, Liu S, Yao Q, Qing S and Lu Z-H, J. Mater. Chem. A, 2019, 7, 21438–21446.

480. Feng C, Hao Y, Zhang L, Shang N, Gao S, Wang Z and Wang C, RSC Adv, 2015, 5, 39878–39883.

481. Zhao X, Xu D, Liu K, Dai P and Gao J, Appl. Surf. Sci, 2020, 512, 145746.

482. Zhang S, Metin O, Su D and Sun S, Angew. Chem., Int. Ed, 2013, 52, 3681–3684.

483. Yu C, Guo X, Shen B, Xi Z, Li Q, Yin Z, Liu H, Muzzio M, Shen M, Li J, Seto CT and Sun S, J. Mater. Chem. A, 2018, 6, 23766–23772.

484. Shimizu K, Sugino K, Sawabe K and Satsuma A, Chem. – Eur. J, 2009, 15, 2341–2351. [PubMed: 19160439]

485. Mamontov G, Grabchenko MV, Sobolev V, Zaikovskii V and Vodyankina O, Appl. Catal., A, 2016, 528, 161–167.

486. Janlamool J and Jongsomjit B, Catal. Commun, 2015, 70, 49–52.

487. Karmakar R, Pahari P and Mal D, Chem. Rev, 2014, 114, 6213–6284. [PubMed: 24823231]

488. Chaudhary S, Shyamlal BRK, Yadav L, Tiwari MK and Kumar K, RSC Adv, 2018, 8, 23152–23162.

489. Sun M, Su L, Dong J, Liu L, Zhou Y and Yin SF, Tetrahedron Lett, 2017, 58, 2433–2437.

490. Kumar MR, Irudayanathan FM, Moon JH and Lee S, Adv. Synth. Catal, 2013, 355, 3221–3230.

491. Almasalma AA and Mejía E, Eur. J. Org. Chem, 2018, 188–195.

492. Chadha R, Maiti N and Kapoor S, J. Phys. Chem. C, 2014, 118, 26227–26235.

493. Ayán-Varela M, Fernández-Merino MJ, Paredes J, Villar-Rodil S, Fernández-Sánchez C, Guardia L, Martínez-Alonso A and Tascón J, J. Phys. Chem. C, 2014, 2, 7295–7305.

494. Zhou Y, Shen Y, Luo X, Liu G and Cao Y, Nanoscale Adv, 2020, 2, 3423–3430.

495. Yadav GD, Chandan PA and Tekale DP, Ind. Eng. Chem. Res, 2012, 51, 1549–1562.

496. Zhou J, Zhang J, Guo X, Mao J and Zhang S, Green Chem, 2012, 14, 156–163.

497. Sun D, Yamada Y and Sato S, Appl. Catal., A, 2014, 475, 63–68.

498. Koley P, Shit SC, Sabri YM, Srinivasa Rao B, Nakka L, Tardio J and Mondal J, ACS Sustainable Chem. Eng, 2021, 9, 3750–3767.

499. Zheng Y, Hou L, Liu M, Newell SE, Yin G, Yu C, Zhang H, Li X, Gao D, Gao J, Wang R and Liu C, Sci. Adv, 2017, 3, e1603229. [PubMed: 28782034]

500. Jafari T, Moharreri E, Amin AS, Miao R, Song W and Suib SL, Molecules, 2016, 21, 900.

501. Huang Z, Miseki Y and Sayama K, Chem. Commun, 2019, 55, 3813–3816.

502. Kamat PV, ACS Energy Lett, 2017, 2, 1586–1587.

503. Liu B, Zhao X, Terashima C, Fujishima A and Nakata K, Phys. Chem. Chem. Phys, 2014, 16, 8751–8760. [PubMed: 24675975]

504. Abedi S and Morsali A, ACS Catal, 2014, 4, 1398–1403.

505. Samanta S, Martha S and Parida K, ChemCatChem, 2014, 6, 1453–1462.

506. Liu P, Yi J, Bao R and Fang D, New J. Chem, 2019, 43, 7482–7490.

507. Sarina S, Waclawik ER and Zhu H, Green Chem, 2013, 15, 1814–1833.

508. Wang P, Huang B, Dai Y and Whangbo MH, Phys. Chem. Chem. Phys, 2012, 14, 9813–9825. [PubMed: 22710311]

509. Shen L, Luo M, Huang L, Feng P and Wu L, Inorg. Chem, 2015, 54, 1191–1193. [PubMed: 25594784]

510. Chen X, Zheng Z, Ke X, Jaatinen E, Xie T, Wang D, Guo C, Zhao J and Zhu H, Green Chem, 2010, 12, 414–419.

511. Awazu K, Fujimaki M, Rockstuhl C, Tominaga J, Murakami H, Ohki Y, Yoshida N and Watanabe T, J. Am. Chem. Soc, 2008, 130, 1676–1680. [PubMed: 18189392]

512. Tee SY, Win KY, Teo WS, Koh LD, Liu S, Teng CP and Han MY, Adv. Sci, 2017, 4, 1600337.

513. Yu B, Zhou Y, Li P, Tu W, Li P, Tang L, Ye J and Zou Z, Nanoscale, 2016, 8, 11870–11874. [PubMed: 27231820]

514. Liu J, Zhang H, Tang D, Zhang X, Yan L, Han Y, Huang H, Liu Y and Kang Z, ChemCatChem, 2014, 6, 2634–2641.

515. Jeong SY, Shin HM, Jo YR, Kim YJ, Kim S, Lee WJ, Lee GJ, Song J, Moon BJ and Seo S, J. Phys. Chem. C, 2018, 122, 7088–7093.

516. Sheu JK, Liao PH, Lee YC, Wang HK and Lee ML, J. Phys. Chem. C, 2020, 124, 9591–9598.

517. Alenzi N, Liao WS, Cremer PS, Sanchez-Torres V, Wood TK, Ehlig-Economides C and Cheng Z, Int. J. Hydrogen Energy, 2010, 35, 11768–11775.

518. Zhang N, Zhang Y, Pan X, Yang MQ and Xu Y-J, J. Phys. Chem. C, 2012, 116, 18023–18031.

519. Iwase A, Ng YH, Ishiguro Y, Kudo A and Amal R, J. Am. Chem. Soc, 2011, 133, 11054–11057. [PubMed: 21711031]

520. Yang Y, Liu E, Dai H, Kang L, Wu H, Fan J, Hu X and Liu H, Int. J. Hydrogen Energy, 2014, 39, 7664–7671.

521. Wu F, Hu X, Fan J, Liu E, Sun T, Kang L, Hou W, Zhu C and Liu H, Plasmonics, 2013, 8, 501–508.

522. Walter MG, Warren EL, McKone JR, Boettcher SW, Mi Q, Santori EA and Lewis NS, Chem. Rev, 2010, 110, 6446–6473. [PubMed: 21062097]

523. Wood A, Giersig M and Mulvaney P, J. Phys. Chem. B, 2001, 105, 8810–8815.

524. Choi Y, Kim HI, Moon GH, Jo S and Choi W, ACS Catal, 2016, 6, 821–828.

525. Martin DJ, Qiu K, Shevlin SA, Handoko AD, Chen X, Guo Z and Tang J, Angew. Chem., Int. Ed, 2014, 53, 9240–9245.

526. Di Y, Wang X, Thomas A and Antonietti M, ChemCatChem, 2010, 2, 834–838.

527. Rathi AK, Kmentová H, Naldoni A, Goswami A, Gawande MB, Varma RS, Kment Š and Zbo il R, ACS Appl. Nano Mater, 2018, 1, 2526–2535.

528. Pieta IS, Rathi A, Pieta P, Nowakowski R, Hołdynski M, Pisarek M, Kaminska A, Gawande MB and Zboril R, Appl. Catal., B, 2019, 244, 272–283.

529. Li H, Gan S, Wang H, Han D and Niu L, Adv. Mater, 2015, 27, 6906–6913. [PubMed: 26422111]

530. Ge L, Han C, Liu J and Li Y, Appl. Catal., A, 2011, 409, 215–222.

531. Qin J, Huo J, Zhang P, Zeng J, Wang T and Zeng H, Nanoscale, 2016, 8, 2249–2259. [PubMed: 26743319]

532. Singh B, Sharma V, Gaikwad RP, Fornasiero P, Zbo il R and Gawande MB, Small, 2021, 2006473, DOI: 10.1002/smll.202006473.

533. Pieta IS, Kadam RG, Pieta P, Mrdenovic D, Nowakowski R, Bakandritsos A, Tomanec O, Petr M, Otyepka M, Kostecki R, Khan MAM, Zboril R and Gawande MB, Adv. Mater. Interfaces, 2021, 2001822, DOI: 10.1002/admi.202001822.

534. Du XL, Wang XL, Li YH, Wang YL, Zhao JJ, Fang LJ, Zheng LR, Tong H and Yang HG, Chem. Commun, 2017, 53, 9402–9405.

535. Jiang XH, Zhang LS, Liu HY, Wu DS, Wu FY, Tian L, Liu LL, Zou JP, Luo SL and Chen BB, Angew. Chem., Int. Ed, 2020, 59, 23112–23116.

536. Majeed I, Manzoor U, Kanodarwala FK, Nadeem MA, Hussain E, Ali H, Badshah A, Stride JA and Nadeem MA, Catal. Sci. Technol, 2018, 8, 1183–1193.

537. Shaik SA, Sengupta S, Varma RS, Gawande MB and Goswami A, ACS Sustainable Chem. Eng, 2021, 9, 3–49.

538. Qin J and Zeng H, Appl. Catal., B, 2017, 209, 161–173.

539. Erwin WR, Coppola A, Zarick HF, Arora P, Miller KJ and Bardhan R, Nanoscale, 2014, 6, 12626–12634. [PubMed: 25188374]

540. Xu D, Yang S, Jin Y, Chen M, Fan W, Luo B and Shi W, Langmuir, 2015, 31, 9694–9699. [PubMed: 26280571]

541. Ji X, Liu B, Ren X, Shi X, Asiri AM and Sun X, ACS Sustainable Chem. Eng, 2018, 6, 4499–4503.

542. Prasad C, Tang H, Liu Q, Bahadur I, Karlapudi S and Jiang Y, Int. J. Hydrogen Energy, 2020, 45, 337–379.

543. Jeon TH, Monllor-Satoca D, Moon GH, Kim W, Kim HI, Bahnemann DW, Park H and Choi W, Nat. Commun, 2020, 11, 967. [PubMed: 32075977]

544. Zhao S, Jin R and Jin R, ACS Energy Lett, 2018, 3, 452–462.

545. Lu Q, Rosen J and Jiao F, ChemCatChem, 2015, 7, 38–47.

546. Lu Q, Rosen J, Zhou Y, Hutchings GS, Kimmel YC, Chen JG and Jiao F, Nat. Commun, 2014, 5, 1–6.

547. Kumar S, Gawande MB, Kopp J, Kment S, Varma RS and Zbořil R, ChemSusChem, 2020, 13, 5231–5238. [PubMed: 32687261]

548. Sharma P, Kumar S, Tomanec O, Petr M, Zhu Chen J, Miller JT, Varma RS, Gawande MB and Zbořil R, Small, 2021, 2006478, DOI: 10.1002/smll.202006478.

549. Kumari G, Zhang X, Devasia D, Heo J and Jain PK, ACS Nano, 2018, 12, 8330–8340. [PubMed: 30089207]

550. Kočí K, Matěj K, Obalová L, Krejčíková S, Lacný Z, Plachá D, Čapek L, Hospodková A and Šolcová O, Appl. Catal., B, 2010, 96, 239–244.

551. Iizuka K, Wato T, Miseki Y, Saito K and Kudo A, J. Am. Chem. Soc, 2011, 133, 20863–20868. [PubMed: 22087856]

552. Ding J, Bu Y, Ou M, Yu Y, Zhong Q and Fan M, Appl. Catal., B, 2017, 202, 314–325.

553. Zhao C, Krall A, Zhao H, Zhang Q and Li Y, Int. J. Hydrogen Energy, 2012, 37, 9967–9976.

554. Gulati U, Chinna Rajesh U, Rawat DS and Zaleski JM, Green Chem, 2020, 22, 3170–3177. [PubMed: 33795971]

555. Nielsen DU, Hu XM, Daasbjerg K and Skrydstrup T, Nat. Catal, 2018, 1, 244–254.

556. Du C, Lan X, An G, Li Q and Bai G, ACS Sustainable Chem. Eng, 2020, 8, 7051–7058.

557. Kan M, Yan ZW, Wang X, Hitt JL, Xiao L, McNeill JM, Wang Y, Zhao Y and Mallouk TE, Angew. Chem., Int. Ed, 2020, 59, 11462–11469.

558. Otgonbayar Z, Youn Cho K and Oh WC, New J. Chem, 2020, 44, 16795–16809.

559. Otgonbayar Z, Cho KY and Oh WC, ACS Omega, 2020, 5, 26389–26401. [PubMed: 33110967]

560. Kumari G, Kamarudheen R, Zoethout E and Baldi A, ACS Catal, 2021, 11, 3478–3486. [PubMed: 33859867]

561. Köhler A, Hellweg S, Escher BI and Hungerbühler K, Environ. Sci. Technol, 2006, 40, 3395–3401. [PubMed: 16749712]

562. Yu L, Wang H, Zhang Y, Zhang B and Liu J, Environ. Sci.: Nano, 2016, 3, 28–44.

563. Dias EM and Petit C, J. Mater. Chem. A, 2015, 3, 22484–22506.

564. Tang J, Zou Z and Ye J, Angew. Chem., Int. Ed, 2004, 43, 4463–4466.

565. Ahmed S, Rasul M, Martens WN, Brown R and Hashib M, Water, Air, Soil Pollut, 2011, 215, 3–29.

566. Dunnill CW, Ansari Z, Kafizas A, Perni S, Morgan DJ, Wilson M and Parkin IP, J. Mater. Chem, 2011, 21, 11854–11861.

567. Pirilä M, Saouabe M, Ojala S, Rathnayake B, Drault F, Valtanen A, Huuhtanen M, Brahmi R and Keiski RL, Top. Catal, 2015, 58, 1085–1099.

568. Liang Y, Guo N, Li L, Li R, Ji G and Gan S, New J. Chem, 2016, 40, 1587–1594.

569. Ma S, Xue J, Zhou Y and Zhang Z, J. Mater. Chem. A, 2014, 2, 7272–7280.

570. Zheng Y, Chen C, Zhan Y, Lin X, Zheng Q, Wei K and Zhu J, J. Phys. Chem. C, 2008, 112, 10773–10777.

571. Zhou W, Leng Y, Hou D, Li H, Li L, Li G, Liu H and Chen S, Nanoscale, 2014, 6, 4698–4704. [PubMed: 24651444]

572. Peng S, Li L, Tan H, Wu Y, Cai R, Yu H, Huang X, Zhu P, Ramakrishna S and Srinivasan M, J. Mater. Chem. A, 2013, 1, 7630–7638.

573. Li J, Cushing SK, Bright J, Meng F, Senty TR, Zheng P, Bristow AD and Wu N, ACS Catal, 2013, 3, 47–51.

574. Zhu M, Chen P and Liu M, ACS Nano, 2011, 5, 4529–4536. [PubMed: 21524132]

575. Yıldırım ÖA, Unalan HE and Durucan C, J. Am. Ceram. Soc, 2013, 96, 766–773.

576. Wang P, Huang B, Qin X, Zhang X, Dai Y, Wei J and Whangbo MH, Angew. Chem., Int. Ed, 2008, 47, 7931–7933.

577. Deng Q, Duan X, Ng DH, Tang H, Yang Y, Kong M, Wu Z, Cai W and Wang G, ACS Appl. Mater. Interfaces, 2012, 4, 6030–6037. [PubMed: 23092309]

578. Chen KH, Pu YC, Chang KD, Liang YF, Liu CM, Yeh JW, Shih HC and Hsu YJ, J. Phys. Chem. C, 2012, 116, 19039–19045.

579. Wei Z, Feng L, Zhi-Ming J, Xiao-Bo S, Peng-Hui Y, Xue-Ren W, Cheng S, Zhan-Qi G and Liang-Sheng L, J. Mater. Chem. A, 2014, 2, 13226–13231.

580. Wang D, Xue G, Zhen Y, Fu F and Li D, J. Mater. Chem, 2012, 22, 4751–4758.

581. Liu C, Yang D, Jiao Y, Tian Y, Wang Y and Jiang Z, ACS Appl. Mater. Interfaces, 2013, 5, 3824–3832. [PubMed: 23551122]

582. Lu D, Wang H, Zhao X, Kondamareddy KK, Ding J, Li C and Fang P, ACS Sustainable Chem. Eng, 2017, 5, 1436–1445.

583. He X, Cai Y, Zhang H and Liang C, J. Mater. Chem, 2011, 21, 475–480.

584. Zhang P, Shao C, Zhang Z, Zhang M, Mu J, Guo Z, Sun Y and Liu Y, J. Mater. Chem, 2011, 21, 17746–17753.

585. Zhang K, Heo N, Shi X and Park JH, J. Phys. Chem. C, 2013, 117, 24023–24032.

586. Pagano R, Quarta A, Pal S, Licciulli A, Valli L and Bettini S, J. Phys. Chem. C, 2017, 121, 27199–27206.

587. Jiao T, Guo H, Zhang Q, Peng Q, Tang Y, Yan X and Li B, Sci. Rep, 2015, 5, 11873. [PubMed: 26183266]

588. Tao X, Zhou Y, Xu K, Wu Y, Mi J, Li Y, Liu Q, Cheng X, Zhao N, Shi H and Yang J, ACS Sustainable Chem. Eng, 2018, 6, 16907–16919.

589. Yang SF, Niu CG, Huang DW, Zhang H, Liang C and Zeng GM, Environ. Sci.: Nano, 2017, 4, 585–595.

590. Shojaie A, Fattahi M, Jorfi S and Ghasemi B, Int. J. Ind. Chem, 2018, 9, 141–151.

591. Zhang H, Liang C, Liu J, Tian Z, Wang G and Cai W, Langmuir, 2012, 28, 3938–3944. [PubMed: 22335447]

592. Li Y, Zhou Y, Zeng W, Gao S, Wu Y and Yang J, ChemistrySelect, 2017, 2, 9947–9952.

593. Zhu M, Chen P and Liu M, Langmuir, 2013, 29, 9259–9268. [PubMed: 23844641]

594. Abinaya M, Rajakumaran R, Chen S-M, Karthik R and Muthuraj V, ACS Appl. Mater. Interfaces, 2019, 11, 38321–38335. [PubMed: 31549800]

595. Kulkarni AA and Bhanage BM, ACS Sustainable Chem. Eng, 2014, 2, 1007–1013.

596. Qi L, Zhang K, Qin W and Hu Y, Chem. Eng. J, 2020, 388, 124252.

597. Liu Q, Zeng C, Ai L, Hao Z and Jiang J, Appl. Catal., B, 2018, 224, 38–45.

598. Tian K, Liu WJ and Jiang H, ACS Sustainable Chem. Eng, 2015, 3, 269–276.

599. Cai J, Huang J, Wang S, Iocozzia J, Sun Z, Sun J, Yang Y, Lai Y and Lin Z, Adv. Mater, 2019, 31, 1806314.

600. Chen Y, Shen C, Wang J, Xiao G and Luo G, ACS Sustainable Chem. Eng, 2018, 6, 13276–13286.

601. Temerov F, Pham K, Juuti P, Mäkelä JM, Grachova EV, Kumar S, Eslava S and Saarinen JJ, ACS Appl. Mater. Interfaces, 2020, 12, 41200–41210. [PubMed: 32820899]

602. Trang TNQ, Phan TB, Nam ND and Thu VTH, ACS Appl. Mater. Interfaces, 2020, 12, 12195–12206. [PubMed: 32013392]

603. Ju L, Wu P, Yang Q, Ahmed Z and Zhu N, Appl. Catal., B, 2018, 224, 159–174.

604. Cheshme Khavar AH, Moussavi G, Mahjoub AR, Luque R, Rodríguez-Padrón D and Sattari M, Sep. Purif. Technol, 2019, 229, 115803.

605. Lang X, Chen X and Zhao J, Chem. Soc. Rev, 2014, 43, 473–486. [PubMed: 24162830]

606. Deng X, Li Z and García H, Chem. – Eur. J, 2017, 23, 11189–11209. [PubMed: 28503763]

607. Yoon TP, Ischay MA and Du J, Nat. Chem, 2010, 2, 527–532. [PubMed: 20571569]

608. Mogal SI, Shah DO, Mukherjee T, Shripathi T and Mishra MK, ACS Omega, 2018, 3, 12802–12812. [PubMed: 31458006]

609. König B, Eur. J. Org. Chem, 2017, 1979–1981.

610. Christopher P, Xin H and Linic S, Nat. Chem, 2011, 3, 467–472. [PubMed: 21602862]

611. Wu T, Liu S, Luo Y, Lu W, Wang L and Sun X, Nanoscale, 2011, 3, 2142–2144. [PubMed: 21451827]

612. Mori K, Kawashima M, Che M and Yamashita H, Angew. Chem., Int. Ed, 2010, 49, 8598–8601.

613. Garg R, Mondal S, Sahoo L, Vinod CP and Gautam UK, ACS Appl. Mater. Interfaces, 2020, 12, 29324–29334. [PubMed: 32484649]

614. Tada H, Ishida T, Takao A, Ito S, Mukhopadhyay S, Akita T, Tanaka K and Kobayashi H, Chem. Phys. Chem, 2005, 6, 1537–1543. [PubMed: 15999384]

615. Mohamed RM and Ibrahim F, J. Ind. Eng. Chem, 2015, 22, 28–33.

616. Fu L, Cai W, Wang A and Zheng Y, Mater. Lett, 2015, 142, 201–203.

617. Kominami H, Yamamoto S, Imamura K, Tanaka A and Hashimoto K, Chem. Commun, 2014, 50, 4558–4560.

618. Yang Z, Xu X, Liang X, Lei C, Cui Y, Wu W, Yang Y, Zhang Z and Lei Z, Appl. Catal., B, 2017, 205, 42–54.

619. Kumar A, Paul B, Boukherroub R and Jain SL, J. Hazard. Mater, 2020, 387, 121700. [PubMed: 31806437]

620. Tsukamoto D, Shiro A, Shiraishi Y, Sugano Y, Ichikawa S, Tanaka S and Hirai T, ACS Catal, 2012, 2, 599–603.

621. Liu Z, Huang Y, Xiao Q and Zhu H, Green Chem, 2016, 18, 817–825.

622. Zhang X, Kumari G, Heo J and Jain PK, Nat. Commun, 2018, 9, 1–10. [PubMed: 29317637]

623. Teržan J, Huš M, Likozar B and Djinovi P, ACS Catal, 2020, 10, 13415–13436.

624. Nasir Baig RB, Verma S, Nadagouda MN and Varma RS, Green Chem, 2016, 18, 1019–1022.

625. Hu C, Mu X, Fan J, Ma H, Zhao X, Chen G, Zhou Z and Zheng N, ChemNanoMat, 2016, 2, 28–32.

626. Verma S, Nasir Baig R, Nadagouda MN and Varma RS, ACS Sustainable Chem. Eng, 2017, 5, 3637–3640. [PubMed: 30245941]

627. Wang L, Yu M, Wu C, Deng N, Wang C and Yao X, Adv. Synth. Catal, 2016, 358, 2631–2641.

628. Wu W, Cui E, Zhang Y, Zhang C, Zhu F, Tung CH and Wang Y, ACS Catal, 2019, 9, 6335–6341.

629. Shah AP, Sharma AS, Sharma VS and Shimpi NG, ACS Appl. Nano Mater, 2020, 3, 1922–1933.

630. Chopra R, Sharma K, Kumar M and Bhalla V, J. Org. Chem, 2016, 81, 1039–1046. [PubMed: 26756525]

631. Landry MJ, Gellé A, Meng BY, Barrett CJ and Moores A, ACS Catal, 2017, 7, 6128–6133.

632. Lei G, Gao PF, Yang T, Zhou J, Zhang HZ, Sun SS, Gao MX and Huang CZ, ACS Nano, 2017, 11, 2085–2093. [PubMed: 28117958]

633. Ellabban O, Abu-Rub H and Blaabjerg F, Renew. Sust. Energ. Rev, 2014, 39, 748–764.

634. Zhou JH and Zhang YW, React. Chem. Eng, 2018, 3, 591–625.

635. Lee SM, Lee H, Kim J, Ahn SH and Chang ST, Appl. Catal., B, 2019, 259, 118045.

636. El Badawy AM, Silva RG, Morris B, Scheckel KG, Suidan MT and Tolaymat TM, Environ. Sci. Technol, 2011, 45, 283–287. [PubMed: 21133412]

637. Wen C, Yin A and Dai WL, Appl. Catal., B, 2014, 160–161, 730–741.

638. Xie C, Niu Z, Kim D, Li M and Yang P, Chem. Rev, 2020, 120, 1184–1249. [PubMed: 31580651]

639. Lamoth M, Jones T, Plodinec M, Machoke A, Wrabetz S, Krämer M, Karpov A, Rosowski F, Piccinin S, Schlögl R and Frei E, ChemCatChem, 2020, 12, 2977–2988.

640. Campbell FW, Belding SR, Baron R, Xiao L and Compton RG, J. Phys. Chem. C, 2009, 113, 14852–14857.

641. Yang M, Lao X, Sun J, Ma N, Wang S, Ye W and Guo P, Langmuir, 2020, 36, 11094–11101. [PubMed: 32838533]

642. Yao W, Jiang X, Li M, Li Y, Liu Y, Zhan X, Fu G and Tang Y, Appl. Catal., B, 2021, 282, 119595.

643. Nazemi M and El-Sayed MA, J. Phys. Chem. C, 2019, 123, 11422–11427.

644. Pan B, Chen F, Kou B, Wang J, Tang Q, Guo L, Wang Q, Li Z, Bian W and Wang J, Nanoscale, 2020, 12, 11659–11671. [PubMed: 32436927]

645. Ko YJ, Choi K, Yang B, Lee WH, Kim JY, Choi JW, Chae KH, Lee JH, Hwang YJ, Min BK, Oh HS and Lee WS, J. Mater. Chem. A, 2020, 8, 9859–9870.

646. Zahran M, Khalifa Z, Zahran MAH and Abdel Azzem M, ACS Appl. Nano Mater, 2020, 3, 3868–3875.

647. Jiang L, Santiago I and Foord J, Langmuir, 2020, 36, 6089–6094. [PubMed: 32403933]

648. Dubouis N and Grimaud A, Chem. Sci, 2019, 10, 9165–9181. [PubMed: 32015799]

649. Asefa T, Acc. Chem. Res, 2016, 49, 1873–1883. [PubMed: 27599362]

650. Zhang L, Jia Y, Yan X and Yao X, Small, 2018, 14, 1800235.

651. Ren X, Lv Q, Liu L, Liu B, Wang Y, Liu A and Wu G, Sustainable Energy Fuels, 2020, 4, 15–30.

652. Zhang L, Jia Y, Yan X and Yao X, Small, 2018, 14, 1800235.

653. Bhatt MD and Lee JY, Energy Fuels, 2020, 34, 6634–6695.

654. Nguyen TP, Tuan Nguyen DM, Tran DL, Le HK, Vo DVN, Lam SS, Varma RS, Shokouhimehr M, Nguyen CC and Le QV, Mol. Catal, 2020, 486, 110850.

655. Qu K, Zheng Y, Zhang X, Davey K, Dai S and Qiao SZ, ACS Nano, 2017, 11, 7293–7300. [PubMed: 28640994]

656. Bello A, Fabiane M, Dodoo-Arhin D, Ozoemena KI and Manyala N, J. Phys. Chem. Solids, 2014, 75, 109–114.

657. Li Z, Wang X, Yin Z, Zhao J, Song M, Wu Z, Li H and Wang X, Carbon, 2020, 161, 726–735.

658. Amin MA, Fadlallah SA and Alosaimi GS, Int. J. Hydrogen Energy, 2014, 39, 19519–19540.

659. Li Z, Fu JY, Feng Y, Dong CK, Liu H and Du XW, Nat. Catal, 2019, 2, 1107–1114.

660. Lu J, Guo J, Song S, Yu G, Liu H, Yang X and Lu Z, RSC Adv, 2020, 10, 38583–38587.

661. Huang JF and Wu YC, ACS Sustainable Chem. Eng, 2018, 6, 8285–8290.

662. Lee CL and Tseng CM, J. Phys. Chem. C, 2008, 112, 13342–13345.

663. Murray BJ, Li Q, Newberg JT, Hemminger JC and Penner RM, Chem. Mater, 2005, 17, 6611–6618.

664. Huang X, Xie M, Chen Y, Zong Q, Liu Z and Jin Y, RSC Adv, 2015, 5, 26150–26156.

665. Ji R, Wang L, Yu L, Geng B, Wang G and Zhang X, ACS Appl. Mater. Interfaces, 2013, 5, 10465–10472. [PubMed: 23978111]

666. Xia X, Shen X, Zhao X, Ye W and Wang C, ChemCatChem, 2015, 7, 2517–2525.

667. Solomon G, Mazzaro R, You S, Natile MM, Morandi V, Concina I and Vomiero A, ACS Appl. Mater. Interfaces, 2019, 11, 22380–22389. [PubMed: 31145582]

668. Yao RQ, Zhou YT, Shi H, Zhang QH, Gu L, Wen Z, Lang XY and Jiang Q, ACS Energy Lett, 2019, 4, 1379–1386.

669. Lu W, Xia X, Wei X, Li M, Zeng M, Guo J and Cheng S, ACS Appl. Mater. Interfaces, 2020, 12, 21569–21578. [PubMed: 32309921]

670. Du N, Wang C, Wang X, Lin Y, Jiang J and Xiong Y, Adv. Mater, 2016, 28, 2077–2084. [PubMed: 26757098]

671. Li C, Yuan Q, Ni B, He T, Zhang S, Long Y, Gu L and Wang X, Nat. Commun, 2018, 9, 3702. [PubMed: 30209252]

672. Ge J, Wei P, Wu G, Liu Y, Yuan T, Li Z, Qu Y, Wu Y, Li H, Zhuang Z, Hong X and Li Y, Angew. Chem., Int. Ed, 2018, 57, 3435–3438.

673. Zhou Y, Lu Q, Zhuang Z, Hutchings GS, Kattel S, Yan Y, Chen JG, Xiao JQ and Jiao F, Adv. Energy Mater, 2015, 5, 1500149.

674. Xia Y, Chem. – Eur. J, 2019, 25, 4244.

675. Cheng H, Wang P, Wang Z, Liu Y and Huang B, Surface Science of Photocatalysis, 2020, pp. 415–452, DOI: 10.1016/b978-0-08-102890-2.00013-0.

676. Uchida T, Mogami H, Yamakata A, Sasaki Y and Osawa M, J. Am. Chem. Soc, 2008, 130, 10862–10863. [PubMed: 18661991]

677. Jiao Y, Zheng Y, Jaroniec M and Qiao SZ, Chem. Soc. Rev, 2015, 44, 2060–2086. [PubMed: 25672249]

678. Nørskov JK, Bligaard T, Rossmeisl J and Christensen CH, Nat. Chem, 2009, 1, 37–46. [PubMed: 21378799]

679. Kang WJ, Cheng CQ, Li Z, Feng Y, Shen GR and Du XW, ChemCatChem, 2019, 11, 5976–5981.

680. Ren Y, Chen Z and Yu X, Chem. – Asian J, 2019, 14, 4315–4321. [PubMed: 31631572]

681. Wang J, Fang W, Hu Y, Zhang Y, Dang J, Wu Y, Zhao H and Li Z, Catal. Sci. Technol, 2020, 10, 154–163.

682. Majee R, Kumar A, Das T, Chakraborty S and Bhattacharyya S, Angew. Chem., Int. Ed, 2020, 59, 2881–2889.

683. Rolly GS, Meyerstein D, Yardeni G, Bar-Ziv R and Zidki T, Phys. Chem. Chem. Phys, 2020, 22, 6401–6405. [PubMed: 32149286]

684. Cao R, Lee JS, Liu M and Cho J, Adv. Energy Mater, 2012, 2, 816–829.

685. Chu S, Cui Y and Liu N, Nat. Mater, 2017, 16, 16–22.

686. Zuliani A, Cano M, Calsolaro F, Puente Santiago AR, Giner-Casares JJ, Rodríguez-Castellón E, Berlier G, Cravotto G, Martina K and Luque R, Sustainable Energy Fuels, 2021, 5, 720–731.

687. Liu J, Zhang H, Qiu M, Peng Z, Leung MKH, Lin WF and Xuan J, J. Mater. Chem. A, 2020, 8, 2222–2245.

688. Chandrasekaran S, Ma D, Ge Y, Deng L, Bowen C, Roscow J, Zhang Y, Lin Z, Misra RDK, Li J, Zhang P and Zhang H, Nano Energy, 2020, 77, 105080.

689. Wang L, Cui L, Ge X, Yue N, He X, Zhang W and Asefa T, Int. J. Hydrogen Energy, 2020, 45, 27230–27243.

690. Chen H, Shi L, Liang X, Wang L, Asefa T and Zou X, Angew. Chem., Int. Ed, 2020, 59, 19654–19658.

691. Zhang Z, Li X, Zhong C, Zhao N, Deng Y, Han X and Hu W, Angew. Chem., Int. Ed, 2020, 59, 7245–7250.

692. Hou Y, Liu Y, Gao R, Li Q, Guo H, Goswami A, Zboril R, Gawande MB and Zou X, ACS Catal, 2017, 7, 7038–7042.

693. Islam DA, Barman K, Jasimuddin S and Acharya H, ChemElectroChem, 2017, 4, 3110–3118.

694. Dong R, Du H, Sun Y, Huang K, Li W and Geng B, ACS Sustainable Chem. Eng, 2018, 6, 13420–13426.

695. Yu M, Moon GH, Castillo RG, DeBeer S, Weidenthaler C and Tuysuz H, Angew. Chem., Int. Ed, 2020, 59, 16544–16552.

696. Zhang Z, Li X, Zhong C, Zhao N, Deng Y, Han X and Hu W, Angew. Chem., Int. Ed, 2020, 59, 7245–7250.

697. Ashok A, Kumar A, Matin MA and Tarlochan F, ACS Omega, 2018, 3, 7745–7756. [PubMed: 31458922]

698. Chala SA, Tsai MC, Su WN, Ibrahim KB, Duma AD, Yeh MH, Wen CY, Yu CH, Chan TS, Dai H and Hwang BJ, ACS Catal, 2018, 9, 117–129.

699. Zhang FF, Cheng CQ, Wang JQ, Shang L, Feng Y, Zhang Y, Mao J, Guo QJ, Xie YM, Dong CK, Cheng YH, Liu H and Du XW, ACS Energy Lett, 2021, 6, 1588–1595.

700. Kumar S, Selvaraj C, Scanlon LG and Munichandraiah N, Phys. Chem. Chem. Phys, 2014, 16, 22830–22840. [PubMed: 25242373]

701. Erikson H, Sarapuu A and Tammeveski K, ChemElectroChem, 2019, 6, 73–86.

702. Furuya N and Aikawa H, Electrochim. Acta, 2000, 45, 4251–4256.

703. Gu S, Sheng W, Cai R, Alia SM, Song S, Jensen KO and Yan Y, Chem. Commun, 2013, 49, 131–133.

704. Varcoe JR, Slade RCT, Wright GL and Chen Y, J. Phys. Chem. B, 2006, 110, 21041–21049. [PubMed: 17048923]

705. Singh P and Buttry DA, J. Phys. Chem. C, 2012, 116, 10656–10663.

706. Holewinski A, Idrobo JC and Linic S, Nat. Chem, 2014, 6, 828–834. [PubMed: 25143220]

707. Cheng Y, Li W, Fan X, Liu J, Xu W and Yan C, Electrochim. Acta, 2013, 111, 635–641.

708. Yuan L, Jiang L, Liu J, Xia Z, Wang S and Sun G, Electrochim. Acta, 2014, 135, 168–174.

709. Pu L, Li K, Chen Z, Zhang P, Zhang X and Fu Z, J. Power Sources, 2014, 268, 476–481.

710. Kim JH, Kim JK, Seo HG, Lim DK, Jeong SJ, Seo J, Kim J and Jung W, Adv. Funct. Mater, 2020, 30, 2001326.

711. Mustain WE, Chatenet M, Page M and Kim YS, Energy Environ. Sci, 2020, 13, 2805–2838.

712. Shumilova NA, Zhutaeva GV and Tarasevich MP, Electrochim. Acta, 1966, 11, 967–974.

713. Sun Y and Xia Y, Science, 2002, 298, 2176–2179. [PubMed: 12481134]

714. Wiley B, Sun Y, Mayers B and Xia Y, Chem. – Eur. J, 2005, 11, 454–463. [PubMed: 15565727]

715. Van Cleve T, Gibara E and Linic S, ChemCatChem, 2016, 8, 256–261.

716. Liu M and Chen W, Nanoscale, 2013, 5, 12558–12564. [PubMed: 24173664]

717. Nie Y, Li L and Wei Z, Chem. Soc. Rev, 2015, 44, 2168–2201. [PubMed: 25652755]

718. Lim EJ, Choi SM, Seo MH, Kim Y, Lee S and Kim WB, Electrochem. Commun, 2013, 28, 100–103.

719. Soo LT, Loh KS, Mohamad AB, Daud WRW and Wong WY, J. Power Sources, 2016, 324, 412–420.

720. Chen L, Cui LL, Wang Z, He X, Zhang W and Asefa T, ACS Sustainable Chem. Eng, 2020, 8, 13147–13158.

721. Guo J, Li H, He H, Chu D and Chen R, J. Phys. Chem. C, 2011, 115, 8494–8502.

722. Park SA, Lim H and Kim YT, ACS Catal, 2015, 5, 3995–4002.

723. Tang Q, Jiang L, Qi J, Jiang Q, Wang S and Sun G, Appl. Catal., B, 2011, 104, 337–345.

724. Goh FWT, Liu Z, Ge X, Zong Y, Du G and Hor TSA, Electrochim. Acta, 2013, 114, 598–604.

725. Liu J, Liu J, Song W, Wang F and Song Y, J. Mater. Chem. A, 2014, 2, 17477–17488.

726. Lee K, Ahmed MS and Jeon S, J. Power Sources, 2015, 288, 261–269.

727. Ryu J, Jang H, Park J, Yoo Y, Park M and Cho J, Nat. Commun, 2018, 9, 3715. [PubMed: 30213933]

728. Lima FHB, de Castro JFR and Ticianelli EA, J. Power Sources, 2006, 161, 806–812.

729. Chen J, Wang Z, Mao J, Liu C, Chen Y, Lu Z and Feng SP, J. Alloys Compd, 2020, 856, 157379, DOI: 10.1016/j.jallcom.2020.157379.

730. Vu TH, Shin D, Jeong J and Lee J, J. Phys. Chem. C, 2016, 120, 22342–22348.

731. Song Y and Chen S, Chem. – Eur. J, 2014, 9, 418–430.

732. Song Y, Liu K and Chen S, Langmuir, 2012, 28, 17143–17152. [PubMed: 23163535]

733. Chen L, Deming CP, Peng Y, Hu P, Stofan J and Chen S, Nanoscale, 2016, 8, 14565–14572. [PubMed: 27417026]

734. Lee CL, Syu CM, Huang CH, Chiou HP, Chao YJ and Yang CC, Appl. Catal., B, 2013, 132–133, 229–236.

735. Miller HA, Bevilacqua M, Filippi J, Lavacchi A, Marchionni A, Marelli M, Moneti S, Oberhauser W, Vesselli E, Innocenti M and Vizza F, J. Mater. Chem. A, 2013, 1, 13337–13347.

736. Wang Y and Balbuena PB, J. Phys. Chem. B, 2005, 109, 18902–18906. [PubMed: 16853433]

737. Loglio F, Lastraioli E, Bianchini C, Fontanesi C, Innocenti M, Lavacchi A, Vizza F and Foresti ML, ChemSusChem, 2011, 4, 1112–1117. [PubMed: 21648096]

738. Yu A, Lee C, Lee NS, Kim MH and Lee Y, ACS Appl. Mater. Interfaces, 2016, 8, 32833–32841. [PubMed: 27934168]

739. Hernández-Rodríguez MA, Goya MC, Arévalo MC, Rodríguez JL and Pastor E, Int. J. Hydrogen Energy, 2016, 41, 19789–19798.

740. Li M, Wang C, Yang Y, Jiang P, Lin Z, Xia G, Yang K, Xu P and Chen Q, ACS Sustainable Chem. Eng, 2018, 6, 14033–14041.

741. Cho YB, Moon S, Lee C and Lee Y, Appl. Surf. Sci, 2017, 394, 267–274.

742. Bordley JA and El-Sayed MA, J. Phys. Chem. C, 2016, 120, 14643–14651.

743. Jin Y, Chen F, Lei Y and Wu X, ChemCatChem, 2015, 7, 2377–2383.

744. Lu Y, Zhang N, An L, Li X and Xia D, J. Power Sources, 2013, 240, 606–611.

745. Wang Q, Chen F, Liu Y, Zhang N, An L and Johnston RL, ACS Appl. Mater. Interfaces, 2017, 9, 35701–35711. [PubMed: 28953357]

746. Jiang K, Sandberg RB, Akey AJ, Liu X, Bell DC, Nørskov JK, Chan K and Wang H, Nat. Catal, 2018, 1, 111–119.

747. Tang L, Wu W, He L, Yu K, Xu T, Zhang Q, Zhang L and Sun L, J. Phys. Chem. Lett, 2019, 10, 1973–1980. [PubMed: 30947503]

748. Shaik SA, Goswami A, Varma RS and Gawande MB, Curr. Opin. Green Sustainable Chem, 2019, 15, 67–76.

749. Ge X, Sumboja A, Wuu D, An T, Li B, Goh FWT, Hor TSA, Zong Y and Liu Z, ACS Catal, 2015, 5, 4643–4667.

750. Liu M, Zhang R and Chen W, Chem. Rev, 2014, 114, 5117–5160. [PubMed: 24666160]

751. Peng Y and Chen S, Green Energy Environ, 2018, 3, 335–351.

752. Sekol RC, Li X, Cohen P, Doubek G, Carmo M and Taylor AD, Appl. Catal., B, 2013, 138–139, 285–293.

753. Huang M, Liu S, Gong S, Xu P, Yang K, Chen S, Wang C and Chen Q, ACS Sustainable Chem. Eng, 2019, 7, 16511–16519.

754. Thanh TD, Chuong ND, Hien HV, Kim NH and Lee JH, ACS Appl. Mater. Interfaces, 2018, 10, 4672–4681. [PubMed: 29336546]

755. Shi F, He J, Zhang B, Peng J, Ma Y, Chen W, Li F, Qin Y, Liu Y, Shang W, Tao P, Song C, Deng T, Qian X, Ye J and Wu J, Nano Lett, 2019, 19, 1371–1378. [PubMed: 30620607]

756. Jin S, Chen M, Dong H, He B, Lu H, Su L, Dai W, Zhang Q and Zhang X, J. Power Sources, 2015, 274, 1173–1179.

757. Zhou R and Qiao SZ, Chem. Mater, 2014, 26, 5868–5873.

758. Lopes JH, Ye S, Gostick JT, Barralet JE and Merle G, Langmuir, 2015, 31, 9718–9727. [PubMed: 26038977]

759. Liu R, Yu X, Zhang G, Zhang S, Cao H, Dolbecq A, Mialane P, Keita B and Zhi L, J. Mater. Chem. A, 2013, 1, 11961–11969.

760. Dembinska B, Brzozowska K, Szwed A, Miecznikowski K, Negro E, Di Noto V and Kulesza PJ, Electrocatalysis, 2018, 10, 112–124.

761. Meng Y, Song W, Huang H, Ren Z, Chen SY and Suib SL, J. Am. Chem. Soc, 2014, 136, 11452–11464. [PubMed: 25058174]

762. Wu L, Xu F, Zhu Y, Brady AB, Huang J, Durham JL, Dooryhee E, Marschilok AC, Takeuchi ES and Takeuchi KJ, ACS Nano, 2015, 9, 8430–8439. [PubMed: 26181235]

763. Ni S, Zhang H, Zhao Y, Li X, Sun Y, Qian J, Xu Q, Gao P, Wu D, Kato K, Yamauchi M and Sun Y, Chem. Eng. J, 2019, 366, 631–638.

764. Holewinski A, Idrobo JC and Linic S, Nat. Chem, 2014, 6, 828–834. [PubMed: 25143220]

765. Davis DJ, Raji ARO, Lambert TN, Vigil JA, Li L, Nan K and Tour JM, Electroanalysis, 2014, 26, 164–170.

766. Kim SJ, Lee SC, Lee C, Kim MH and Lee Y, Nano Energy, 2018, 48, 134–143.

767. Choi S, Park Y, Choi J, Lee C, Cho HS, Kim CH, Koo J and Lee HM, ACS Sustainable Chem. Eng, 2021, 9, 7519–7528.

768. Xu Z, Zhang X, Wang X, Fang J, Zhang Y, Liu X, Zhu W, Yan Y and Zhuang Z, ACS Nano, 2021, 15, 7131–7138. [PubMed: 33821618]

769. Wang M, Wang C, Liu J, Rong F, He L, Lou Y, Zhang Z and Du M, ACS Sustainable Chem. Eng, 2021, 9, 5872–5883.

770. Fan L, Xia C, Yang F, Wang J, Wang H and Lu Y, Sci. Adv, 2020, 6, eaay3111. [PubMed: 32128404]

771. Bushuyev OS, De Luna P, Dinh CT, Tao L, Saur G, van de Lagemaat J, Kelley SO and Sargent EH, Joule, 2018, 2, 825–832.

772. Dahl S and Chorkendorff I, Nat. Mater, 2012, 11, 100–101. [PubMed: 22270823]

773. Gattrell M, Gupta N and Co A, J. Electroanal. Chem, 2006, 594, 1–19.

774. Mikkelsen M, Jørgensen M and Krebs FC, Energy Environ. Sci, 2010, 3, 43–81.

775. Hernández S, Amin Farkhondehfal M, Sastre F, Makkee M, Saracco G and Russo N, Green Chem, 2017, 19, 2326–2346.

776. Wu X, Guo Y, Sun Z, Xie F, Guan D, Dai J, Yu F, Hu Z, Huang YC, Pao CW, Chen JL, Zhou W and Shao Z, Nat. Commun, 2021, 12, 660, DOI: 10.1038/s41467-021-20960-8. [PubMed: 33510153]

777. Hori Y, Wakebe H, Tsukamoto T and Koga O, Electrochim. Acta, 1994, 39, 1833–1839.

778. Back S, Yeom MS and Jung Y, ACS Catal, 2015, 5, 5089–5096.

779. Salehi-Khojin A, Jhong HRM, Rosen BA, Zhu W, Ma S, Kenis PJA and Masel RI, J. Phys. Chem. C, 2013, 117, 1627–1632.

780. Ma S, Lan Y, Perez GM, Moniri S and Kenis PJ, ChemSusChem, 2014, 7, 866–874. [PubMed: 24474718]

781. Tornow CE, Thorson MR, Ma S, Gewirth AA and Kenis PJA, J. Am. Chem. Soc, 2012, 134, 19520–19523. [PubMed: 23167268]

782. Lu Q, Rosen J, Zhou Y, Hutchings GS, Kimmel YC, Chen JG and Jiao F, Nat. Commun, 2014, 5, 3242. [PubMed: 24476921]

783. Kim C, Jeon HS, Eom T, Jee MS, Kim H, Friend CM, Min BK and Hwang YJ, J. Am. Chem. Soc, 2015, 137, 13844–13850. [PubMed: 26447349]

784. Hatsukade T, Kuhl KP, Cave ER, Abram DN and Jaramillo TF, Phys. Chem. Chem. Phys, 2014, 16, 13814–13819. [PubMed: 24915537]

785. Hsieh YC, Senanayake SD, Zhang Y, Xu W and Polyansky DE, ACS Catal, 2015, 5, 5349–5356.

786. Schmitt KG and Gewirth AA, J. Phys. Chem. C, 2014, 118, 17567–17576.

787. Kim C, Eom T, Jee MS, Jung H, Kim H, Min BK and Hwang YJ, ACS Catal, 2016, 7, 779–785.

788. Abeyweera SC, Yu J, Perdew JP, Yan Q and Sun Y, Nano Lett, 2020, 20, 2806–2811. [PubMed: 32197043]

789. Xi W, Ma R, Wang H, Gao Z, Zhang W and Zhao Y, ACS Sustainable Chem. Eng, 2018, 6, 7687–7694.

790. Hu H, Liu M, Kong Y, Mysuru N, Sun C, Gálvez-Vázquez MDJ, Müller U, Erni R, Grozovski V, Hou Y and Broekmann P, ACS Catal, 2020, 10, 8503–8514.

791. Fan T, Wu Q, Yang Z, Song Y, Zhang J, Huang P, Chen Z, Dong Y, Fang W and Yi X, ChemSusChem, 2020, 13, 2677–2683. [PubMed: 32020717]

792. Pan Y, Paschoalino WJ, Bayram SS, Blum AS and Mauzeroll J, Nanoscale, 2019, 11, 18595–18603. [PubMed: 31578539]

793. Zeng J, Zhang W, Yang Y, Li D, Yu X and Gao Q, ACS Appl. Mater. Interfaces, 2019, 11, 33074–33081. [PubMed: 31424903]

794. Chang Z, Huo S, Zhang W, Fang J and Wang H, J. Phys. Chem. C, 2017, 121, 11368–11379.

795. Shan C, Martin ET, Peters DG and Zaleski JM, Chem. Mater, 2017, 29, 6030–6043.

796. Wang J, Li Z, Dong C, Feng Y, Yang J, Liu H and Du X, ACS Appl. Mater. Interfaces, 2019, 11, 2763–2767. [PubMed: 30620171]

797. Ting LLR, Piqué O, Lim SY, Tanhaei M, Calle-Vallejo F and Yeo BS, ACS Catal, 2020, 10, 4059–4069.

798. Dong WJ, Yoo CJ, Lim JW, Park JY, Kim K, Kim S, Lee D and Lee JL, Nano Energy, 2020, 78, 105168.

799. Zheng T, Jiang K and Wang H, Adv. Mater, 2018, 30, 1802066.

800. Wang J, Li Z, Dong C, Feng Y, Yang J, Liu H and Du X, ACS Appl. Mater. Interfaces, 2019, 11, 2763–2767. [PubMed: 30620171]

801. Chen C, Li Y, Yu S, Louisia S, Jin J, Li M, Ross MB and Yang P, Joule, 2020, 4, 1688–1699.

802. Chang CJ, Hung SF, Hsu CS, Chen HC, Lin SC, Liao YF and Chen HM, ACS Cent. Sci, 2019, 5, 1998–2009. [PubMed: 31893230]

803. Park H, Choi J, Kim H, Hwang E, Ha DH, Ahn SH and Kim SK, Appl. Catal., B, 2017, 219, 123–131.

804. Lum Y and Ager JW, Energy Environ. Sci, 2018, 11, 2935–2944.

805. Zhang Q, Tao S, Du J, He A, Yang Y and Tao C, J. Mater. Chem. A, 2020, 8, 8410–8420.

806. Yang Y, Ajmal S, Feng Y, Li K, Zheng X and Zhang L, Chem. – Eur. J, 2020, 26, 4080–4089. [PubMed: 31535739]

807. Irtem E, Arenas Esteban D, Duarte M, Choukroun D, Lee S, Ibáñez M, Bals S and Breugelmans T, ACS Catal, 2020, 10, 13468–13478.

808. Marti N, Reller C, Macauley C, Löffler M, Reichert AM, Reichbauer T, Vetter KM, Schmid B, McLaughlin D, Leidinger P, Reinisch D, Vogl C, Mayrhofer KJJ, Katsounaros I and Schmid G, Energy Environ. Sci, 2020, 13, 2993–3006.

809. Nguyen VH, Thi Vo TT, Huu Do H, Thuan Le V, Nguyen TD, Ky Vo T, Nguyen BS, Nguyen TT, Phung TK and Tran VA, Chem. Eng. Sci, 2021, 232, 116381.

810. Gawande MB, Fornasiero P and Zbo il R, ACS Catal, 2020, 10, 2231–2259.

811. Zhang Q and Guan J, Adv. Funct. Mater, 2020, 30, 2000768.

812. Liu L and Corma A, Chem. Rev, 2018, 118, 4981–5079. [PubMed: 29658707]

813. Huang Z, Gu X, Cao Q, Hu P, Hao J, Li J and Tang X, Angew. Chem., Int. Ed, 2012, 51, 4198–4203.

814. Huang Z, Zhang J, Du Y, Zhang Y, Wu X and Jing G, ChemCatChem, 2020, 12, 561–568.

815. Li Y, Chen C, Cao R, Pan Z, He H and Zhou K, Appl. Catal., B, 2020, 268, 118747.

816. Zhang N, Zhang X, Tao L, Jiang P, Ye C, Lin R, Huang Z, Li A, Pang D, Yan H, Wang Y, Xu P, An S, Zhang Q, Liu L, Du S, Han X, Wang D and Li Y, Angew. Chem., Int. Ed, 2021, 60, 6170–6176.

817. Zaidman B, Wiener H and Sasson Y, Int. J. Hydrogen Energy, 1986, 11, 341–347.

818. Yu X and Pickup PG, J. Power Sources, 2008, 182, 124–132.

819. Clark EL, Hahn C, Jaramillo TF and Bell AT, J. Am. Chem. Soc, 2017, 139, 15848–15857. [PubMed: 28988474]

820. Hoang TTH, Verma S, Ma S, Fister TT, Timoshenko J, Frenkel AI, Kenis PJA and Gewirth AA, J. Am. Chem. Soc, 2018, 140, 5791–5797. [PubMed: 29620896]

821. Li F, Li YC, Wang Z, Li J, Nam DH, Lum Y, Luo M, Wang X, Ozden A, Hung SF, Chen B, Wang Y, Wicks J, Xu Y, Li Y, Gabardo CM, Dinh CT, Wang Y, Zhuang TT, Sinton D and Sargent EH, Nat. Catal, 2020, 3, 75–82.

822. Zhang W, Xu C, Hu Y, Yang S, Ma L, Wang L, Zhao P, Wang C, Ma J and Jin Z, Nano Energy, 2020, 73, 104796.

823. Liu P and Nørskov JK, Phys. Chem. Chem. Phys, 2001, 3, 3814–3818.

824. Lewalska-Graczyk A, Pieta P, Garbarino G, Busca G, Holdynski M, Kalisz G, Sroka-Bartnicka A, Nowakowski R, Naushad M, Gawande MB, Zbo il R and Pieta IS, ACS Sustainable Chem. Eng, 2020, 8, 7244–7255.

825. Asefa T and Huang X, Chem. – Eur. J, 2017, 23, 10703–10713. [PubMed: 28397303]

826. Wu J, Ma S, Sun J, Gold JI, Tiwary C, Kim B, Zhu L, Chopra N, Odeh IN, Vajtai R, Yu AZ, Luo R, Lou J, Ding G, Kenis PJA and Ajayan PM, Nat. Commun, 2016, 7, 13869. [PubMed: 27958290]

827. Alves DCB, Silva R, Voiry D, Asefa T and Chhowalla M, Mater. Renew. Sustain. Energy, 2015, 4, 2.

828. Lv K, Fan Y, Zhu Y, Yuan Y, Wang J, Zhu Y and Zhang Q, J. Mater. Chem. A, 2018, 6, 5025–5031.

829. Wang L, Higgins DC, Ji Y, Morales-Guio CG, Chan K, Hahn C and Jaramillo TF, Proc. Natl. Acad. Sci. U. S. A, 2020, 117, 12572–12575. [PubMed: 31980521]

830. Wang Y, Wang D, Dares CJ, Marquard SL, Sheridan MV and Meyer TJ, Proc. Natl. Acad. Sci. U. S. A, 2018, 115, 278–283. [PubMed: 29279386]

831. Fan T, Wu Q, Yang Z, Song Y, Zhang J, Huang P, Chen Z, Dong Y, Fang W and Yi X, ChemSusChem, 2020, 13, 2677–2683. [PubMed: 32020717]

832. Nam DH, Shekhah O, Lee G, Mallick A, Jiang H, Li F, Chen B, Wicks J, Eddaoudi M and Sargent EH, J. Am. Chem. Soc, 2020, 142, 21513–21521. [PubMed: 33319985]

833. Yuan X, Wu Y, Jiang B, Wu Z, Tao Z, Lu X, Liu J, Qian T, Lin H and Zhang Q, ACS Appl. Mater. Interfaces, 2020, 12, 56642–56649. [PubMed: 33284596]

834. Lamaison S, Wakerley D, Blanchard J, Montero D, Rousse G, Mercier D, Marcus P, Taverna D, Giaume D, Mougel V and Fontecave M, Joule, 2020, 4, 395–406.

835. Shan W, Liu R, Zhao H, He Z, Lai Y, Li S, He G and Liu J, ACS Nano, 2020, 14, 11363–11372. [PubMed: 32790343]

836. Martín AJ, Shinagawa T and Pérez-Ramírez J, Chem, 2019, 5, 263–283.

837. Guo X, Du H, Qu F and Li J, J. Mater. Chem. A, 2019, 7, 3531–3543.

838. Smil V, Nature, 1999, 400, 415.

839. Ma H, Chen Z and Wang Z, Nanoscale, 2021, 13, 1717–1722. [PubMed: 33427282]

840. Garcia-Segura S, Lanzarini-Lopes M, Hristovski K and Westerhoff P, Appl. Catal., B, 2018, 236, 546–568.

841. Xu H, Ithisuphalap K, Li Y, Mukherjee S, Lattimer J, Soloveichik G and Wu G, Nano Energy, 2020, 69, 104469.

842. Iwamoto M, Akiyama M, Aihara K and Deguchi T, ACS Catal, 2017, 7, 6924–6929.

843. Huang H, Xia L, Shi X, Asiri AM and Sun X, Chem. Commun, 2018, 54, 11427–11430.

844. Li Y, Yu H, Wang Z, Liu S, Xu Y, Li X, Wang L and Wang H, Chem. Commun, 2019, 55, 14745–14748.

845. Zhao X, Yin M, Ma L, Liang L, Liu C, Liao J, Lu T and Xing W, Energy Environ. Sci, 2011, 4, 2736–2753.

846. Tiwari JN, Tiwari RN, Singh G and Kim KS, Nano Energy, 2013, 2, 553–578.

847. Feng Y, Liu H and Yang J, Sci. Adv, 2017, 3, e1700580. [PubMed: 28695199]

848. Bai J, Liu D, Yang J and Chen Y, ChemSusChem, 2019, 12, 2117–2132. [PubMed: 30834720]

849. Shi Q, Zhang P, Li Y, Xia H, Wang D and Tao X, Chem. Sci, 2015, 6, 4350–4357. [PubMed: 29218206]

850. Zhang H, Shang Y, Zhao J and Wang J, ACS Appl. Mater. Interfaces, 2017, 9, 16635–16643. [PubMed: 28445028]

851. Zhang S, Liu K, Liu Z, Liu M, Zhang Z, Qiao Z, Ming L and Gao C, Nano Lett, 2021, 21, 1074–1082. [PubMed: 33448860]

852. Njoki PN, Roots MED and Maye MM, ACS Appl. Nano Mater, 2018, 1, 5640–5645.

853. Satyanarayana M, Rajeshkhanna G, Sahoo MK and Rao GR, ACS Appl. Energy Mater, 2018, 1, 3763–3770.

854. Tang J, Chen D, Li C, Yang X, Liu H and Yang J, RSC Adv, 2017, 7, 3455–3460.

855. Xiong L, Sun Z, Zhang X, Zhao L, Huang P, Chen X, Jin H, Sun H, Lian Y, Deng Z, Rummerli MH, Yin W, Zhang D, Wang S and Peng Y, Nat. Commun, 2019, 10, 3782. [PubMed: 31439841]

856. Bartrom AM and Haan JL, J. Power Sources, 2012, 214, 68–74.

857. Han SH, Liu HM, Bai J, Tian XL, Xia BY, Zeng JH, Jiang JX and Chen Y, ACS Appl. Energy Mater, 2018, 1, 1252–1258.

858. Mohammadinejad R, Karimi S, Iravani S and Varma RS, Green Chem, 2016, 18, 20–52.

859. Jebakumar Immanuel Edison TN and Sethuraman MG, ACS Sustainable Chem. Eng, 2013, 1, 1326–1332.

860. Li C and Yao Y, Chem. Phys. Lett, 2020, 761, 137726.

861. Zhang QY, He X and Zhao L, Chem. Sci, 2017, 8, 5662–5668. [PubMed: 28989604]

862. Yang Y, Zhang H, Wang J, Yang S, Liu T, Tao K and Chang H, J. Mater. Chem. A, 2019, 7, 11497–11505.

863. Bai Z, Shi M, Zhang Y, Zhang Q, Yang L, Yang Z and Zhang J, Green Chem, 2016, 18, 386–391.

864. Boukil R, Tuleushova N, Cot D, Rebiere B, Bonniol V, Cambedouzou J, Tingry S, Cornu D and Holade Y, J. Mater. Chem. A, 2020, 8, 8848–8856.

865. Khalifa Z, Zahran M, Zahran MA-H and Azzem MA, RSC Adv, 2020, 10, 37675–37682.

866. Chouhan N, Ameta R and Meena RK, J. Mol. Liq, 2017, 230, 74–84.

867. Zhang W, Xiao B and Fang T, Chemosphere, 2018, 191, 324–334. [PubMed: 29045933]

868. Singh A, Hou WC, Lin TF and Zepp RG, Environ. Sci. Technol, 2019, 53, 11162–11169. [PubMed: 31479236]

869. Singh A, Hou WC and Lin TF, Chemosphere, 2021, 272, 129825.

870. Rizzello L and Pompa PP, Chem. Soc. Rev, 2014, 43, 1501–1518. [PubMed: 24292075]

871. Tortella GR, Rubilar O, Durán N, Diez MC, Martínez M, Parada J and Seabra AB, J. Hazard. Mater, 2020, 390, 121974. [PubMed: 32062374]

872. Akter M, Sikder MT, Rahman MM, Ullah AKMA, Hossain KFB, Banik S, Hosokawa T, Saito T and Kurasaki M, J. Adv. Res, 2018, 9, 1–16. [PubMed: 30046482]

873. Yu SJ, Yin YG and Liu JF, Environ. Sci.: Processes Impacts, 2013, 15, 78–92.

874. Massarsky A, Trudeau VL and Moon TW, Environ. Toxicol. Pharmacol, 2014, 38, 861–873. [PubMed: 25461546]

875. McGillicuddy E, Murray I, Kavanagh S, Morrison L, Fogarty A, Cormican M, Dockery P, Prendergast M, Rowan N and Morris D, Sci. Total Environ, 2017, 575, 231–246. [PubMed: 27744152]

876. Garg S, Li M, Weber AZ, Ge L, Li L, Rudolph V, Wang G and Rufford TE, J. Mater. Chem. A, 2020, 8, 1511–1544.

877. Masa J, Andronescu C and Schuhmann W, Angew. Chem., Int. Ed, 2020, 59, 15298–15312.
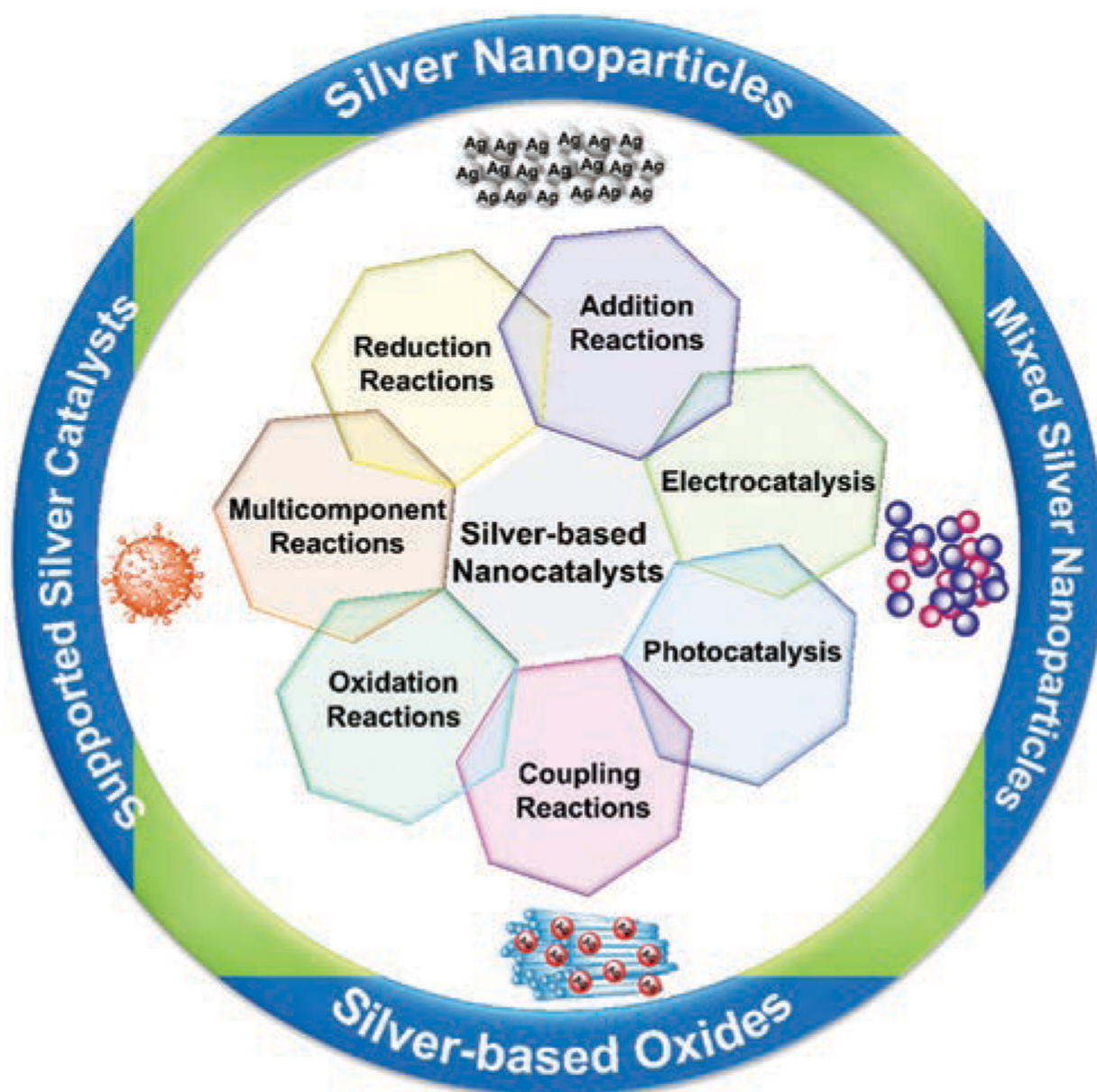
Fig. 1.
Applications of nanosilver-based catalysts.
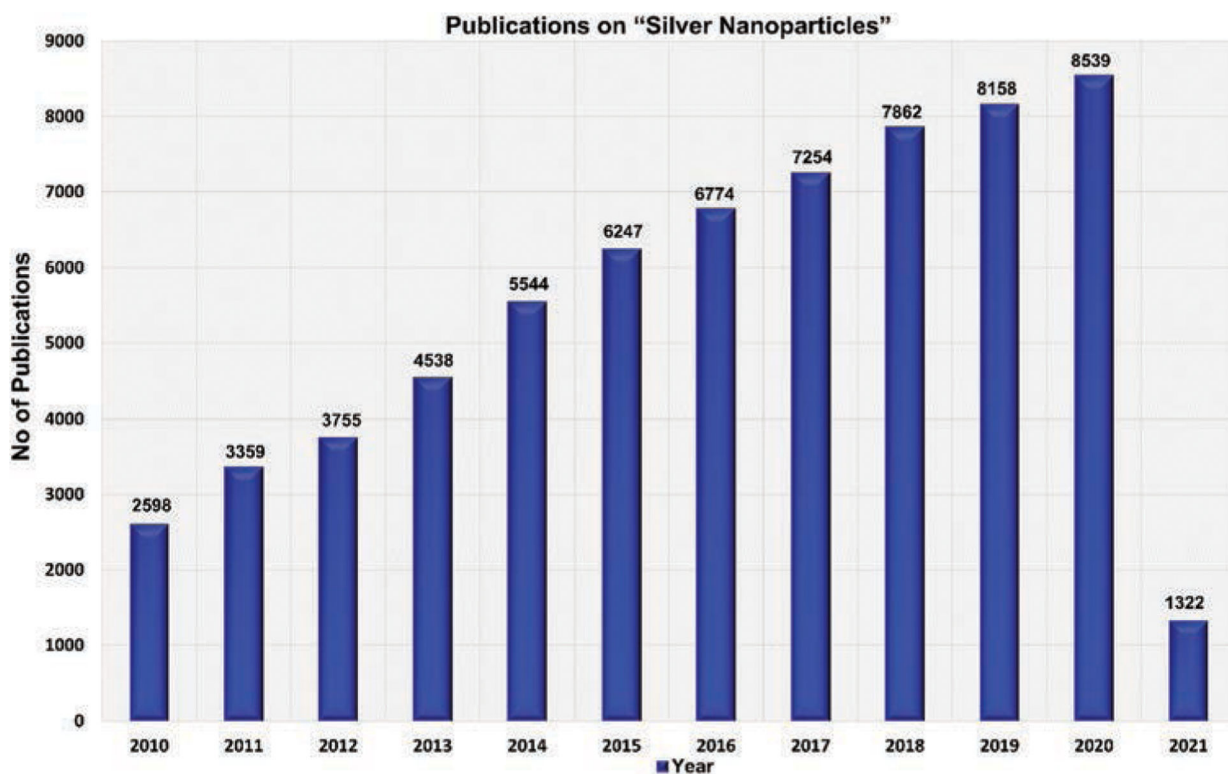
Fig. 2.

Publications identified *via* keywords 'silver nanoparticles' from 2010 to March 2021. The number of publications for the search all field: 'silver nanoparticles', timespan: 2011–2021, indexes = SCI-EXPANDED, SSCI, A&HCI, as found in Web of Science (date: 26th March 2021).
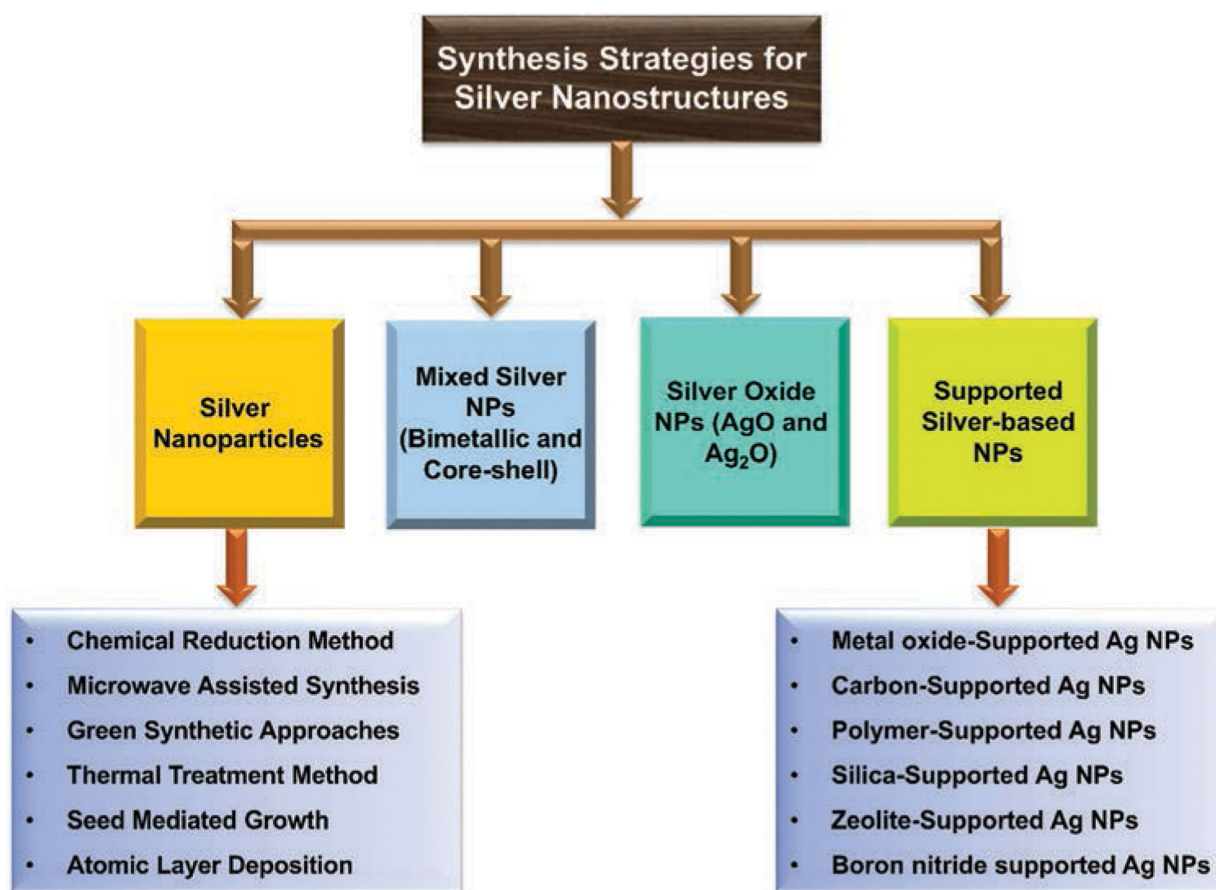
Fig. 3.
Methods for fabrication of different Ag-based nanostructures.
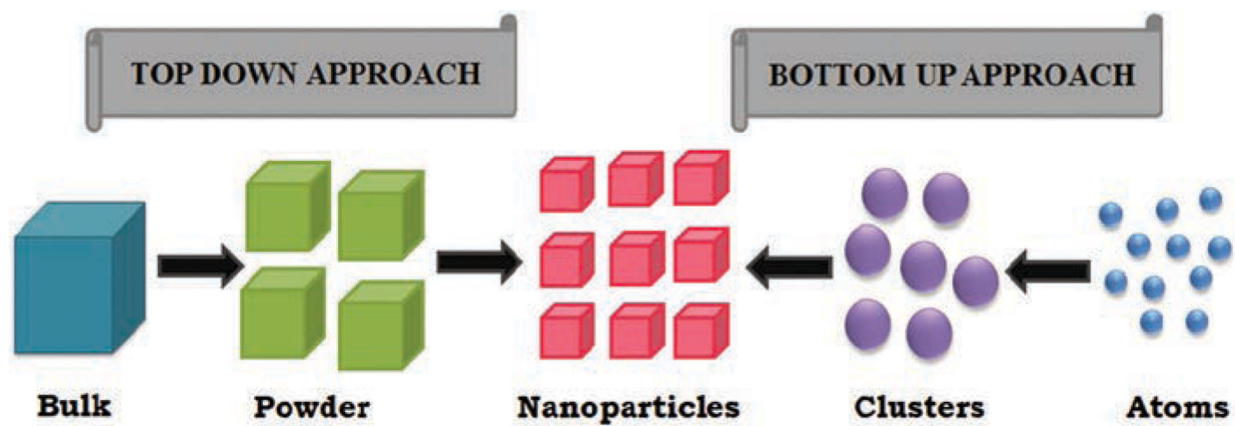
Fig. 4.
Top-down and bottom-up approach for fabricating Ag NPs.
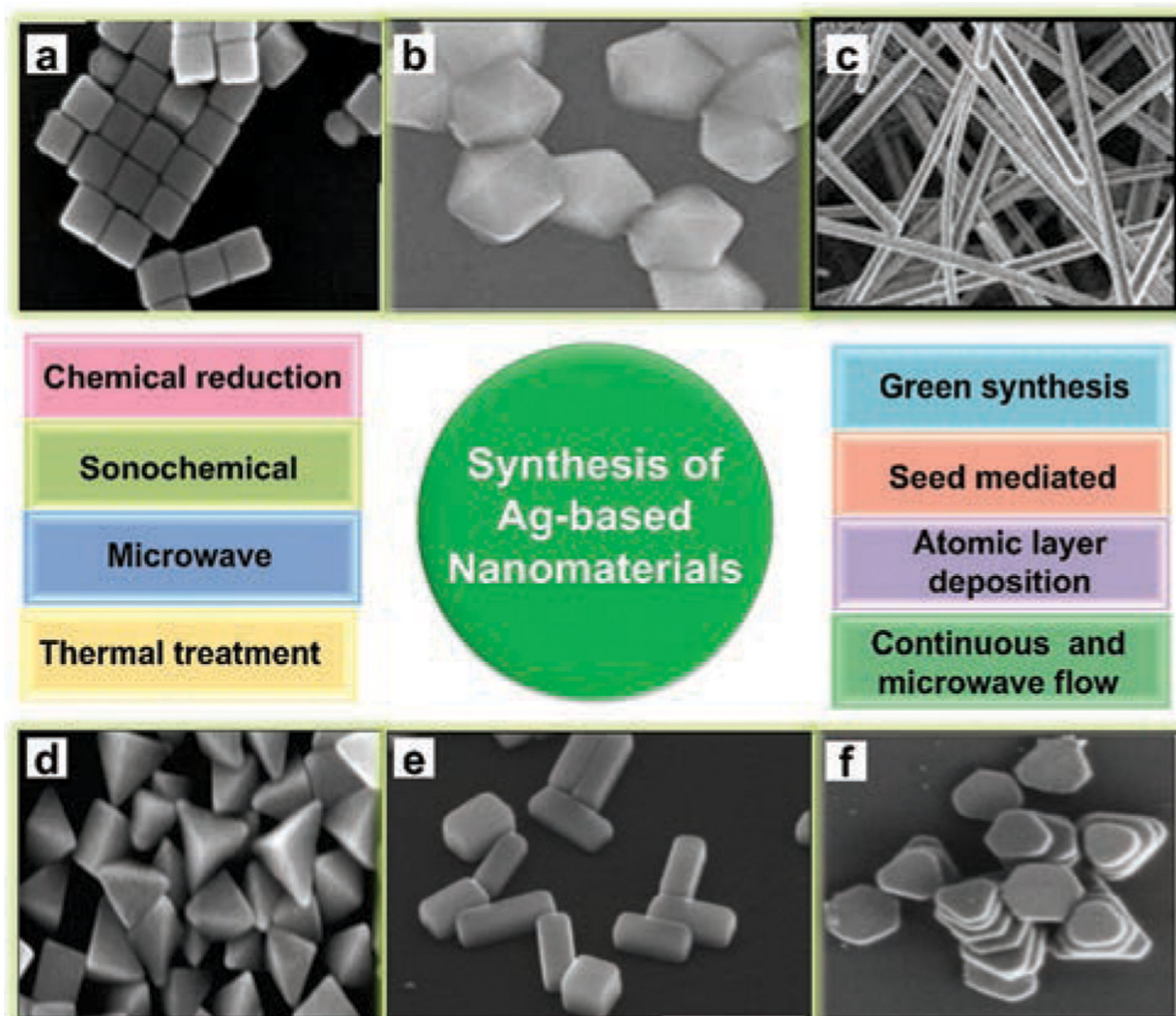
Fig. 5.
Major synthetic approaches for the fabrication of Ag NPs. (a) Reproduced from ref. 24 with permission, John Wiley and Sons, copyright 2008. (b) Reproduced from ref. 20 with permission, Elsevier, copyright 2006. (c) Reproduced from ref. 22 with permission, Elsevier, copyright 2013. (d) Reproduced from ref. 25 with permission, American Chemical Society, copyright 2006. (e) Reproduced from ref. 23 with permission, American Chemical Society, copyright 2007. (f) Reproduced from ref. 21 with permission, Royal Society of Chemistry, copyright 2017.
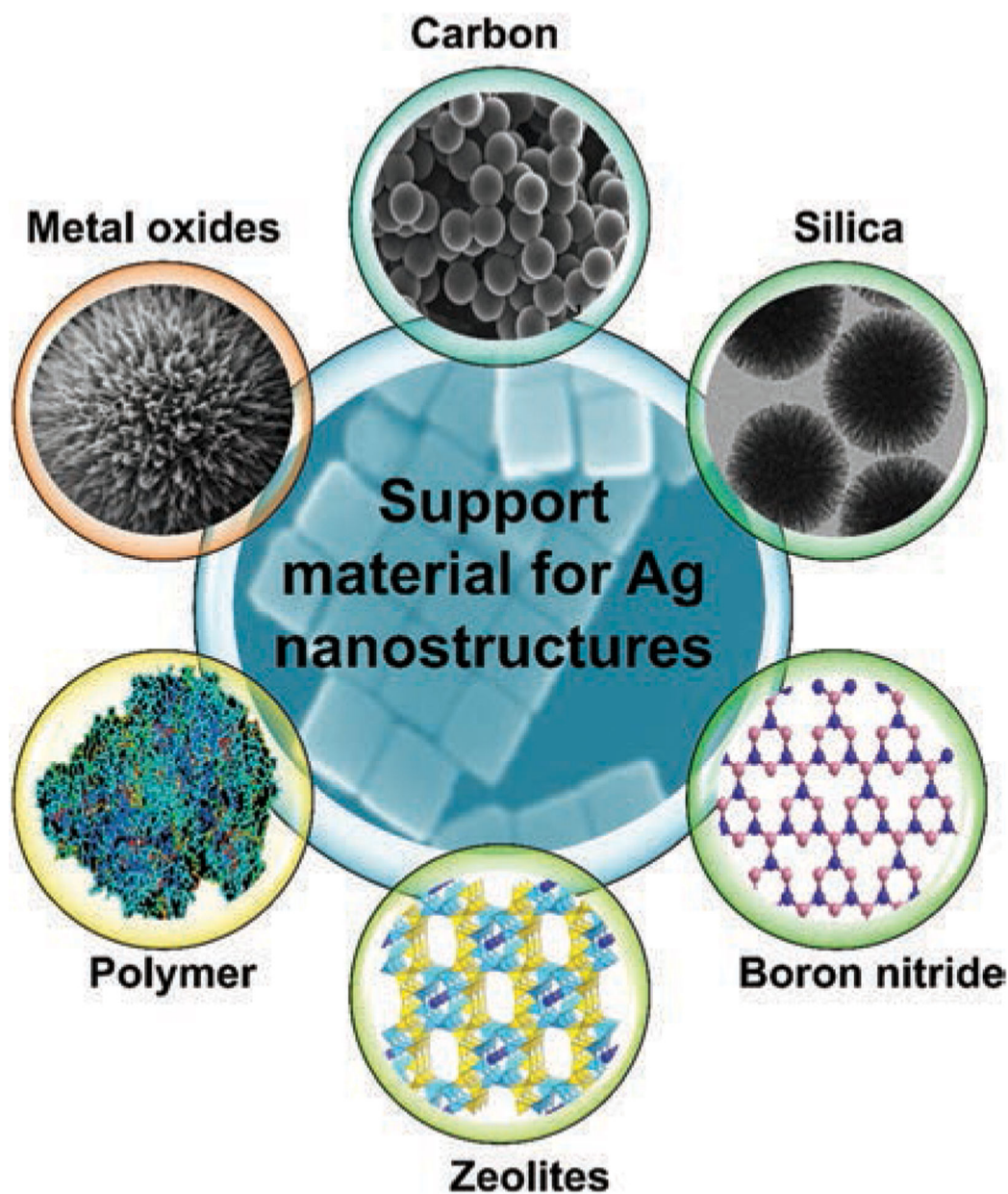
Fig. 6.
Support materials used to anchor Ag NPs. (a) Centre image—reproduced from ref. 24 with permission, John Wiley and Sons, copyright 2008. (b) Metal oxides—reproduced from ref. 224 with permission, Royal Society of Chemistry, copyright 2014. (c) Carbon—reproduced from ref. 225 with permission, Royal Society of Chemistry, copyright 2016. (d) Silica— reproduced from ref. 226 with permission, Royal Society of Chemistry, copyright 2015.
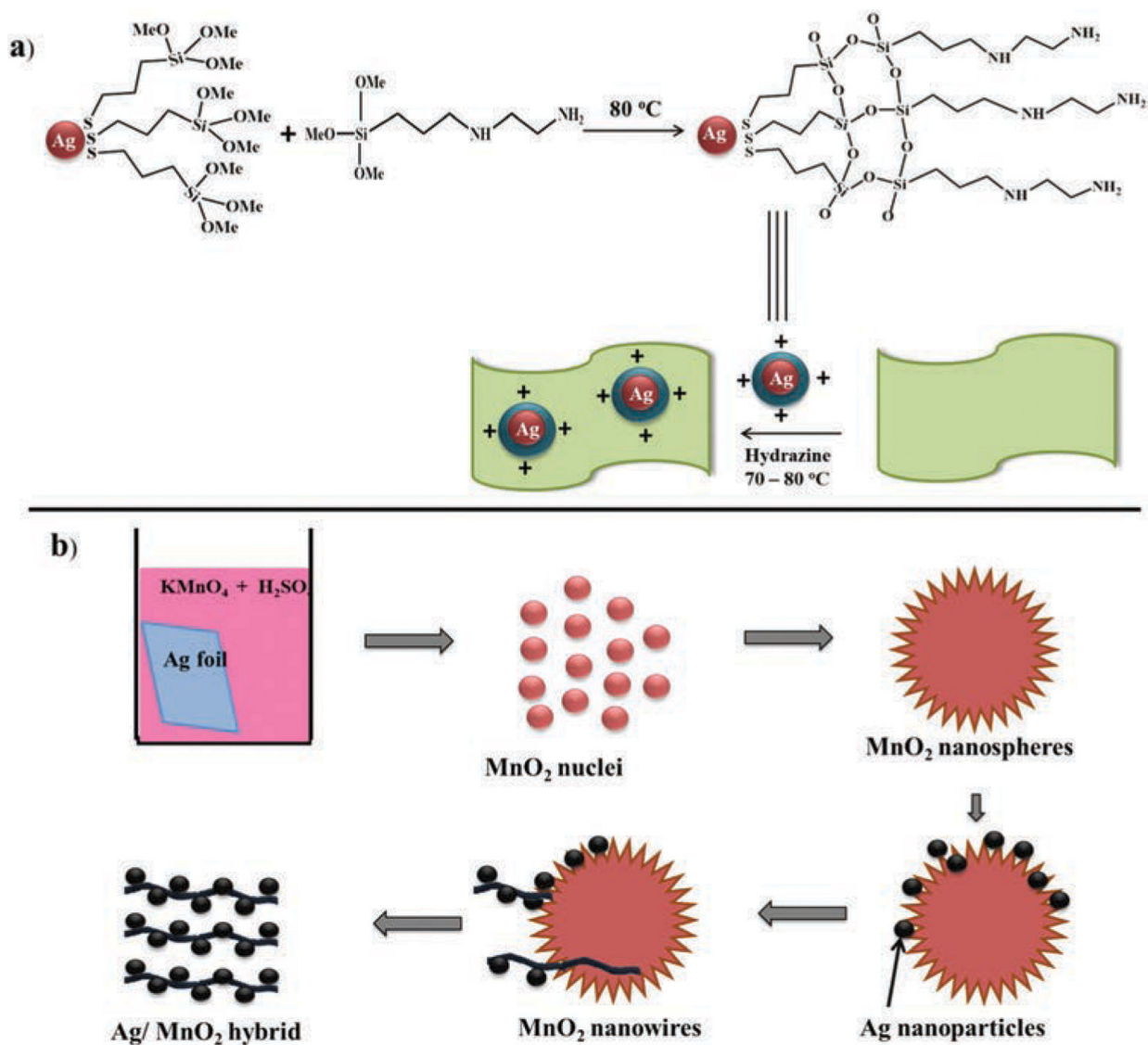
Fig. 7.
Synthetic pathway used to produce differently supported Ag nanocomposite materials: (a) fabrication of a reduced graphene oxide–silver nanoparticle (rGO–Ag) composite and (b) schematic illustration of the synthesis of MnO_2 nanowire supported Ag NPs.
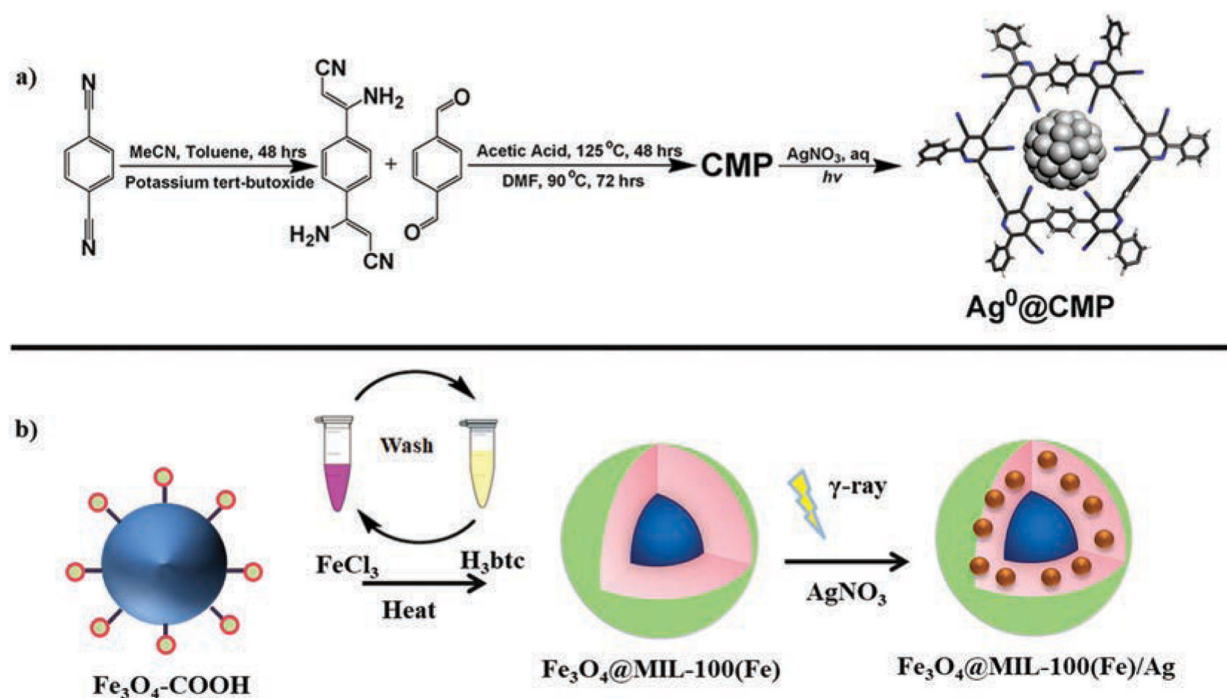
Fig. 8.
Synthesis of supported Ag composite materials. (a) Fabrication route of CMP for Ag nanoparticle immobilization. Reproduced from ref. 308 with permission, American Chemical Society, copyright 2017. (b) Synthetic pathway of Fe$_3$O$_4$@MIL-100(Fe)/Ag.
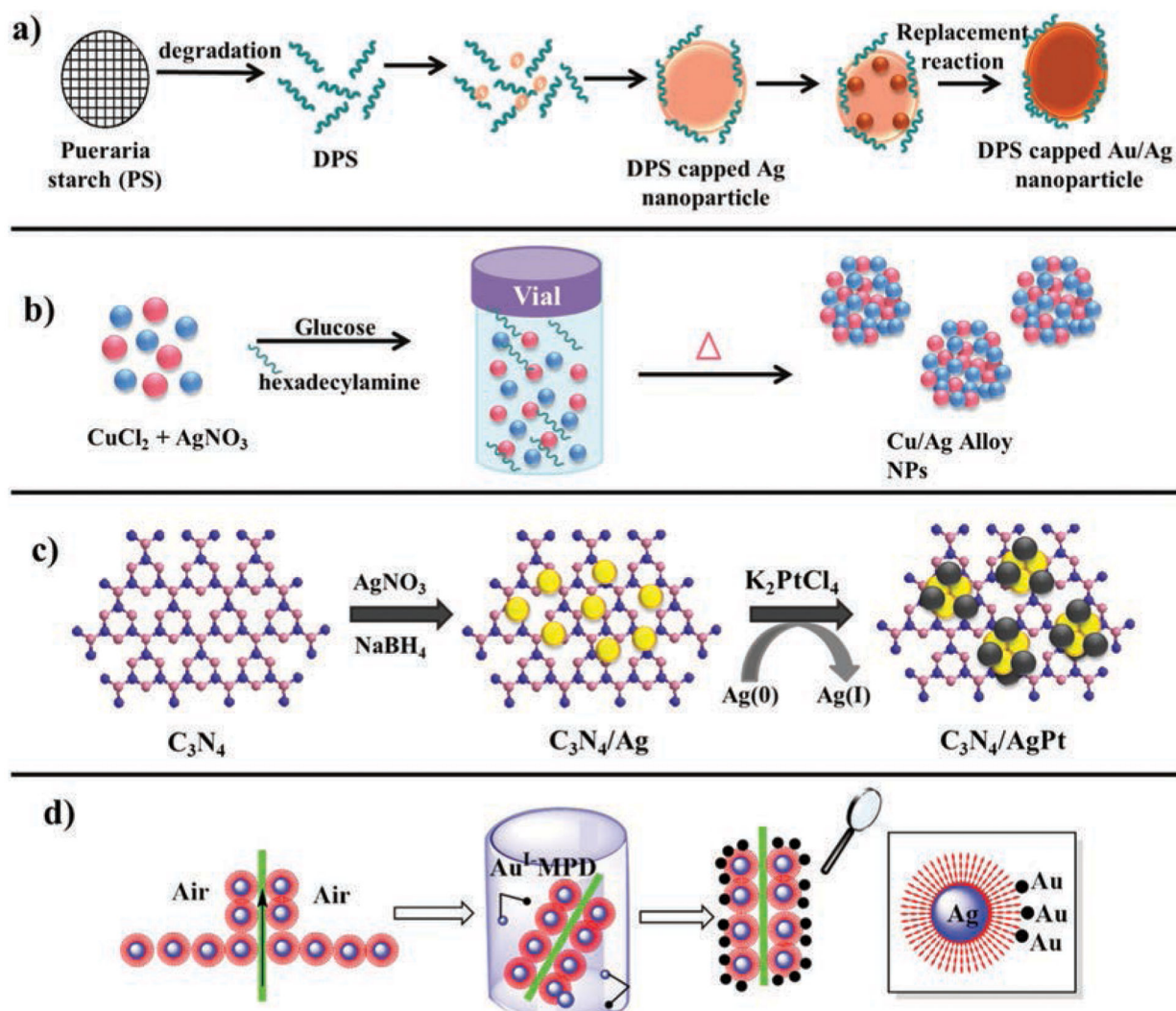
Fig. 9.
Various mixed Ag NPs. (a) Fabrication of DPS (degraded pueraria starch) capped bimetallic Au/Ag NPs. (b) One-pot synthesis of Cu/Ag bimetallic NPs. (c) Synthetic pathway of AgPt bimetallic NPs on C_3N_4 surface *via* galvanic exchange. (d) Synthesis of bimetallic AgAu Janus NPs.
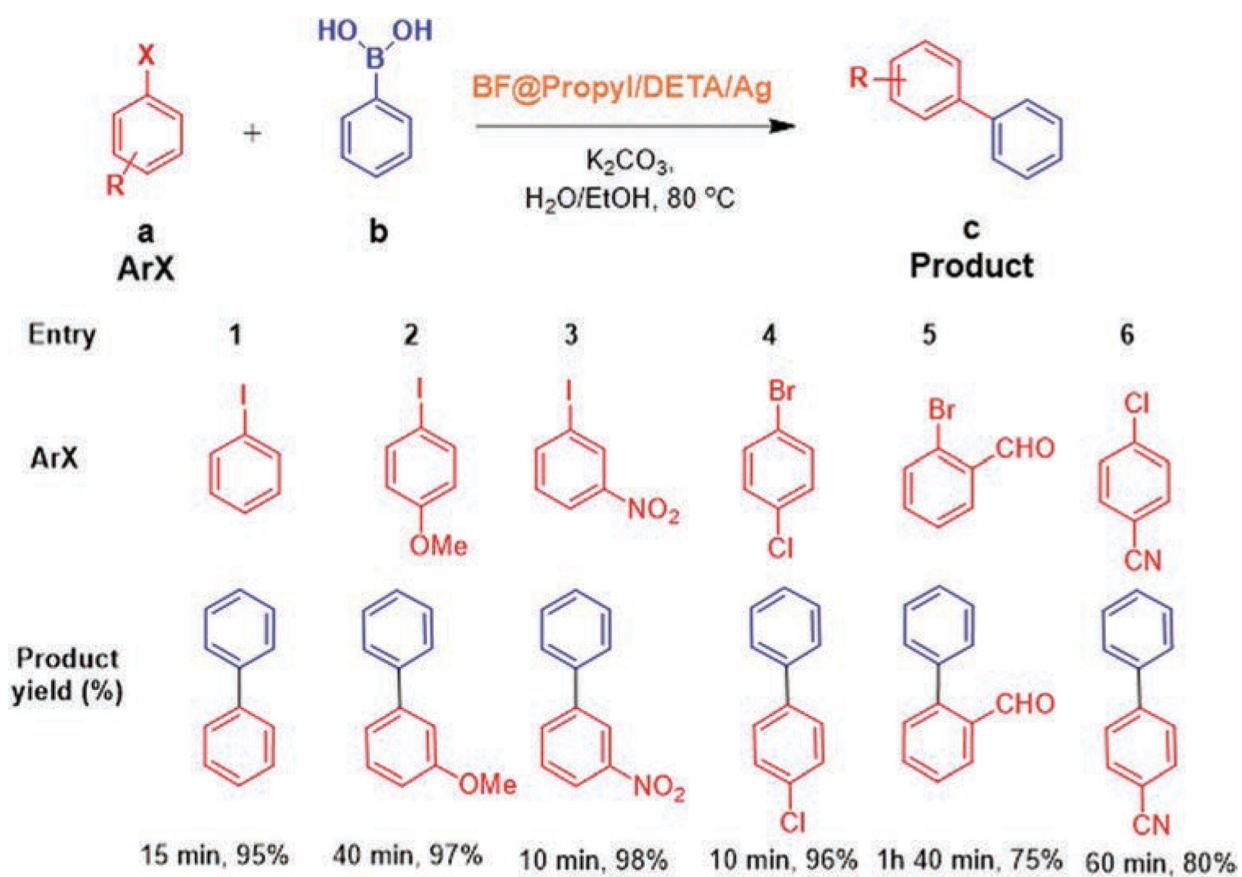
Fig. 10.
Suzuki Miyaura coupling of aryl halides and phenylboronic acid catalyzed by a BF@Propyl/
DETA/Ag nanocomposite.
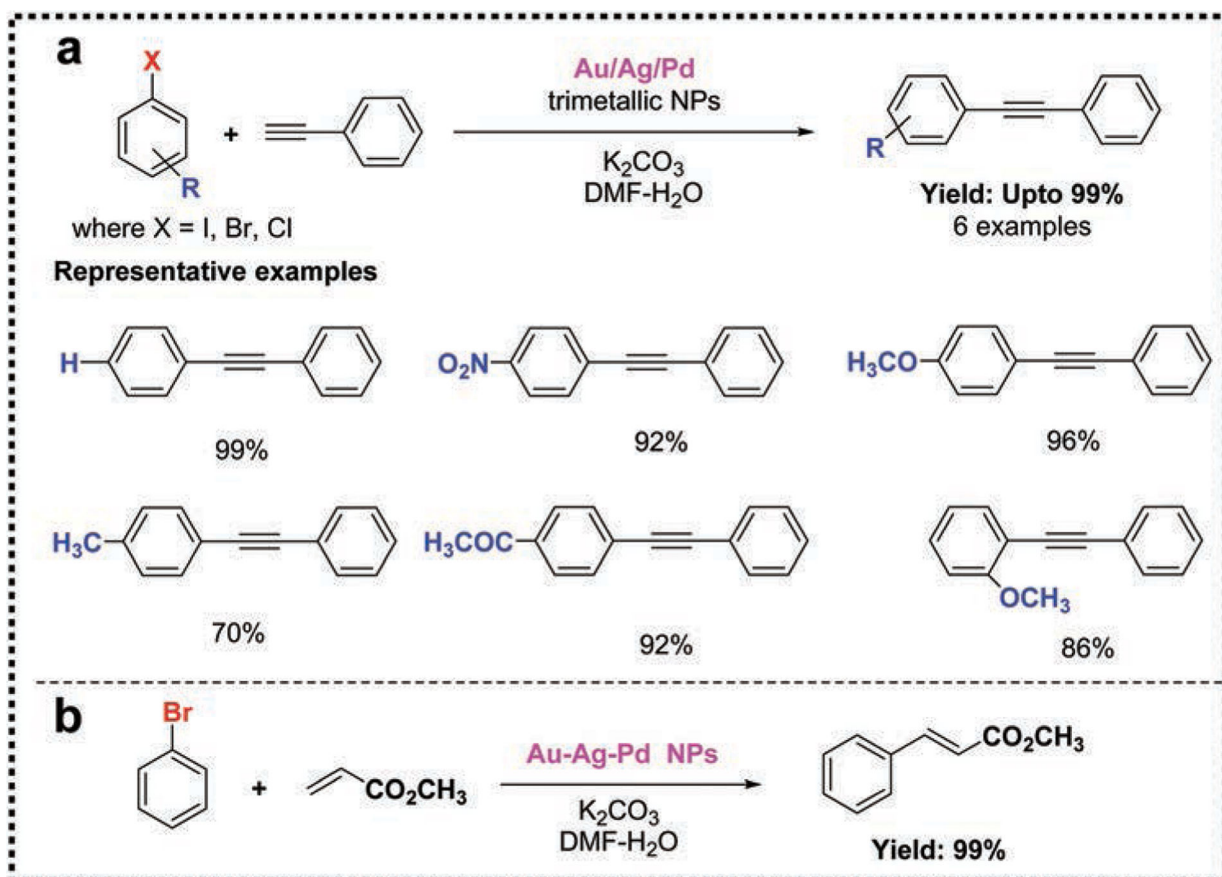
Fig. 11.
(a) Sonogashira C–C coupling reaction catalyzed by Au/Ag/Pd trimetallic NPs, and (b) Au–Ag–Pd NPs catalysed Heck coupling reaction.
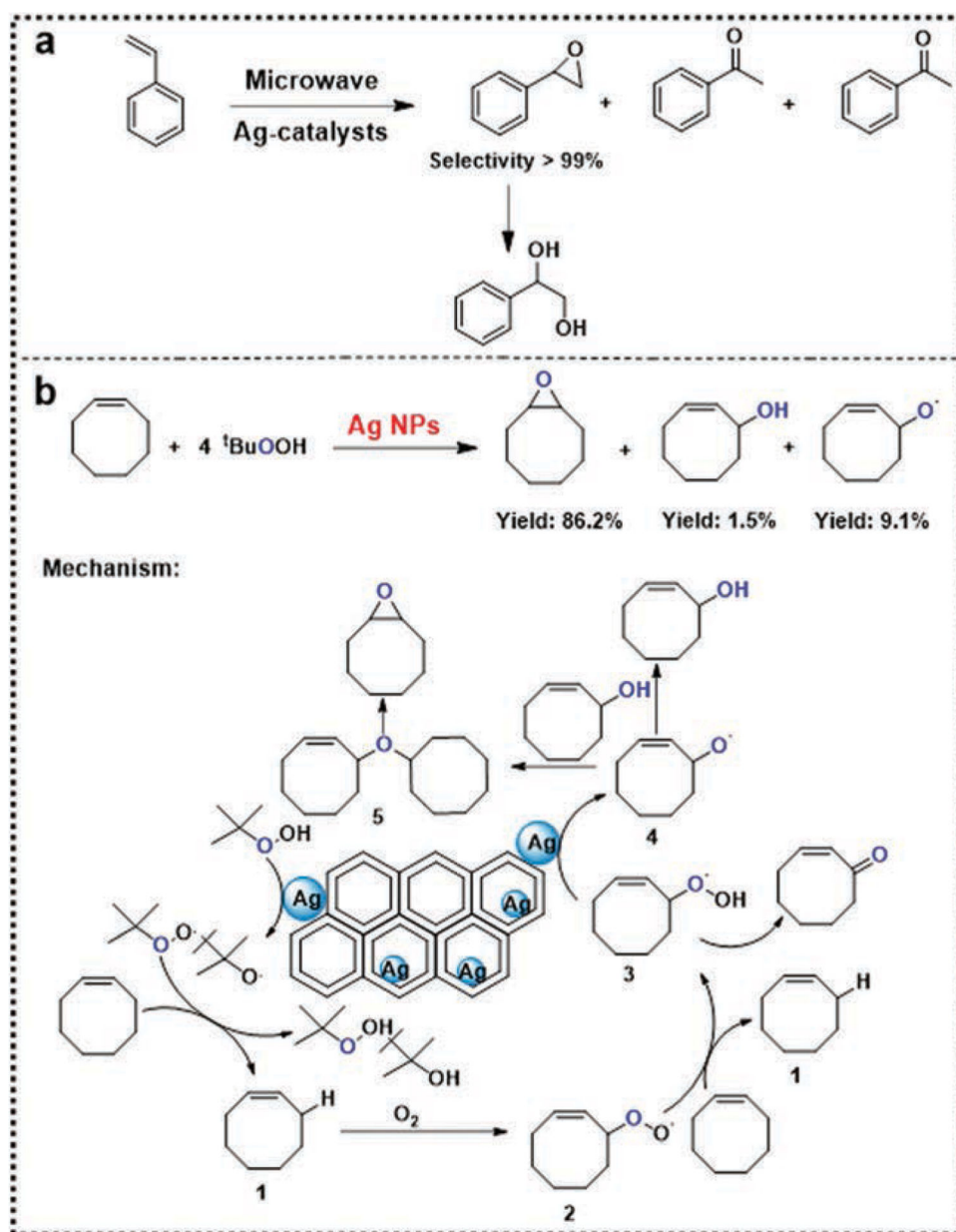
Fig. 12.
(a) Reaction products obtained in the oxidation of styrene with supported Ag NPs on hybrid films. (b) Proposed mechanism for (*Z*)-cyclooctene epoxidation on the MCM-41 supported Ag catalyst.
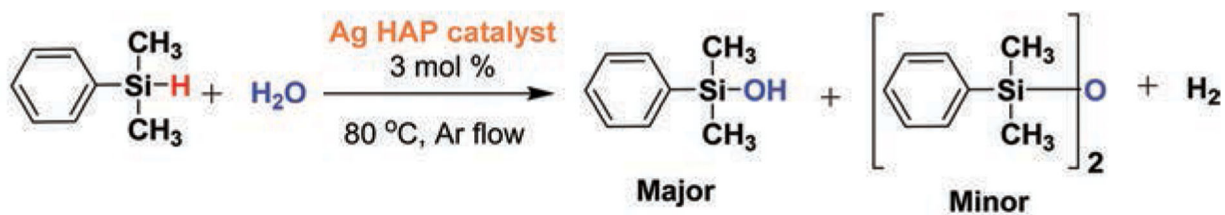
Representative examples of silanol (Major)
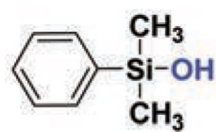
Conv. 99%, Sel. 99%
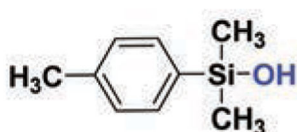
Conv. 99%, Sel.99%
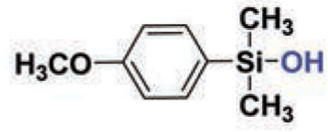
Conv. 97%, Sel.99%
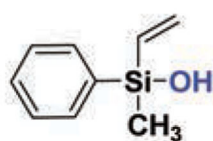
Conv. 97%, Sel.99%
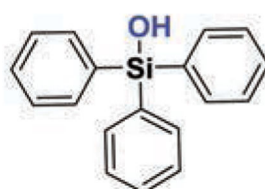
Conv. 99%, Sel. 99%
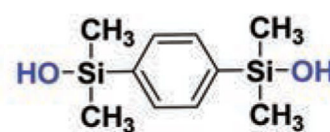
Conv. 96%, Sel. 99%

Fig. 13.
Oxidation of dimethylphenylsilane using a Ag-HAP catalyst.
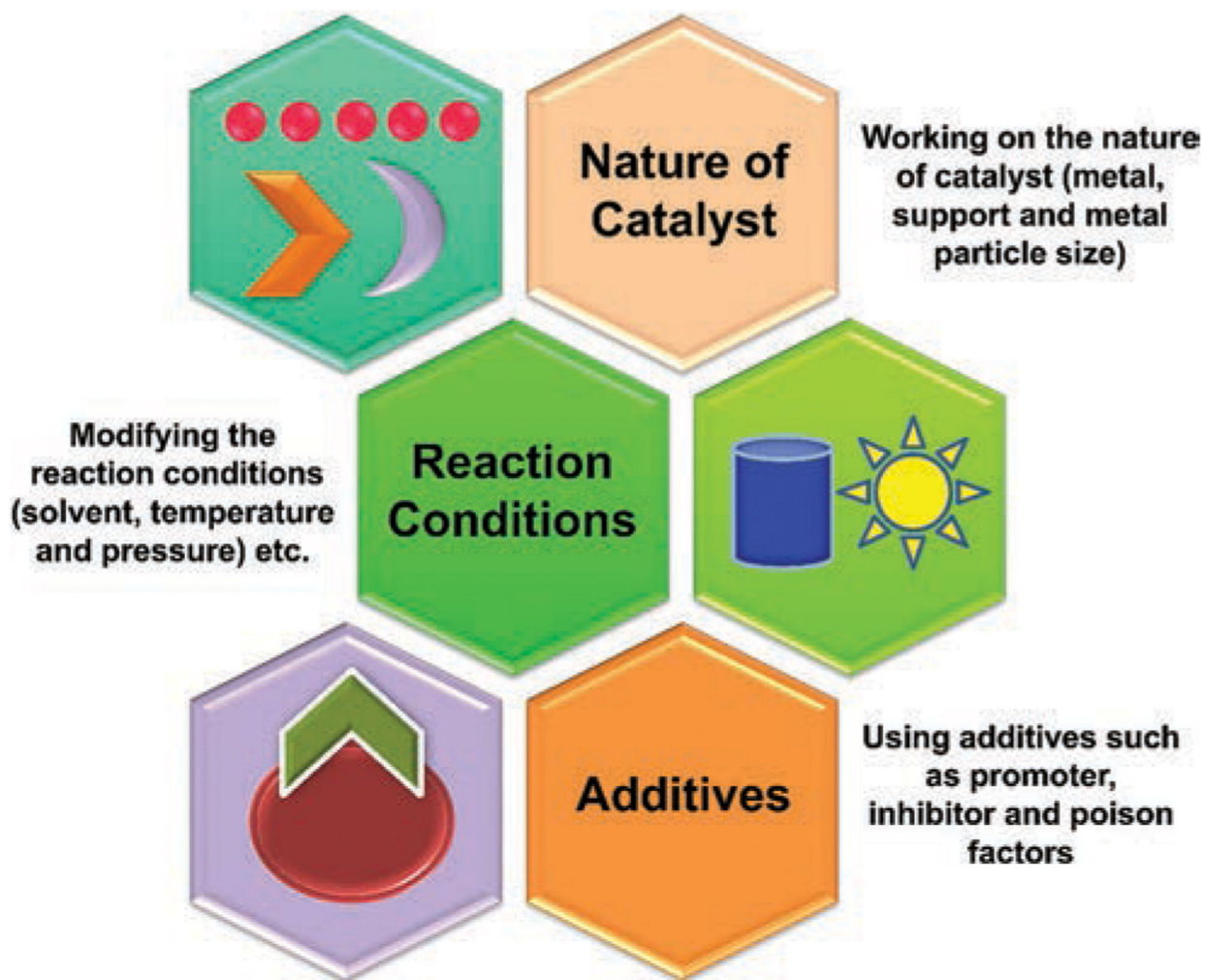
Fig. 14.
Different approaches for accomplishing selective catalytic hydrogenation of nitroarenes.
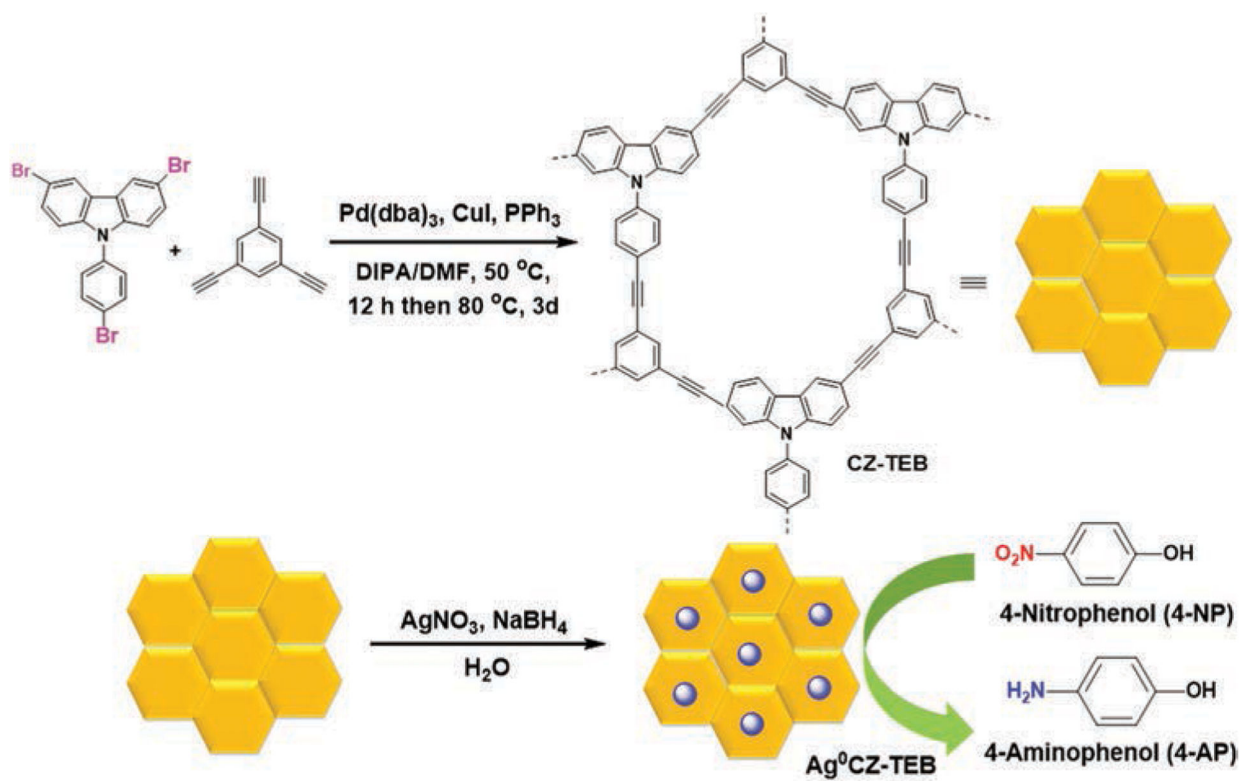
Fig. 15.
Illustration of the synthetic pathway of CZ–TEB for Ag NPs immobilization and its
application in reduction of 4-NP.
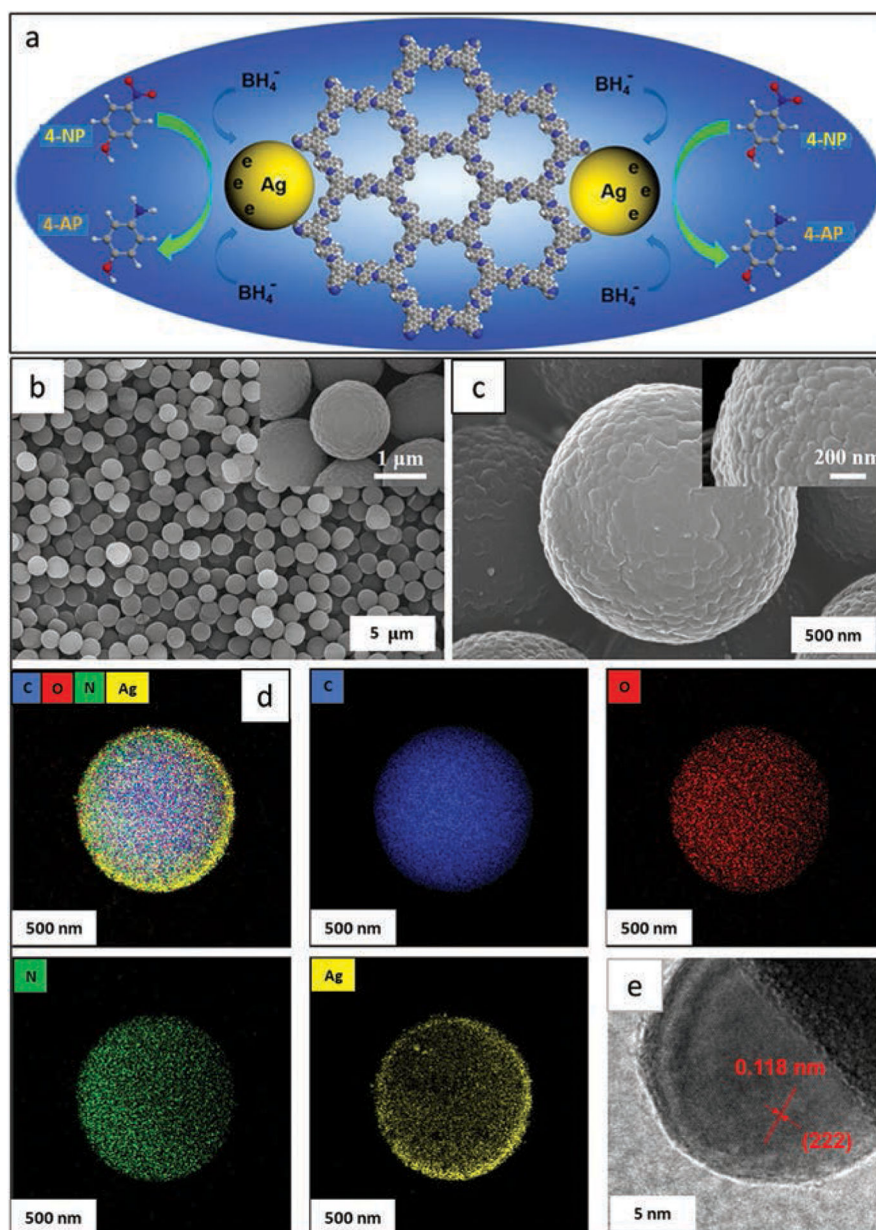
Fig. 16.
(a) Schematic of 4-NP reduction using $NaBH_4$ in the presence of Ag NPs@SCOF microspheres and (b and c) SEM images of the SCOF and Ag NPs@SCOF respectively. (d) STEM-EDX elemental mapping images of C, O, N, and Ag. (e) HR-TEM image of the Ag NPs@SCOF. Reproduced from ref. 428 with permission from American Chemical Society, copyright 2021.
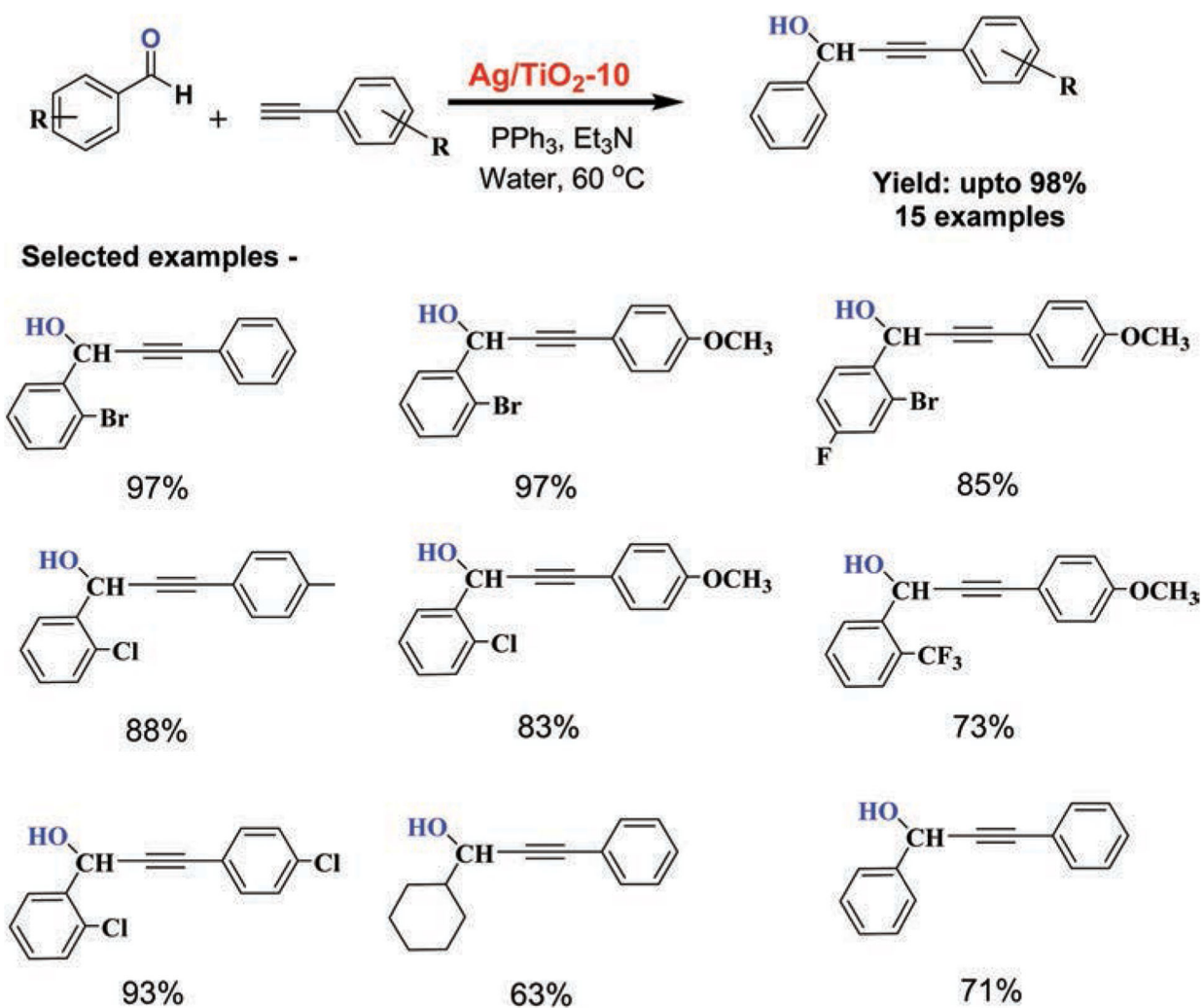
Fig. 17.
TiO$_2$ supported Ag NP-catalyzed 1,2-addition of alkynes to aldehydes.
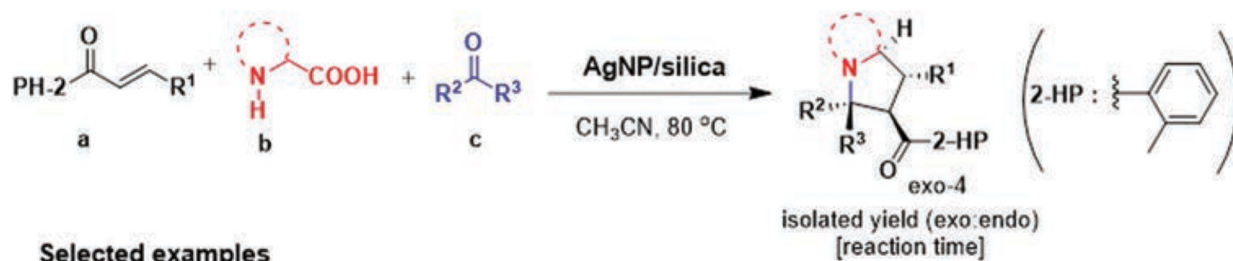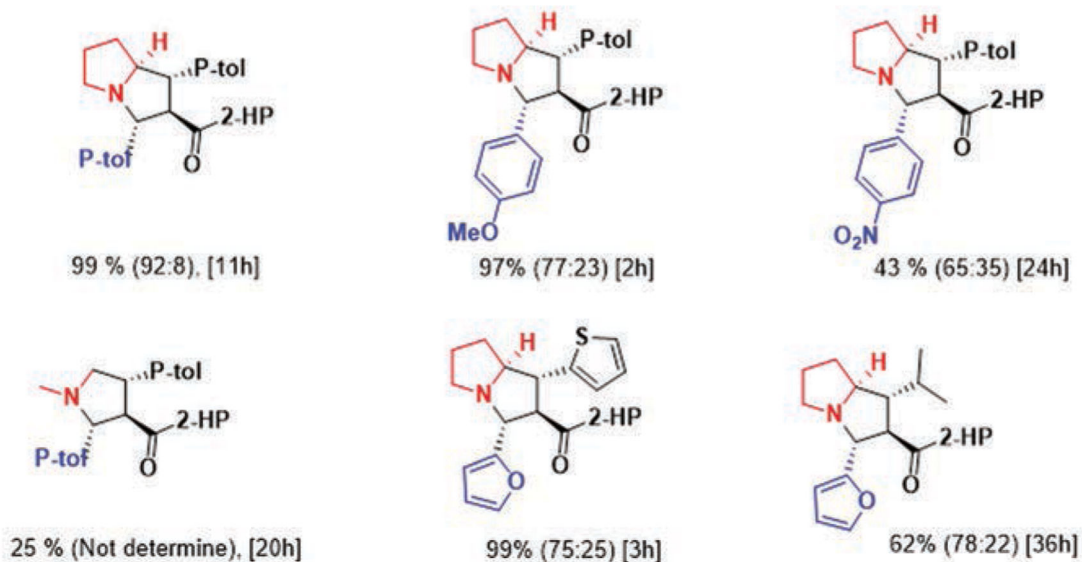
Fig. 18.
Ag/silica-catalyzed [3+2]-cycloaddition reaction.
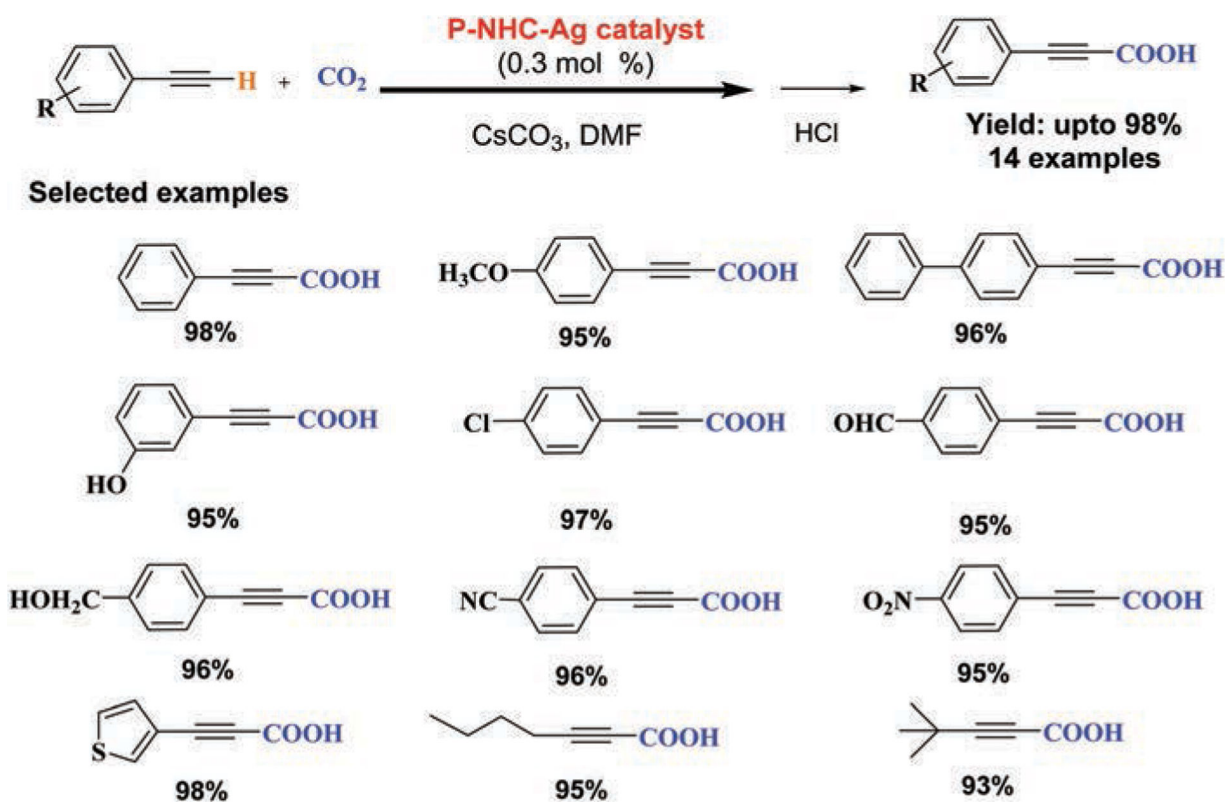
Fig. 19.
N-Heterocyclic carbene polymer supported Ag NPs catalyzed carboxylation of terminal alkynes with CO_2.
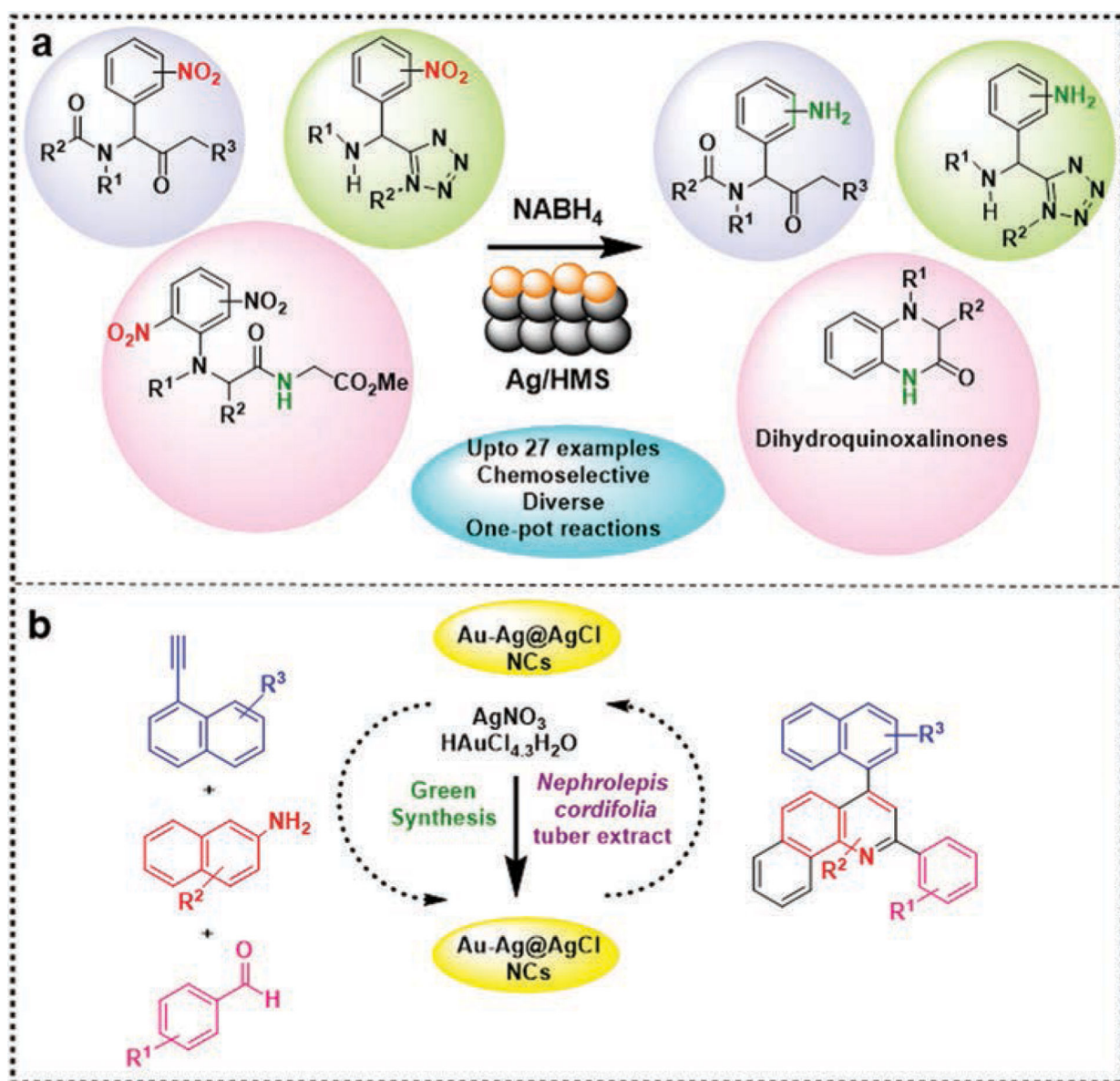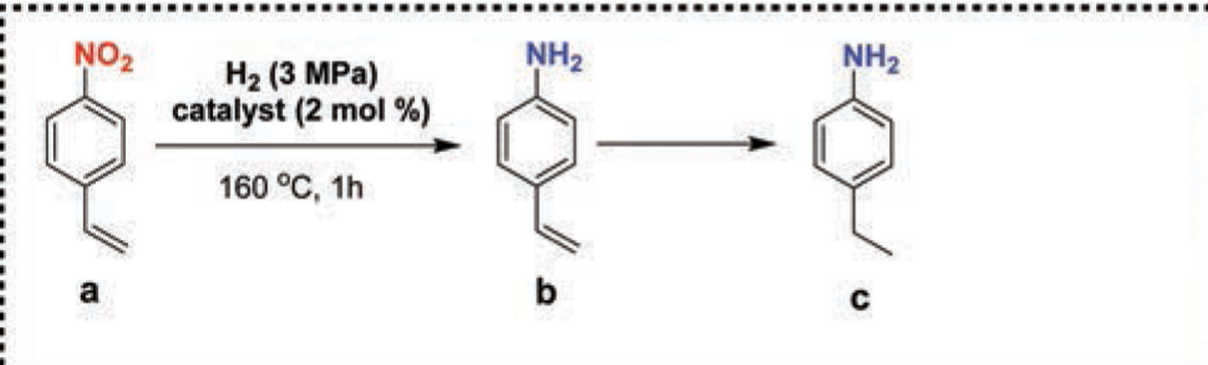
Fig. 20.
(a) Ag/HMS (10) –NaBH$_4$ catalyzed chemoselective reduction of the multifunctional nitro compounds synthesized by the Ugi-Smiles and Ugi-4C reactions, and (b) green synthesis of Au–Ag@AgCl NCs for catalyzing the multicomponent domino annulation–aromatization for obtaining quinolines.

Fig. 21.
Hydrogenation of 4-nitrostyrene by various catalysts.

Entry	Catalysts-X[b]	Selectivity		Conversion rate (%)
		b	c	
1	Ag/WO$_3$-2.6	98	0	11
2	Ag/Al$_2$O$_3$-0.9	96	3	100
3	Ag/Al$_2$O$_3$-1.1	95	2.9	100
4	Ag/TiO$_2$-1.3	92	1.4	100
5	Ag/sepiolite-3.7	89	1.4	100
6	Ag/ZrO$_2$-1.6	74	3.0	61
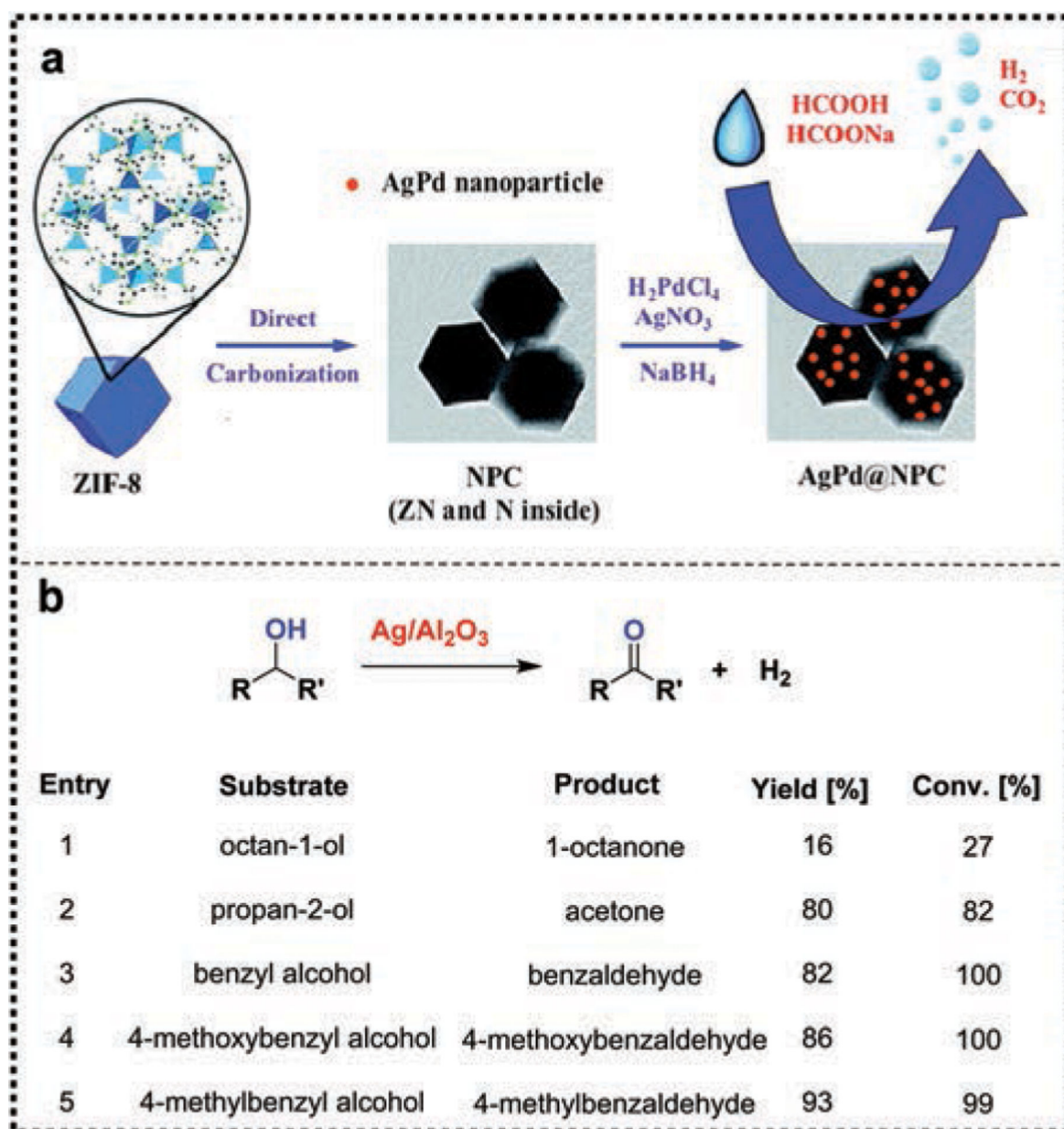
Fig. 22.
(a) The dehydrogenation of formic acid by using a AgPd@NPC catalyst. Reproduced from ref. 480 with permission, Royal Society of Chemistry, copyright 2015. (b) Dehydrogenation of various alcohols by using a Ag/Al_2O_3 catalyst (reaction conditions: 1.0 mmol of substrate, 3 mL of toluene, 2.0 mol% of a Ag/Al_2O_3-5 catalyst stirred at 373 K for 24 h).
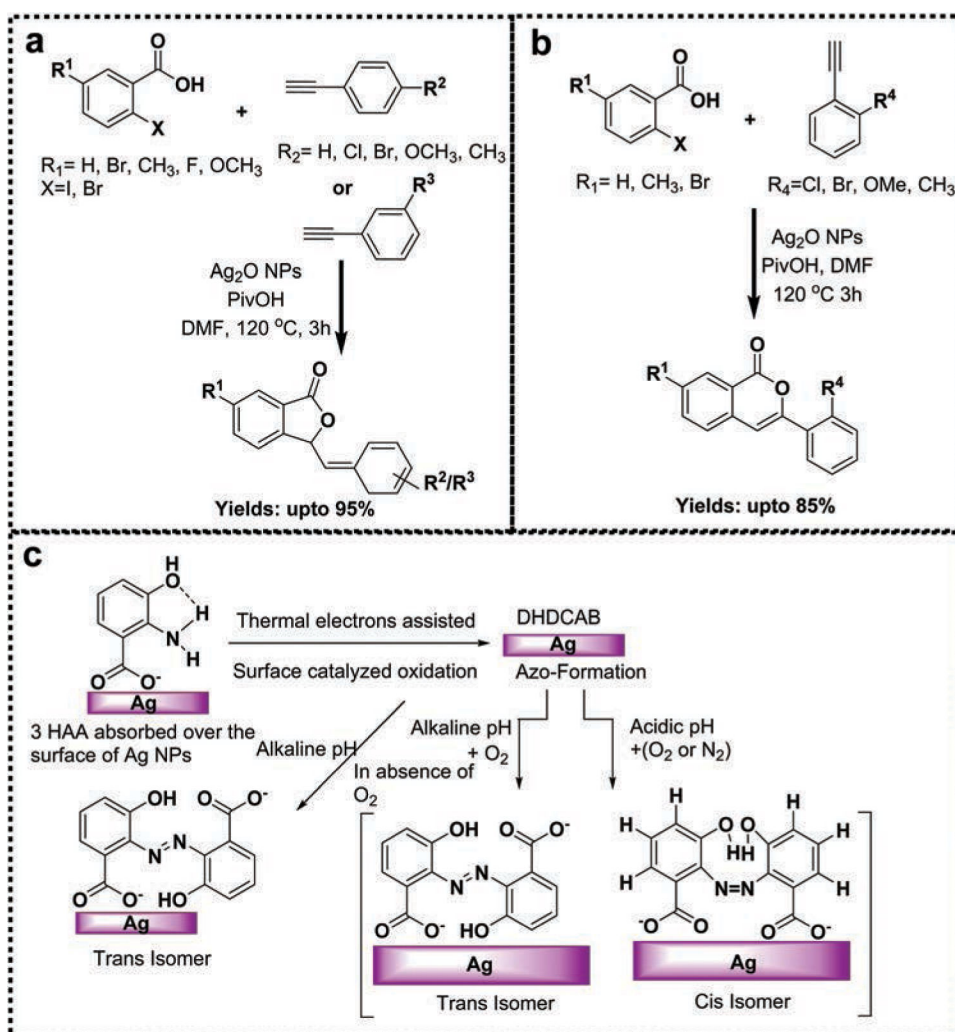
Fig. 23.
(a) Synthesis of 3-ylidenephthalides and (b) synthesis of isocoumarins, and (c) illustration of the formation of the azo derivative of HAA.
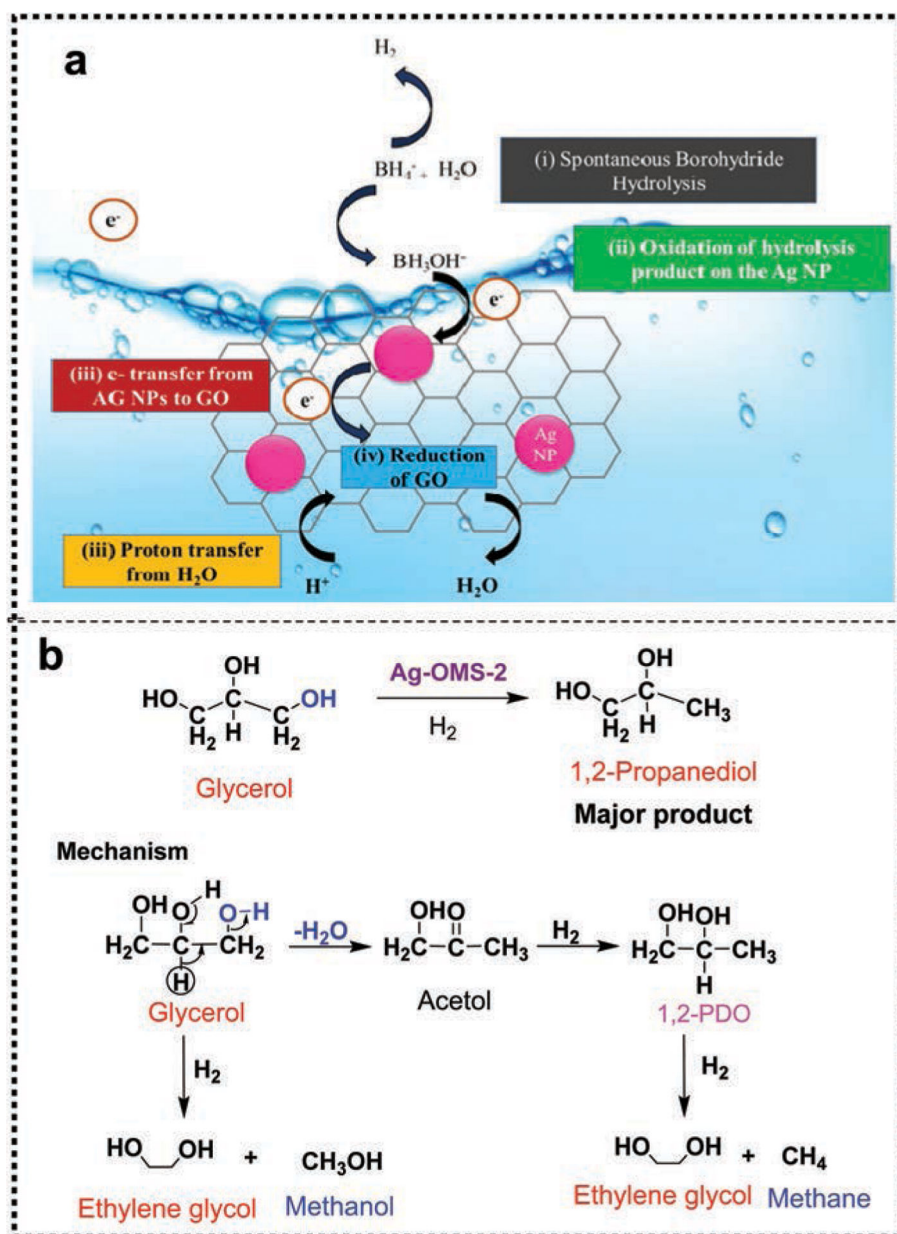
Fig. 24.

(a) Proposed mechanism for the reduction of aqueous GO dispersions with NaBH$_4$ catalyzed by Ag NPs. Reproduced from ref. 493 with permission, Royal Society of Chemistry, copyright 2014. (b) Products for glycerol hydrogenolysis over Ag-OMS-2.
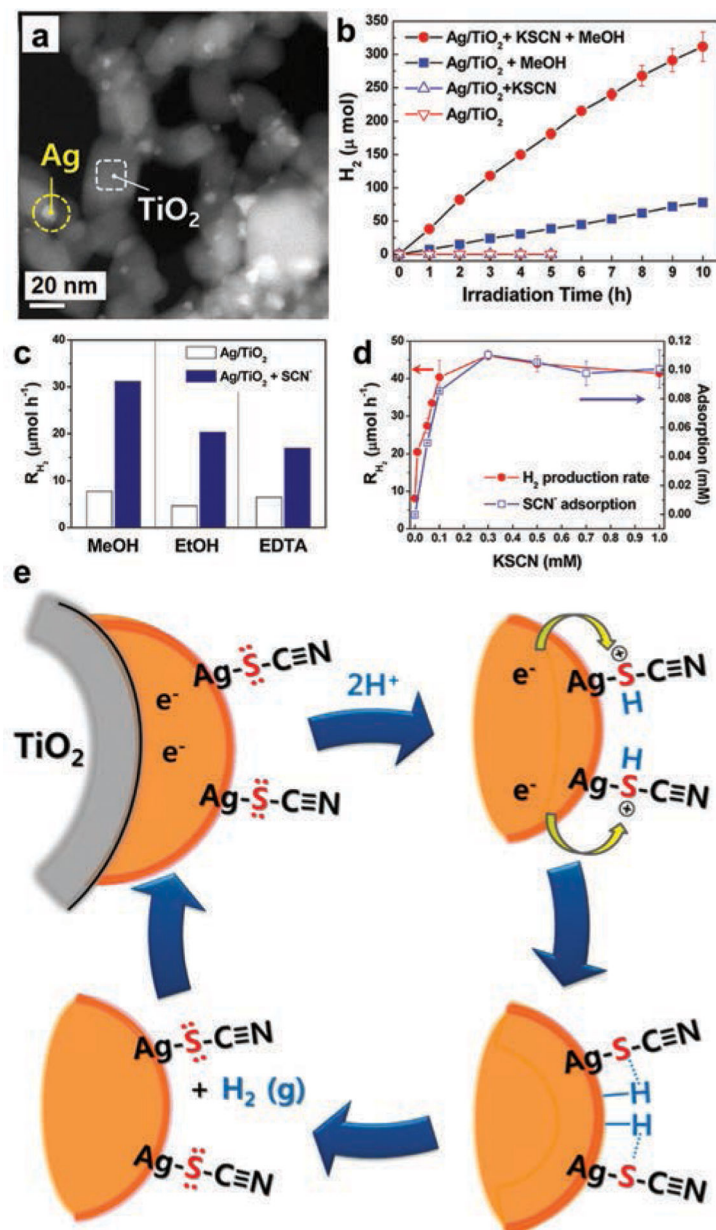
Fig. 25.

(a) Dark-field STEM images of thiocyanate-modified Ag/TiO$_2$, (b) time profiles of photocatalytic HER on Ag/TiO$_2$ with and without thiocyanate. Rate of H$_2$ production (R_{H_2}) (µmol h^{-1}) (c) in the presence of ethanol, methanol, and EDTA as electron donors. (d) Effect of KSCN concentration on the rate of H$_2$ production (left axis) and the adsorbed amount of thiocyanate on 3.0 wt% of Ag supported TiO$_2$ (right axis), (e) proposed mechanistic pathway to the production of H$_2$ under photocatalytic conditions over thiolate-adsorbed Ag/TiO$_2$. Reproduced from ref. 524 with permission, American Chemical Society, copyright 2016.
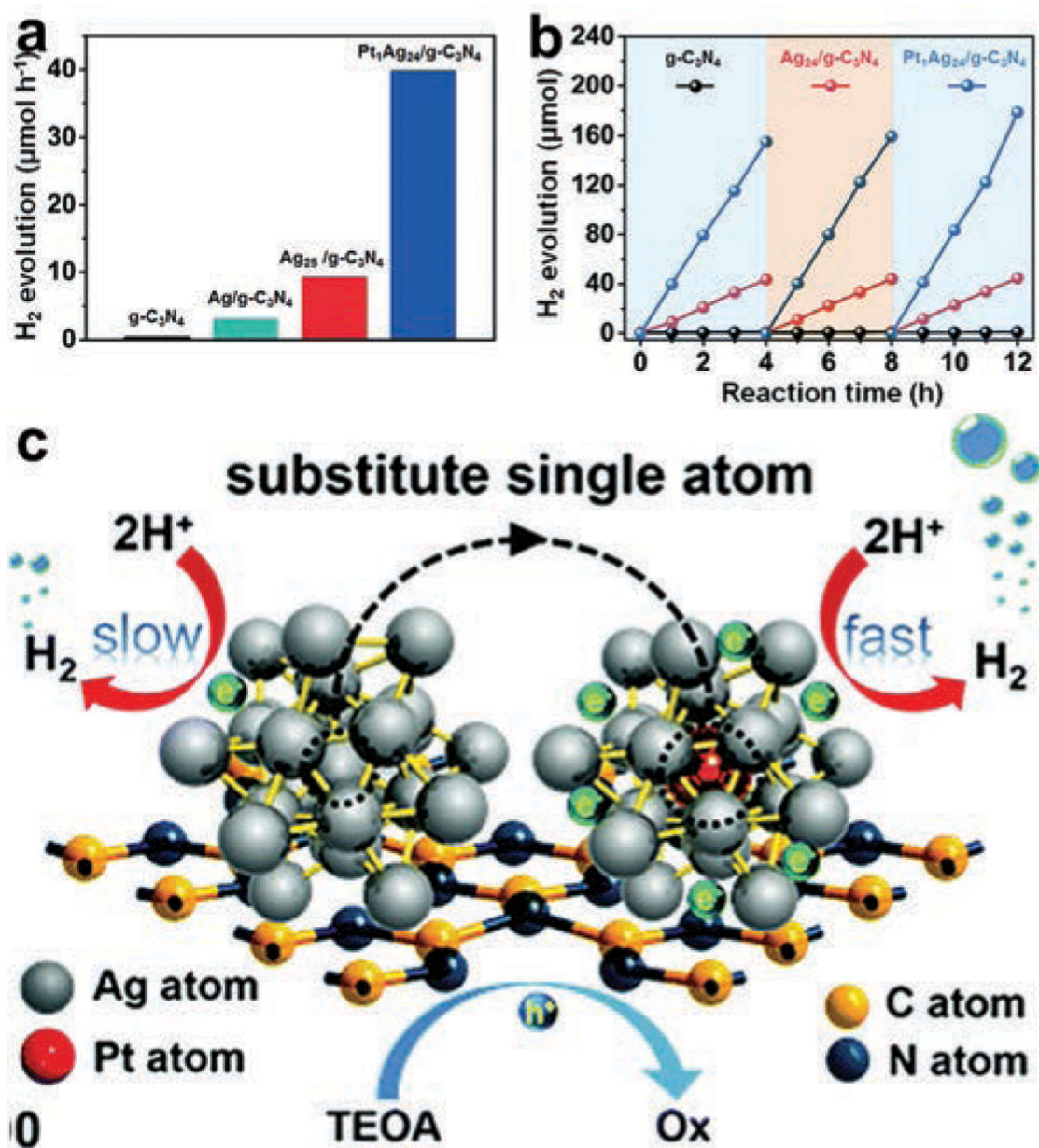
Fig. 26.
Comparison of g-C_3N_4, Ag_{25}/g-C_3N_4, and Pt_1Ag_{24}/g-C_3N_4 catalyst activity. (a) Photocatalytic HER performance, (b) cycling runs for the HER under photocatalytic conditions, (c) schematic mechanism for photocatalytic HER. Reproduced from ref. 534 with permission The Royal Society of Chemistry, copyright 2017.
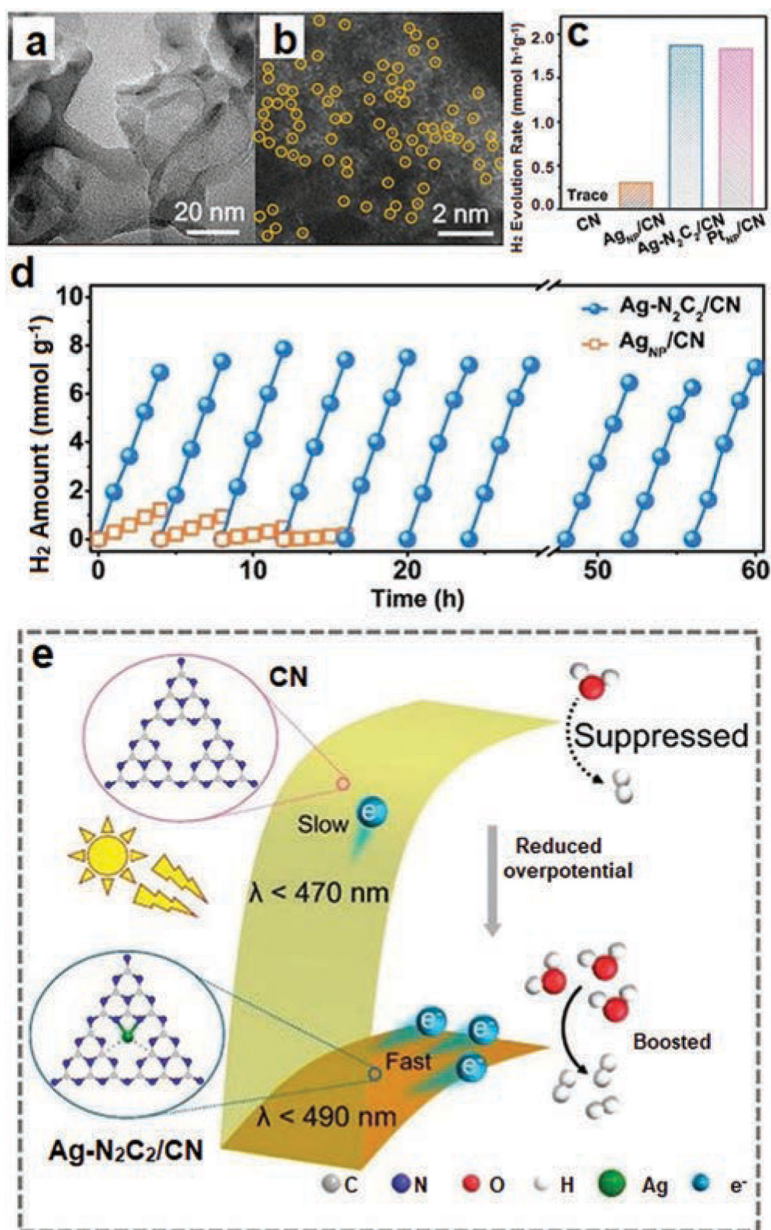
Fig. 27.
Schematic of the Ag–N$_2$C$_2$/CN photocatalyst. (a) HR-TEM and (b) AC-HAADF-STEM images, (c) H$_2$ evolution rates of Ag–N$_2$C$_2$/CN, Ag$_{NP}$/CN, and Ag–N$_4$/CN samples, and (d) comparison of the stability of Ag$_{NP}$/CN and Ag–N$_2$C$_2$/CN for the photocatalytic H$_2$ evolution. Reproduced from ref. 535 with permission John Wiley and Sons, copyright 2020.

Fig. 28.
(a) Mechanistic pathway for reduction of CO_2 under photocatalytic conditions over $BaLa_4Ti_4O_{15}$ with Ag cocatalysts by different methods. Reproduced from ref. 551 with permission, American Chemical Society, copyright 2011. (b) Schematic illustration depicting Ag NPs/carbon fibers mediated photocatalytic reduction of CO_2. Reproduced from ref. 552 with permission, Elsevier, copyright 2017.
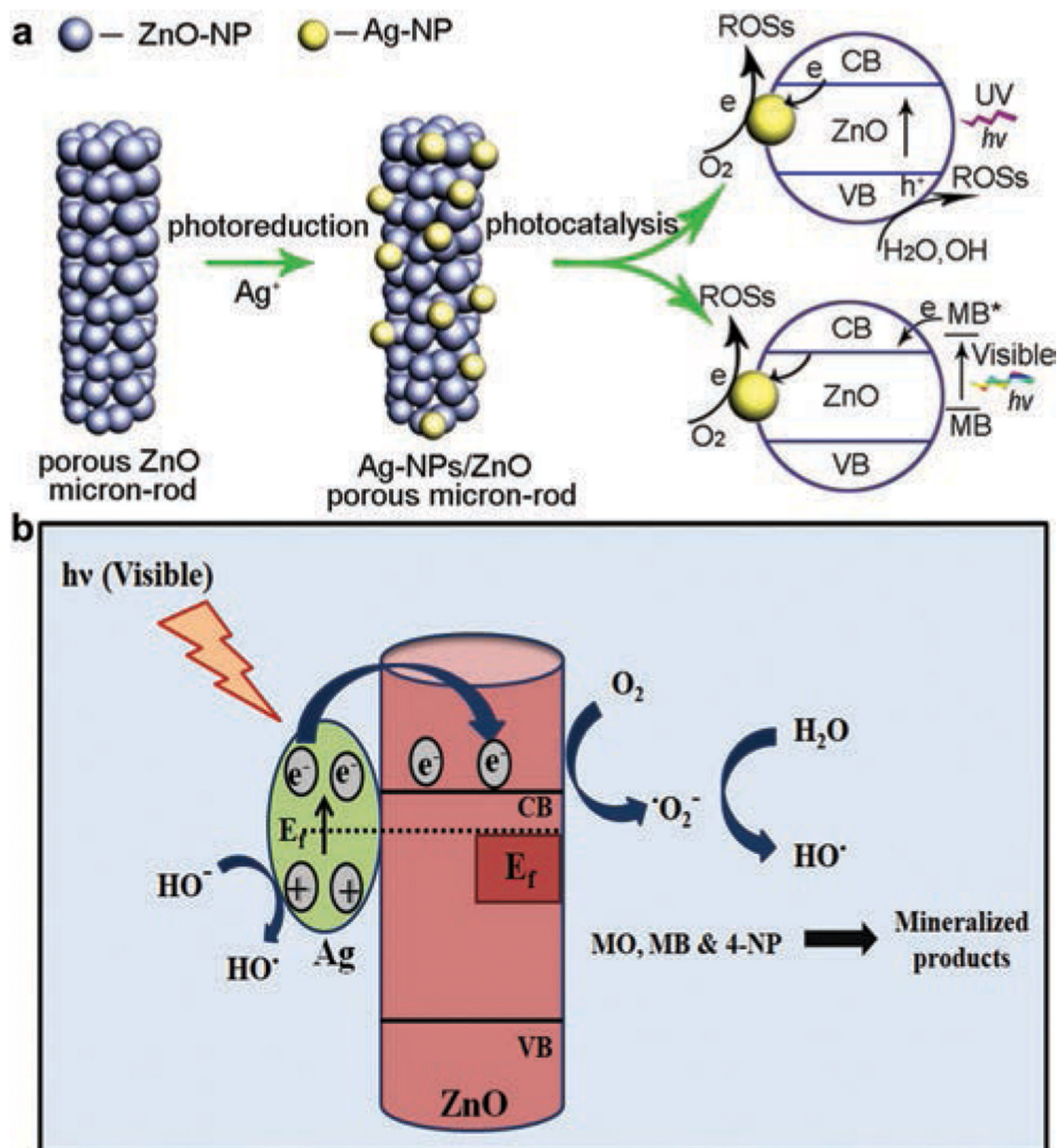
Fig. 29.
(a) Schematic depiction of MB degradation under UV and visible light irradiation in the presence of Ag–NPs/*n*ZnO microstructures. Reproduced from ref. 577 with permission, American Chemical Society, copyright 2012. (b) Diagrammatic representation illustrating photocatalytic degradation of MO, MB and 4-NP by the Ag–ZnO composite. Reproduced from ref. 284 with permission, American Chemical Society, copyright 2013.
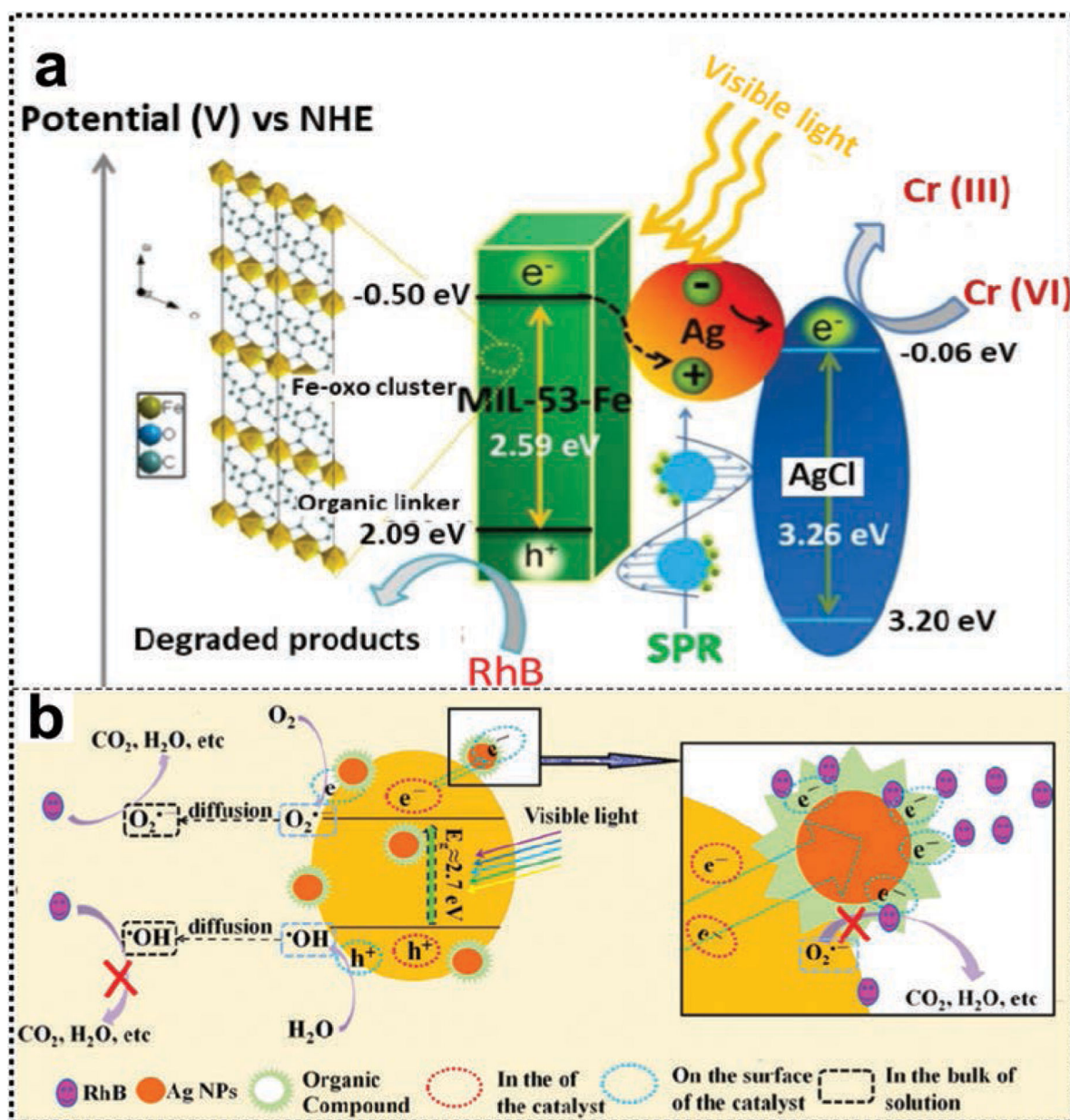
Fig. 30.

(a) Plasmonic Z-scheme photocatalytic mechanism of Ag/AgCl@MIL-53-Fe under visible light irradiation. Reproduced from ref. 597 with permission from Elsevier, copyright 2018. (b) The mechanism of the RhB degradation using Ag/C_3N_4 photocatalyst in the bulk of solution (*p*-benzoquinone, *t*-butanol, and methanol). Reproduced from ref. 598 with permission, American Chemical Society, copyright 2015.
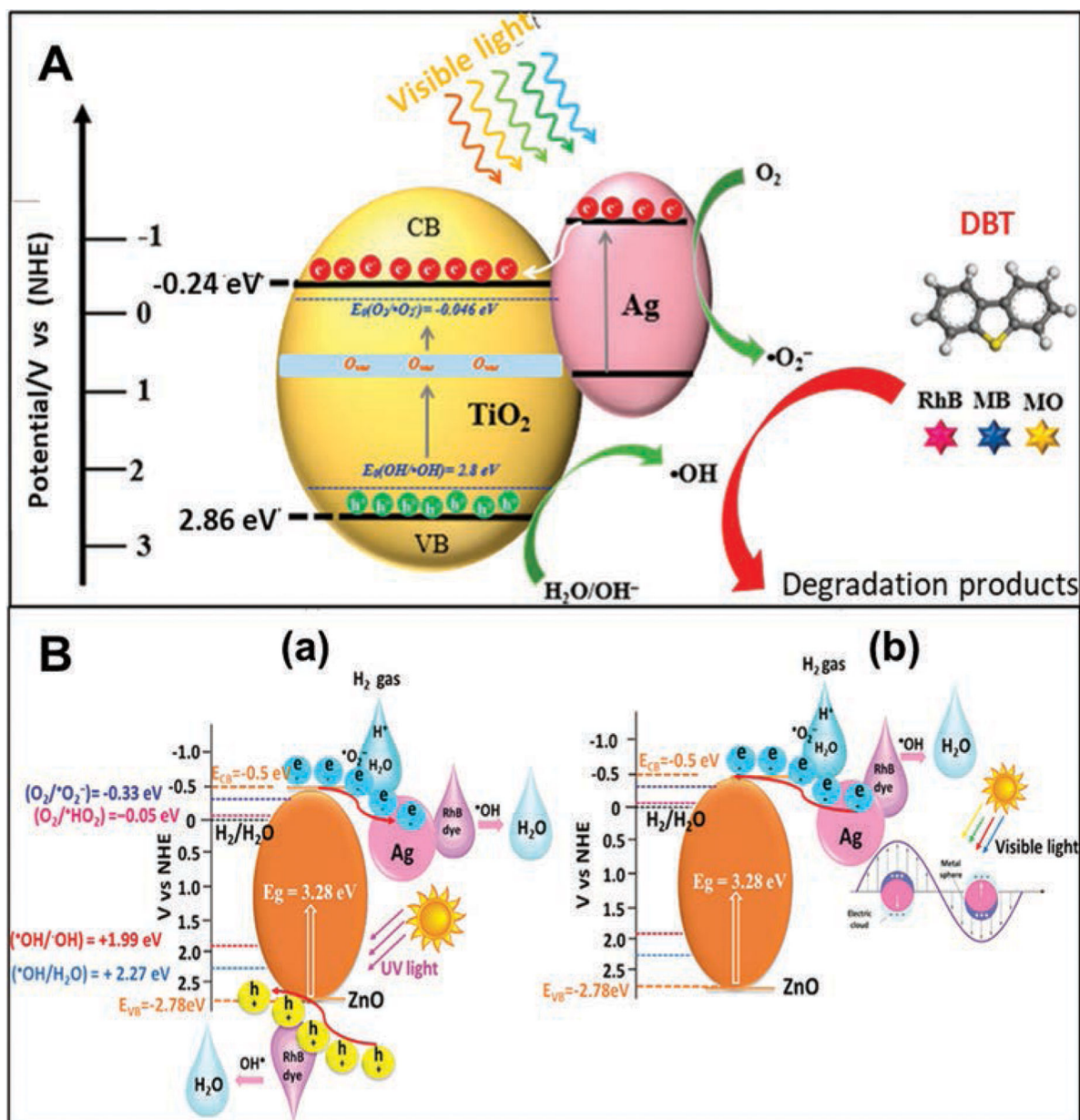
Fig. 31.
(A) Schematic behaviour of charge carriers in the Ag–TiO$_2$/PG catalyst under visible light irradiation. Reproduced from ref. 600 with permissions, with permission, American Chemical Society, copyright 2018. (B) Schematic illustration of the charge-transfer mechanism in the Ag-loaded ZnO nanostructures under (a) UV light and (b) visible light irradiation. Reproduced from ref. 602 with permission, American Chemical Society, copyright 2020.
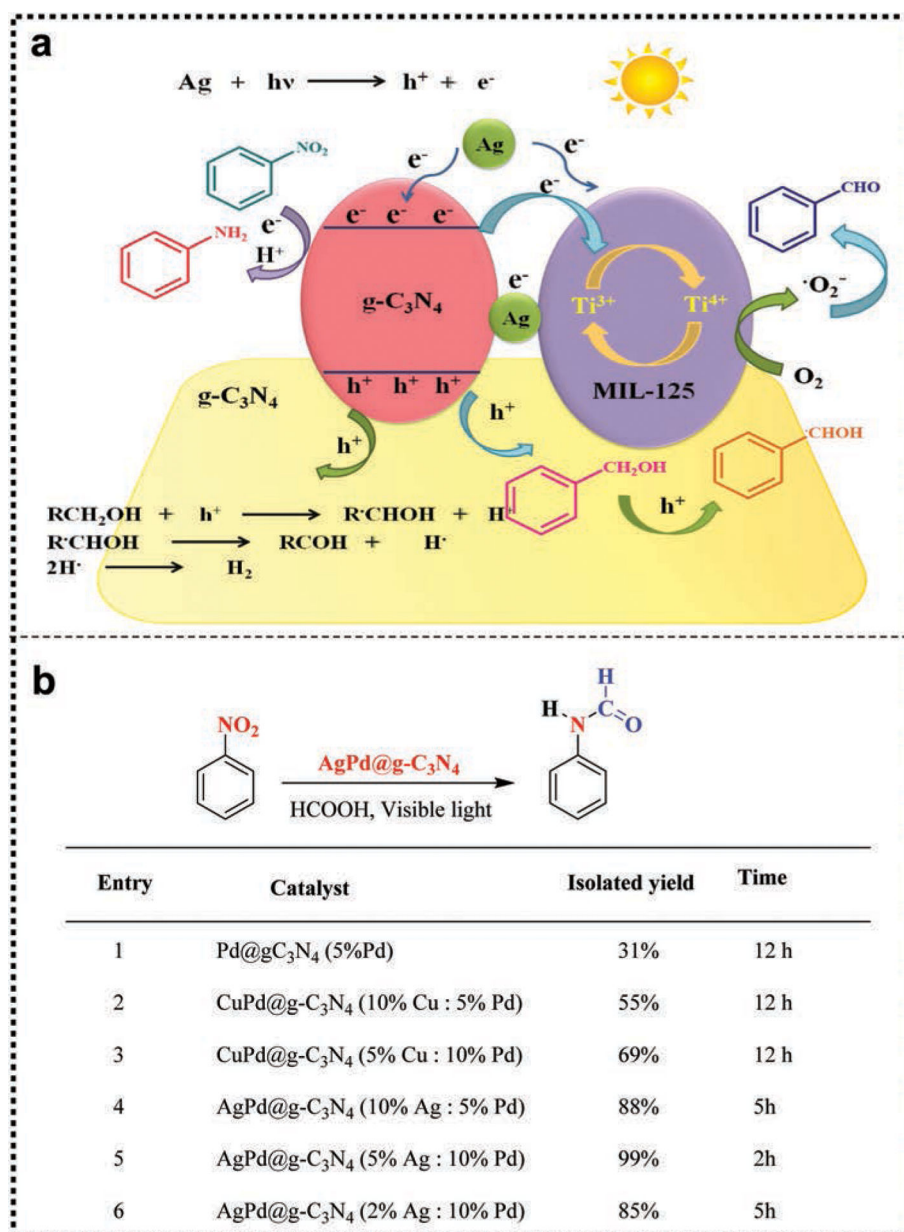
Fig. 32.
(a) Schematic illustration showing photocatalytic oxidation and reduction processes of the MIL-125/Ag/g-C$_3$N$_4$ composite. Reproduced from ref. 618 with permission, Elsevier, copyright 2017. (b) *N*-Formylation by using a AgPd@g-C$_3$N$_4$ catalyst.
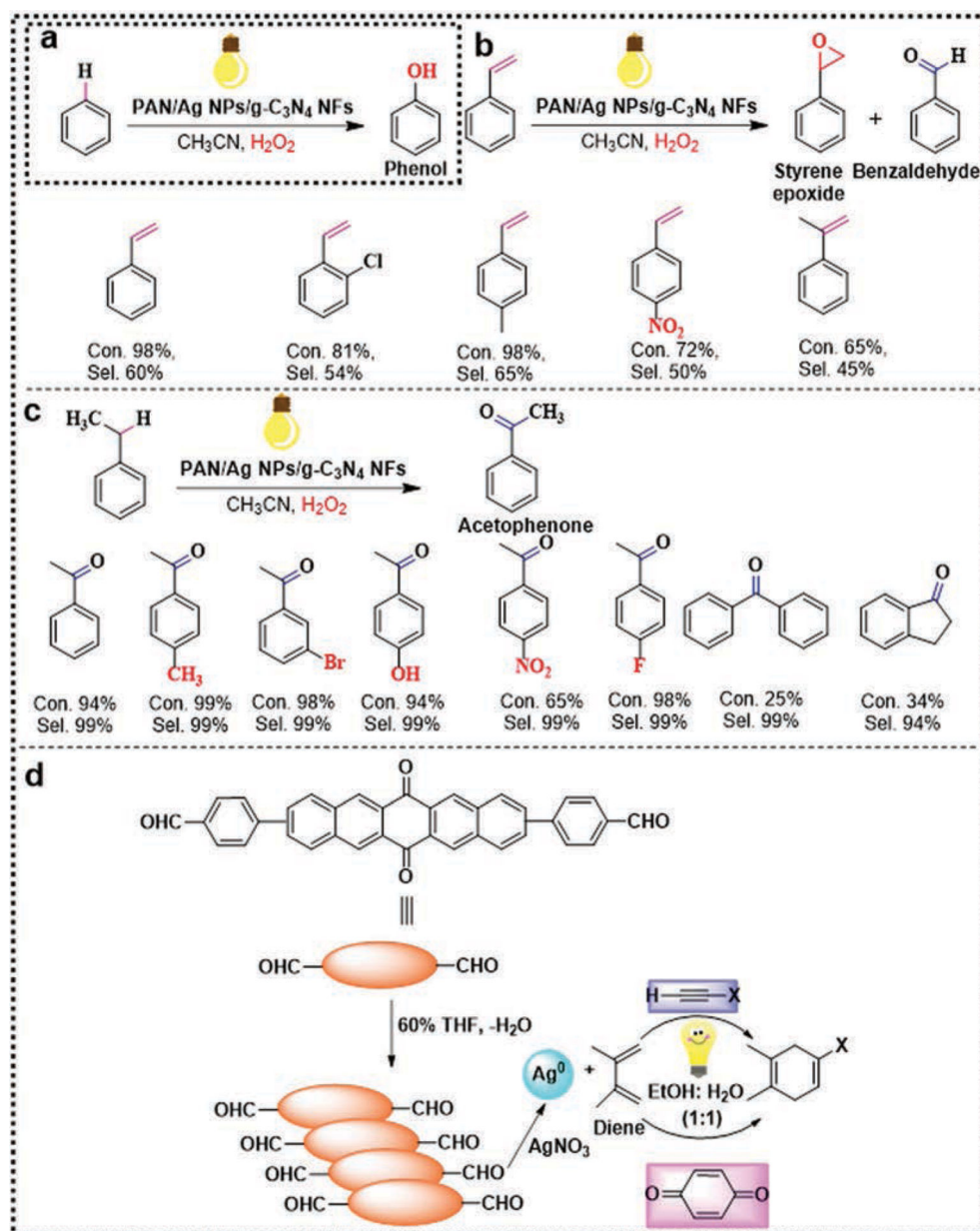
Fig. 33.
Selectivity and conversion rate of PAN/Ag NPs/g-C$_3$N$_4$ catalyzed oxidation reactions, (a) C–H oxidation of benzene, (b) styrene and substituted styrene's to styrene epoxide, (c) C–H oxidation of various −CH$_2$ bonded substrates, and (d) Ag NPs served as a photocatalyst for the DA reaction.
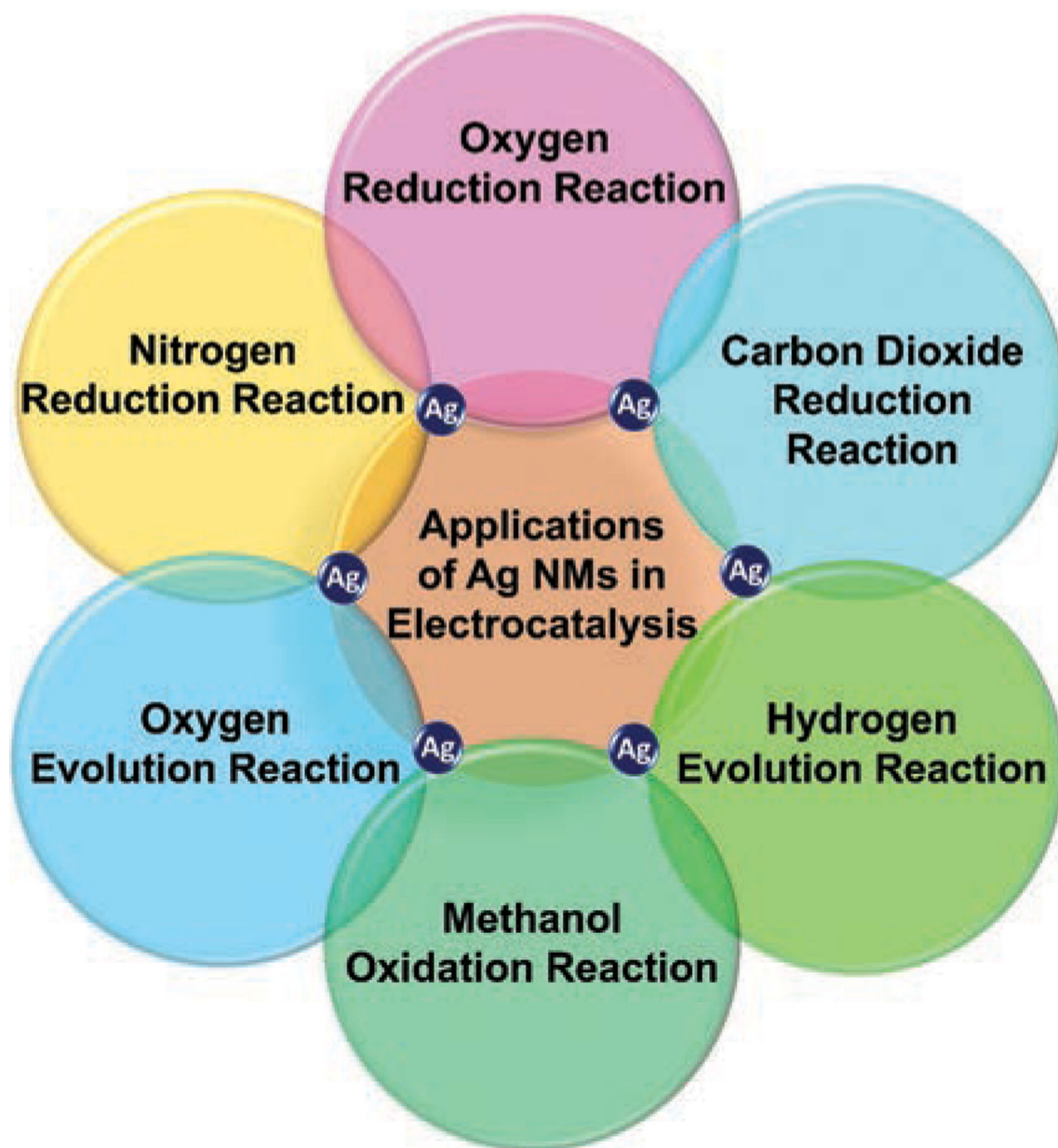
Fig. 34.
Schematic representation of electrocatalytic applications of silver nanocatalysts.
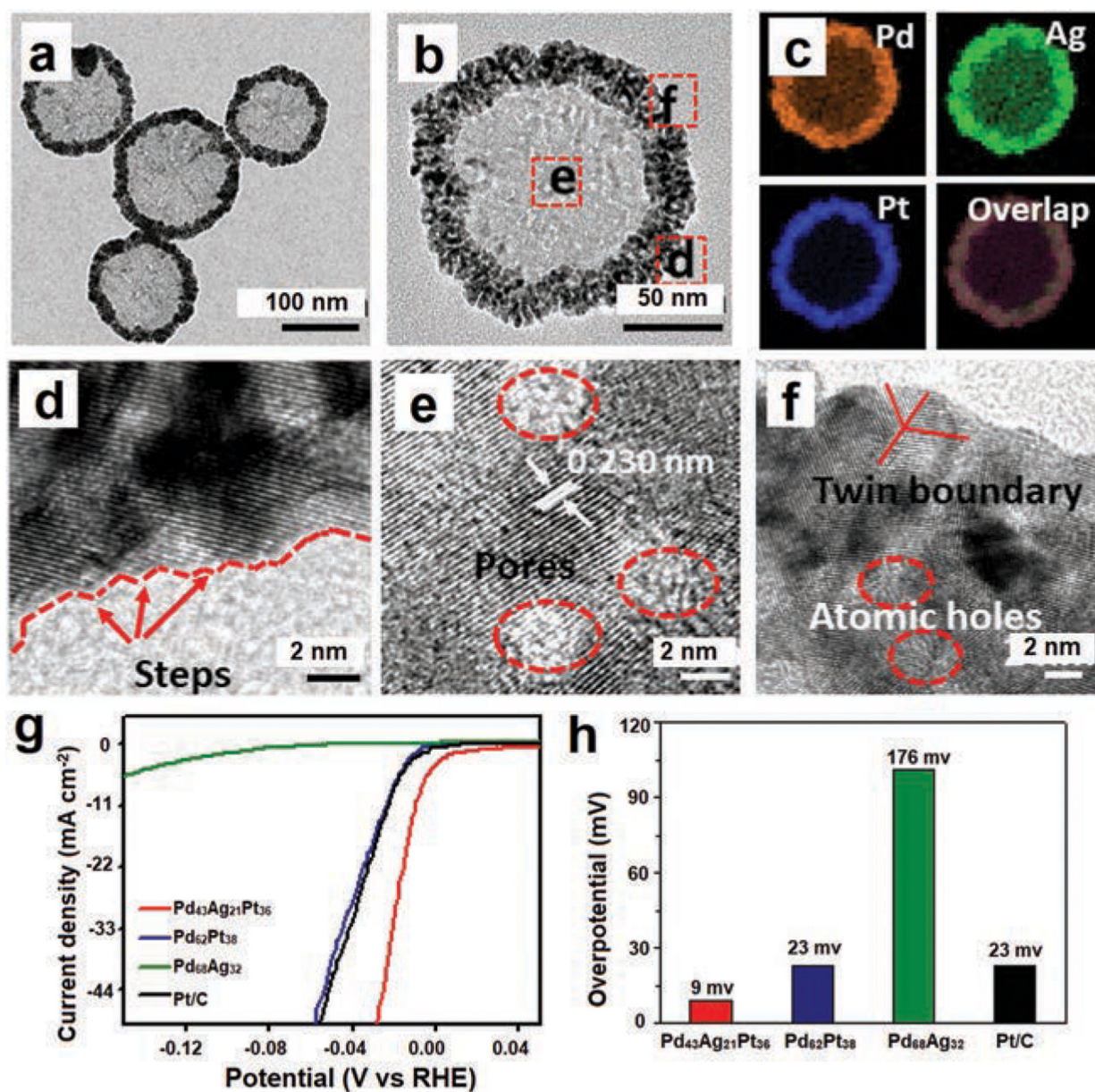
Fig. 35.

Schematic of $Pd_{43}Ag_{21}Pt_{36}$ nanowheels and electrocatalytic HER performance. (a and b) TEM images, (c) EDS elemental mapping, (d–f) HRTEM images, (g) LSV curves, and (h) overpotential of 9 mV at a 10 mA cm^{-2} current density. Reproduced from ref. 669 with permission, American Chemical Society, copyright 2020.
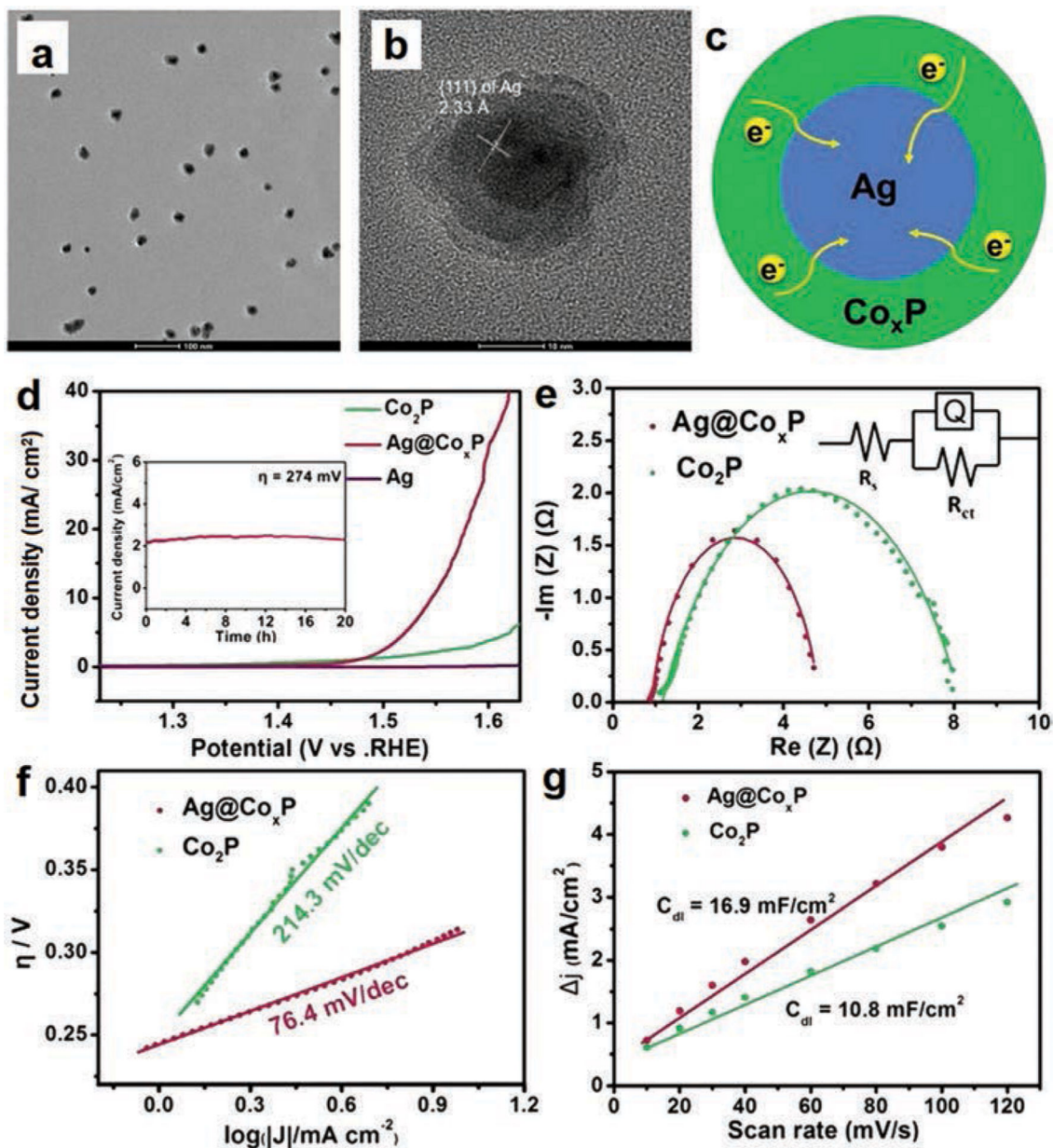
Fig. 36.
Schematic of core–shell Ag@Co$_x$P NPs and electrocatalytic OER performance. (a) TEM image, (b) HRTEM image, and (c) pictorial representation of the electron migration between the Co$_x$P shell and the Ag core. Electrocatalytic activity comparison of Ag@Co$_x$P and Co$_2$P. (d) Polarization curves depicting the overpotential, (e) Nyquist plots describing the equivalent circuit model, (f) Tafel slope demonstrated by polarization curves, and (g) linear relationship between *j* and the scan rate. Reproduced from ref. 692 with permission American Chemical Society, copyright 2017.
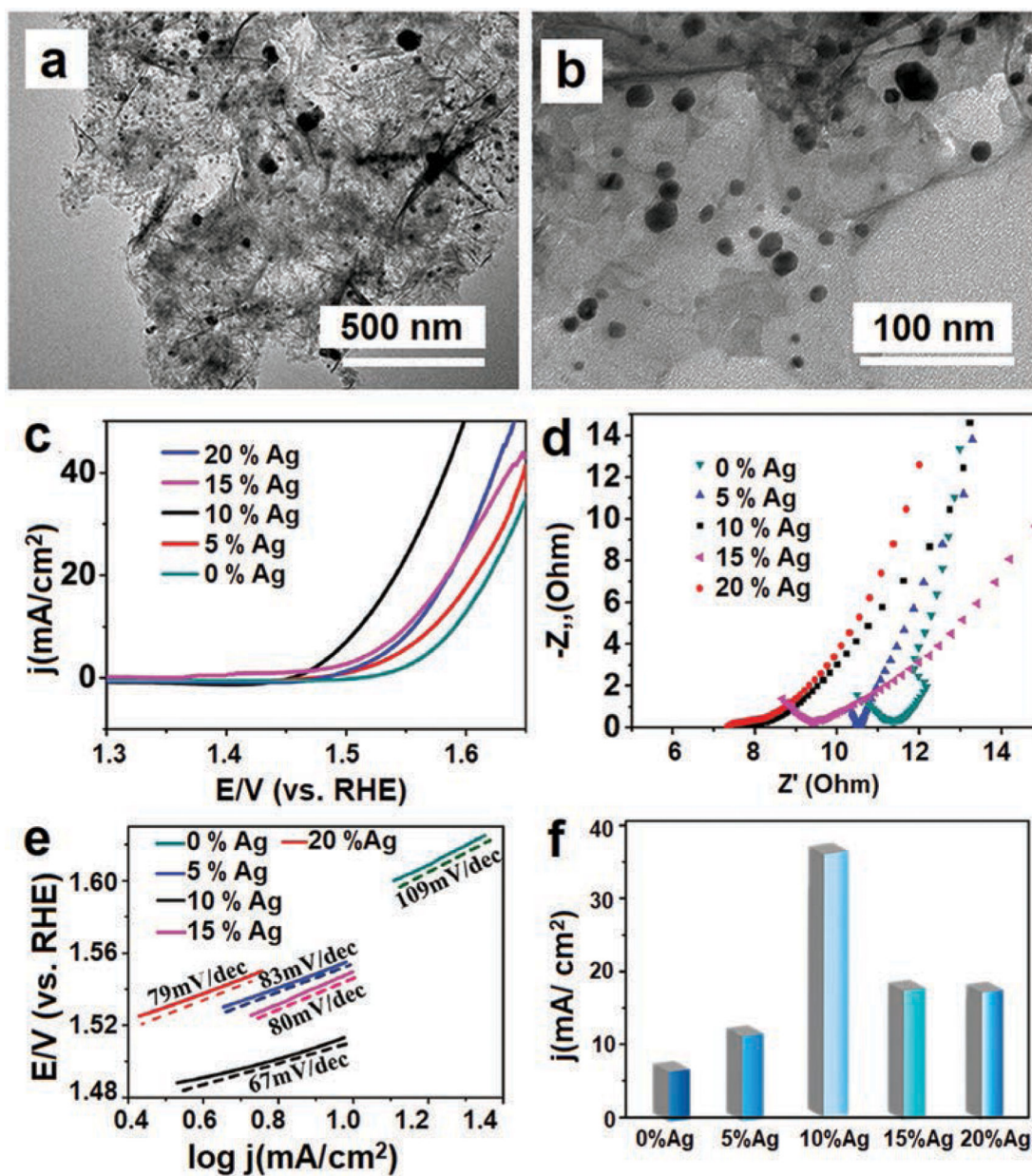
Fig. 37.
Schematic of Ag-decorated Co(OH)$_2$ nanosheets and its electrocatalytic OER performance.
(a and b) TEM images, (c) LSV curves, (d) EIS curves, (e) Tafel slope, and (f) current
densities at a 0.35 V overpotential of different compositions of Ag-decorated Co(OH)$_2$
nanosheets. Reproduced from ref. 694 with permission, American Chemical Society,
copyright 2018.
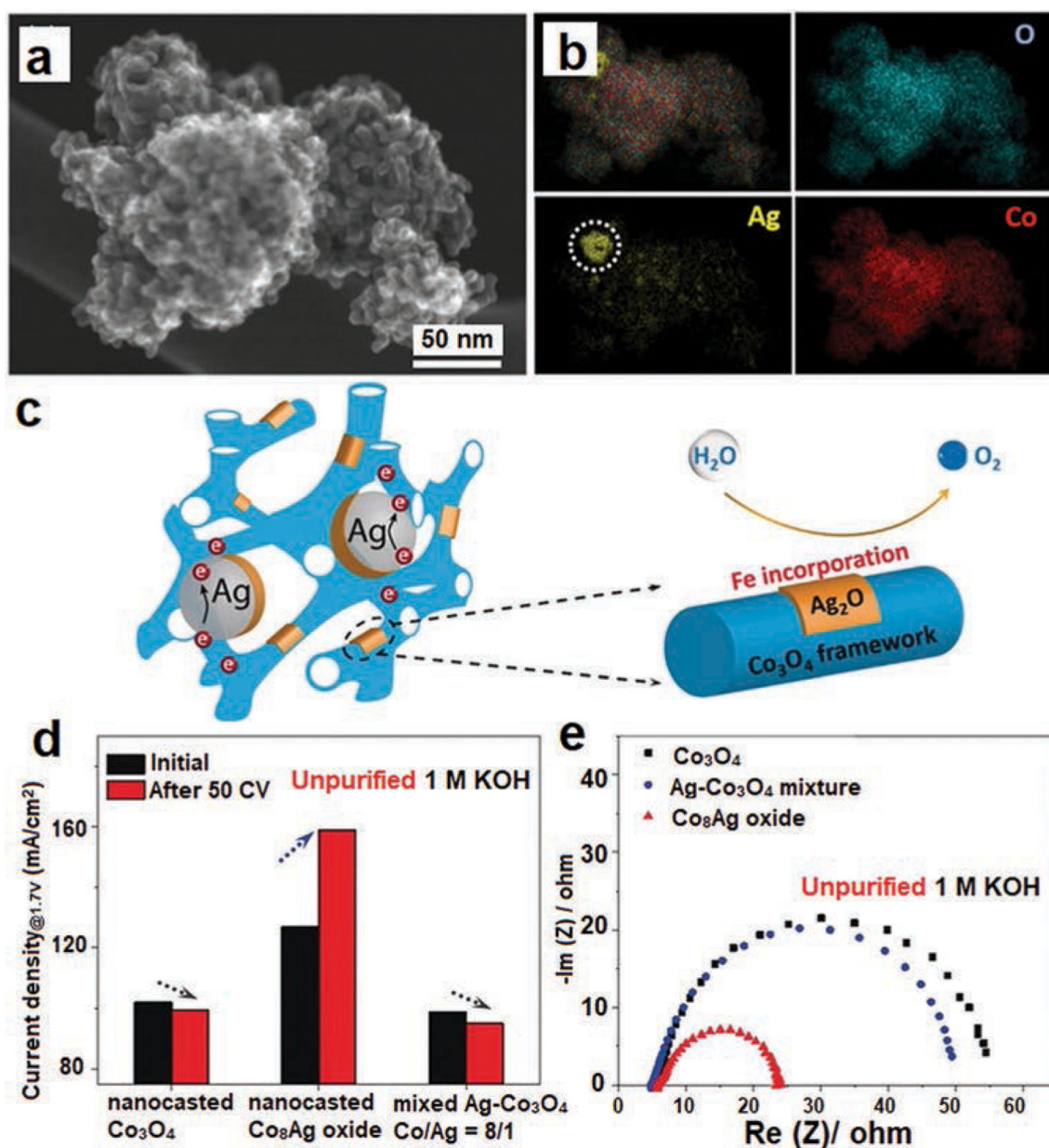
Fig. 38.
Schematic of the Ag–Co oxide nanocomposite. (a) HR-SEM image, (b) elemental mapping images, (c) pictorial representation of the role of Ag metallic particles and Ag_2O clusters in the Co_8Ag oxide structure, (d) a comparison of current density obtained before and after 50 CV at 1.7 V_{RHE}, and (e) Nyquist plots of nanocast Co_3O_4. Reproduced from ref. 695 with permission, John Wiley and Sons, copyright 2020.
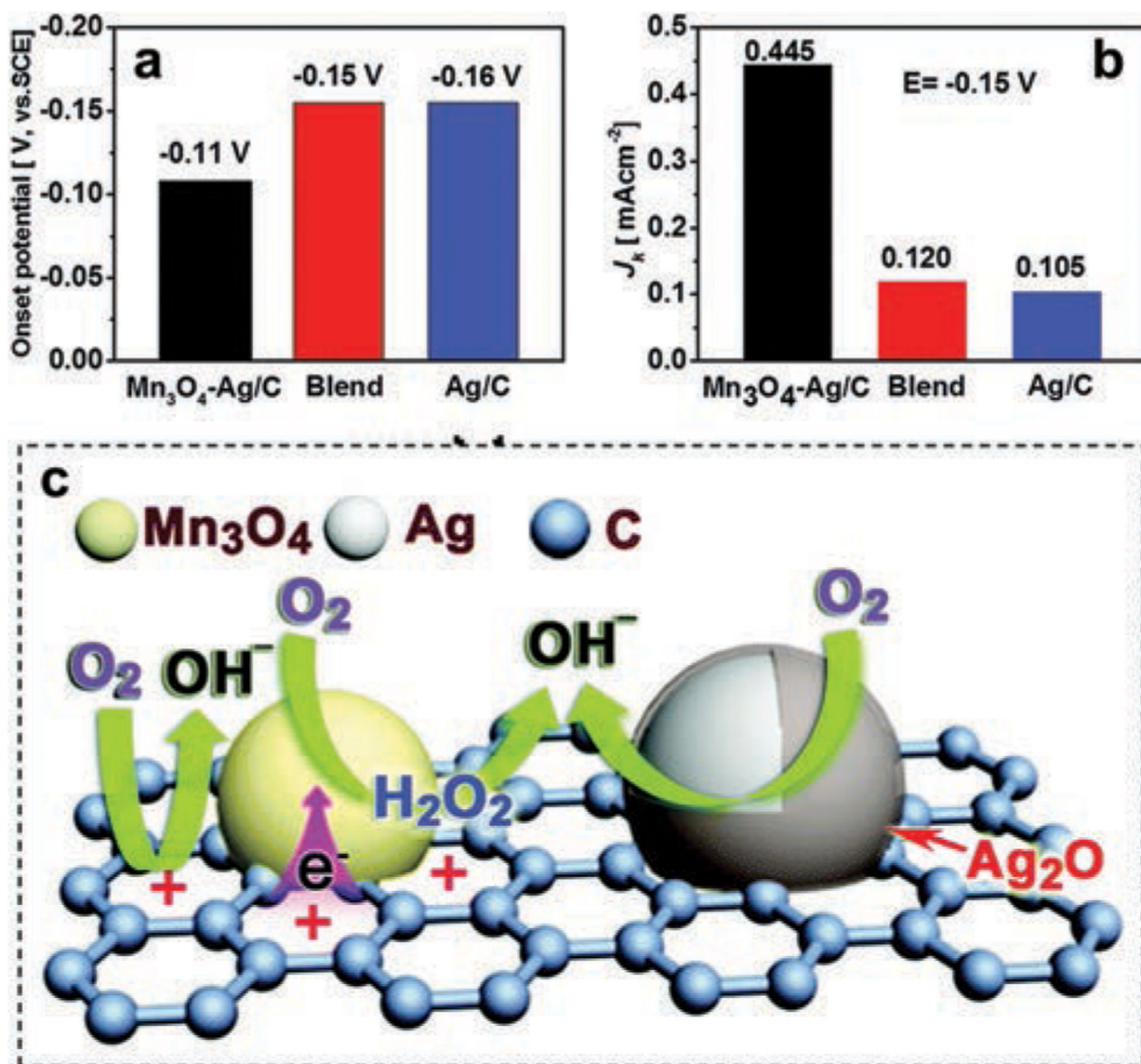
Fig. 39.
The comparison of electrocatalytic behaviour of synthesized Ag–Mn$_3$O$_4$/C, Ag/C, the blend, and a commercial Pt/C; (a) onset potential, (b) kinetic current densities, and (c) the depicted proposed mechanism for electron interaction-enhanced oxygen reduction and H$_2$O$_2$ degradation. Reproduced from ref. 725 with permission, Royal Society of Chemistry, copyright 2014.
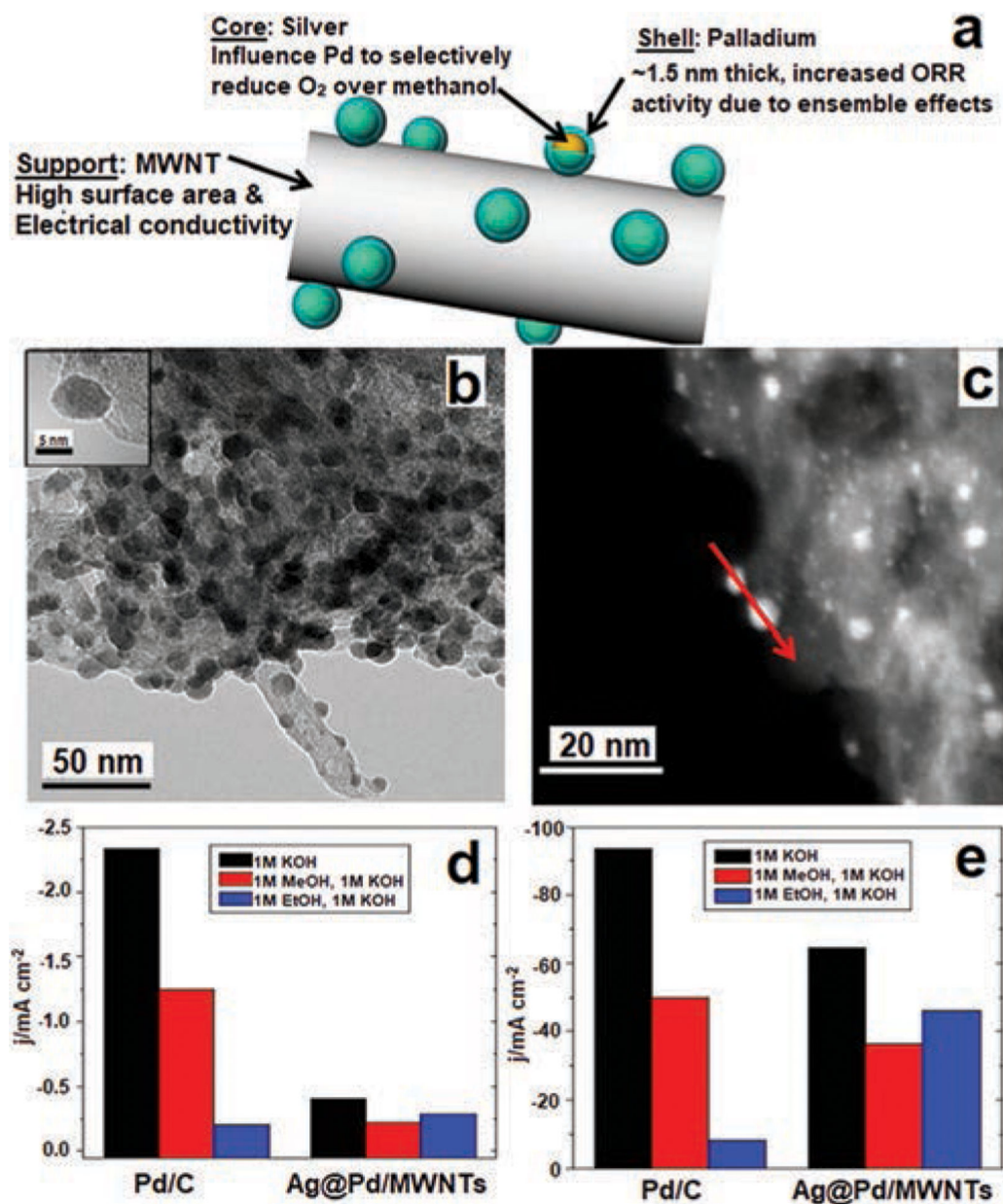
Fig. 40.
Schematic of the Ag@Pd/MWNTs catalyst, (a) pictorial representation of catalyst
properties, (b and c) TEM images and activity comparison of Pd/C and Ag@Pd/MWNTs at
−0.1 V, (d) current density, and (e) mass activity. Reproduced from ref. 752 with permission,
Elsevier, copyright 2013.
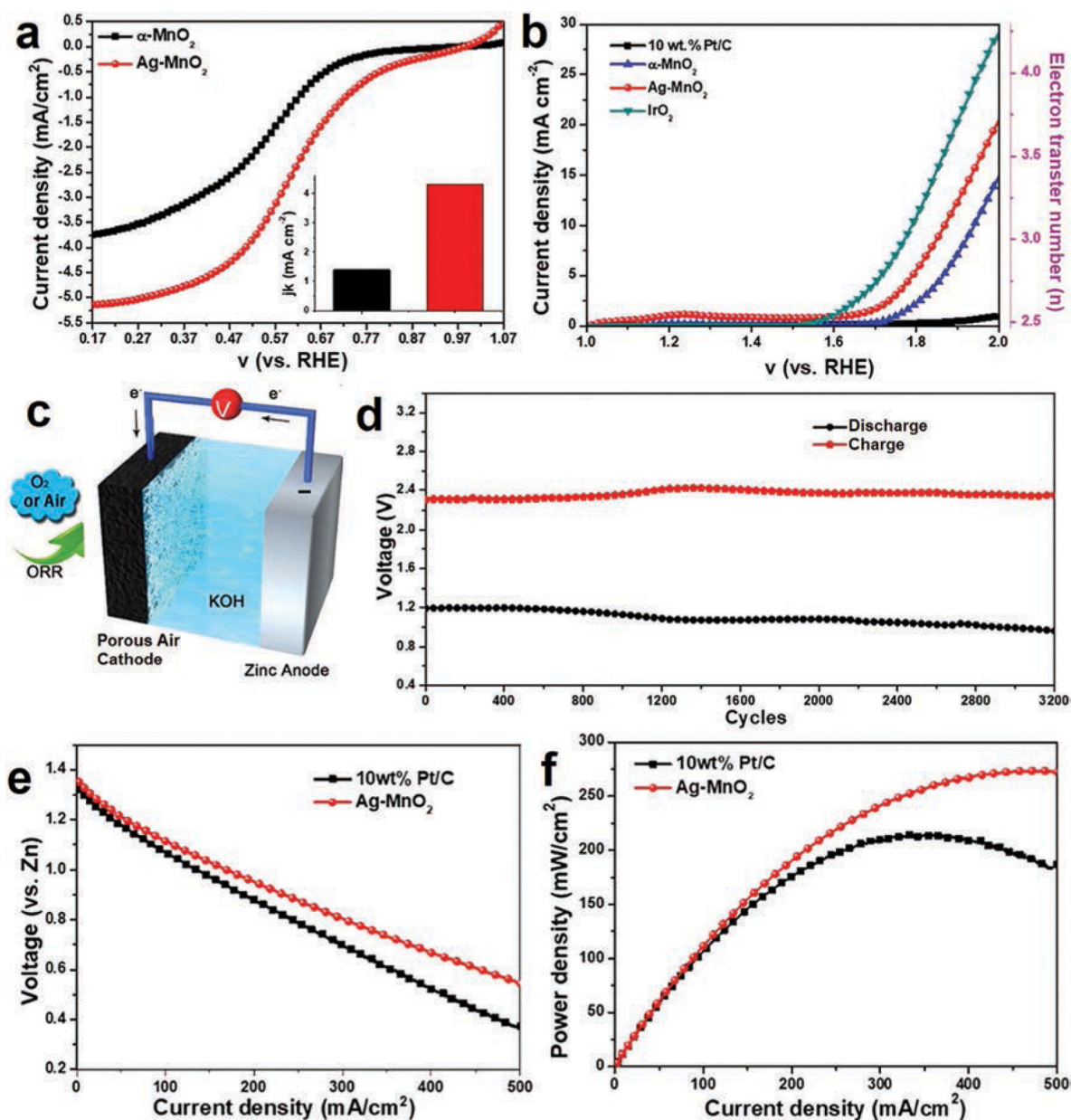
Fig. 41.
Electrocatalytic performance of Ag–MnO$_2$ catalyst, (a) ORR polarization curves, (b) OER polarization curves, (c) pictorial representation of ZAB, (d) operational stability of Ag–MnO$_2$ based ZAB, (e) profile of current–voltage, and (f) powder density *vs.* current density for Ag–MnO$_2$ and Pt/C ORR catalysts in ZAB. Reproduced from ref. 763 with permission Elsevier, copyright 2019.
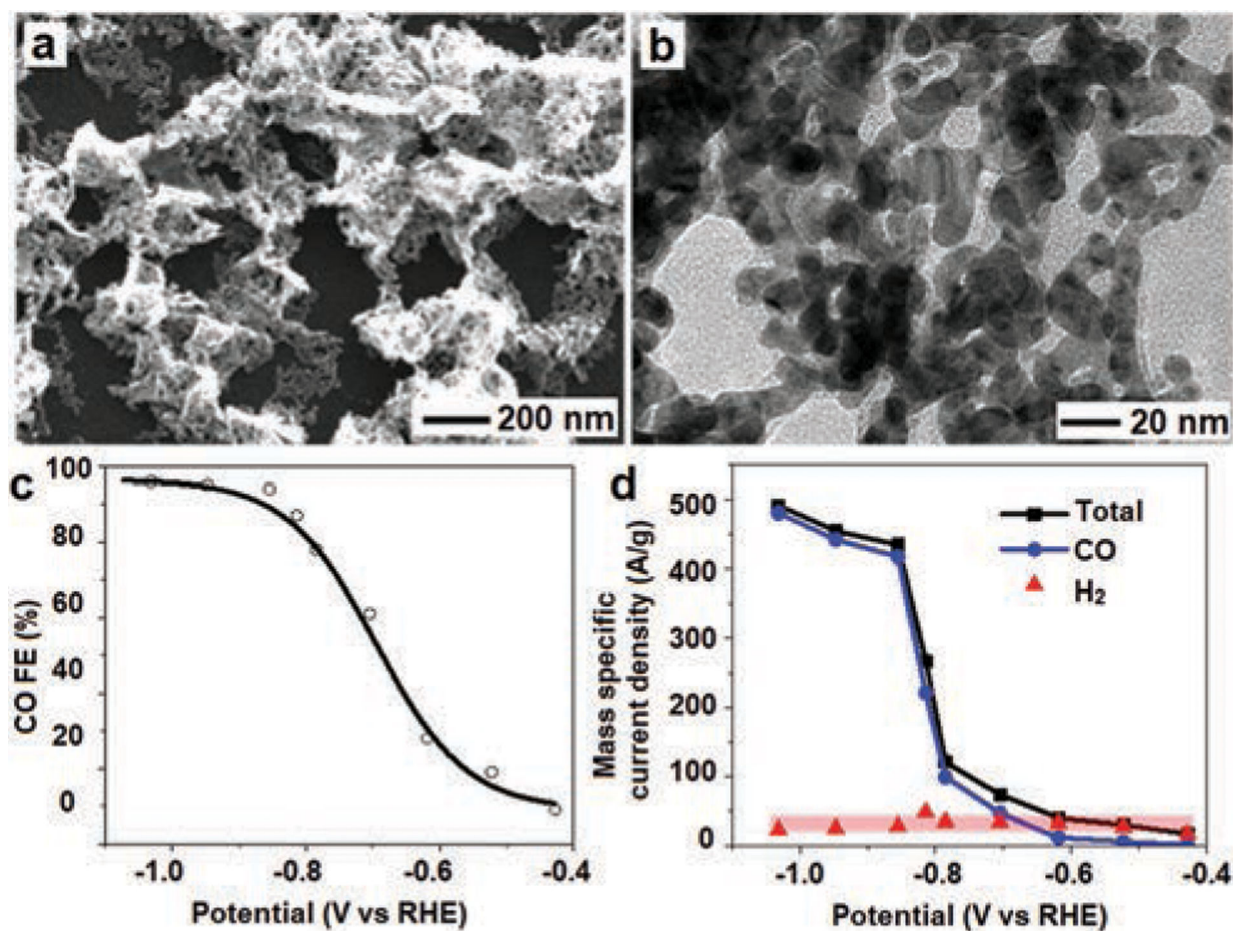
Fig. 42.
Schematic of porous Ag nanostructure, (a) SEM image, (b) TEM image, (c) FE of CO production from the EC-CO$_2$RR, (d) mass-specific current density for electrochemical reduction of CO$_2$ to CO (blue), hydrogen production from the HER (red), and overall electrochemical reduction reactions (black). Reproduced from ref. 788 with permission American Chemical Society, copyright 2020.
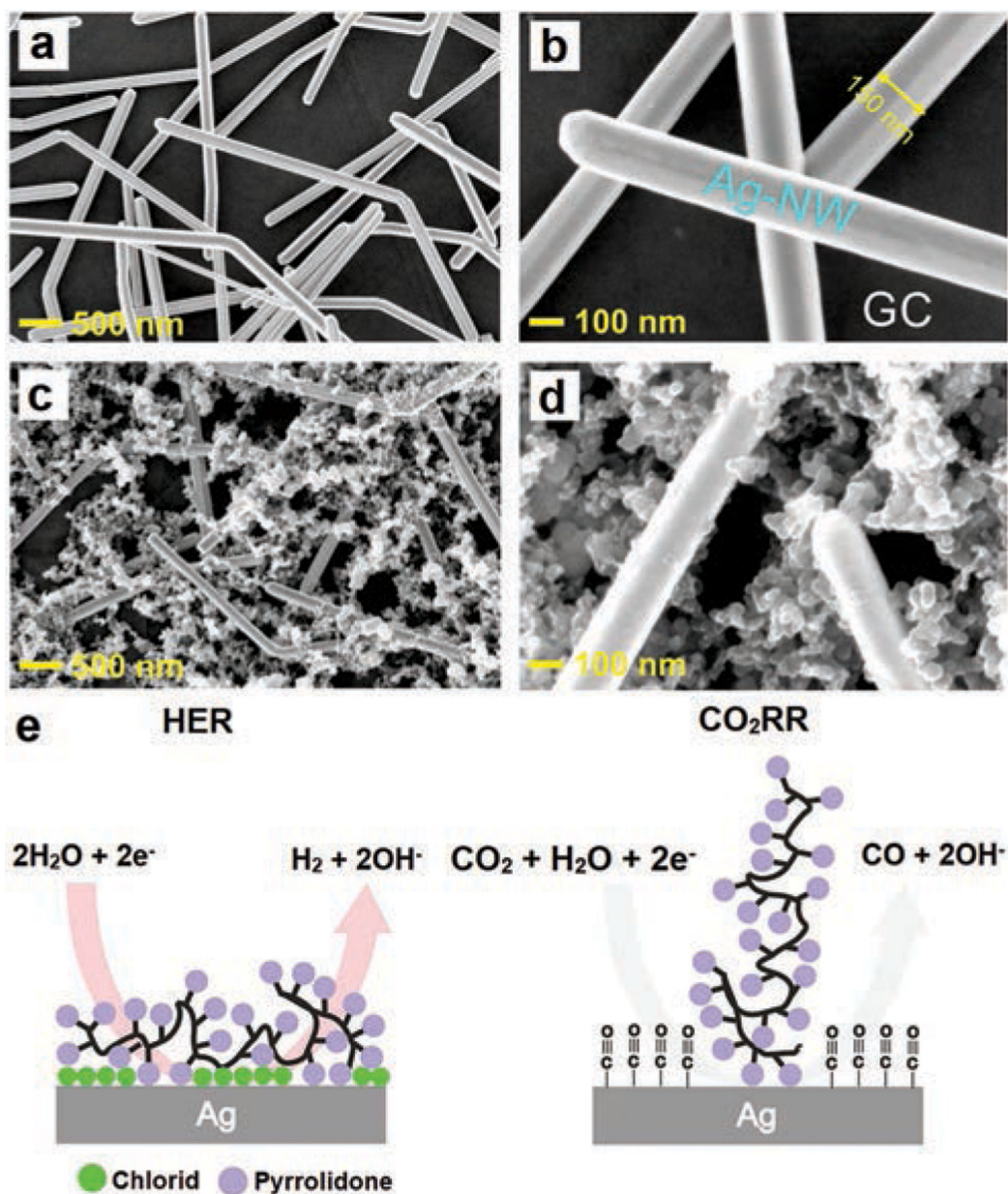
Fig. 43.
SEM images: (a and b) Ag-NWs supported with a glassy carbon (GC) electrode, (c and d) Ag-NWs supported with carbon, and (e) schematics of the PVP and Cl terminated Ag surface. Reproduced from ref. 790 with permission, American Chemical Society, copyright 2020.
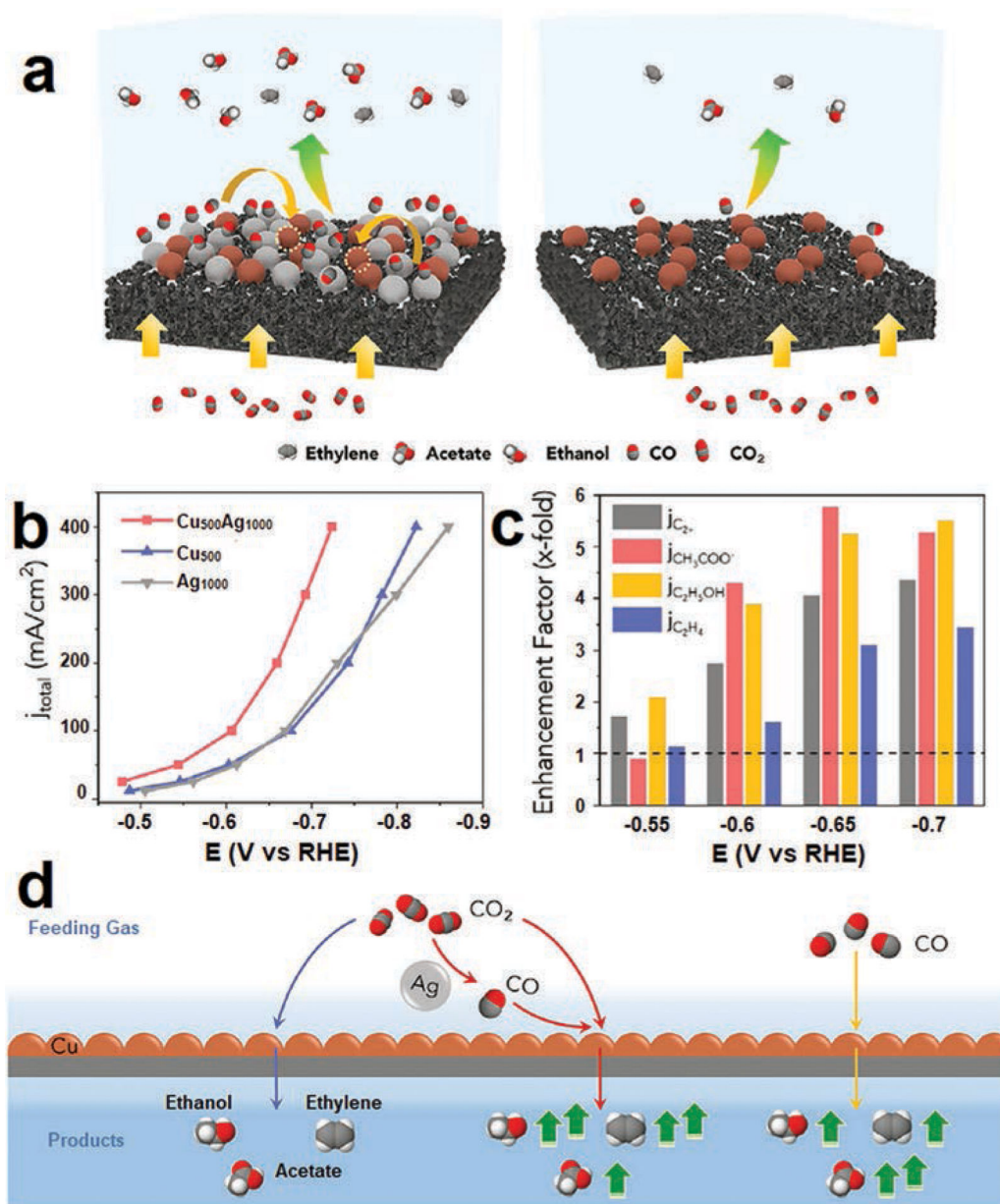
Fig. 44.
(a) Schematic representation of the EC-CO_2RR over the Cu–Ag tandem catalyst, (b) Cu–Ag based catalyst efficiency comparison with partial current density, (c) EFs for overall C_{2+} and individual products and (d) difference in catalytic activity due to the change in local environment. Reproduced from ref. 801 with permission, Elsevier, copyright 2020.
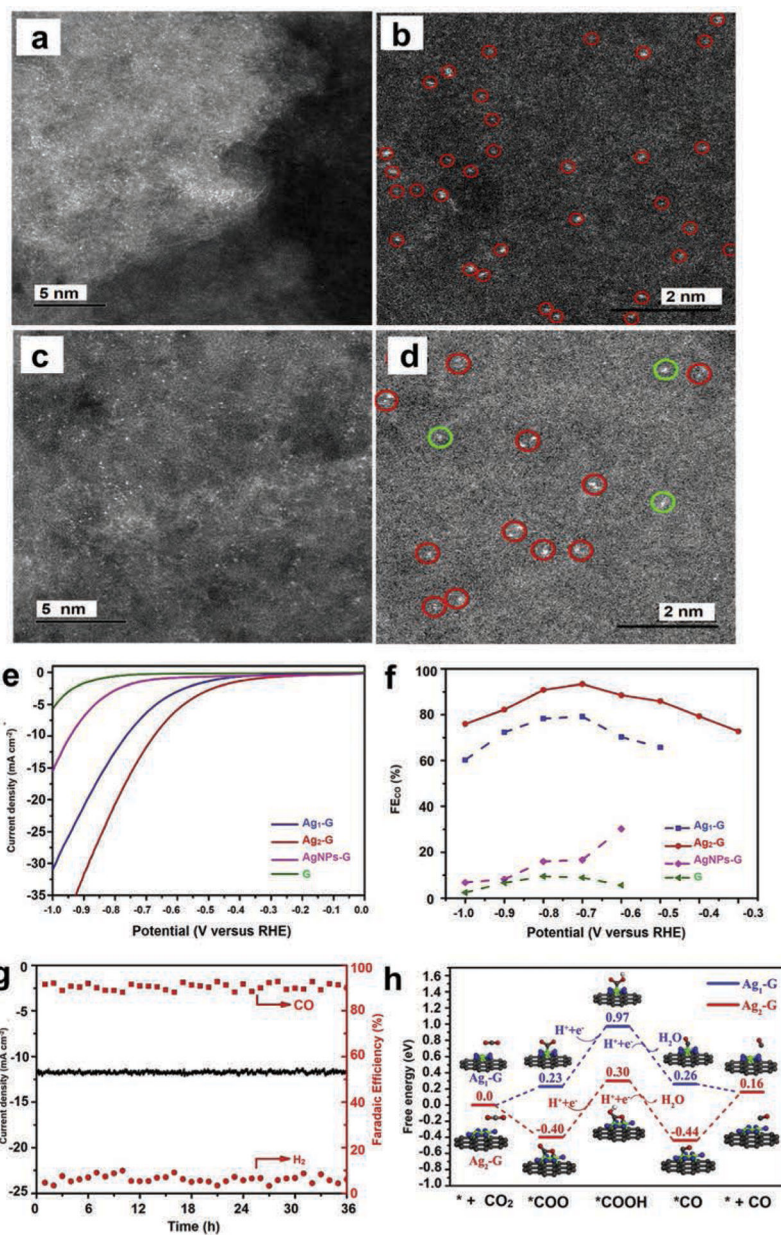
Fig. 45.

(a and b) AC HAAD STEM and enlarged HAAD STEM image of Ag_1-G, and (c and d) AC HAAD STEM and enlarged HAAD STEM image of Ag_2-G, respectively. Schematic of Ag_2-G catalyst performance for the EC-CO_2RR, (e) current density by LSV curves, (f) FE for the production of CO, (g) catalyst operational stability test, and (h) calculations of the CO_2RR's free energy using DFT. Reproduced from ref. 815 with permission, Elsevier, copyright 2020.
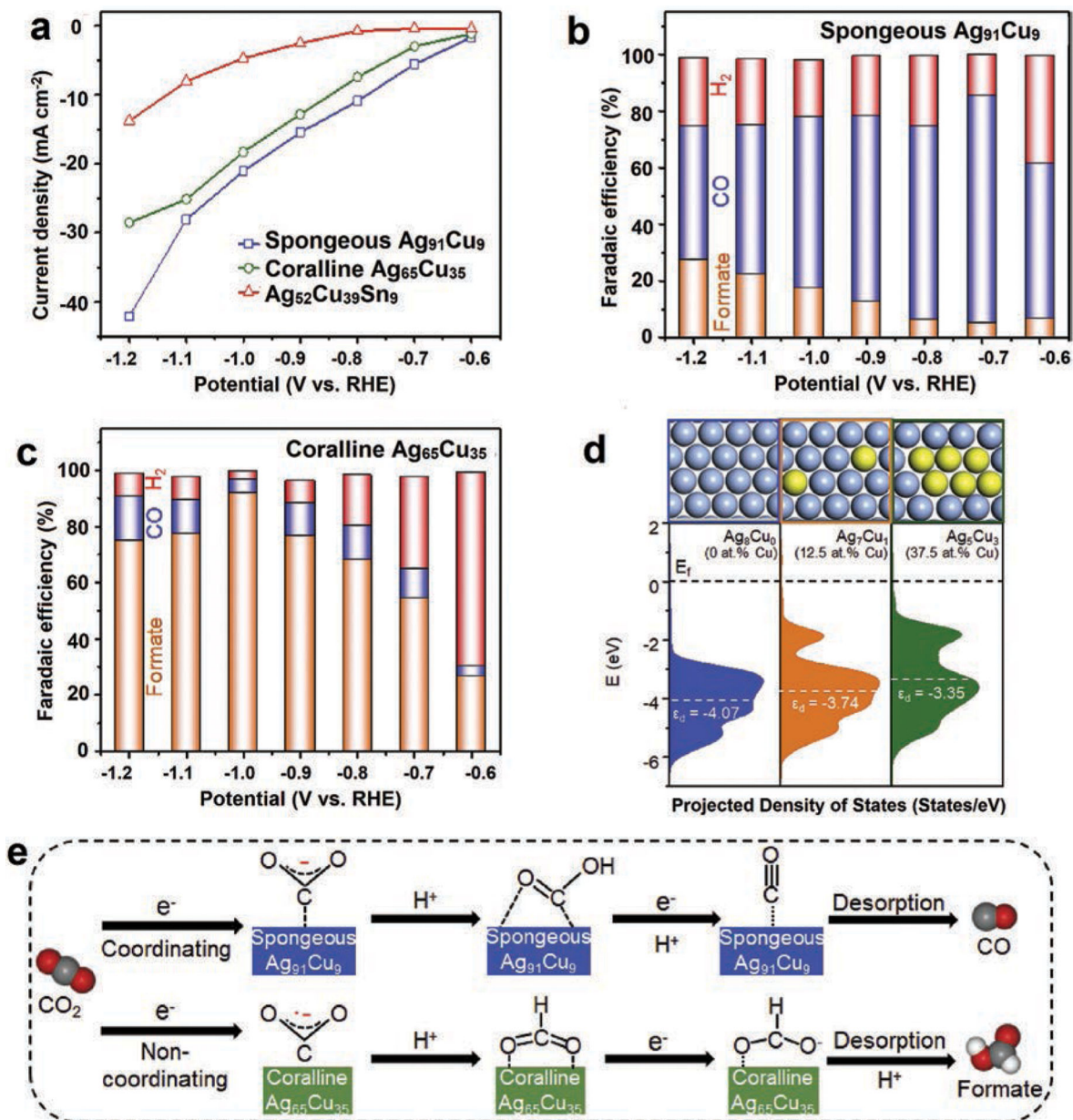
Fig. 46.

(a) Current densities of Ag/Cu-based alloy nanostructures, (b) FE of CO_2 reduction products over the spongeous $Ag_{91}Cu_9$ nanocomposite, (c) FE of CO_2 reduction products over coralline $Ag_{65}Cu_{35}$, (d) effect of variations in Cu enrichment on d-band electronic states of surface atoms on $Ag_8Cu_0(111)$, $Ag_7Cu_1(111)$ and $Ag_5Cu_3(111)$, and (e) mechanistic pathway for the reduction of CO_2 electrocatalytically over spongeous $Ag_{91}Cu_9$ and coralline $Ag_{65}Cu_{35}$ nanocatalysts. Reproduced from ref. 822 with permission, Elsevier, copyright 2020.
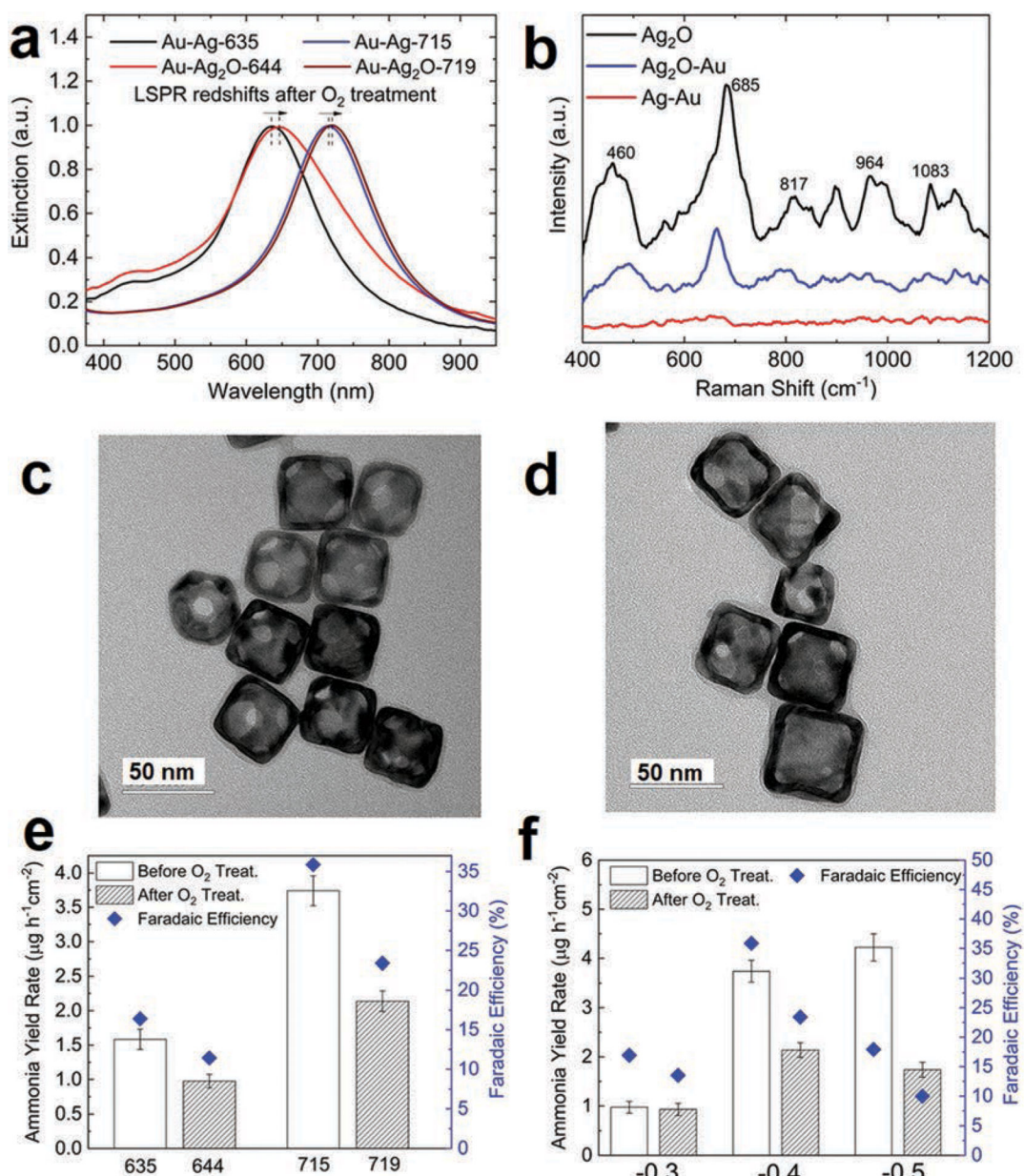
Fig. 47.

Before and after O_2 treatment UV-vis extinction spectra of bimetallic Au–Ag nanocages (a) with different LSPR peak positions, and (b) SERS spectra. TEM images of (c) Ag_2O–Au-644, (d) Ag_2O–Au-719, (e) FE, and ammonia yield rate for Au–Ag bimetallic nanocages before and after O_2 treatment with various LSPR peak positions in 0.5 M $LiClO_4$ aqueous solution at the potential of 0.4 V *vs.* RHE, (f) in a 0.5 M $LiClO_4$ aqueous solution, ammonia yield rate, and FE were measured at different applied potentials. Reproduced from ref. 643 with permission, American Chemical Society, copyright 2019.
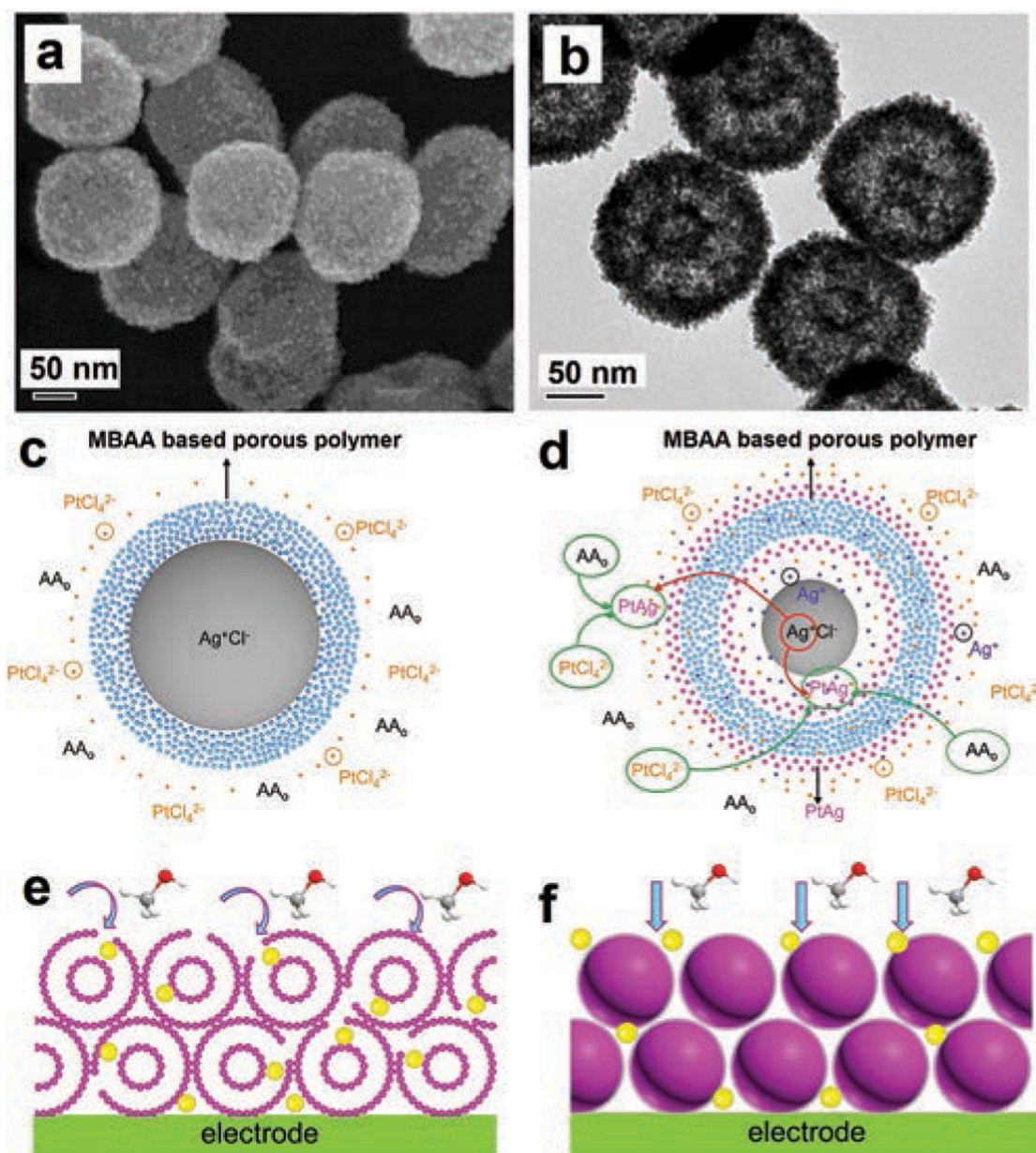
Fig. 48.
Schematic of Pt-Ag DSNCs. (a) SEM image, (b) TEM image. The mechanism of formation of Pt-Ag DSNCs at different time intervals (c) after 10 min and (d) after 30 min. The mass transport during MOR in (e) Pt–Ag DSNCs and (f) commercial Pt black NPs. Reproduced from ref. 642 with permission, Elsevier, copyright 2021.

Table 1

Key advantages and disadvantages of various techniques utilized for preparing Ag NPs

S. no.	Synthesis technique	Advantages	Disadvantages	Applications	Industrial scale up	Environmental safety	Ref.
1	Chemical reduction method	• Produces Ag nanoparticles with well-defined size, dimension, composition and structure • Nanoparticles formed with good homogeneity and narrow size distribution • Easier to manipulate growth and morphology by simply monitoring the reaction conditions like concentration, capping or stabilizing agent, type of solvent	• Drawbacks include toxicity, poor reducing ability and high cost of the reducing agent involved • Formation of toxic by-products	• Catalysis (photo/electro/liquid phase) • Electrical Percolation	• No, in view of toxicity associated	• No	218
2	Sonochemical mediated synthesis	• Expeditious, environmentally benign and facile method for producing Ag nanostructures • Faster rate of reaction • Encompasses ambient operating conditions • Compared to other methods, leads to the production of Ag NPs of reduced size • Low dispersion of nanoparticles observed	• Rate of sonochemical reduction depends on the ultrasonic frequency • Challenging to control size and shape of nanoparticles • Difficult in scaling to larger installations • Exact mechanism of formation of nanoparticles is still unknown	• Catalysis (photo/liquid phase) • Biomedical (antibacterial and antioxidant) • Drug delivery • Cosmetics	• Yes	• Yes	135, 196
3	Microwave assisted synthesis	• Rapid and selective heating • High heating rate and increased reaction kinetics • Excellent control over the reaction parameters • High yield and improved selectivity	• Insufficient large penetration depth of microwaves during large batch reactions produces heating via convention rather than direct dielectric heating • Non-uniform heating occurs as MW dependent on wavelength; non-uniformity of electric	• Catalysis • Agro based applications • Antibacterial and antioxidant activities • Catalytic degradation of dyes	• Yes	• Yes	150, 219

S. no.	Synthesis technique	Advantages	Disadvantages	Applications	Industrial scale up	Environmental safety	Ref.
		• Greater reproducibility	field with wavelength causes non-uniformity in temperature	• Water purification			
		• High throughput synthesis	• Electrical discharge phenomenon leading to burning of the sample's surface				
		• Generates monodispersed, crystalline and high purity Ag nanostructures within few minutes	• In-depth or detailed mechanism for Ag NPs synthesis using MW irradiations is not elucidated; theoretical or computer simulations of microwave heating mechanisms can be used				
			• Lack of scalability for industrial applications				
			• Requires polar solvents				
			• Detailed experimental studies to identify the exact effect involved: thermal or non-thermal is required				
4	Green synthetic approaches	• Eco-friendly and low-toxic method for fabricating Ag NPs	• Reproducibility of the synthetic process has to be upgraded	• Drug delivery	• Yes	• Yes	96, 218, 220
		• Economical and cost-effective approach (phytoconstituents play dual role of reducing and stabilizing agent)	• Scaling up to the industrial level	• DNA analysis and gene therapy			
			• Mechanism of NP synthesis through bioreduction reaction requires additional experimentation	• Cancer treatment			
		• No expensive equipment required		• Antimicrobial agents			
		• Less waste generation	• Difficult to achieve proper control over size and distribution of nanoparticles	• Biosensors			
		• Inherently safer technique (occurrence of accidents is negligible)		• Catalysis			
			• Effective control of the monodispersity is required	• SERS			
		• Plants extracts are biocompatible; nanoparticles synthesized using this technique can be further utilized in pharmaceutical and biomedical fields	• Identification and purification of individual phytoconstituent	• Magnetic resonance imaging (MRI)			

EPA Author Manuscript

EPA Author Manuscript

EPA Author Manuscript

S. no.	Synthesis technique	Advantages	Disadvantages	Applications	Industrial scale up	Environmental safety	Ref.
5	Thermal treatment method	• Convenient and economical technique for Ag NPs synthesis • Generates stable, monodispersed and controlled nanometric sized particles • By regulating annealing temperature, heating time and heating rate, shape as well as size of ensuing NPs can be meticulously controlled	responsible for bioreduction is necessary • Proper kinetic characterization of thermal decomposition processes is required that would eventually provide key knowledge pertaining to controlling the reaction process as well as properties of Ag NPs formed. • Involves high temperature conditions and thus proper safety measures should be taken	• Biomedical applications • Catalysis	• No	• No	191
6	Continuous flow and microwave flow assisted synthesis	• Fast and efficient mixing of reagents • Precise control over mixing and reaction parameters (temperature and pressure) • Enhanced yield accompanied with low impurities • Constant product (nanoparticles) formation; high efficiency • High reproducibility • Scalable from pilot to full commercial process • Improved thermal (safety) management due to closed systems; interaction with hazardous chemicals is minimized • Microwave assisted flow reactors generates large quantities of NPs • Greener technique from quality, safety,	• High cost of equipment involved • Possibility of settling of nanoparticles so-formed, sticking up in pipes which increases the flow resistance, makes the heat exchange process difficult and sometimes also results in product contamination • After every reaction, overall assembly requires washing with solvents so as to eliminate the leftovers, thus making it a costly operation process • Suitable methods need to be developed so that reagents and solvents can be recovered and recycled • Special emphasis should be given to sustainable reactor design, temperature distribution monitoring tools within the MW compartment and theoretical modeling and computational simulations of MW flow system	• Biodiesel synthesis • Catalysis • Biomedical imaging	• Yes	• Yes	196, 202, 203

S. no.	Synthesis technique	Advantages	Disadvantages	Applications	Industrial scale up	Environmental safety	Ref.
7	Seed mediated growth	environmental and economic perspective • Offers staggering degree of control over size, shape, structure and composition of the resulting Ag nanocrystals • Possible to manipulate the conditions of the nanocrystal growth	• Fundamental growth mechanism or mechanism of reduction still remains elusive • Reproducibility for production of Ag nanocrystals needs to be enhance • Time intensive as well as expensive; one-pot reactions wherein nucleation and growth occur together but in two temporarily separate steps should be designed	• Bactericidal and therapeutic applications • Catalysis • LSPR sensing • Electronics	• Yes	• Yes	208, 209
8	Atomic layer deposition	• An accurate and controlled method to produce high quality Ag films of specified thickness and composition • Ensures conformality control • In comparison to other techniques, require low temperature conditions	• One of the major drawbacks is that ALD processes are very time-consuming as involves slow deposition rates • Since it requires high precision, it leads to high usage of precursor gas and energy • Volatile precursors are favored that do not undergo decomposition easily • Low material utilization efficiency • Instrument or equipment employed are highly expensive which ultimately increases the cost of production	• Catalysis • Biomedical • Plasmonics • Analytical methods	• Yes	• No	215